JULY, 2017 Ph.D in Civil Engineering GULER FAKHRADDIN MUHYADDIN

GAZIANTEP UNIVERSITY

GRADUATE SCHOOL OF

NATURAL & APPLIED SCIENCES

FIBER REINFORCED UHPC AND ITS EFFECT ON LOAD CARRYING CAPACITY OF COMPOSITE TUBE MEMBERS ACCORDING TO CURRENT DESIGN CODES

Ph.D. THESIS
IN
CIVIL ENGINEERING

BY

GULER FAKHRADDIN MUHYADDIN

JULY 2017

Fiber Reinforced UHPC and its Effect on Load Carrying Capacity of Composite Tube Members According to Current Design Codes

Ph.D. Thesis
in
Civil Engineering

University of Gaziantep

Supervisor
Assoc. Prof. Dr. Esra Mete Güneyisi

by

Guler Fakhraddin MUHYADDIN

July 2017

REPUBLIC OF TURKEY
UNIVERSITY OF GAZİANTEP
GRADUATE SCHOOL OF NATURAL & APPLIED SCIENCES
CIVIL ENGINEERING DEPARTMENT

Name of the thesis: Fiber Reinforced UHPC and Its Effect On Load Carrying Capacity of Composite Tube Members According to Current Design Codes.

Name of the student: Guler Fakhraddin MUHYADDIN

Exam date: 31/07/2017

Approval of the Graduate School of Natural and Applied Sciences

Prof. Dr. A. Necmeddin YAZICI
Director

I certify that this thesis satisfies all the requirements as a thesis for the degree of Philosophy of Doctorate.

Prof. Dr. Abdulkadir ÇEVİK
Head of Department

This is to certify that we have read this thesis and that in our consensus/majority opinion it is fully adequate, in scope and quality, as a thesis for the degree of Doctor of Philosophy.

Assoc. Prof. Dr. Esra METE GÜNEYİSİ
Supervisor

Examining Committee Members:	Signature
Prof. Dr. Hanifi ÇANAKCI	....
Assoc. Prof. Dr. Ali Fırat ÇABALAR	....
Assoc. Prof. Dr. Esra METE GÜNEYİSİ	....
Assist. Prof. Dr. Hatice Öznur ÖZ	....
Assist. Prof. Dr. Hasan Erhan YÜCEL	....

I hereby declare that all information in this document has been obtained and presented in accordance with academic rules and ethical conduct. I also declare that, as required by these rules and conduct, I have fully cited and referenced all material and results that are not original to this work.

Guler Fakhraddin MUHYADDIN

ABSTRACT

FIBER REINFORCED UHPC AND ITS EFFECT ON LOAD CARRYING CAPACITY OF COMPOSITE TUBE MEMBERS ACCORDING TO CURRENT DESIGN CODES

MUHYADDIN, Guler Fakhraddin
Ph.D. in Civil Engineering
Supervisor: Assoc. Prof. Dr. Esra METE GÜNEYİSİ
July 2017
207 Pages

The main objective of using reinforced ultra-high performance concrete (UHPC) by different type and volume of fibers with concrete filled steel tube (CFST) structure is to minimize the size of the structural steel tube and to improve the mechanical, fracture, and shrinkage properties of concrete core. This provides high strength and performance for the composite elements. Accordingly, this thesis consists of two parts: First describes the experimental behavior of UHPC reinforced with various fiber types and concentrations. While the second part presents the research results of the structural behavior of axially loaded steel tube column filled with ultra-high performance fiber reinforced concrete (UHPFRC). For this, 19 UHPC mixtures containing micro-steel, hooked-steel, and micro glass fibers up to 2% volume fractions were produced. All designed mixtures were tested for the mechanical, fracture and physical performance. On the other hand, three outer diameters to wall thickness D/t ratios (30, 60, and 90) corresponded by 300, 450, and 600 MPa of yield strength (f_y) of the steel tube were used to calculate the axial load capacity (N_u) of circular CFSTs infilled with mentioned UHPFRCs via design equations given by Eurocode 4 (EC4), American Concrete Institute (ACI), American Institute of Steel Construction (AISC), Architectural Institute of Japan (AIJ), and Chinese (DL/T) codes. The results of code comparison revealed that AIJ and DL/T were so near to EC4 followed by AISC then ACI.

Keywords: Axial capacity; Concrete filled steel tube column; Fracture properties; Mechanical properties; Physical properties; Ultra high performance fiber reinforced concrete.

ÖZET

FİBER TAKVİYELİ UYPB VE MEVCUT TASARIM KODLARINA GÖRE BUNLARIN KOMPOSİT TÜP ELEMANLARIN YÜK TAŞIMA KAPASİTESİNE ETKİSİ

MUHYADDIN, Guler Fakhraddin
Doktora Tezi, İnşaat Mühendisliği Bölümü
Tez Yöneticisi: Doç. Dr. Esra METE GÜNEYİSİ
Temmuz 2017
207 Sayfa

Beton dolgulu çelik tüp (BDÇT) yapısal sistemlerde farklı tip ve hacimlerde fiber takviyeli ultra yüksek performanslı beton (UYPB) kullanmanın asıl amacı, yapısal çelik tüpün boyutunu en aza indirgemek ve beton çekirdeğin mekanik, kırılma ve büzülme özelliklerini iyileştirmektir. Bu durum kompozit elemanlar için yüksek dayanım ve performans sağlamaktadır. Bu tez iki kısımdan oluşmaktadır. İlk kısım çeşitli fiber türleri ve konsantrasyonları ile takviye edilmiş UYPB'un deneysel davranışını içermektedir. İkinci kısımda, ultra yüksek performanslı fiber takviyeli beton (UYPFTB) ile doldurulmuş eksenel yüklü çelik tüp kolonların yapısal davranışının araştırma sonuçlarını içermektedir. Bu amaçla, 2% hacim fraksiyonlarına kadar mikro-çelik, çengelli çelik ve mikro cam elyaf içeren 19 UYPB karışımı incelendi. Tasarlanan tüm karışımlar mekanik, kırılma ve fiziksel performans açısından test edildi. Öte yandan, çelik tüpün akma dayanımın (f_y) 300, 450 ve 600 MPa olduğu ve çap-et kalınlık oranın 30, 60 ve 90 olduğu durumlar için, BDÇT' lerin kapasitesi hesaplandı. Bunun için Avrupa (Eurocode 4, EC4), Amerika (ACI, AISC), Japonya (AIJ) ve Çin (DL/T) tasarım kollarında verilen denklemler kullanıldı. Kod karşılaştırması sonuçları, AIJ ve DL/T'nin EC4'e yakın olduğunu, bunu AISC ve ardından ACI izlediğini ortaya koymuştur.

Anahtar Kelimeler: Eksenel yük kapasitesi; Beton dolgulu çelik tüp kolon; Kırılma özellikleri; Mekanik özellikler; Fiziksel özellikleri; Ultra yüksek performanslı fiber takviyeli beton.

To all members of my sweet family

ACKNOWLEDGEMENTS

First, I would like to thank ALL MIGHT GOD for giving me the will to be powerful and efficient in achieving my thesis. I would like to express my genuine thanks to my supervisor Assoc. Prof. Dr. Esra METE GÜNEYİSİ for her encouragement, professional support, and guidance.

My deepest appreciation and immense pleasure to Assoc. Prof. Dr. Mehmet GESOĞLU who has the attitude and a substance of genius. I am more than thankful to him for encouraging and trusting me. I am also very grateful to him for his persistent support, valuable advice, and productive reviews of my study through the period of this project.

I am very greatly obligated to show gratitude to Dr. Diler ASAAD; he is my nearest, dearest friend and my husband for his support and guidance. I feel fortunate to have such friend and husband. He always said funny words to me which is very valuable for me to release stress after the hard and intensive working days, especially for my final Ph.D. studying phase.

I express my deepest gratitude to my family for all their love, support, and encouragement throughout my life to this point. Without their encouragement, this work would not have been possible. I especially want to thank my parents Fakhreddin MUHYADDIN and Wedad FATTAH. I will always be grateful for everything they have done and owe them a debt that never can be repaid. Thank you for everything.

Finally, and the most thoughtfully difficult, but the most emotionally vital, I say. I have to pronounce the last but the greatest thanks. This is turned to my siblings for their sacrifices and for the love and encouragements proved to me during my studies.

TABLE OF CONTENTS

Page

LIST OF TABLES

LIST OF FIGURES

LIST OF SYMBOLS/ ABREVIATIONS

ACI	American Concrete Institute
AISC	American Institute of Steel Construction
AS	Australian Standards
ASTM	American Society for Testing and Materials
b/t	Width/Thickness Ratio
CCR	Concrete Contribution Ratio
CFST	Circular Concrete Filled Steel Tubular
CPWD	Central Public Works Department
CRC	Compact Reinforced Composites
D/t	Diameter-to-Thickness
DSP	Ultra-Fine Particles
E	Modulus of Elasticity
EC4	Eurocode 4
FBG	Fiber Bragg Gratings
FRC	Fiber Reinforced Concrete
f_{st}	Splitting Tensile Strength
GEP	Gene Expression Programming
G_F	Fracture energy
GFRC	Glass Fiber Reinforced Concrete
GFUHPRC	Ultra-High Perf. Reinforced Concrete Containing Glass fibers
HFRCC	Hybrid Fiber Reinforced Cement-Based Composites
HPC	High Performance Concrete
HPFRC	High-Performance Fiber Reinforced Composites

HRWR	High-Range Water-Reducing Admixture
HSC	High-Strength Concrete
ITZ	Interfacial Transition Zone
l_{ch}	Characteristic Length
LVDT	Linear Variable Displacement Transducer
MDF	Macro-Defect Free
MIT	Massachusetts Institute of Technology
MSCC	Multi-Scale Cement Composite
NSC	Normal Strength Concrete
N_u	Ultimate Strength
PNF	Processed Natural Fibers
PNFRC	Processed Natural Fiber Reinforced Concretes
PP	Polypropylene
RPC	Reactive Powder Concretes
SCC	Self-Compaction Concrete
SF	Silica Fume
SP	Superplasticizer
SRA	Shrinkage Reducing Admixture
TS	Turkish Standard
UHPC	Ultra High Performance Concrete
UHPCFT	Circular Ultra-High-Performance Concrete-filled Steel Tube
UHPFRC	Ultra-High Performance Fiber-Reinforced Concretes
UHP-HFRC	Ultra-High Performance Hybrid Fiber Reinforced Concrete
UHS	Ultra High Strength
UNF	Unprocessed Natural Fibers
UPV	Ultrasonic Pulse Velocity
w/b	Water to Binder Ratio

CHAPTER 1

INTRODUCTION

1.1 Ultra High Perforormance Fiber Reinforced Concrete (UHPFRC)

Many huge strategic projects such as coupling beams in high-rise buildings, precast members, infrastructure rehabilitations, blast resistant structures, and special facilities like nuclear waste storage containers require ultra high performance concrete (UHPC) [1]. Investigations over the past years have yielded an innovative classification of highly resilient concrete called reactive powder concretes (RPC), nowadays it is labeled and classified as ultra-high performance cementitious composites or concrete. UHPC is one of the newest developments in concrete technology, and remedies the lack of many concretes [2]. Producing UHPC necessitates a large cement content of 900e1200 kg/m3, silica fume (SF) of 10-30% by weight of the cement, very fine quartz sand (0.15- 0.40 mm) instead of using coarse aggregates, a water-binder (w/b) ratio less than 0.2, and an effective superplasticizer (SP) for the workability [3-7]. The mechanical properties that can be achieved include the compressive strength of greater than 150 MPa, flexural strength of 30-60 MPa, splitting tensile strength higher than 7 MPa as well as Young's modulus up to 60 GPa [8-11].

For the practical structural applications, nonetheless, the brittle behavior of plain UHPC has been one of a major problem for its practical applications resulting in the main obstacles [12]. Thus, promoting UHPCs via different types and shapes of fibers significantly improve ductility, strain hardening behavior, fracture toughness, impact resistance and energy absorption capacity, in addition, to prevent or control initiation, propagation, or coalescence of cracks [13-16]. Mechanically, UHPC reinforced by fibers is named as an ultra high performance fiber reinforced concrete (UHPFRC) that can resist the tensile stress through composite action between the cementitious matrix and embedded fibers. When a crack occurs, micro fibers can bridge the potential cracks that triggered to provide resistance to crack propagation, whereas relatively longer fibers provide resistance to crack opening, thus enhancing the structural behavior and durability [17]. In addition, it is well known of fibers afford some of the stress that takes place in the matrix themselves and transmits the other portion of stress to the stable cement matrix due to stress transfer ability of randomly distributed fibers [18-20]. Moreover, the ideal displacement feature of concrete that reinforced by fibers is recognized to elongate the required strain hardening and strain softening properties when subjected to loading. [21, 22]. Overall, the fiber characteristics such as strength, stiffness, shape, aspect ratio, Poisson’s ratio as well as orientation and distribution of the fibers effect on the performance of UHPFRC such as stiffness, ductility, shrinkage, the physio-chemical and frictional bond properties at the interface between matrix and fiber [23-28].

There are many attempts to increase the performance of UHPCs using fibers of different features. For instance, Kim et al. [29] studied flexural behaviors of UHPC after adding different types of macro steel fibers. They observed that twisted steel and hooked steel fibers delivered superior flexural strength, deflection, and energy absorption capacity than that of steel straight fibers. Yoo et al. [30] concluded that the fracture parameters and all mechanical properties of UHPFRC were linearly improved with increasing steel fiber content in spite of the fact of modest change in the first cracking was detected. Lee and Chisholm [31] studied the effect of straight steel fibers with the aspect ratio of 65 on the mechanical properties of RPC. The addition of 2% steel fibers led to primarily improved the tensile strength of the composite apart from a marked increase in the compressive strength. Wille et al. [27] carried out an experimental study on the tensile behavior of different UHPFRC mixes using four types of high strength steel fibers. It was observed that both the tensile strength and the maximum post-cracking strains were significantly improved by using deformed steel fiber instead of smooth one. Additionally, Hoagn et al. [32] studied the effects of short and long steel fibers (the aspect ratios of 85 and 70, respectively) on the properties of UHPCs. Test results indicated that a reasonable combination of two steel fibers guaranteed the high flowability as well as the flexural strength of 20 MPa, and the compressive strength exceeding 150 MPa. In spite of many investigating the use of steel fibers in UHPCs, there are few studies on the UHPCs reinforced with micro glass fibers and/or with hooked steel fibers. Ghorpade [33] utilized to reinforce the UHPC by incorporating 12 mm long glass fibers at of 0.5, 1.0, and 1.5% volume concentrations. The maximum compressive, splitting tensile, and flexural strengths were achieved at 1% fiber content. Moreover, Yoo and Yoon [34] studied the structural UHPC beams reinforced with different steel bars. They concluded an enhancement of ductility and post-peak response with the usage of twisted steel fibers and increased length of smooth steel fibers. Furthermore, Aydın and Baradan [35] and Yoo et al. [36] executed flexural behaviors of UHPC beams incorporated with different fiber lengths. The results showed that the long steel fibers are more efficient than short steel fibers in improving fracture energy and flexural results due to increase in bonding area between the long fibers and matrix.

1.2 Concrete Filled Steel Tubular Structural Members

Through the last few years, with the increasing usage of composite construction worldwide, there is a growing interest in exploiting concrete filled steel tubes (CFSTs) as the main column member. Whereas these sorts of composite members are utilized as structural columns, specifically in high-rise buildings, they may be exposed to a high shearing force in addition to moments caused by the wind or seismic actions. Thus, it is very important to examine the behaviour of CFST columns in axial compression [37, 38]. Owing to their effective usage of construction material these members are perfectly suitable for all applications. CFST structure is a type of the composite steel-concrete structures used presently in civil engineering field [38]. CFST are composite structures of steel tube and in-filled concrete; they are exploiting the advantages of both steel and concrete. They consist of a hollow steel section of circular or rectangular shape filled with plain or reinforced concrete. They are more usually used in the construction of high-rise buildings, bridges, subway platforms, barriers, multistory buildings as columns and beam-columns, and as beams in low-rise industrial buildings wherever a robust and efficient structural system is required [39, 40]. Their usage delivers outstanding static and earthquake-resistant properties, for instance, high strength, high ductility, high stiffness, excellent structural dimensional stability and high load carrying capacity. In circular sections by reason of the confinement of the concrete is much more since the steel may develop an effective hoop tension. Conversely the flat sides of a rectangular tube are not effective in resisting perpendicular pressure [41].

1.3 Application and Benefit of CFST Columns

- Higher confinement in the concrete due to the cover of structural steel tube

In the CFST the steel tube surrounding a concrete column not only assists in carrying the axial load but also confines the concrete, it acts as a longitudinal and transverse reinforcement which puts the concrete under a triaxial state of stress, therefore improves both axial load resistance, strength and ductility of CFST members. CFST with circular cross-sections had a higher confinement than CFST with rectangular cross sections, attributable to the shape of circular section provides the higher hoop stresses. This confinement is similarly influenced by the diameter-to-thickness ratio (*D/t*) of the tubes. In Figure 1a, it obviously demonstrates that the ultimate strength for a CFST is even larger than the summation of the strength of the steel tube and the RC column, which is described as "1(steel tube) + 1(concrete core) greater than 2 (simple summation of the two materials)" [42]. While the Figure 1b displays a schematic view of the load versus deformation relationship of the hollow steel tube, the concrete stub column by itself and the CFST. It can be realized that the ductility of the CFST is considerably enhanced when matched to those of the steel tube and the concrete alone.

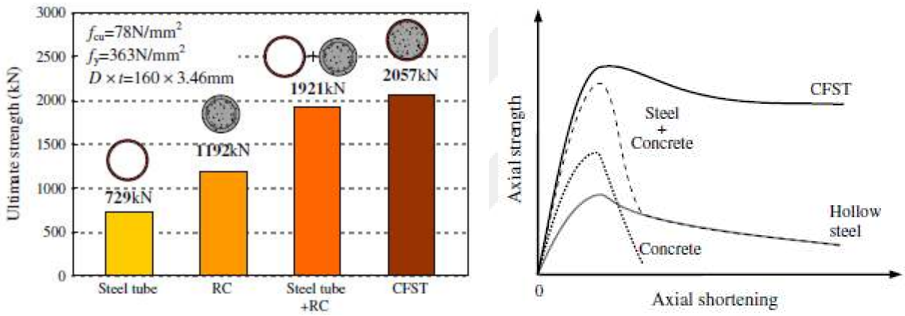

(a) (b)

Figure 1.1. Axial compressive behavior of CFST stub column [42]

- Delay of the local steel buckling

Attributable to the existence of the concrete core, the inherent buckling problem related to thin-walled steel tubes is as well delayed or prevented. In CFST even if the concrete cracks, the delay of local buckling will still happen as the concrete expands and endures against the steel tube, maintaining the concrete-steel contact. Because of the concrete core forces all local buckling modes outward, thinner steel sections may be used that still certify the yield strength will be reached in the tube before buckling occurs. The rectangular and square cross sections had greater local buckling than circular cross sections [42].

- Higher compressive strength and flexural strength

The concrete filling gives a higher load compressive capacity without increasing the outer dimensions so that the strength, stiffness, and ductility of the structures constructed from CFSTs can be enhanced simultaneously. Since the function of longitudinal reinforcement and transverse confinement can be picked up due to the presence of the steel tubes, the traditional longitudinal and transverse reinforcement may be eliminated. This type of column also maintains higher ductility, compressive strength, and flexural strength when high strength concrete is used [42].

- Earthquake and fire resistance

In seismic design, there are important structural aspects to be considered which are the strength, ductility, and the hysteretic behavior. CFST columns demonstrated a favorable energy dissipation capacity. Therefore, the ideal system for many seismic-resistant structures is the CFST columns. With the increase of the axial load level, the ductility and the energy dissipation ability of the concrete-encased CFST columns decreased [42].

Whenever the concrete-encased CFST exposed to severe earthquakes, concrete encasement cracks are resulting in a reduction of stiffness, nevertheless the steel core offers shear capacity and ductile resistance to subsequent cycles of overload [43]. For seismic design, the steel tube similarly prevents spalling of the concrete and minimizes congestion of reinforcement in the connection region principally Compared to reinforced concrete columns with transverse reinforcement.

For CFST, the concrete filling can considerably increase the fire resistance. As the heat is absorbed by the concrete core, the temperature in the steel tube increases much slower than that of the plain hollow steel tubes. Besides, the outer tube provides a confinement to the concrete core when subjected to the fire, the spalling of the concrete core consequently can be prevented [42].

- Rapid construction

In CFST structures the steel tube acts as the framework, which decreases workload in contrast to the RC construction, there was the tedious process of framework preparation and steel fixing [44]. First, the hollow steel tubes were designed alone in such a way that they are capable of supporting the floor load up to three or four storey height. Next, the upper floors were accomplished, then the concrete was pumped into the tubes from the bottom. After the concrete has hardened and the composite action has been advanced, the system can attain its final strength and stiffness, to sustenance the designated gravity and lateral loads. In moderate- to high-rise construction, CFST column can arise more quickly than an equivalent reinforced concrete structure as the steelwork can precede the concrete by several stories [45].

Because of modern pumping facility and the presence of high performance concrete make pumping three or four storey readily feasible. In consequence of the simplicity of the construction system, the project can be accomplished in great speed [40]. the constructions costs may be condensed as a result of the fast erection and optimal design. Owing to its higher strength, a composite column is lighter than a typical RC column with a parallel strength, which decreases the loads on and cost of the foundation, the cost and amount of reinforcement bars. Because of the steel section can word as formwork and is stiffened by the concrete in CFST columns, is much lighter than a conventional steel column, consequently its more economical than reinforced columns [46].

1.4 Research Significance

This thesis studied the properties of UHPFRC and steel tublar columns filled with UHPFRC. To this aim, experimental and numerical analysis was performed. The experimental program was conducted to achieve UHPC having the best mechanical, flexural performance, early-age shrinkage properties according to different types of macro and micro fibers. Three groups of UHPCs were designed in which micro steel, hooked steel, and micro glass fibers were utilized equally by a volume up to 2% to produce UHPFRCs. In the numerical study, the structural behavior of UHPFRC filled steel tublar columns subjected to uniaxial compression loading conditions was examined. For this, various D/t ratio and yield strength of steel tube, as well as the compressive strength of concrete core, were used in the analysis. The axial column strength was evaluated and compared to formulations of the existing design codes, i.e. EC4, ACI, AISC, AIJ, and DL/T.

1.5 Outline of the Thesis

In the present Ph.D. thesis, the total work is demonstrated by five chapters;

Chapter 1 is a general introduction and the significance of the thesis

Chapter 2 is the literature reviews on the compounds as well as mechanical, flexural, physical properties, and structural applications of UHPFRCs. The properties of the composite members and the structural performance of the CFST columns are discussed in this chapter.

Chapter 3 this chapter covers highlights of the experimental test and numerical anlysis in this work. The properties of all materials used, mix design, mixing techniques, the preparation of test samples, and testing procedures are stated. The properties of CFST columns, analysis steps as well as the design code formulations are given in this chapter.

Chapter 4 contains the experimental and numerical results and discussion of the mechanical, fracture, load displacement behavior, physical properties, and findings, on the axial load capacity of circular CFST members with UHPC using the different volume of fibers.

Chapter 5 is a key to the main conclusions from the results of this study.

CHAPTER 2

LITERATURE REVIEW AND BACKGROUND

2.1 Fiber Reinforced Concrete (FRC)

From the point of view of structural engineering, to upgrade or increase the flexural resistance, crack resistance, durability and other performances, fibers can be applied to meet the requirement. For example, in the beam-column node, the of steel fiber reinforced concrete (FRC) improves the seismic intensity of the node. It was well known that concrete made from cement is relatively strong in compression but weak in tension and tends to be brittle [47]. Fibers have been used to reinforce brittle materials since ancient times. Straw was used to reinforcing sun-baked bricks, and horsehair was used to reinforce masonry mortar and plaster. A pueblo house built around 1540, believed to be the oldest house in the U.S., is constructed of sun-baked adobe reinforced with straw [48]. In more recent times the asbestos fiber was extensively used throughout the world today, especially in structural components like wall panels, roofs, and gates to name a view. However, primarily due to health hazards associated with asbestos fibers, alternative fibers were introduced as a replacement introduced throughout the 1960s and 1970s [49]. After asbestos fibers, steel fibers were one of the first possible alternatives to steel bar reinforcing, with the first patent being applied for in 1874. During the early 1960s in the United States, the first major investigation was made to evaluate the potential of steel fibers as a reinforcement for concrete [50]. It was however only in the early 1970’s that the use of these fibers on a large scale was noticed in the USA, Japan and in Europe. Examples of existing structures build from steel and other FRCs include ground supported slabs, suspended slabs, pile supported slabs, tunnel panel segments (The Channel Tunnel Rail Link project) and various in-situ concrete structures like a 210m long 6 m high wall that is 310 mm thick in Belgium to name a few [51]. Since then, a substantial amount of research, development, experimentation, and industrial application of steel FRC has occurred.

In the late 1950s in the USSR first attempted use, of glass fibers in concrete [52]. Ordinary glass fibers, such as borosilicate E-glass fibers recognized quickly that, they are attacked and eventually destroyed by the alkali in the cement paste. Alkali-resistant glass fibers containing zirconia form produced after Considerable development work [53]. This led to a considerable number of commercialized products. Glass FRC in the U.S. is currently applied for the production of exterior architectural cladding panels. Initial attempts at using synthetic fibers (nylon, polypropylene) were not as successful as those using glass or steel fibers [54, 55]. However, new approaches of fabrication and new categories of organic fibers have led investigators to conclude that both synthetic and natural fibers can successfully reinforce concrete [56, 57].

Throughout the world, considerable research, development, and applications of FRC are taking place. Industry interest and potential business opportunities are evidenced by continued new developments in fiber reinforced construction materials. The use of discontinuous steel reinforcing elements such as nails, wire segments, and metal chips involved in experimental trials and patents to improve the properties of concrete date from 1910 [58]. The toughness behavior of the fiber-matrix composite enhanced through the use of fibers after it has cracked [59]. Therefore, fibers incorporate a wide range of engineering materials, (including ceramics, plastics, cement, and gypsum products) in modern times to enhance composite properties. The enhanced properties include tensile strength, compressive strength, elastic modulus, crack resistance, crack control, durability, fatigue life, resistance to affect and abrasion, shrinkage, expansion, thermal characteristics, and fire resistance.

2.1.1 Fiber Types, Properties, and its Applications

The enhanced mechanical and shrinkage properties are the desired result of adding fibers to any concrete mix. The improvements gained by using fibers depend on the properties of the fiber that include the fiber material as well as fiber length and geometry to name a few. Fiber is a small discrete reinforcing material; various materials are used to produce fibers in different shapes and size [48]. Steel fibers, synthetic fibers, glass fibers and organic or natural fibers are the main distinctly fibers used currently. Table 2.1 shows some of the fibers from every category along with the basic material properties.

Table 2.1. Properties of various fiber types [60, 61]

Type	Specific Gravity	Tensile Strength (MPa)	Elastic Modulus (GPa)
Acrylic	1.16-1.18	296-1000	14-19
Aramid I	1.44	2930	62
Aramid II	1.44	2344	117
Carbon I	1.9	1724	380
Carbon II	1.9	2620	230
Nylon	1.14	965	5
Polyester	1.34-1.39	228-1103	17
Polyethlene	0.92-0.96	76-586	5-117
Polypropylene	0.9-0.91	138-690	3.0-5.0
Alkali-resistant	2.7-2.74	2448-2482	79-80
Non Alkali-resistant	2.46-2.54	3103-3447	655-72
Coconut	1.12-1.15	120-200	19-26
Sisal	-	276-568	13-26
Bagasse	1.2-1.3	184-290	15-19
Steel	7.8	1000-3000	200
Glass	2.6	2000-4000	80

All fibers are either characterized as macro or micro fibers. Macro fibers or structural fibers are having the lengths between 19-60 mm. These fibers are expected to bridge cracks and provide structural support for the hardened state of concrete. Nevertheless, micro fibers are included in a mix to help improve the fresh and early-age tensile- and flexural strength of concrete. These fibers provide the necessary resistance to tensile forces developed by drying shrinkage as well as plastic shrinkage. Micro fibers range between 2-10 mm in length and nominal diameters of 0.1-1 mm [51].

Fiber aspect ratio is a numerical parameter, which is defined as the fiber length, divided by an equivalent fiber diameter [l/d]. Typical aspect ratio ranges from 30 to 150 for length dimensions of 0.1 to 7.62 cm typical fiber diameters are 0.25 to 0.76 mm for steel and 0.02 to 0.5 mm for plastic. When the deflection corresponding to the ultimate flexural strength is exceeded, the plain concrete fails suddenly, whereas FRC continues to sustain considerable loads even at deflections considerably in excess of the fracture deflection of the plain concrete [62].

Steel FRC is a composite material which is made up from hydraulic cement containing coarse or fine aggregate and steel fibers as reinforcing. Different geometrical forms, size, shape and surface structure of fibers produced, due to different manufacturing processes and different materials to improve the bond characteristics between fiber and the concrete matrix, however, trying to prevent fiber bundling from occurring during the mixing process. Figure 2.1 shows some of the most used fiber geometries for steel fibers [51].

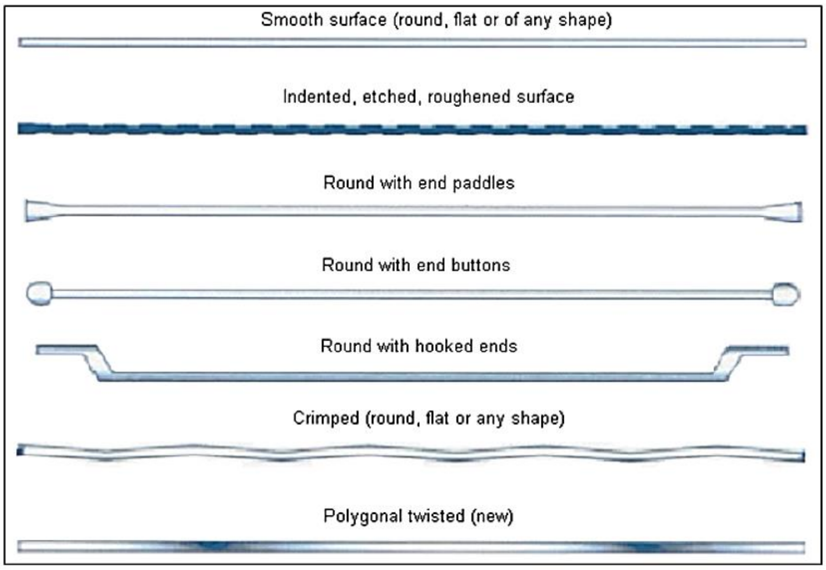

Figure 2.1. Steel fiber geometries [51]

The types of steel fibers are defined by [63] as Type I: cold-drawn wire, Type II: cut sheet, Type III: melt-extracted, Type IV: mill cut, and Type V: modified cold-drawn wire. Most of the fibers are supplied as single fibers. However, some are magnetically aligned and some glued together in bundles in order to ensure a better distribution after casting. Consequently, the effect of the fibers on the behavior of concrete under load is fairly different. In the case of fibers that are pulled out after the creation of macroscopic matrix cracks it ranges from crack control to an increase of the post peak load in case of fibers with an anchorage working up to steel tensile rupture [64].

Steel fiber reinforcement makes the concrete tougher and more ductile by offering a solution to the problem of cracking. Over the past three decades' extensive research and field trials carried out it has also been proved, that addition of steel fibers to conventional plain or reinforced and prestressed concrete members at the time of mixing/production imparts improvements to several properties of concrete, mainly those related to strength, performance, and durability. Concretes when reinforced with steel fibers behave as a composite material with properties significantly different from conventional concrete because of the weak matrix in FRC, fibers uniformly distributed across its entire mass, get strengthened enormously. The propagation of micro-cracks presents in the matrix assist by the randomly-oriented steel fibers, once the load applied to the member first the fiber improved the overall cracking resistance of the matrix itself, and later by bridging across even smaller cracks formed after the, so preventing them widening into major cracks [65] (Figure 2.2).

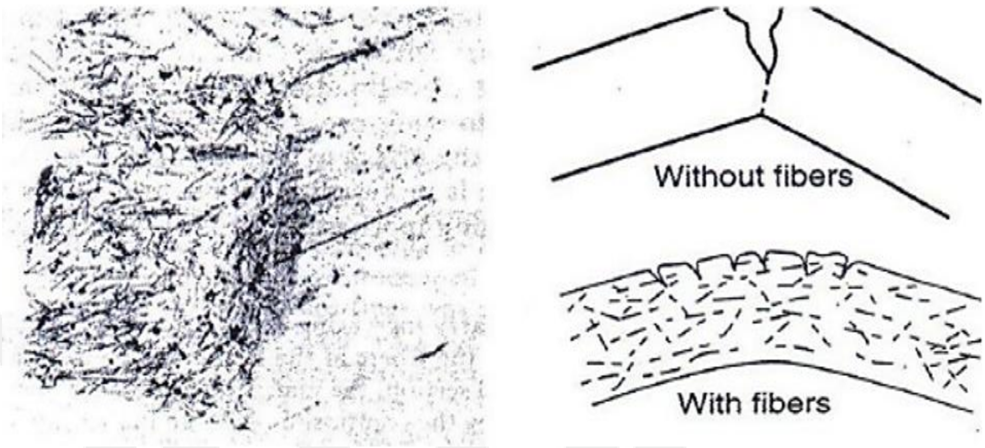

Figure 2.2. Effect of fibers and the failure mechanism [65]

Generally, Steel FRC is very ductile and particularly well suited for structures which are required to exhibit: resistance to splitting/spalling, erosion and abrasion, high thermal/ temperature resistance, resistance to seismic hazards (Earthquake resistance), high fatigue strength resistance to impact, blast and shock loads, shrinkage control of concrete, and tensile strength, very high flexural, shear. Moreover, the following factors controlling Steel FRC are as; Aspect ratio, volume fraction, fiber reinforcing index, critical length, balling of fibers, and good mix design. Glass FRC includes essentially of a cementitious matrix composed of cement, sand, water, and admixtures, in which short length glass fibers are dispersed. The fibers in this composite lead to an increase in the tension and impact strength of the material [66]. In the early l960s, much of the original research implemented on glass fiber reinforced cement paste. This work used conventional borosilicate glass fibers (E-glass) and soda-lime-silica glass fibers (A-glass) [48]. Figure 2.3 shows the glass fiber shape.

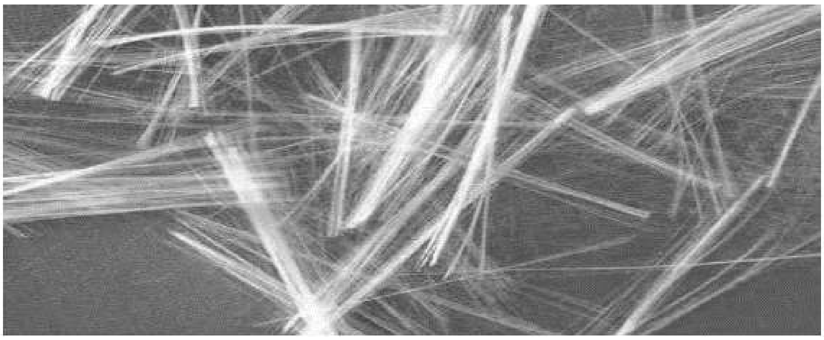

Figure 2.3. Glass fibers [62]

At the beginning of the glass fiber development, one of the most concerning problems were found that glass fiber loses its strength rather quickly (which became fragile with time), due to the high alkalinity of the cement mortar (pH$\geq$ 12.5). Consequently, significant progress has been made, new types of alkali-resistant glass fibers and with mortar additives that prevent the processes that lead to the embrittlement of glass FRC, by this way, the problem is practically solved [66-69].

Reinforced concrete normally occupy civil structures suffer from corrosion of the steel by the salt, which consequences in the failure of those structures. To enhance the life cycle of those civil structures constant maintenance and repair is needed. To diminish the failure of the structures made of reinforcing concrete. There are many ways; the custom method is to adhesively bond polymer fiber composites onto the structure. Therefore, resultant composite toughness and tensile strength increased and the cracking and deformation characteristics improved [70]. Nevertheless, this method adds another layer, which is prone to degradation. Degradation takes place when these fiber polymer composites exposed to marine environment due to surface blistering. Thus, the adhesive bond strength is reduced, which results in the de-lamination of the composite [62].

Numerous natural reinforcing materials can be found at low levels of cost and energy by locally available manpower and technical know-how. Such fibers are used in the manufacture of low fiber content FRC and rarely have been used in the manufacture of thin sheet high fiber content FRC. These fibers are usually referred to as unprocessed natural fibers. Nevertheless; other natural fibers are obtainable that have been processed to enhance their properties. These fibers are typically referred to as processed natural fibers and concrete made from them as processed natural FRC. Many fibers have been used to reinforce several building materials until a recently little scientific effort has been devoted to the use of natural fibers for reinforcement

[48]. The use of some of the best known natural fibers such as wood, sisal jute, bamboo, coconut asbestos, rockwool, sugarcane bagasse, plantain (banana), palm, etc. [62].

Research and development in the petrochemical and textile industries result in man-made synthetic fibers. Acrylic, aramid, carbon, nylon, polyester, polyethylene and polypropylene are fiber types that have been tried in the use of structural concrete. Structural reinforcement doesn't provide its benefits until concrete hardens. They correspondingly enhance some of the properties of hardened concrete [70]. Synthetic FRC presently exists worldwide, primarily in applications of cast-in-place concrete (such as slabs-on-grade, pavements, and tunnel linings) and factory manufactured products (such as cladding panels, siding, shingles, and vaults) [71].

Synthetic fiber volume contents used in applications today are 0.1-0.3%, which is referred to as low volume percentage, and 0.4-0.8 %, which is referred to as a high-volume percentage. To control plastic shrinkage cracking, most synthetic fiber applications are at the 0.1% by volume level. Uses include precast products, shotcrete, and cast-in-place elements. Usually, the fiber length is 19 to 64 mm with the predominance of demand for 19 or 38 mm long fibers [48].

2.2 Ultra High Performance Concrete (UHPC)

2.2.1 Advances in Structural Concrete Strength

Concrete strength is usually used in structural applications has often lagged behind the threshold strengths achieved through material development during the advances in the 150-year history of concrete [72]. This tendency is doubted to be because of an increase in material cost accompanying increases in strength and to a general reluctance to use new materials in practical applications. The concrete compressive strength development over 100 years is presented in Figure 2.4. Furthermore, the significant achievements of concrete technology in the last 40 years can be seen in Figure 2.5 [73, 74].

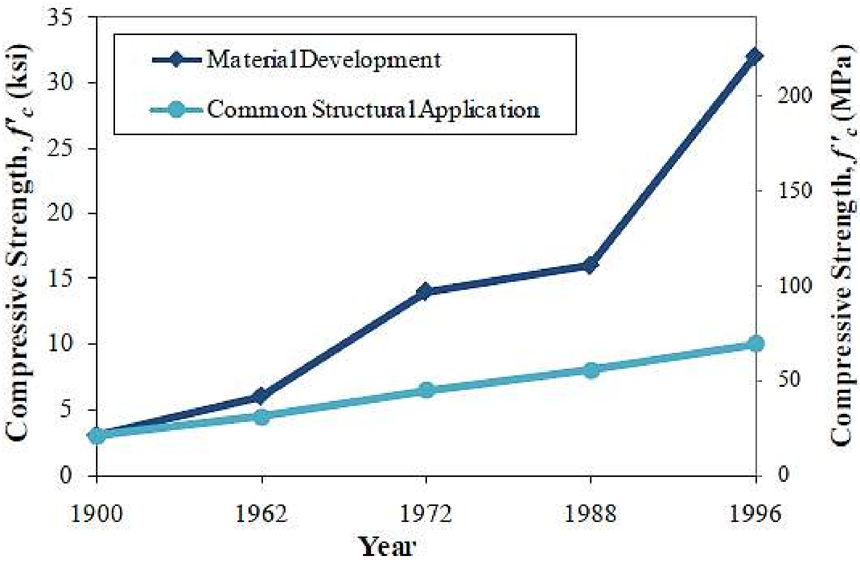

Figure 2.4. Development of concrete strength over 100 years [73]

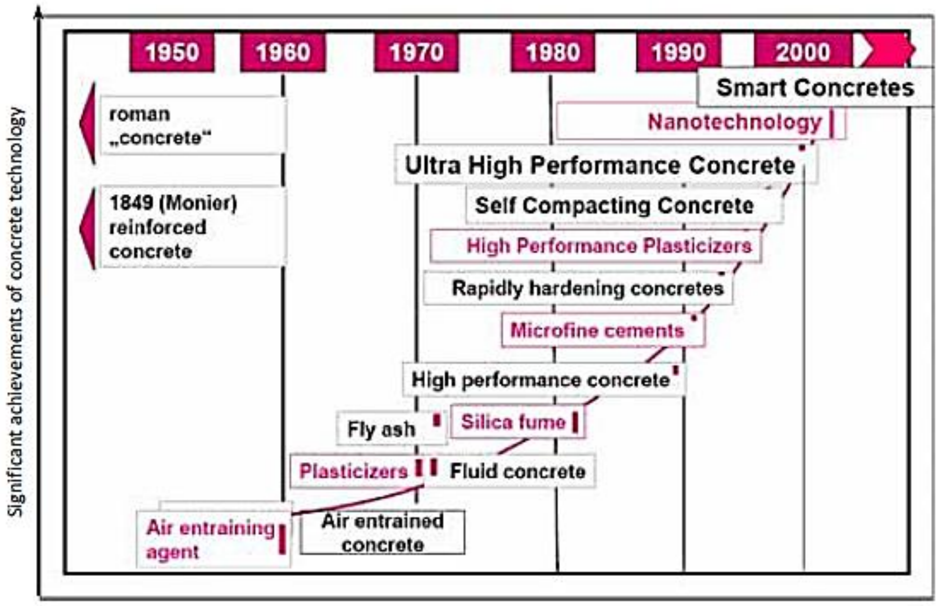

Figure 2.5. Developments in concrete technology in the last 40 years [74]

It can be realized that the concrete technology development advanced slowly during the 1960s with the maximum compressive strength of 15-20 MPa**.** Over a period of about 10 years, it was multiplied by three to 45-60 MPa with an important advance by using water reducers. By the early 1970s, compressive strengths stopped increasing at about 60 MPa, when a technological barrier was reached that could not be surmounted with the raw materials then available**.** Moreover, the w/b ratio not reduced any further by the water reducers that were normally available at that time [75]. During the 1980s, it began to be comprehended that the high-range water reducers, named superplasticizers, were more powerful than lignosulfonates and could be used to reduce w/b ratios down to 0.30 increasingly**.** Decreasing the w/b ratio beneath this was taboo till Bache (1981) stated that by lowering the w/b ratio of a particular concrete down to 0.16, using a very high dosage of superplasticizer and a new ultrafine cement substitute (silica fume), he had been able to reach a compressive strength of 280 MPa within the compacted granular materials by optimizing the grain size distribution of the granular skeleton [75].

Over the past 30 years, the results of careful thinking how to exploit these technological breakthroughs and/or some fundamental knowledge about low-porosity materials has run to the progress of a number of cement-based materials that existent notable mechanical properties. The introduction of ultra-high strength and ultra-high performance concrete (UHPC) is a comparatively recent expansion in concrete technology [3] developed reactive powdered concrete (RPC), which is the latest ultra-high-strength cement-based material that has been developed recently. The ultimate strength that is not likely to be achieved is up to 800 MPa**.** The w/b ratio of these materials is much lower than that of high-performance concrete it lies in the 0.10 to 0.20 range in order to attain the densest packing possible in the hardened product.

A very beneficial brief look at how UHPC is capable of attaining such high strength [76]: 'We know how to make 150 MPa concrete on an industrial basis. Because at such a level of strength it is the coarse aggregate which becomes the weakest link in concrete, it is only necessary to take out coarse aggregate, to be able to increase the concrete compressive strength and make RPC having a compressive strength of 200 MPa; it is only necessary to confine this RPC in thin walled stainless steel tubes to see the compressive strength increased to 375 MPa; and when the sand is replaced by a metallic powder, the compressive strength of concrete increases to 800 MPa. Optimization is required to realize UHPC achieve more common use in structural applications, and optimization can only be accomplished by exhaustively understanding the material behavior and its engineering properties and by adapting to newer, more well-organized cross-sectional shapes [77].

2.2.2 Development of UHPC

One of the significant departure from the design premise of high performance concrete (HPC) mixes is the UHPC. The "minimum defect" concept– producing a material with a minimum amount of defects, such as micro-cracks and interconnected pore spaces that more closely method the potential ultimate strength of the components and enhance durability resulted in UHPC [77]. There is approaches in developing minimum defect materials, macro-defect free (MDF) and densified small particle or densified system with ultra-fine particles (DSP) concretes [78]. Polymers used to fill in pores in the concrete matrix in the MDF method. Very demanding manufacturing conditions required in this process, involving laminating the material by passing it through rollers. The properties of MDF concrete, which can have tensile strengths up to 150 MPa, require pressing, are vulnerable to water, have a large number of creeps, and are very brittle. While the DSP concretes, comprise high amounts of superplasticizer and silica fume. DSP concretes also use extremely hard coarse aggregates or eliminate them entirely to avoid the aggregates from being the weakest component of the mix. Extreme manufacturing conditions not required in DSP concretes that MDF concretes do. However DSP concretes have a much lower tensile strength and, like MDF concretes, are very fragile. The ductility was considered to improve each concrete type by the addition of steel fibers, nonetheless by the addition of fibers MDF concretes become too viscous and unworkable. Consequently, DSP concrete was enhanced with fibers, subsequent in UHPC.

In different countries and by different manufacturers several forms of UHPC have been developed. The main difference between the brands of UHPC is the type and amount of fibers used. Up to the present time, there are four main categories of UHPC including ceracem/BSI, compact, reinforced composites (CRC), multi-scale cement composite (MSCC), and reactive powder concrete (RPC) [77]. Ceracem/BSI comprises coarse aggregates, which are eliminated in the other three sorts of UHPC [79]. While in CRC and MSCC both use high amounts of fiber and use different fiber sizes than those used in RPC [78]. Additionally, two percent of steel fibers occupy of the concrete mixture by volume in RPC. RPC has become one of the principal types of UHPC, and one such product is marketed under the name Ductal by the French companies Lafarge, Bouygues, and Rhodia.

In UHPC, the mismatch in elastic moduli is eliminated by selecting constituent materials with similar elastic moduli [80]. In normal concrete and HPC, a weak transition zone also exists in the interface between the aggregate and paste [81]. A representation of the force transfers through normal concrete compared to UHPC presented in Figure 2.6. The aggregates become inclusions that form a rigid skeleton in normal concrete. Shear and tensile stresses grow at the interfaces between the aggregates, forming small cracks approximately proportional in size to the maximum aggregate diameter when a compressive force is applied. Conversely, in UHPC, the aggregates are a set of inclusions in a continuous matrix, and the aggregate diameters are much smaller. So the compressive force can be conveyed by the matrix instead of by a rigid skeleton of aggregates, which diminishes the stresses that develop at the paste-aggregate interface. In UHPC a much more uniform stress distribution done through the transmittal of stresses by both the aggregates and the surrounding matrix, which can reduce the potential for shear and tensile cracking at the interface [10].

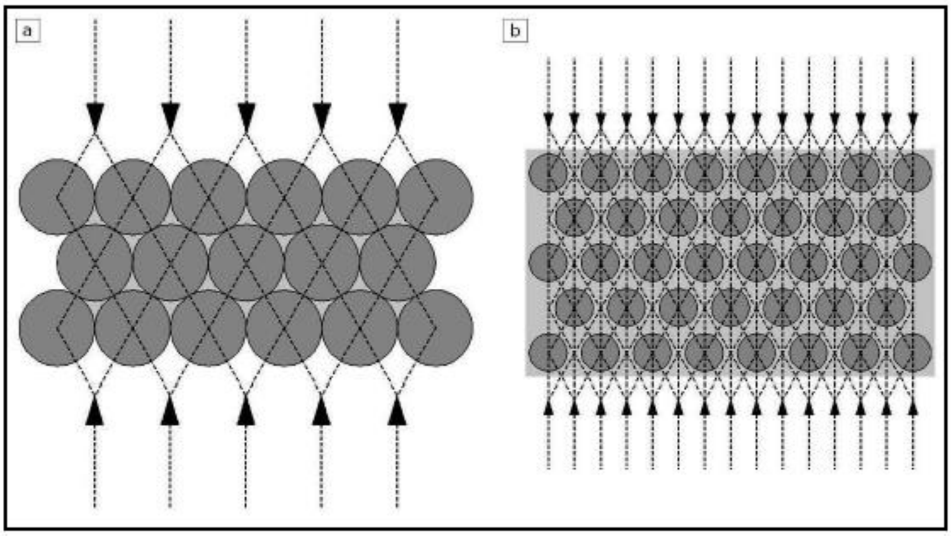

Figure 2.6. Force transfer mechanisms in a) normal concrete and b) UHPC [82]

Several authors identified the basic principles used in UHPC [10, 83-85], which can be précised as follows: i) enhancement of homogeneity by elimination of coarse aggregate; resulting in a decrease in the mechanical effects of heterogeneity, ii) enhancement of the packing density by optimization of the granular mixture through a wide distribution of powder size classes, iii) improvement of the properties of the matrix by the addition of a pozzolanic admixture, such as silica fume, iv) improvement of the matrix properties by reducing w/binder ratio, v) enhancement of the microstructure by post-set heat-treatment; and vi) enhancement of ductility by including small steel fibers. Concrete with very high compressive strength is produced through the application of the first five principles. The accumulation of the steel fibers aids to improve both the tensile strength and the ductility [10].

2.2.3 Design of UHPC

A challenge has been made in the development of ultra-high performance fiber reinforced concrete (UHPFRC) mixtures without heat or pressure treatment due to its large array of influencing parameter [86]. These comprise properties and particle size of the material component, mixture proportions, the mixing procedure and test method. The correlation between flow ability and packing density of the paste appraised by various researches. The notion is to optimize the mixtures developed to decrease the effort needed to attain high compressive strength (exceeding 150 MPa) devoid of the need for special heat or pressure treatment [86, 87]. Wille et al. [86] achieved compressive strength exceeding 200 MPa at 28 days on 50 mm cubes with no heat or pressure curing by optimizing the cementitious matrix, packing density, and flowability; using very high strength, fine-diameter steel fibers; and tailoring the mechanical bond between the steel fiber and cement matrix. In addition, a tensile strength of 34.6 MPa at a strain of 0.46 percent was accomplished. Total properties of material are a function of both macro-level properties and micro-level properties according to Polystructural theory [88]. Consequently, it is convenient to look at the different components of a typical UHPC mix, besides the microstructural properties of the mix. Reliance on the application and supplier different mixtures of UHPFRC materials may be used. Table 2.2 shows samples of composition and properties of NSC, HSC, and UHPC.

UHPC is well-known as a fine-grained concrete with a very high binder content and a very low w/c ratio. Using the packing density optimization principle, the choice of the components of UHPC. The mix is as well-proportioned in such a way that the fine aggregates will be a set of movable inclusions in the matrix, instead of a rigid skeleton. Packing optimization is done through using smaller particles to fill the voids between sand particles. Nonetheless a rigid skeleton of sand particles would still stay [89].

The wide distribution of granular class's advantages to not merely maximize density and make a more uniform stress distribution when the matrix is loaded nevertheless similarly contributes to the flowability of the mixture. The smaller grains assist as a lubricant, permitting sand particles of the same size to move past each other with minimal interference. Typically, UHPC mixes can be made to be self-compacting, no vibration to place needful [82]. The workability considerably decreased in normal FRC, when the coarse aggregate sizes are about the same as the fiber lengths through creating interferences between the fibers and aggregates. Though in UHPC, no such interference occurs because even the largest sand particles are over 20 times smaller than the fiber length.

The density of UHPC is higher than HPC or normal concrete, Since UHPC has a very compact microstructure, and the weight per cubic foot is also slightly increased. Table 2.3 displays a comparison between the typical densities of UHPC, HPC, and normal concrete mixes. The density of UHPC is higher than that of normal concrete or HPC, on the other hand, the slight increase in weight is easily offset by the much higher strength of UHPC. (2510 kg/m^3) was approximately the average reported value for the density of UHPC mixes from 17 published mix descriptions.

UHPCs are categorized by extremely high packing densities [10, 83-85]. These densities can be attained by optimizing the proportioning of constituents. Within the aggregate skeleton, the particles should be selected to fill up the voids between large particles with smaller particles and so on, foremost to a smaller volume of gaps. The ratio of the volume of solids to a given volume, i.e., the idea of packing density is introduced to appraise the arrangement of the granular mixture. The idea of packing density how can be applied to three granular systems, i.e. single-, binary-, and ternary-systems [90].

Table 2.2. Typical properties of NSC, HSC and UHPC [77, 85]

Material characteristics	**NSC**	**HSC**	**UHPC**
Component (kg/m^3)			
Portland cement	< 400	400	600-1000
Coarse aggregate	≈ 1000	900	-
Sand	≈ 700	600	1000-2000
Silica fume	-	40	50-300
Reinforcement/Fibers	designed	designed	40-250
Superplasticizer	-	5	10-70
Water	> 200	100-150	110-260
Maximum aggregate size (mm)	19.0-25.5	9.5-12.5	0.15-0.6
w/c ratio (by weight)	0.4-0.7	0.24-0.38	0.14-0.27
w/b ratio (by weight)	-	< 0.38	< 0.27
Properties (at 28 days)			
Density (kg/m^3)	2000-2800	2000-2800	2320-2760
Porosity (%)	20-25	10-15	2-6
Compression strength (MPa)	< 60	60-100	> 150
Tensile strength(MPa)	< 3	< 5	> 8
Initial modulus of elasticity (GPa)	≈ 30	< 45	50-70
Fracture energy (J/m^2)	30-200	< 150	< 90 without fibers > 10000 with fibers

Table 2.3. Comparison of density of NSC, HPC, and UHPC [91-93]

Concrete Type	Typical Density Range
NSC	2290-2400 kg/m^3
HPC	2430-2480 kg/m^3
UHPC	2320-2760 kg/m^3

2.2.4 Advantages of UHPC in Structural Engineering

The below are the summarized common advantages of UHPC [77, 94-96]:

1. The better alternative to HPC is UHPC besides it has the potential to compete structurally with steel.

2. In order to reduce the dead-load and less limited shapes of its structural members used UHPC with its superior strength combined with higher shear capacity is the best way. Compared to normal or high-strength concrete UHPC can lead to longer span structures with reduced member sizes, and to a sharp decrease in the volume and the self-weight with UHPC members. For instance, Figure 2.7 displays beam made from UHPC, steel, prestressed, and reinforced concrete with equal moment capacities [97]. Entertainingly, the UHPC beam wants only half the section depth of the reinforced or pre-stressed concrete beams, which in turn diminishes its weight by 70% or further. Similarly, the UHPC beam has the same section depth as the steel beam which, in this situation, is only slightly lighter than the UHPC member.

3. The advantageous regarding service life and reduced maintenance costs are because of the superior durability properties of UHPC. Several of the specific deterioration problems associated with concrete reinforcement can be lessened in UHPC because of its dense matrix and the decline or elimination of steel reinforcement that is typically essential in concrete members.

The improvement of UHPC with these advantages offers several attractive applications in the construction industry. The UHPC can be applied in numerous features: security industry, offshore, wear protection, concrete repair, prefab structures, industrial floors, pavements and new applications [84, 95, 96]. Big ceramic metal-based hybrid structures can be prepared by combining UHPC with other materials that display unique combinations of high strength in all directions, with extreme hardness, and very high fracture toughness. This makes it not only conceivable to design and to build large structures and extremely thin, elegant and daringly designed structures, on the other hand, to make non-brittle ceramics for medical (bone replacements and implants) and industrial applications (pumps, tooling, and engines) [97].

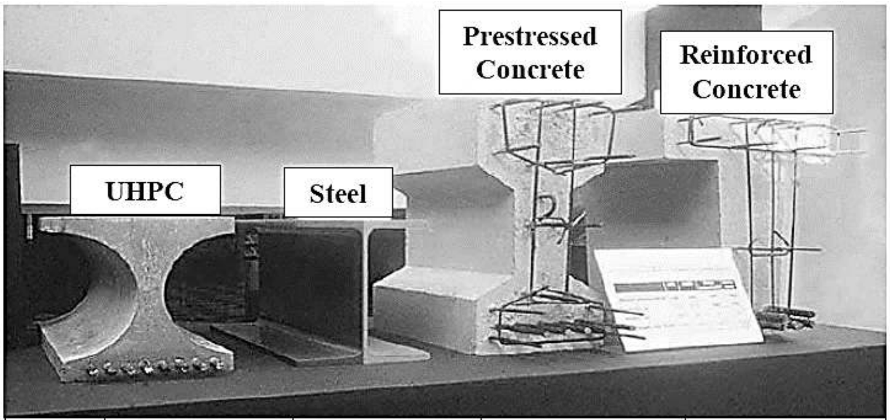

Material	UHPC	Steel	Prestressed Concrete	Reinforced Concrete
Depth	14 in. (360 mm)	14 in. (360 mm)	28 in. (700 mm)	28 in. (700 mm)
Weight	94 lb/ft (141 kg/m)	75 lb/ft (110 kg/m)	313 lb/ft (466 kg/m)	355 lb/ft (528 kg/m)

Figure 2.7. UHPC, steel, pre-stressed, and reinforced concrete beams with equal moment capacities [97]

4. With UHPC the total amount of materials savings required may also be recognized in other types of applications besides flexural members. Compared to normal concrete the UHPC cross-sectional area of compressive members may be reduced because of UHPC's high compressive strength, while slenderness ratios may restrict the reduction in cross-section for those members. Through UHPC using, the cross-sectional area of some 17-m tall columns in a cement silo in Detroit, Michigan, were reduced by 75 percent compared to normal concrete [98]. These reductions in material supplement decrease in dead weight and rise in the usable floor or overhead space. UHPC similarly can be used to reduce cross-sectional area compared to normal concrete in piping applications as shown in Figure 2.8 [99].

Figure 2.8. Reduction in pipe wall thickness of UHPC (right) compared to an equivalent pipe in normal concrete (left) [99]

2.2.5 Structural Applications of UHPC

In the 1990 three French companies: Bouygues, Lafarge, and Rhodia developed UHPC (specifically in the form of RPC or Ductal) [100]. The Arc Majeur project for the A6 motorway in France: a monumental sculpture, 54 m high was designed in 1996 by the artist Bernar Venet.

The pedestrian and bicycle bridge over the Magog River in Sherbrooke, Quebec in July 1997 was the first engineering structure in the world to be built out of this type of UHPC [81, 101]. As displayed in Figure 2.9, the spanning is 60 m, this precast, the pre-stressed pedestrian bridge is a post-tensioned open-web space RPC truss, with four access spans made of HPC. The main span is a gathering of six 10 m prefabricated match-cast segments.

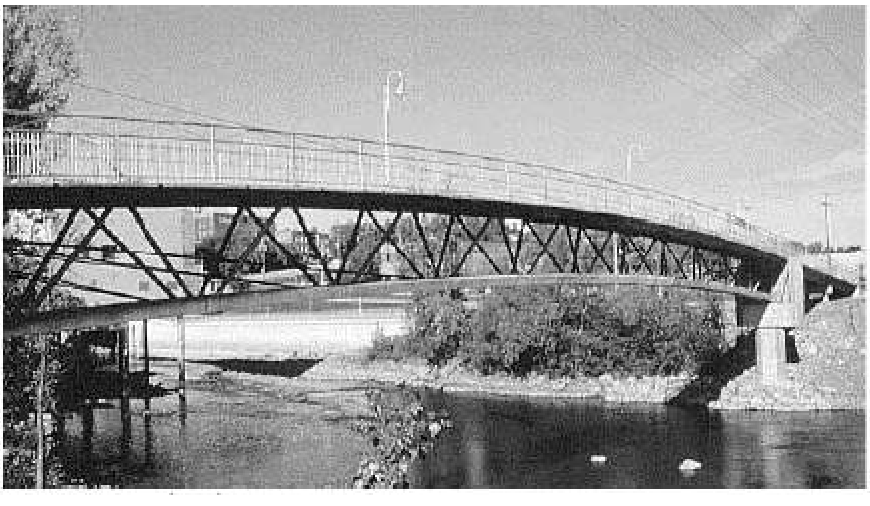

Figure 2.9. Sherbrooke footbridge general view [101]

A ribbed slab 30 mm thick is the cross section material, and a transverse prestressing made of greased-sheathed monostrands. The truss webs are produced from RPC restrained in stainless steel tubes, revealed in Figure 2.10.

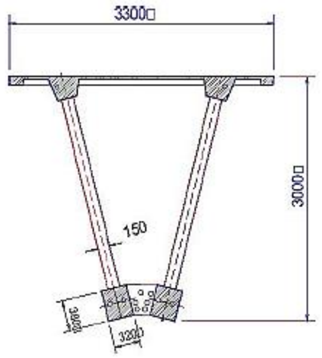

Figure 2.10. Typical cross section of Sherbrooke footbridge [101]

The structure is longitudinally pre-stressed through an internal pre-stressing located in each longitudinal flange in addition to an external pre-stressing anchored at the upper part of the end diaphragms and deviated in blocks located at the level of the lower flange. The greased-sheathed monostrands and miniaturized anchorage confirmed the connection between the flanges and truss diagonals.

1. Precast pre-stressed UHPC beams plus girders for a cooling tower at the Cottenom Nuclear Power Plant in France in 1999, was the another early use of the material [102]. Figure 2.11 illustrates some of the girders and casting beds for the 2,600 precast UHPC beams that were created for the exchange body of the cooling tower. For this project UHPC was selected by Electricité de France as a lightweight and durable alternative that would decrease foundation loads and yet be able to endure freeze-thaw cycles in an aggressive environment.

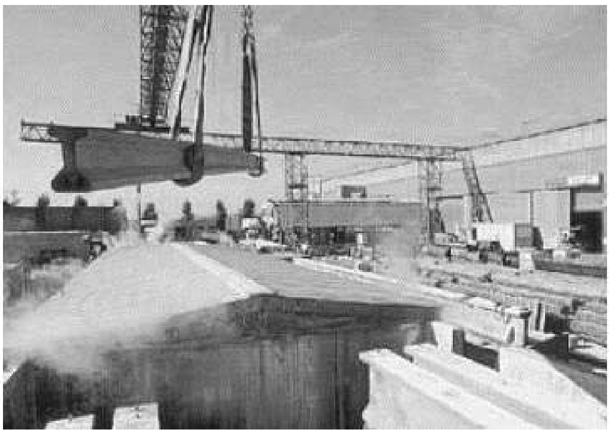

Figure 2.11. View of precasting area for UHPC beams for Cottenom Nuclear Power Plant [102]

2. In the Chryso plant in Sermaises, France a UHPC footbridge has similarly been built [103]. The 19-m walkway is supported on pillars with no reinforcement. It was selected as an alternative to the traditional wood and steel alternative and can convey six times the requisite design load. In this application UHPC's fire resistance properties, are principally important, allowing for the proximity of large quantities of chemicals.

3. Schmidt and Fehling [84] state that Germany has correspondingly built a long-span UHPC pedestrian bridge. In Wapello County, Iowa, United States the first UHPC vehicular bridge in North America, the Mars Hill Bridge, was built [100]. The Mars Hill Bridge is one of the highlighted UHPC ventures.

4. Through the years 2000 and 2001 the French Government, represented by its Regional Department of Public Works for the Drôme district with the support of the Service d.Etudes Techniques des Routes et Autoroutes and the Centre d.Etudes Techniques de l.Equipement of Lyonthe first road bridge UHPC constructed was Bourg les valence bridges, built by the contractor Eiffage Construction with BSI on Valence bypass. Each bridge with two isostatic spans of around 20 m. The road deck was prepared continuously by placing in situ UHPC among the two spans as presented in Figure 2.12.

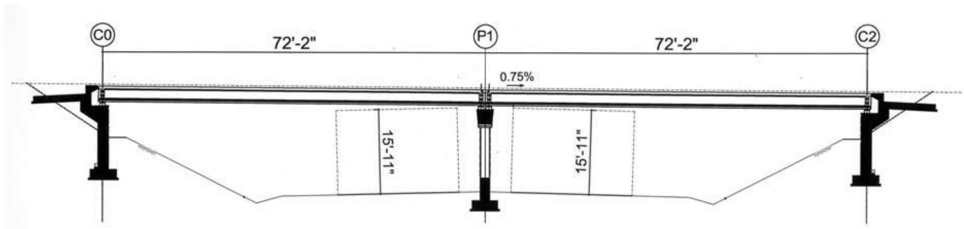

Figure 2.12. Longitudinal cross-section of OA4 [104]

As revealed in Figure 2.13 a 9 m wide road pavement supported by each deck with 1 m and 2 m sidewalks. Transversally, the two decks are same; they are constructed on an assembly of five π-shaped precast beams made from BSI, longitudinally stitched together with in situ UHPC.

Altogether the beams are pre-stressed by pre-tension. There is no transverse pre-stress, with no transverse passive reinforcement, but where π -shaped beams are transversally sewed together.

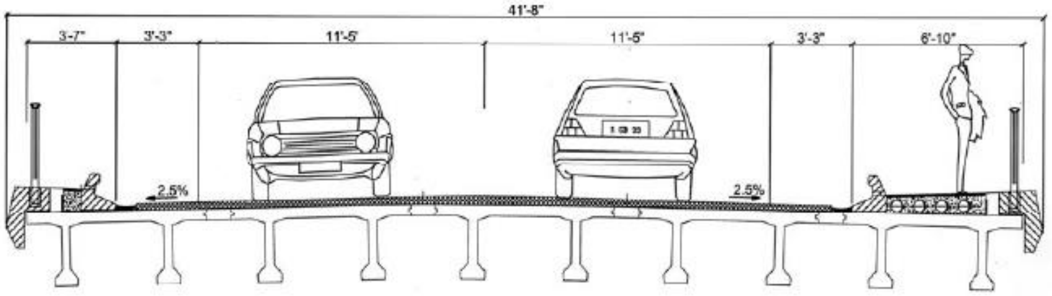

Figure 2.13. Typical cross-section of Bourg-lèsValence bridges [104]

5. The contractor Bouygues built a footbridge over the Han River in 2001 and 2002, the bridge running through Seoul in South Korea. Jointly conceived by the City of Seoul and "France's Year 2000 Committee" to commemorate the new Millennium, the footbridge represents the collaboration and friendship between South Korea and France. As displayed in Figure 2.14, it is constructed of an arch spanning 120 m, and two steel access spans.

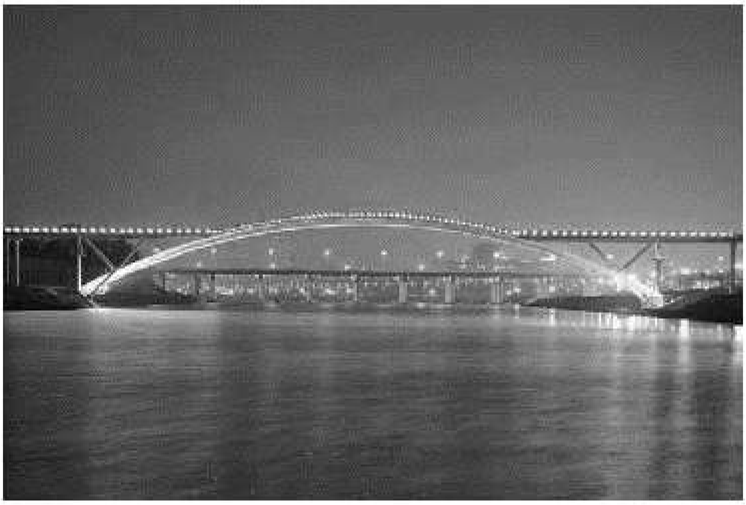

Figure 2.14. General view of Seoul footbridge [105]

The arch with a π-shaped cross-section 1.30 m deep, presented in Figure 2.15. A ribbed slab 30 mm thick is the upper, and a transverse pre-stressing made of greased sheathed mono-strands. The webs are inclined outward, and the web is 160 mm thick. The arch is prefabricated segments with the assembly of six 20 m, associated with site using temporary supports. The components are tacked together by an internal longitudinal pre-stressing located in haunches in the lower and the upper parts of the webs [106].

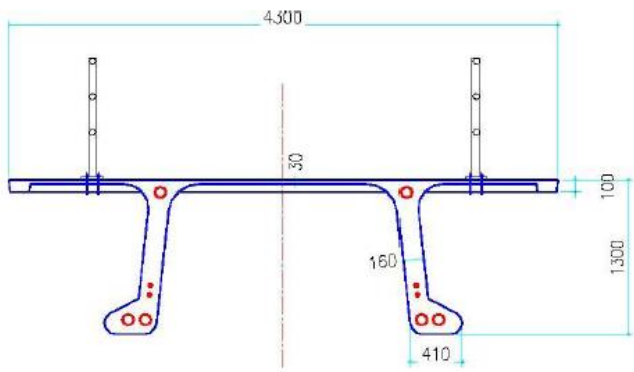

Figure 2.15. Cross-section of Seoul footbridge [106]

This very thin structure has frequencies of vibration sensitive to the pedestrian traffic. To decrease the effect of the first three kinds of vibration of the footbridge, vibration calculation has been carried out, and adjusted mass dampers have been fitted.

The first Ductal footbridge constructed in Japan with a span of 50 m. The deck is a simple beam 2.4 m wide with circular web holes. The structure is longitudinally pre-stressed via external pre-stressing with no passive reinforcement. At the end of 2002, this footbridge was accomplished, shown in Figure 2.16 [107].

Figure 2.16. Footbridge project in Sakata City. Japan [107]

6. Through using UHPC beams and permanent UHPC formwork panels overlain by a reinforced concrete deck the Shepherd Creek Road Bridge in New South Wales, Australia, has been built [108]. The four-lane bridge was 600-mm deep, 15-m long UHPC beams spaced 1.3 m away from each other. The weight of the UHPC beams was described to be half much as the other normal concrete beams, plus the UHPC formwork panels were only 25-mm thick.

7. The two bridges over a highway near the city of Bourg-Lès-Valence, France UHPC in the form of BSI or Ceracem has been used [109]. In Saint-Pierre-la-Cour, France a bridge with 19-m long over a railroad has also been built from UHPC [110].

A 12.6-m wide bridge with the half weighs a continuous reinforced concrete road and a bicycle lane as an alternative of normal concrete. Figure 2.17 illustrates some of the bridges and footbridges defined overhead.

Figure 2.17. Examples of UHPC bridges and footbridges: a) Footbridge of Peace in South Korea, b) Shepherd Creek Road Bridge in Australia, c) Sakata Mirai footbridge in Japan, and d) Papatoetoe footbridge in New Zealand [97, 103, 110]

In order to support a high floor in a cement silo in Detroit, Michigan, United States four UHPC columns were used [111]. The columns were 17-m tall, 76-cm square and reinforced with only four 13-mm diameter pre-stressing strands. The columns raised in just one day plus it is a quarter of the size of the normal concrete alternative. UHPC was likewise used in columns in the Queen Sofia Museum in Madrid, Spain [103]. The first cast-in-place UHPC project was the 32-cm diameter steel columns were filled with UHPC. By the addition of UHPC, the flexural and compressive capacity of the 16-m tall columns increased.

8. On a clinker silo in Joppa, Illinois, United States the first long-span roof in the world built from UHPC was finished in 2001 [112]. Due to the light weight of the UHPC roof, there is no negatively impact the foundation design of the 18-m diameter silo. A mechanical penthouse supported by a roof which comprises of 13-mm thick ribbed panels. Compared to 35 days for steel roofs on adjacent silos, the UHPC roof took only 11 days to install.

9. Shawnessy LRT station in Calgary, Canada, is one of the most well-known UHPC structures in the world is displayed in Figure 2.18. The design flexibility gave by UHPC permitted the architect to achieve their desire for a free-flowing form design for this building. To confirm the satisfactory performance of the 24 UHPC

architectural shell canopies that were used for the station before their installation full-scale load tests were used. The canopies are shield waiting passengers from the weather and were only 20-mm thick [97]. Each pair of canopy pieces is supported on a single UHPC column.

Figure 2.18. Shawnessy LRT station with UHPC canopies [97]

10. For the Monaco underground train station, UHPC has been used to building acoustic panels [102]. To support in panel acoustic properties. The thin and light UHPC panels were cast with small holes. The nonflammable panels make an aesthetically pleasing, bright environment for passengers plus they are resilient to impact. Along with a roadway in Châtellerault, France acoustic panels have also been used, due to its resistance to car pollution and de-icing salts [103].

11. For the Rhodia Research Center in Aubervilliers, France UHPC has been used for façade panels [103]. UHPC can similarly be used in decorative panels, as the panels can be cast with various surface finishes and can be dyed or painted. Moreover, UHPC applied to sculptures, most notably the Martel Tree in Boulogne-Billancourt, France [102].

12. The eight bus shelters in Tucson, Arizona, United States, that protect passengers from extreme sun and heat which is made of UHPC so, it can be used for urban furniture [111]. Furthermore, UHPC can be utilized for interior furnishings, containing tables, chairs, countertops, sinks, planters, tiles, and even security-type applications like safes [97].

13. According to investigated applications, the bridges be one of the areas of greatest potential for UHPC, for the reason that its high loads, long spans, and sometimes harsh environments. Some of the completed or ongoing investigation on using UHPC in bridge applications comprises:

Steel-free post-tensioning: as renowned formerly some of the first research including UHPC was directed to develop nonmetallic anchorage systems [113]. Steel-free bridge decks: according to an investigation by Hassan and Kawakami's composite panels composed of UHPC and cast-in-place FRC display strong potential [114]. Ribbed deck slabs: for box girder bridges an optimized UHPC deck containing a ribbed upper slab could be used. Because of this resulting system, a decline in weight though maintaining sufficient stiffness and easy prefabricated construction would provide [73]. Box girders: as noted earlier a UHPC box girder with the similar depth, load requirements, and top area could be built with only one third of the total amount of material compared to normal concrete [6]. Π-shaped girders: investigators at the Massachusetts Institute of Technology (MIT) designed two 21.3-m long, 2.4-m wide Π-shaped girders and installed in an experimental test bridge at FHWA’s testing facility in McLean, Virginia, United States [103]. Protective layers: to protect normal concrete structures UHPC may be used compositely on them. One theory uses UHPC for an abrasion layer and the curb, barrier, and deck edge on a normal concrete box girder [115].

14. Other Structures

Due to the high strength and high durability of UHPC give benefits potential for a wide variety of uses. Some of the studies on non-bridge structural members consist of: Impact-resistant structures: an investigation on the CRC type of UHPC shows the material is less sensitive than normal strength FRC to impact loading rate [116]. Earthquake-resistant structures: due to UHPC’s high strength and ductility, the investigation is being conducted on using pre-stressed UHPC elements for earthquake-resistant structures [117]. Spherical dome roof: using 30-mm thick stiffened UHPC plates as well as post-tensioned arching beams a dome with 120-m diameter has been designed [118]. Railway walkway braces: because of the deterioration of existing concrete foot-walk braces, deliberation of UHPC as an alternative. The ductility of UHPC provides cautioning to maintenance staff before the walkway braces fail [119]. Nuclear waste containers: radioactive waste containers used must resist impact without losing integrity. UHPC is being deliberated as current FRC containers do not meet requirements [120]. Hot water tanks for solar energy storage: UHPC can use in the prefabricated shell elements because of the high density of UHPC and its high strength make it a favorable material for underground hot-water tanks [121]. Well cover plates: UHPC has been considered as a ductile and cost-effective alternate to cast-iron cover plates on wells and underground civil configurations [122].

15. According to theorized applications, at this point, some applications of UHPC have not been investigated nevertheless are interesting areas of possible future research and implementation. These theorized applications comprise the following: tunnel liners [123]; caissons, reservoirs, and coatings [7]; bunkers, structures of military and strategic importance, gas tanks, defense shelters, crash barriers, and heavy-duty runways [116]; and sheet piling, heavily loaded industrial floors, transportation routes, and flood barriers [124].

16. According to mixed applications, the realization of punched and thin acoustic sound panels for the underground Monaco railway station 1500 m^2 of panels 30 m^3 of concrete.

The realization of architectural wall panels for Rhodia head office in Aubervilliers. In seawall anchors on Reunion Island, UHPC has been used for anchor blocks, where 6300 plates were used to stabilize a sea wall (see Figure 2.19). The low maintenance related with the durability of UHPC led to further cost savings of 18 percent plus The UHPC plates cost competitive with the cast iron alternative [102]. Similarly, UHPC anchors were used in Calgary, Alberta, Canada for a post-tensioned, soil anchor precast retaining wall system in front of a bridge abutment. The realization of stays for a treatment reservoir of rainwater in Les Houches, France. In the pylons of Sungai Muar bridge in Malaisia as the injection of curved saddles for stay cables, as a display in Figure 2.20. The realization of foundations blocks for the roof of the Cluses toll-gate on A40 motorway, Germany. As seen in Figure 2.21.

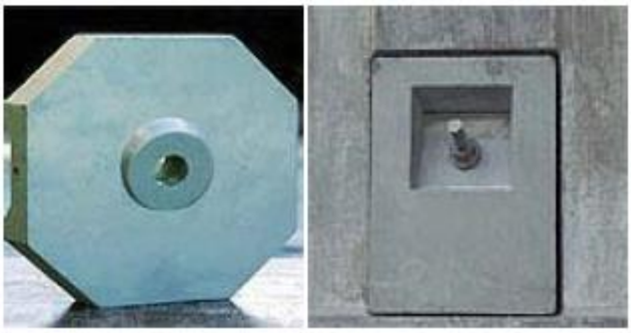

Figure 2.19. Anchor plates for seawall on Reunion Island (left) and soil wall in Calgary (right) [102]

Figure 2.20. Curved saddles for stay cables in Sungai Muar Bridge [105]

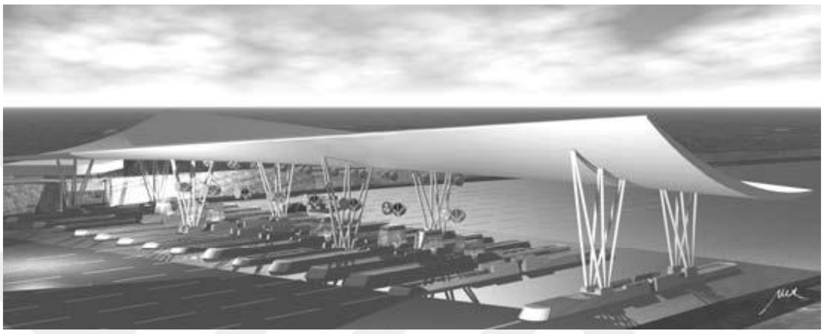

Figure 2.21. Roof of the Cluses toll-gate on A40 motorway [104]

2.3 Composite Columns

A composite column is a compression member known as a combination of concrete and one or more steel sections, in such a way that the resulting arrangement works as a single item [125]. It was well known that concrete is perfect in compression and steel is excellent in tension and by fitting together the two materials structurally these strengths can capitalize consequently, a light weight and very highly efficient design can build. Additionally, they display a higher level of performance compared while the two materials functioned individually [126].

2.3.1 Background on Composite Columns

In 1940 for the first time in construction, the composite columns were used. However, in various countries around the world, the year 1970 is marked the evolution of concrete filled steel tubes. many of those countries for the use of CFST have developed a design code and specifications. From the steel or concrete design approaches, these specifications have been created [126]. The effective approach has been acknowledged for enhancing structural performance is the usage of composite action.

For a better understanding of composite columns specially concrete filled steel tube (CFST) columns, essential amount of works have been designed during the last 40 years. All over the world what attracts the attention of investigators is that CFST columns can substitute the standard structural columns like reinforced concrete structures, structural steel that comprise reinforced concrete and the structural steel alone with an improved performance additionally construction cost reduced to the minimum. Therefore, that is why it is principally very beneficial in tall buildings where high strength is needed, and the flexibility of the open space is required for the maximum range of applications [37].

Due to its rapidity of construction, higher load-carrying capacity, stiffness which results from combining the rigidity of reinforced concrete with structural steel sections and their light weight, which similarly reduces the size and cost of structural foundations. Also, there are huge interests of using composite systems for the seismic resistance design. Furthermore, when the two steel and concrete used together we take advantage of both steel and concrete properties, as concrete supplies its inherent mass, stiffness, and economy. However steel provides strength and its light weight [127].

2.3.2 Types of Composite Columns

The two basic categories of composite columns are concrete-encased, those with the steel section encased in concrete (either partially or wholly) and those with the steel section filled with concrete, concrete filled steel tube (CFST) [125].

One of the mutual and widespread columns is the encased steel profile, where a steel H-section is encased in concrete. Occasionally, structural pipe, tube, or built up section is placed as a replacement for of the H-section. The concrete encasement improves the behavior of the structural core by reinforcing it, as well as making it more effective against both the local and overall buckling [37]. The concrete encasement can be either encased wholly or partially as revealed in Figure 2.22.

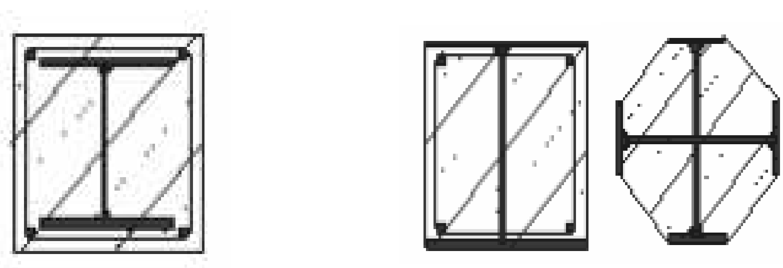

a) b)

Figure 2.22. Concrete encased columns; a) fully encased and b) partially encased [37]

The load-bearing concrete encasement implements the further function of fire-proofing the steel core. The cross sections, which usually are square or rectangular, must have one or more longitudinal bars located in every single corner and these have to be tied via lateral ties at regular vertical intervals in the manner of a reinforced concrete column. Strength, confinement, and ductility of the column increased through these ties. Additionally, throughout construction, the longitudinal bars displacement stopped, and buckling of these same bars outward under load resisted, which would cause spalling of the outer concrete cover even at low load levels, particularly in the case of eccentrically loaded columns [42].

Figure 2.23 displays the cross section of concrete filled steel tube. These varieties of composite column comprise a steel hollow tube of different shape (circular, square, rectangular, etc.) filled with concrete or concrete with transverse and longitudinal reinforcement [37, 128].

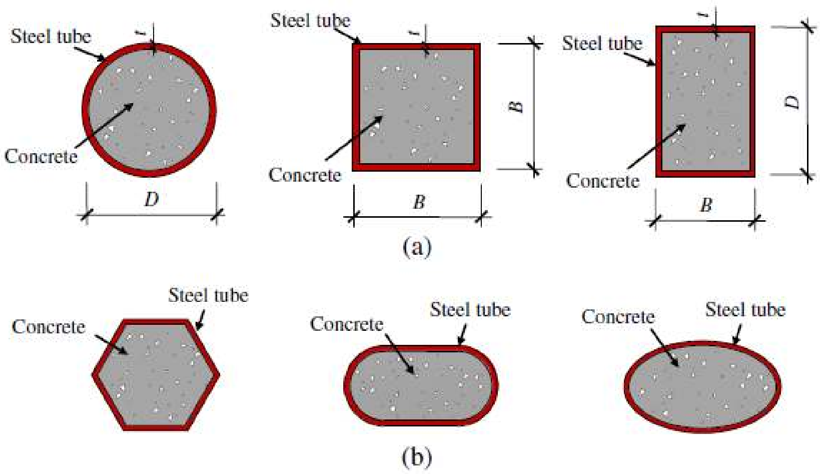

Figure 2.23. Typical CFST sections [42]

Concrete filled steel tube may be the most effective in the application of materials for column cross sections. It increases the strength and stiffness of the column through providing forms for the inexpensive concrete core. Moreover, the steel shell supplies transverse confinement to the concrete since its relatively high stiffness and have tensile resistance; these steel shells make the filled composite column very ductile with the notable toughness to endure local overloads [42].

2.3.3 Advantages of Concrete Filled Steel Tube (CFST) Composite Columns

There are several distinct advantages of using CFST rather than other types of columns.

The following are the main benefits of CFST:

- The steel tube in CFST columns restrains the concrete and whereas the concrete delays the occurrence of local buckling of steel tube so, the axial and flexural capabilities are improved. Similarly, an excellent energy absorption capacity is realized because that the steel tube restrains the entire concrete core in the circumferential direction [129].
- The concrete core and steel tube are completely compatible and complementary to each other as they have nearly the similar thermal expansion [37].
- Composite columns, predominantly those uses CFSTs, allows very rapid construction, so the long term formwork construction is not required. Besides, the waiting time needed for concrete curing is not needed since the constructions of the upper story can continue formerly the curing of concrete in the lower story [37].
- CFST members are considerably more economical than the steel members because usage of steel in CFST is less. Additionally, the steel tube can be used as a formwork for casting the concrete therefore in the construction process there will be cost savings [129].
- The structure fire resistance can enhance because of the concrete inside the steel tube consequently the fire proof material requirement can be reduced [130].
- The ductility requirement for earthquake resistant design is certainly attained through using CFST once compared with the common reinforced concrete columns. The vibrations because of earthquakes and winds can similarly be reduced due to its higher rigidity [37].
- Proper for tall buildings, bridges and other types of structures because of high strength and flexibility [128].
- The steel section can substitute the function of transverse confinement and longitudinal reinforcement by carrying both longitudinal and transverse loads besides simultaneously providing a confinement. Consequently, the usage of transverse and longitudinal reinforcement may be eliminated [37].
- The system considered as an advantageous in carrying large axial load benefitting from the interaction between the concrete and the steel section [128].

2.3.4 Applications of CFST

Buildings constructed with CFST has increased quickly in the last few decades. A numerous number of buildings had been built with CFT columns around the world. Some of them are presented below. Figures 2.24 to 2.34 also show such examples.

1. First Street Plaza in San Francisco California [131]
2. Sannomiya Grand Building in Japan [132]
3. Millennium Tower in Austria Vienna- Austria [133]
4. The Two Union Tower in Seattle, USA [134].
5. International Finance Center Tower 2 in Hong Kong – China [135]
6. Parking deck "DEZ" in Innsbruck - Austria [136]
7. Redevelopment of the Hilton Hotel –Cheung Kong Center in Hong Kong - China [135].
8. Composite multi-story steel-framed constructions (Building used for commercial located in London and car industry factory building in Germany) [137].
9. SEG plaza in Shenzhen in China [42].
10. Ruifeng building in Hangzhou in China [42].
11. Wangcang East River Bridge in China [42].
12. Canton Tower in Guangzhou [42]
13. A power plant workshop using CFST columns in China [42]

Figure 2.24. First Street Plaza in San Francisco California (left) [131] and Sannomiya Grand Building in Japan (right) [132]

Figure 2.25. Millennium Tower in Austria Vienna- Austria in the right [133] and Two Union Tower in Seattle, the USA in the left [134]

Figure 2.26. International Finance Center Tower 2 in Hong Kong -China [135]

Figure 2.27. Parking deck "DEZ" in Innsbruck – Austria [136]

Figure 2.28. Redevelopment of the Hilton Hotel –Cheung Kong Center in Hong Kong - China [135]

Figure 2.29. Composite multi-storey steel-framed constructions (Building used for commercial located in London and car industry factory building in Germany) [137]

Figure 2.30. SEG plaza in Shenzhen in China [42]

Figure 2.31. Ruifeng building in Hangzhou in China [42]

Figure 2.32. Wangcang East River Bridge in China [42]

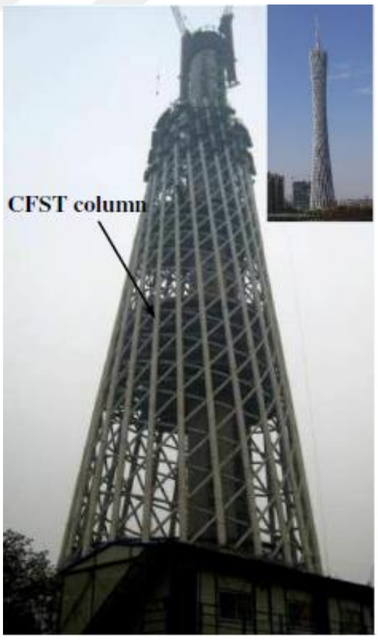

Figure 2.33. Canton Tower China [42]

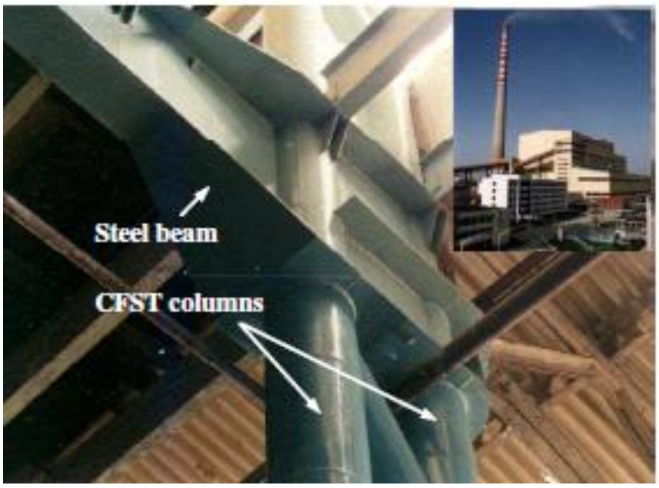

Figure 2.34. A power plant workshop using CFST columns China [42]

2.3.5 Previous Studies on Structural Behavior of CFST

Sakino et al. [138] investigated centrally loaded hollow and CFST short columns. A total of 114 specimens were prepared and tested. Four different parameters have been tested; the shape of steel tube (circular and square), tensile strength which ranges from 400 to 800 MPa, diameter-to-thickness ratio, and concrete compressive strength which varies from 20 MPa to 80 MPa. They recommended design formulas to calculate the ultimate capacities of CFST columns with both circular and square specimens. For an ultimate strength (N_u) of axially loaded circular CFST short columns, a formula below has proposed.

$$N_u = A_s \sigma_{sz} + A_c \sigma_{ccB} \tag{2.1}$$

Where A_c and A_s is the area of concrete and the area of steel tube at the cross section, respectively. σ_{sz} and σ_{ccB} are the axial stress of steel tube in yield condition and the strength of confined concrete, respectively.

Moreover, the axial load capacity of square CFST short columns could be estimated the equation below.

$$N_u = A_s \sigma_{scr} + A_c \gamma_U f'_c \tag{2.2}$$

Where σ_{scr} is the ultimate compressive stress of square steel tubes, taken as the minimum value of yield, γ_U is the strength reduction factor for concrete (γ_U = 51.67 $D_c^{\,-20.11}$), and f'_c is the cylinder strength of concrete.

They similarly showed that the difference between the ultimate strength and the nominal squash load circular CFST columns could be assessed as a linear function of the yield strength of the steel tube [138].

Giakoumelis and Lam [139] studied the behavior of circular concrete-filled steel tubes with various concrete strengths under axial load. They observed the effects of steel tube thickness, the bond strength between the concrete and the steel tube, and the confinement of concrete. A total of 15 specimens were tested using 30, 60 and 100 N/mm2 concrete strength and with a D/t ratio from 22.9 to 30.5. All the columns were 114 mm in diameter and 300 mm in length. The experimental column strengths measured are compared with the values predicted by Eurocode 4 (EC4, 1998), Australian Standards (AS4100, 1998) and American Codes (ACI318, 1995). They showed that the effect caused by concrete shrinkage was critical for high-strength concrete and negligible for normal strength concrete. Figure 2.35 demonstrates the comparison of Eurocode 4 with experimental results, for both Non-Greased and Greased Specimens.Through the experiments all of the codes predicted fewer values than those calculated. Therefore, EC4 gave the best estimation of the axial capacity for both CFST with normal and high concrete strength. The most difference between the experimental value and predicted values of the ultimate capacity of EC4 was 17%.

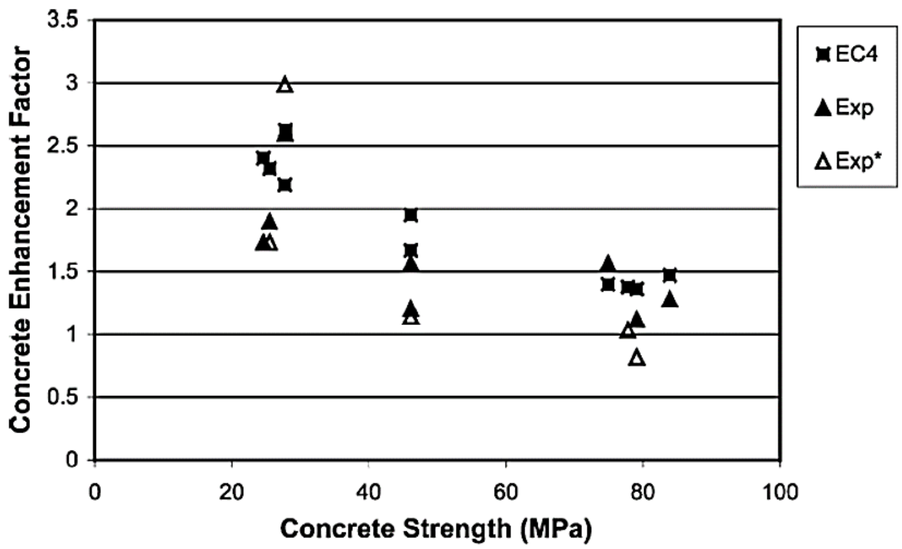

Figure 2.35. Comparison of Eurocode 4 with experimental results [139]

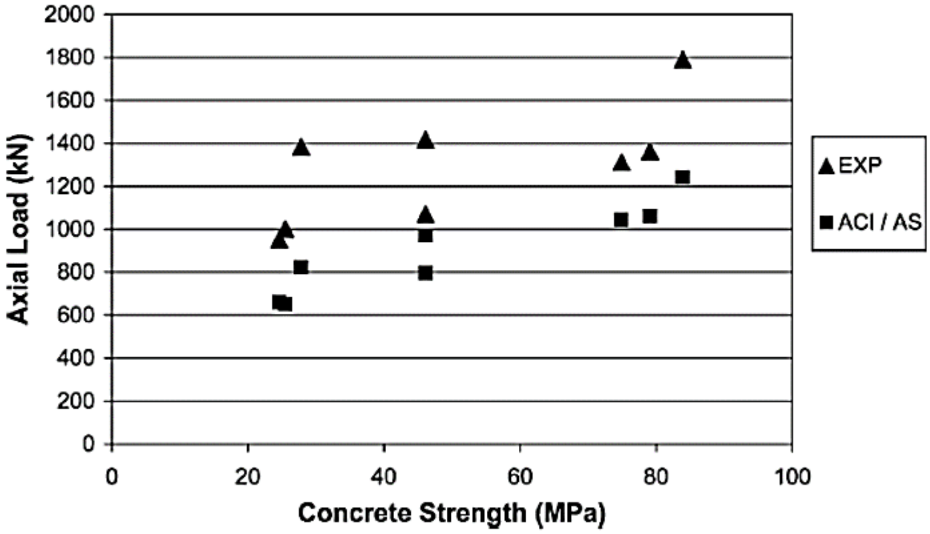

Figure 2.36. Comparison of ACI and AS with experimental results [139]

Nevertheless, for ACI and AS the predicted axial capacity was 35% less than the values from experiments as displayed in Figure 2.36. Additionally, when the concrete strength increased the effects of the bond of the steel tube and concrete core became more critical. For the normal strength concrete, the reduction of the ultimate capacity of the column was very small. Conversely, for a high-strength concrete, the difference between greased and non-greased was 17%.

Schneider et al. [140] described the design and construction of a type of moment-resisting joint in recent times applied for two low-rise buildings in Vancouver, Washington U.S.A. The joint comprises a structural steel wide-flange shape penetrating continuously through a composite concrete-filled steel tube (CFST). Using American Concrete Institute's ACI-318 and the American Institute of Steel Construction 1994 AISC/LRFD provisions, the strength and stiffness of the CFT column were estimated and compared with both specifications. For strength each specification produces somewhat different values. Nonetheless, the stiffness estimation varies most considerably between the two provisions. Finally, one method to estimate joint strength, which is shown to depend significantly on joint configuration, is provided. The flexural stiffness computed using *ACI-318,* and *AISC/LRFD* specifications are presented in Figure 2.37 As shown, flexural stiffness varies significantly between the two specifications and is consistently different for increasing concrete strength.

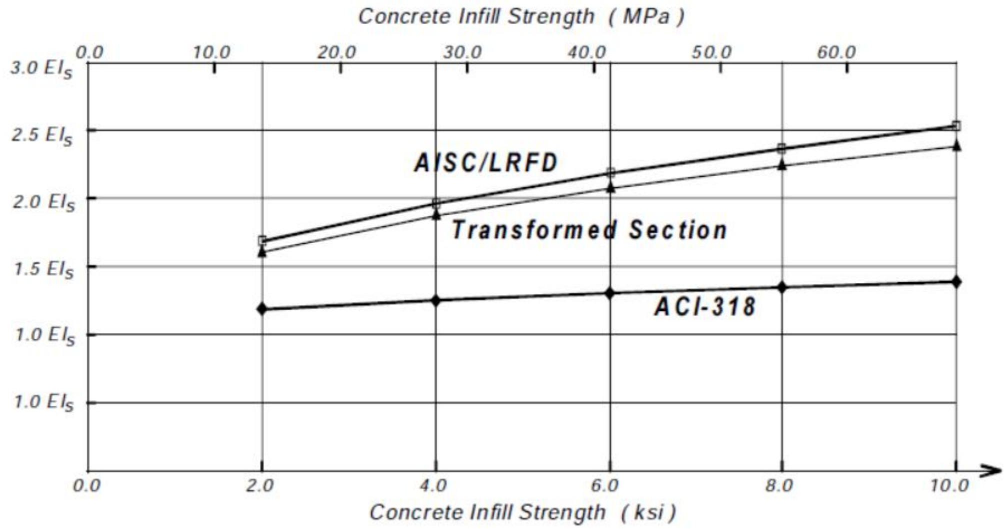

Figure 2.37. Computed Flexural Stiffness of ACI-318 and AISC/LRFD Provisions [140]

The test results showed that flexural capacity computed by the ultimate strength method, as allowed by the AISC/LRFD steel specification, resulted in more capacity than provided by the ACI-318 concrete specification. On the hand, the computed flexural stiffness varied as much as 60% for the column sizes.

Gupta et al. [141] studied the behavior of circular concentrically loaded concrete filled steel tube columns till failure. They investigated the effect of diameter and (D/t) ratio of a steel tube on the load carrying capacity of eighty-one specimens concrete filled tubular columns, and the effect of the grade of concrete and volume of fly ash in concrete was also examined. On the other hand, the effect of these parameters on the confinement of the concrete core was similarly considered. The diameter to wall thickness ratio was between 25 to39, and the length to tube diameter ratio was 3 to 8. The strength test results were compared with the corresponding findings of the available literature results of concrete filled tubular columns. Moreover, a nonlinear finite element model was developed to study the load carrying mechanism of CFSTs using the Finite Element code ANSYS. Figure 2.38 depicts the typical load–compression curves for two modes of collapse for different concretes. It was established that for both modes of the collapse of concrete filled tubular columns at a given deflection the load carrying capacity decreases with the increase in 15% volume of fly ash up to 20% but it again increases at 25% fly ash volume in concrete.

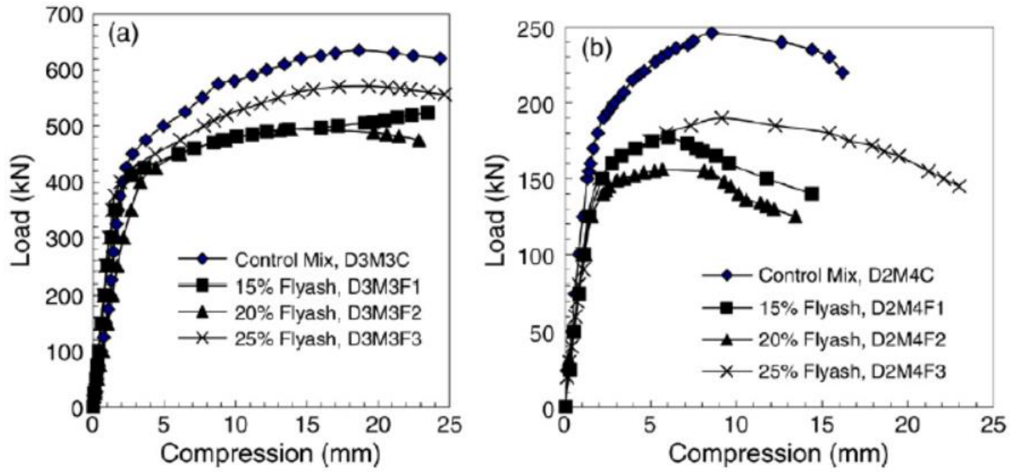

Figure 2.38. Load–compression curves of CFST for different concretes (a) 75 mm diameter and (b) 50 mm diameter CFST [141]

Furthermore, for smaller D/t ratio, it was perceived that steel tube provides good confinement effect to concrete. On the other hand, from the bare tube results, it was established that the load carrying capacity of the steel tube per unit volume decreases as the D/t ratio increases. As shown in Figure 2.43. They suggested that it was essential to fix the correct D/t ratio to make optimum usage of the material.

Evirgen et al. [142] conducted tests to determine compressive strength, modulus of elasticity and steel tensile of sixteen hollow cold formed steel tubes and 48 concrete filled steel tube specimens are used for axial compression tests. They examined the effects of (b/t) ratio, the compressive strength of concrete and geometrical shape of cross section parameters on ultimate loads, axial stress, ductility, and buckling behavior. For the experimental method circular, hexagonal, rectangular and square sections, 18.75, 30.00, 50.00, 100.00 (b/t) ratio values and 13, 26, 35 MPa concrete compressive strength values were selected. Analytical models of specimens are established using a finite element program (ABAQUS), and the results are compared. Table 2.4 shows the change of ultimate axial stress capacity of composite sections. Maximum increment ratios are seen from the table in the circular sections at 167.8%. The increment ratio is enhanced on both the thickening of steel tube and adecrease of compressive strength of the concrete. This behavior also consists of aconfinement effect along all lateral directions on rounded specimens.

Table 2.4. Change of ultimate axial stress capacity of composite sections [142]

Domain parameter	Increment ratio (%)					
Shape ofsection	Circular	Hexagonal		Square		Rectangular
	167.8	150.8		91.1		64.7
Thickness ofsteel (mm)	1.5	3		5		8
	40.4	99.5		215.9		298.3
Compressive strength of concrete (MPa)	13.3		26		35.3	
	291.6		122.7		76.3	

Moreover, the average ductility values were calculated as 19.8, 11.6, 4.0and 3.1 for the circular, hexagonal, square and rectangular specimens respectively. It can be seen that rounded specimens have a higher ductility than angulars pecimens. Also, 15–20% or fewer differences were obtained between the experimental and FEM results for all samples. However, some specimens approached to nearly 40%. These differences can often result from possible geometric or material imperfections.

Ajel and Abbas [128] considered the structural behavior of concrete - filled steel tube columns through experimental and analytical studies. They determined the effect of concrete compressive strength, the thickness of steel tube, stiffeners and longitudinal reinforcement of 16 square samples with dimensions of 150 mm ×150 mm × 300 mm height, and 15 circular samples of 150 mm diameter and height of 300 mm. Using three dimensional finite element representation of ANSYS computer program, the tested samples were studied analytically. To simulate concrete and steel tube 8 nodes brick elements SOLID 65 and SOLID 45 were used correspondingly. Whereas 2 nodes element LINK 8 are used for steel rebar.

The results of analytical method display that, the convergence between analytical and experimental failure load varied from 2 to 15 %. However, the effect of compressive strength of concrete on columns having width/thickness (b/t) or diameter/thickness (d/t) 37.5 is greater than columns which have (b/t) or (d/t) 50. On the other hand, columns filled with normal concrete (25 MPa) deformations are larger than those of columns filled with high strength concrete (60 MPa). Once of (b/t) or (d/t) decreases the effect of (b/t) and (d/t) ratio on the ultimate strength of (CFST) columns will have a reverse action, it caused an increasing in the ultimate load capacity of columns which is from 4.47 to13.37 % for square and for circular samples from 8 to 12.14% depending on the type of stiffened, compressive strength of concrete and ratio of (b/t) and (d/t) [128].

Bedage and Shinde [38] calculated the accuracy of codal design approach by comparing experimental results with the analytical results obtained using EC4, ACI-318 and AISC-LRFD, for prediction of load carrying capacity of CFST columns under axial compression, by conducting concrete filled steel tubes of length 300 mm, thickness 1 to 3 mm for circular, square and rectangular cross section with three different grades of concrete. 200 T capacity compression testing machine is used for experimental investigation. The experimental results are compared with analytical results obtained by a stated code of practices. Figure 2.39, 2.40, and 2.41 displays the comparison of test results with a codal design for different concrete grades. It can be established that EC4 gives conservative results. From which it is observed that EC4 gives conservative results with experimental results and EC4 provisions may be used for the further analytical study to develop an expression to predict the section capacity CFST columns. As the grade of concrete increases the load carrying capacity is also increased.

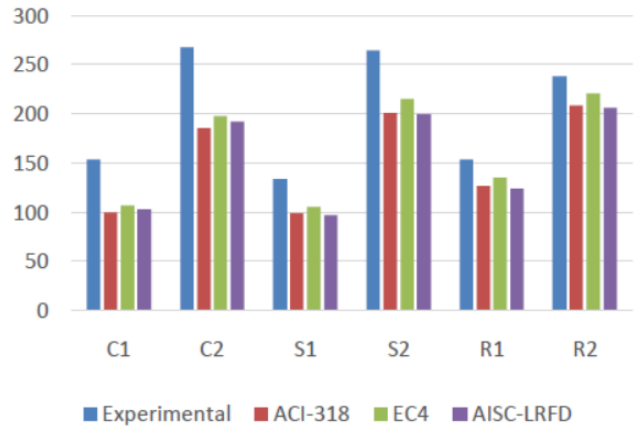

Figure 2.39. Comparison of test results and different code of practices with M20 concrete [38]

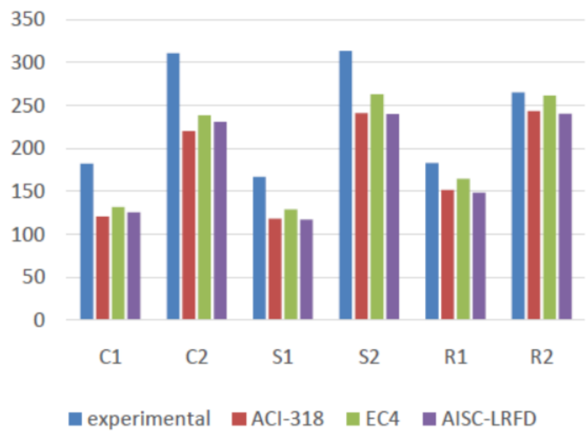

Figure 2.40. Comparison of test results and different code of practices with M30 concrete [38]

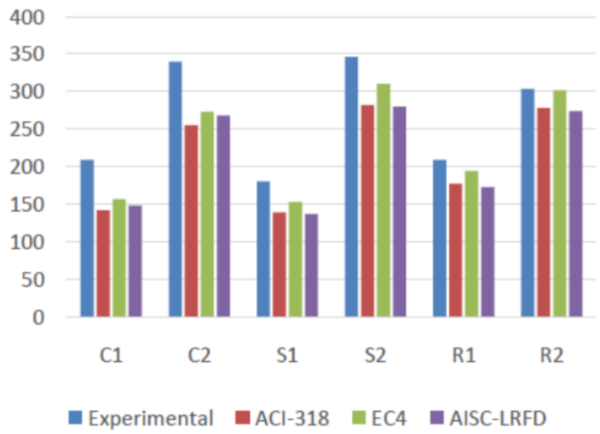

Figure 2.41. Comparison of test results and different code of practices with M40 concrete [38]

Güneyisi et al. [143] presented a new formulation for the axial load carrying capacity (Nu) of circular concrete filled steel tubular (CFST) short columns having various geometrical and material properties. For training and testing of the prediction model. 314 comprehensive experimental data samples obtained from previous studies were examined to prepare a data set.

The prediction parameters were selected as the outer diameter of column (D), wall thickness (t), the length of column (L), the compressive strength of concrete (fc), and yield strength of steel (fy). Gene expression programming (GEP) used for the prediction the model. The proposed model was compared with available ones presented in the current design codes (ACI, Australian Standards, AISC, AIJ, Eurocode 4, DL/T, and CISC) and some existing empirical models proposed by previous researchers. The statistical parameters also evaluated the prediction performance of all models. Figure 2.42 the comparison of the proposed GEP model with existing equations given in (a) design codes and (b) previous studies Its evident that the GEP model was much better than the available formulae, yielding higher correlation coefficient and lower error [143].

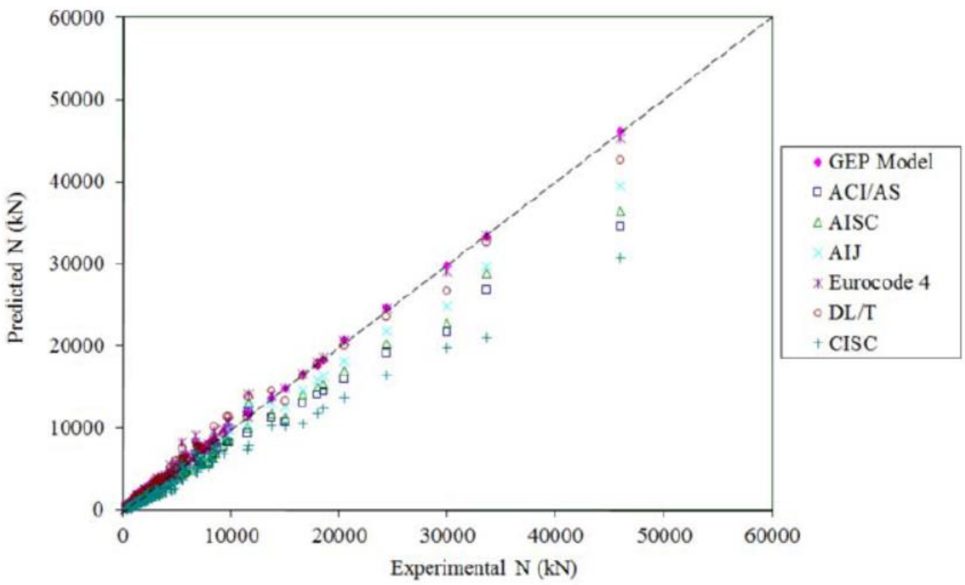

(a) Design codes

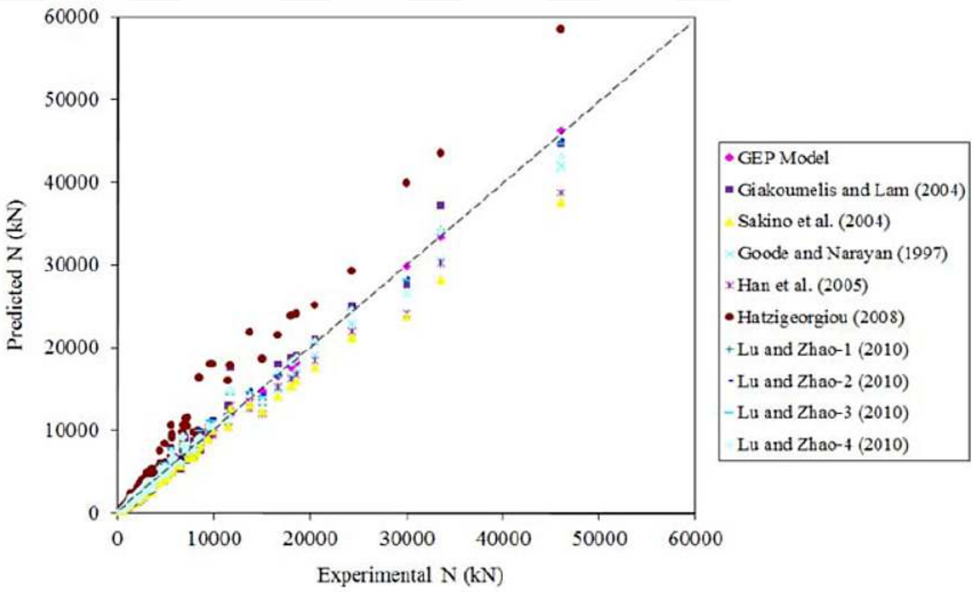

(b) Previous studies

Figure 2.42. Comparison of the proposed GEP model with existing equations given in (a) design codes and (b) previous studies [143]

Hafiz [144] investigated the behavior of concrete filled tabular columns under axial compression loading. Therefore, the axial strength of CFST columns and their corresponding confinement factors have been evaluated using Eurocode-4 design mechanism and CESC 28:90 design mechanism. Numerical analysis has been done using three dimensional non-linear finite element software ABAQUS 6.13. The analytical and numerical results obtained are compared with each other. For this study 12 circular CFST specimen having steel tubes of different thickness and in filled with the various grades of concrete are chosen from the literature. Table 2.5 illustrates the comparison of the analytical and numerical results.

With the increase in the length of CFST column, load carrying capacity decreases as seen from the above table. However, load carrying capacity of CFST columns decreases with increase in D/t ratio. On the other hand, unconfined columns buckle more than confined counterparts and slenderness ratio plays a vital role in the strength calculation of column and its behavior.

Table 2.5. Comparison of analytical and the numerical results [144]

Specimen label	Tested by	Test load (MPa)	Eurocode-4		CECS 28:90		ABAQUS	
			Pu (MPa)	% error	Pu (MPa)	% error	Pu (MPa)	% error
7a	Gardner	1966	1501	-23.65	1760	-10.48	1923	-2.19
7b		1970	1501	-23.8	1760	-10.66	1937	-2.38
8a		1984	1397	-29.58	1601	-19.3	1951	-1.66
1-3Y6	Cheng 1988	1647	1426	-13.42	1817	9.35	1607	-2.4
2-3Y4		1033	856	-17.13	1054	2	998	-3.39
3-3Y3		602	505	-16.11	619	2.74	623	3.37
4-3Y2		334	261	-21.85	312	-6.58	318	-4.79
5-3Y1.5		273	236	-13.55	273	0	284	3.87
S3LA	Sakino 1985	628	600	-4.46	617	-1.75	603	-3.98
S3HA		660	731	9.71	843	21.71	638	-3.33
S6LA		954	923	-3.24	886	-7.13	911	-4.51
S6HA		971	1039	6.54	1120	13.3	924	-4.84

2.3.6 Previous Studies on CFST with UHPC

Liu and Gho [46] studied the axial load behaviour of rectangular concrete-filled steel tubular (CFST) stub columns. They tested a total of 26 specimens under concentric compression. The primary test parameters were material strengths (f'_c = 55-106 MPa; f_y = 300 and 495 MPa) and cross-sectional aspect ratio (1.0–2.0). Through a comparison between design codes of axial load capacity, they observed that ACI and AISC give safe estimation by 7 and 8 and 2%, respectively. In contrast, EC4 overestimates the ultimate capacity of the specimens fabricated from mild steel and high-strength concrete. Moreover, they developed a fiber model to evaluate the axial load behavior of the specimens. Calibration of the model against the test data suggests that it can closely predict the non-linear behavior of high-strength rectangular CFST stub columns.

Ellobody et al. [145] studied the behavior and design of axially loaded concrete-filled steel tube circular stub columns and investigated the effects of different concrete strengths and cross-section geometries on the strength and behaviour of concrete-filled compact steel tube circular stub columns. They examined 40 concrete-filled compact steel tube circular column strengths ranging from 30 to 110 Mpa with different external diameters of the steel tube-to-plate thickness (D/t) ratio ranging from 15 to 70 was achieved using the finite element analysis. Accurate nonlinear material models for confined concrete and steel tubes were used. The column strengths and load–axial shortening curves were calculated. The results obtained from the finite element analysis were verified against experimental results. The column strengths predicted from the finite element analysis were compared with the design strengths calculated using the American, Australian and European specifications. They found that the design strengths given by the American Specifications and Australian Standards are conservative, while those of the European code is un conservative. Reliability analysis was performed to evaluate the current composite column design rules.

Liu [146] explored the behaviour of high-strength rectangular concrete-filled steel tubular columns subjected to eccentric loading throghout experimental and analytical model. He tested four slender and 16 stub CFT columns to investigate their structural behaviour. The test parameters were material strengths (f_y = 495 MPa, f'_c = 60 MPa), cross-sectional aspect ratio (1.0–2.0), slenderness ratio (10 and 60) and load eccentricity ratio (e/H = 0.10–0.42). He observed favourable ductility performance for all specimens during the tests. Experimental failure loads are employed to calibrate the specifications in the design codes EC4, ACI, and AISC. Table 2.6 displayed the comparison of test, codes and the proposed model. EC4 overestimates the failure loads of the specimens by 4% found from the table. ACI and AISC conservatively predict the failure loads by 14% and 24%, respectively. An analytical model is developed to predict the behaviour of high-strength rectangular CFT columns subjected to eccentric loading. Calibration of the model against the test results shows that it closely estimates the ultimate capacities of the columns by 3%.

Yu et al. [147] studied the possibility of using thin-walled hollow structural steel (HSS) columns filled with very high strength SCC. They conducted tests on 28 HSS columns filled with great strength SCC, the main parameters varied are section types, circular and square; slenderness ratio, from 12 to 120; and load eccentricity ratio, from

0 to 0.6. Comparisons are made with predicted column strengths using the existing codes such as AISC, EC4, and DBJ13-51-2003. They concluded that the ductility for very high strength SCC filled steel tubes is smaller than that for normal strength concrete filled steel tubes, in particular for axially loaded columns. Similarly, Comparisons are made with predicted section capacity using the existing codes, such as AISC, EC4 and DBJ13-51 2003. They established that these codes are acceptable for prediction of the member capacities of high strength SCC filled HSS columns. On the other hand, it seems some codes do give slightly higher predictions on the member capacities of columns with square sections.

Table 2.6. Comparison of tests, codes and proposed model [146]

No.	B X H X t (mm)	λ	e (mm)	e/H	Ne (kN)	Ne /Nc			
						EC4	ACI	AISC	Proposed model
S1	120 X 120 X 4	10	15	0.13	1294	1.01	1.13	1.22	1.04
S2	120 X 120 X 4	10	25	0.21	1125	1.01	1.15	1.28	1.05
S3	120 X 120 X 4	10	30	0.25	949	0.93	1.07	1.2	0.96
S4	150 X 100 X 4	10	45	0.38	810	0.92	1.12	1.24	1
S5	150 X 100 X 4	10	15	0.1	1422	1.02	1.13	1.22	1.04
S6	150 X 100 X 4	10	30	0.2	1190	1.03	1.17	1.3	1.07
S7	150 X 100 X 4	10	45	0.3	964	0.97	1.16	1.28	1.04
S8	150 X 100 X 4	10	60	0.4	763	0.88	1.09	1.2	0.96
S9	180 X 90 X 4	10	20	0.11	1491	1.02	1.13	1.23	1.09
S10	180 X90 X 4	10	30	0.17	1319	1	1.13	1.25	1.09
S11	180 X 90 X 4	10	40	0.22	1208	1.01	1.16	1.3	1.12
S12	180 X 90 X 4	10	50	0.28	1051	0.96	1.14	1.26	1.08
S13	130 X 130 X 4	10	15	0.12	1472	0.99	1.12	1.21	1.01
S14	130 X 130 X 4	10	25	0.19	1305	1.01	1.15	1.29	1.05
S15	130 X 130 X 4	10	40	0.31	1022	0.94	1.12	1.26	1.01
S16	130 X 130 X 4	10	55	0.42	789	0.84	1.05	1.17	0.93
L1	150 X 100 X 4	60	15	0.1	1130	0.97	1.21	1.28	1.02
L2	150 X 100 X 4	60	30	0.2	884	0.95	1.21	1.25	1.02
L3	150 X 100 X 4	60	45	0.3	711	0.9	1.17	1.2	1
L4	150 X 100 X 4	60	60	0.4	617	0.89	1.18	1.2	1.01
Mean						0.96	1.14	1.24	1.03
SD						0.06	0.04	0.04	0.05
COV						0.06	0.04	0.03	0.05

Liew and Xiong [148] studied the performance of 27 axially loaded column specimens, comprising 18 steel tubes infilled with ultra-high strength concrete (UHSC) of compressive strength nearly 200 MPa, four steel tubes infilled with normal strength concrete (NSC) and five hollow steel tubes. Steel fibres were added into the

UHSC to study their effect in enhancing the ductility and strength. They also investigated Concrete filled double-tube columns for potential application in multi-storey and high-rise constructions. They revealed that UHSC filled tubular columns achieved ultra-high load-carrying capacities. Nonetheless they could become brittle after the maximum load was attained. Also, the ductility and strength of composite columns infilled with UHSC were improved by applying load only on the concrete core, adding steel fibres into the concrete core or increasing the steel contribution ratio. Comparison of test results with Eurocode 4's predictions indicates that the Eurocode 4 method could be safely extended to predict the compressive resistance of UHSC filled composite stub columns. On average, Eurocode 4 approach underestimated the resistance by 14.6% if the confinement effect was not considered and by 3.5% if the confinement effect has been examined for all the specimens containing UHSC. Nevertheless, to confirm sufficient ductility, it is recommended that a minimum steel contribution ratio of 0.30 or 1% steel fibres should be used.

Liew and Xiong [149] examined the axially loaded ultra-high strength concrete (UHSC) filled single- and double-tubular columns. The UHSC compressive strength is up to 200 MPa. Steel fibres were added to study the effect in enhancing the ductility and strengths. For comparison, normal strength concrete filled steel tubular columns were similarly considered. Test results were compared with the predictions by Eurocode 4 approach. Their results displayed that Eurocode 4 approach underestimates the resistance of UHSC filled steel single- and double-tubular columns by 7.7% and 13.5% respectively when the confinement effect is not considered and by 0.5% and 3.7% when the effect is considered. They concluded that Eurocode 4 approach could be safely extended to predict the plastic cross-sectional resistances of UHSC filled tubular columns. Nevertheless, the steel contribution ratio should be greater than 0.30 or more than 0.5% steel fibres should be added to keep adequate performance in ductility.

Guler et al. [150] examined some performance indices of circular ultra-high-performance concrete-filled steel tube (UHPCFT) columns under monotonic axial compression., Termed concrete contribution ratio (CCR), strength enhancement index (SI) and ductility index (DI), in relation to the diameter-to-thickness ratio (D/t) of the UHPCFT columns were investigated. The obtained axial bearing capacities of the UHPCFT columns compared with Eurocode 4, American Concrete Institute, Australian Standards and Architectural Institute of Japan design codes. They indicated that increasing the steel tube thickness from 2.5 mm to 3.65 mm improves the DI by 69%, but the SI only by 5%.

Lu et al. [151] studied the effects of the concrete strength, the thickness of steel tube and the steel fiber volume fraction on the ultimate strength and the ductility behavior of steel fiber reinforced concrete-filled steel tube columns. They tested 36 specimens, with nine plain UHPC-filled steel tube specimens and 27 UHPFRC-filled steel tube specimens under axial load. Figure 2.43 illustrated Comparisons of axial load−axial shortening responses regarding (a) concrete strength, (b) thichness of steel tube, (c) steel fiber volume fraction. They indicated that the addition of steel fibers in concrete could considerably improve the ductility and the energy dissipation capacity of the concrete-filled steel tube columns and delay the local buckling of the steel tube. They proposed an analytical model to estimate the load capacity for steel tube columns filled with both plain concrete and steel fiber reinforced concrete. Also, they found that the predicted results are in good agreement with the experimental ones obtained in this work and literatures.

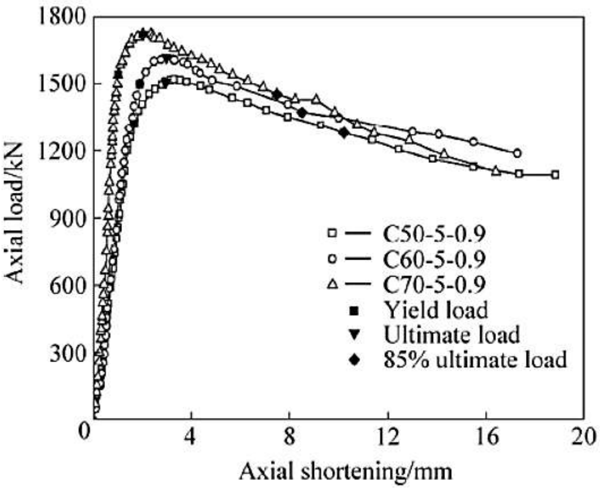

(a)

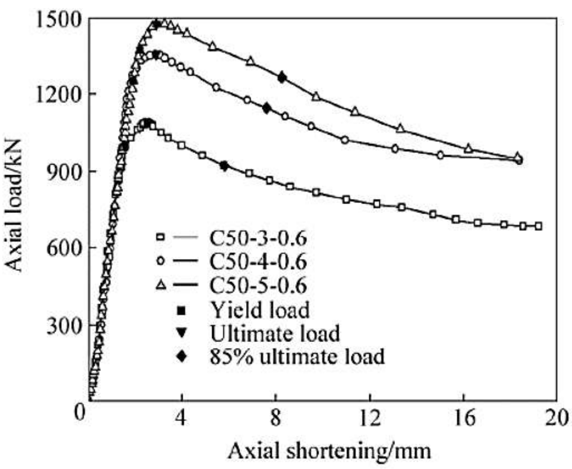

(b)

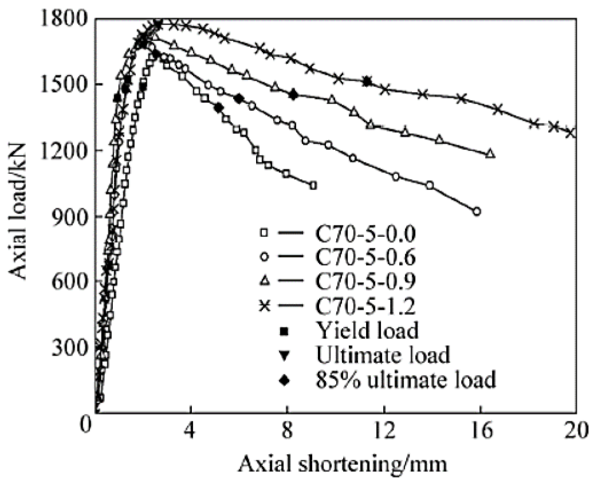

(c)

Figure 2.43. Comparisons of axial load–axial shortening responses regarding (a) concrete strength, (b) thichness of steel tube, (c) steel fiber volume fraction [151]

Zhang et al. [152] explored an investigation on ultra-high performance concrete infilled double-skin tube columns subjected to close-in blast loading on two types of concrete filled double skin tube (CFDST) columns one with both inner and outer tubes circular and the other one with both squares. The main test parameters included the explosive charge weight and the magnitude of the axial load. After the blast tests, they found that there was no visible buckling nor ruptures on the steel tubes and only minor cracks, of no more than 1mm width, in the core concrete when the outer steel tube was removed. Also, it is marked that CFDST column has excellent blast resistance. This feature has the potential to be used in high-value structures which may be the targets of terrorist attacks, such as embassies, government buildings, and critical infrastructures. CFDST columns filled with UHPC can effectively withstand severe blast load without failure. On the other hand, they found that the UHPC filled CFDST can better delay/prevent concrete crushing and steel buckling when compared to normal strength concrete filled CFDST, therefore, have an overall of global flexural response as opposed to localized structural failure, the peak reflected pressures and impulses measured by the pressure transducer yield 18% and 20% error respectively compared to the CONWEP-predictions, the increase in explosive charge weight caused a larger midspan deflection, with this effect being more noticeable on axialload- free specimens rather than axially-loaded specimens And finally the presence of an axial compressive load, corresponding to approximately 20% of the squash load, led to a slight reduction in the peak deflection in two comparative cases.

Zhang et al. [153] observed the residual behaviors of ultra-high performance concrete infilled double-skin steel tubular columns after close-in blast loading of eight CFDST columns, including 3 square ones and five circular ones, under different blast loads with two axial load levels. Next, all CFDST columns were subjected to static axially compressive load until failure. They found that the CFDST columns with smaller permanent displacement had larger peak residual axial capacity and the CFDST columns which were not subjected to axial load during the blast test exhibited more ductile behavior than those which were axially loaded during the blast test as shown in Figure 2.44.

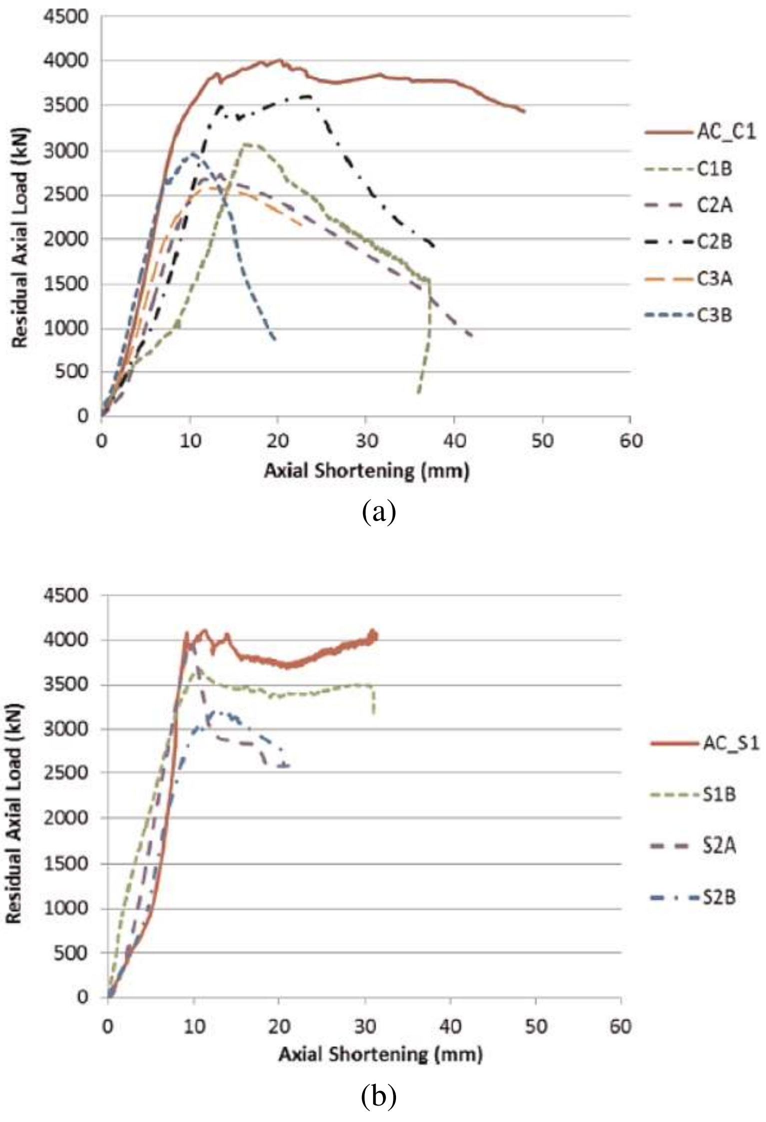

Figure 2.44. The residual axial load vs. axial shortening histories for (a) circular specimens, (b) square samples [153]

Also, they perceived that specimens after the damage indices of all CFDST specimens were less than 0.4, as displayed in Table 2.7. They indicated that the CFDST specimens were able to retain more than 60% of its axial load capacity even after severe blast loading.

Table 2.7. Failure modes of all specimens [153]

Label	Failure modes	Damage index
S1B	Local buckling at ends	0.09
S2A	Local buckling at mid-span	0.01
S2B	Local buckling at mid-span and ends	0.21
C1B	Local buckling at mid-span and ends	0.23
C2A	Outer steel rupture at mid-span	0.32
C2B	Local buckling at mid-span	0.10
C3A	Global flexural failure	0.36
C3B	Outer steel rupture at mid-span	0.38

Xiong et al. [154] considered the behavior of concrete filled steel tubes (CFSTs) subject to flexural loads with high tensile steel and ultra-high strength concrete at ambient temperature. They used high tensile steel with yield strength up to 780 Mpa and ultra-high strength concrete with compressive cylinder strength up to 180 Mpa. The test results seek to clarify if the cross-section plastic moment resistance can be achieved if high tensile steel and ultra-high strength concrete are used in CFST members. The maximum moment resistance from tests was compared with the analytical results predicted by Eurocode 4 method. Then design recommendations were provided so that Eurocode 4 method could be safely extended to determine the flexural resistance of CFST members with high tensile steel and ultra-high strength concrete. In cases where the CFST members are subject to cyclic flexural loading, degradation of flexural stiffness during unloading and reloading occurs when the load level is higher than 0.7. On the other hand, a new database with a total of 78 test data for CFSTs flexural members has been recognized. Similarly, they showed that EC 4 prediction ratios of CFST members with UHSC have higher reliability than those with normal strength concrete and high strength concrete. Conversely, the reliability is lower for the CFSTs made of HTS when compared with those with the mild steel.

Xiong et al. [155] investigated the behavior of CFSTs with high and ultra-high-strength materials at ambient temperature. They obtained the axial performance of 56 short CFSTs through using high tensile steel with yield strength up to 780 Mpa and ultrahigh strength concrete with compressive cylinder strength up to 190 Mpa.

Therefore, experimental and analytical methods were adopted where the test results were compared with the predictions by various design codes world widely, and design recommendations were therefore proposed so that the prediction methods could be safely extended to the short CFSTs with the high- and ultra-high- strength materials. The comparisons of test results with the Eurocode 4 predictions have indicated that the Eurocode 4 method can provide conservative predictions if the confinement effect is not considered and the Class 3 steel sections are not used. The limitations on concrete classes and steel grades could be safely extended for the UHSC with characteristic compressive strength up to 190 MPa and the HTS with yield strength up to 780 Mpa for the short CFST columns, except the double-tube CFSTs with the welded HTS plates.

Moreover, the other codes (AISC 360-10, ACI 318R, AS 4100, AS 3600, AIJ, CISC) gave conservative predictions for the CFSTs with the UHSC and HTS, except AIJ and CISC slightly overestimated the axial resistance in average for the circular double-tubes. However, all design codes over-predicted the resistance for the double-tube CFSTs using HTS. This needs further study. Alternatively, a reduction factor of 0.8 may be adopted for the ultimate axial resistance as shown in Table 2.8.

Kharoob et al. [156] investigated the behavior of beam-high performance fiber reinforced CFST column (beam-HPFR CFST column joints). They tested a total of four exterior joints specimens experimentally. Therefore, moment- relative rotation relationships and their characteristics are evaluated regarding initial stiffness, moment capacities, and ductility. The test parameters are the thickness of the flush end plate and the ratio of the steel fiber. The results are analyzed and compared with the EC3 prediction. From Table 2.9 and 2.10 they showed that the initial stiffness and the maximum deflection of the steel beam increase with increasing the steel fiber ratio. Also, the rotation capacity of beam-HPFR CFST column joints exceeds 0.04 rad and increases up to 0.08 rad by increasing the ratio of fiber. Hence, the ductility of the current joints satisfies the necessary ductility for the seismic provisions for special moment frames AISC, 2010. Finally, the finite element model (FEM) using ABAQUS program is used based on the test geometry. The FEM is verified by comparing with the current experimental results. The FEM model predicts well the complete moment-relative rotation curves for the tested specimens regarding initial stiffness, strength, rotation capacity and maximum vertical displacement of beams. Furthermore, the failure mode of the FE provides good agreement with the experimental results as demonstrated in Table 2.11.

Table 2.8. Comparisons between test results and code predictions for square CFSTs [155]

No.	Ntest (kN)	Npl,Rk1 (kN).	Ntest/Npl,Rk1	Avg.	St.Dev
(a) Hollow HTS tubes (2 data)					
HS1	3695	3828	0.965	1.092	0.180
HS2	6456	5296	1.219		
(b) UHSC filled mild steel single-tubes (5 data)					
S11	5953	5351	1.113	1.139	0.039
S12	5911	5427	1.089		
S13	6039	5269	1.146		
S14	6409	5534	1.158		
S15	6285	5284	1.189		
(c) UHSC filled HTS single-tubes (10 data)					
S1	6536	6428	1.017	1.099	0.055
S2	6715	6511	1.031		
S3	6616	6337	1.044		
S4	7276	6629	1.097		
S5	6974	6354	1.097		
S6	8585	7579	1.133		
S7	8452	7652	1.105		
S8	8687	7500	1.158		
S9	8730	7756	1.126		
S10	8912	7515	1.186		
(d) UHSC filled HTS double-tubes (4 data)					
DS1	7058	7975	0.885	0.908	0.040
DS2	7143	8045	0.888		
DS3	7032	7900	0.890		
DS4	7880	8143	0.968		

Table 2.9. Comparison of moment resistance between the experimental and predicted results [156]

Specimen	$M_{0,Exp}$ [kNm]	$M_{ul,Exp}$ [kNm]	$\theta_{r,ul,Exp}$ [rad]	$M_{u,Rd}$ [kNm]	M_{EC3} [kNm]	$M_{ul,Exp}/M_{u,RD}$	$M_{ul,Exp}/M_{EC3}$
J1	3.5	18.1	0.048	22.19	18.55	0.83	1
J2	4.1	19.2	0.072	23.31	18.55	0.82	1.04
J3	6.06	18.97	0.054	23.59	18.55	0.8	1.02
J4	8.26	20.2	0.08	21.13	18.55	0.96	1.09
Mean						0.85	1.04

Table 2.10. Comparison of initial stiffness between the experimental and predicted results [156]

Specimen	$S_{J,ini,Exp}$ [kN m/rad]	$S_{J,ini,EC3}$[kN m/rad]	$S_{J,ini,Exp}/S_{J,ini,EC3}$	$S_{J,ini,\ mod}$ [kN m/rad]	$S_{J,ini,Exp}/S_{J,ini,\ mod}$
J1	2333	928	2.51	2346	0.99
J2	2844	934	3.05	2390	1.19
J3	14,063	927	15.16	13,351	1.05
J4	14,768	927	15.94	14,992	0.99

Table 2.11. Comparison between the current FE and the experimental results [156]

Specimen	$M_{ul,Exp}$ [kN m]	$M_{ul,FE}$ [kN m]	$M_{ul,FE}/M_{ul,Exp}$	$\delta_{ul,Exp}$ [mm]	$\delta_{ul,FE}$ [mm]	$\delta_{ul,FE}/\delta_{ul,Exp}$
J1	18.1	17	0.94	40	41.2	1.03
J2	19.2	18.8	0.98	65	62.9	0.97
J3	18.97	18.44	0.97	50	47.7	0.95
J4	20.2	19.8	0.98	75	65.9	0.88
Mean			0.97			0.96
Standard deviation			0.014			0.041

Al Zand et al. [157] considered the behavior of various sections of rectangular CFST beams strengthened and/or repaired with unidirectional carbon fiber reinforced polymer (CFRP) sheets and the effects of the U-shaped wrapping scheme using multiple CFRP layers applied at various beam lengths. They demonstrate the cross-sections classification and moments improvement ratio of repairing models. From this table they demonstrated that the moment capacity of strengthened CFST beams increased significantly with increasing CFRP layers; for instance, it increased by approximately 40% and 55% for beams with compact and slender sections, respectively, when wrapped with 4 CFRP layers and the capacity of damaged CFST beams has improved over 65% when repaired with 2 CFRP layers. Furthermore, the effects of wrapping the beam along 75% of its length achieved a similar enhancement ratio and behavior as that of the beam with wrapping along 100% of its length for the same CFRP layers.

CHAPTER 3

METHODOLOGY

3.1 General

The investigational program it has been implemented in present thesis contained two phases. The first is involved of the experimental investigation on UHPC with different types of fibers. After designing the mixture with sufficient flowability, the specimens were tested for evaluating the physical, mechanical, and fracture behavior. In the second phase, the numerical analysis was performed to examine the structural response of the composite columns made of UHPC under the axial compression. To this aim, different diameter to thickness (D/t) ratio and steel tube yield strength as well as the compressive strength of infill UHPC were used in the analysis. The details of the experimental and numerical study are given below.

3.2 Experimental Investigation

3.2.1 Materials

The cement used in this study was Portland cement (PC) (CEM I 52.5 R) conforming to the TS EN 197 [158]. The Blaine specific surface area and specific property are 394 m^2/kg and 3.15, respectively. Commercial silica fume (SF) was used as the supplementary cementitious material. The BET specimen surface area and specific gravity are 21080 m^2/kg and 2.2, respectively the properties of PC and SF are given in Table 3.1. A polycarboxilate-based type superplasticizer (SP) was used to fulfill the workability specifications in ASTM C 494 [159]. Table 3.2 provides the properties of the SP.

Table 3.1. Properties of PC, and SF

Constituent (%)	PC	SF
CaO	62.12	0.45
SiO_2	19.69	90.36
Al_2O_3	5.16	0.71
Fe_2O_3	2.88	1.31
MgO	1.17	-
SO_3	2.63	0.41
K_2O	0.88	1.52
Na_2O	0.17	0.45
Cl	0.0093	-
Loss on ignition	2.99	3.11
Insoluble residue	0.16	-
Free CaO	1.91	-

Table 3.2. Properties of SP

Properties	Results
Appearance	Light brown to yellow liquid
Specific gravity at 20°C	1.08 ± 0.02 gm/cm^3
PH- value	7 ± 1
Alkali content (%)	≤ 1
Chloride content (%)	≤ 0.1

A commercial quartz aggregate with a specific gravity 2.65 was utilized in three fractions, namely 0-0.4, 0.6-1.2, and 1.2-2.5 mm. Figure 3.1 shows the three sizes of the aggregate used. To provide fiber reinforcement, micro steel brass coated (MSF), hooked end steel (HSF), and micro glass (MGF) fibers were used were used at different volume fractions. The properties of the fibers are presented in Table 3.3.

Figure 3.1. Sizes of Quartz aggregates

Table 3.3. Physical, mechanical properties and aspect ratios of fibers

Fiber name	Length (L) (mm)	Diameter (d) (mm)	Aspect ratio (L/d)	Density (g/cm ^{3})	Tensile strength (N/mm^2)
Micro steel	6	0.16	37.5	7.17	2250
Hooked steel	30	0.55	55	7.85	1345
Micro glass	13	0.018	722	2.6	2000

3.2.2 Mixture Proportioning

The mixture design consisted of three groups of concretes UHPFRC, each of which contains six mixes accounting for 0.25, 0.5, 0.75, 1, 1.5 and 2% of micro steel fiber, hooked steel fiber, and micro glass fiber, respectively. The control UHPC was also produced with a w/b ratio of 0.195 and 1200 kg/m^3 of total binder. SF was used at 20% of PC by weight in all of the mixes. The slump flow of the mixes was almost constant which was achieved by using SP in varying amounts. To keep the SP demand in a reasonable dosage, a relatively high w/b ratio of 0.195 was adopted. The mixtures in Table 3.4 were designated according to the fiber type (MSF, HSF, and MGF) followed by the fiber volume fraction. For example, MSF0.25 indicates the mixture containing 0.25% of micro steel fiber.

Table 3.4. Mixture design of UHPFRC

Group	Mix no.	PC (kg/m^3)	SF (kg/m^3)	Water (kg/m^3)	SP (kg/m^3)	Fiber (kg/m^3)	Quartz aggregate (kg/m^3)	Fresh density (kg/m^3)
	Control	960.0	240.0	234.0	45.0	0.0	793.7	2273
1	MSF0.25	960.0	240.0	234.0	45.0	17.9	787.1	2284
	MSF 0.5	960.0	240.0	234.0	45.0	35.9	780.5	2295
	MSF 0.75	960.0	240.0	234.0	45.0	53.8	773.8	2307
	MSF 1	960.0	240.0	234.0	45.0	71.7	767.2	2318
	MSF 1.5	960.0	240.0	234.0	45.0	107.6	754.0	2341
	MSF 2	960.0	240.0	234.0	45.0	143.4	740.7	2363
2	HSF0.25	960.0	240.0	234.0	45.0	19.6	786.4	2285
	HSF 0.5	960.0	240.0	234.0	45.0	39.3	779.2	2297
	HSF 0.75	960.0	240.0	234.0	45.0	58.9	771.9	2310
	HSF 1	960.0	240.0	234.0	45.0	78.5	764.7	2322
	HSF 1.5	960.0	240.0	234.0	57.0	117.8	720.7	2330
	HSF 2	960.0	240.0	234.0	57.0	157.0	706.2	2354
3	GF0.25	960.0	240.0	234.0	45.0	6.5	791.3	2277
	GF 0.5	960.0	240.0	234.0	45.0	13.0	788.9	2281
	GF 0.75	960.0	240.0	234.0	42.0	19.5	793.9	2289
	GF 1	960.0	240.0	234.0	39.0	26.0	798.8	2298
	GF 1.5	960.0	240.0	234.0	78.0	39.0	698.3	2249
	GF 2	960.0	240.0	234.0	96.0	52.0	649.3	2231

The mixtures were prepared using a vertical axis, high speed Hobart type mixer (see Figure 3.2a) with a mixing speed of as high as 470 rpm. Firstly, dry powders and aggregates were mixed at 100 rpm for about 3 min as shown in Figure 3.2b. After adding half of water, the mixture was remixed for about 5 min at 100 rpm, and the situation of the mixture was like Figure 3.2c. The SP and remaining water were added to the premixed material, and mixing was resumed at 470 rpm for about 3 min. Finally, fibers added to the fresh UHPC for additional 2 min for completing production of UHPFRC as illustrated in Figure 3.2d then Fresh concretes were poured into the molds and compacted by using a vibrating table.

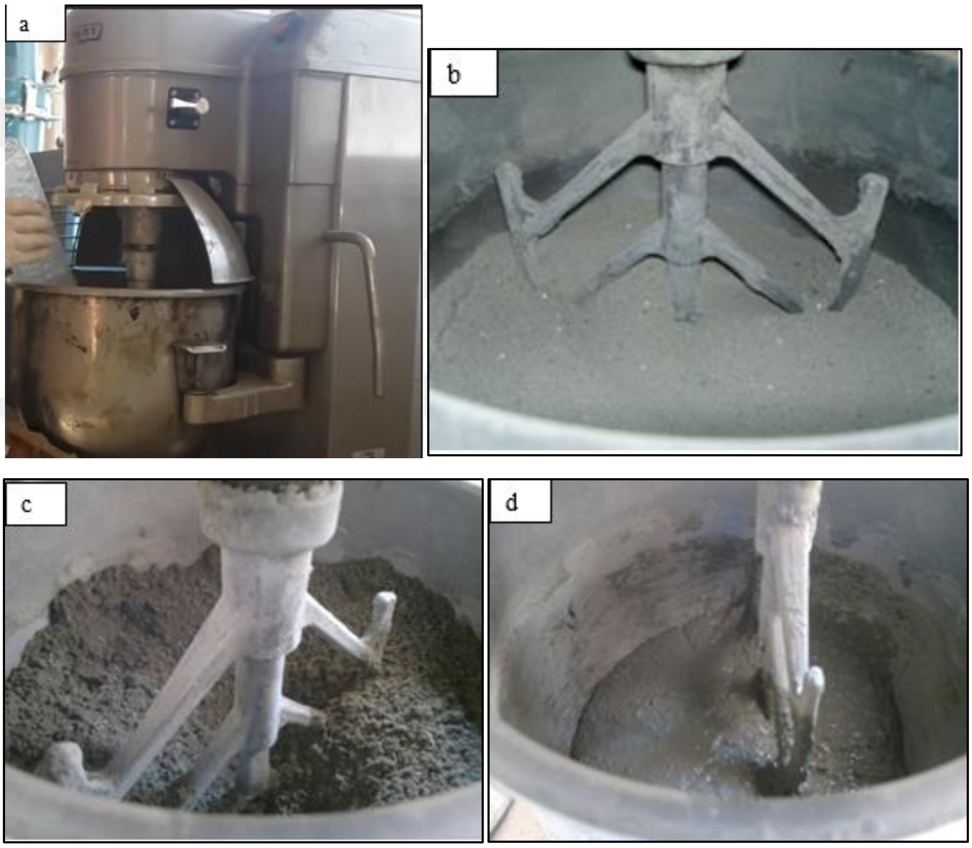

Figure 3.2. Procedure of producing UHPFRC

The specimens were covered with polyethylene sheets and kept in the molds for 16 h at room temperature of 22 ± 2 ºC. After that, they were cured in standard conditions of water curing until the testing age (Figure 3.3a). On the other hand, the models for the drying shrinkage, weight loss, restrain shrinkage measurements were subjected to air-dry after demolding at 23 ± 2 °C and 50 ± 5% relative humidity until the end of the drying period (Figure 3.3b). However, the process for autogenous shrinkage test is different; a Teflon sheet was placed inside the mold to avoid the restraint of concrete from the frictional force between UHPFRCs and the molds. The top surface of the specimen was sealed with the polyester film once the mold was filled totally to avoid moisture evaporation. After 16 hours, specimens were molded instantaneously, wrapped with aluminum adhesive tape to guarantee the equivalent constant temperature, and simulating humidity room. Sealed samples are demonstrated in Figure 3.3c.

(a) Water cured samples

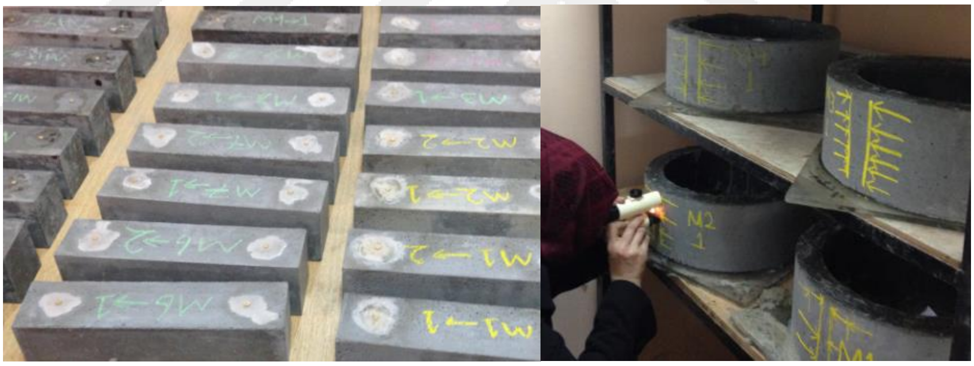

(b) Dry curing samples for dry shrinkage and restrain shrinkage

(c) Sealed curing for autogenous shrinkage

Figure 3.3. Conditioning of samples

3.2.3 Testing Procedures

3.2.3.1 Tests on Fresh Property

The mini-slump flow test was used to measure the flow of UHPFRC using recommended by EFNARC [160] (see Figure 3.4). After fresh UHPFRC poured to the mini cone and the cone was lifted straight upwards to allow the fresh on the plate, the flow value of the designed concrete was calculated as the average of two measured diameters of the mixture. The UHPFRC mixes had flow values that organized by using a suitable amount of superplasticizer, as presented in Table 3.4.

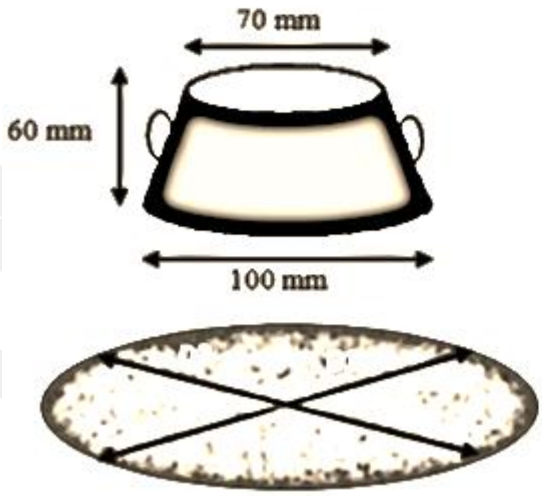

Figure 3.4. Mini-slump flow test

3.2.3.2 Mechanical Property

Compression test was conducted on 50 and 100 mm cubes at 7, 28, 56, 90, and 180 days with respect to ASTM C39 [161]. A digital testing machine of 3000 kN capacity at a rating load of 0.9 kN/s was used. The average of three samples in this study is presented for each result. Splitting test of UHPFRCs was performed on 100 mm cubes at 28 days at a rating load of 0.2 kN/s as per ASTM C496 [162]. The test was implemented on three samples for each mixture. Static modulus of elasticity was determined on 150 mm cubes at 28 days in accordance with ASTM C469 [163]. For this, the cube specimens were loaded and unloaded three times up to 40% of the ultimate load which was determined from the compression test. The first set of the readings from each cube was discarded, and the elastic modulus was reported as the average of the other two sets of readings.

3.2.3.3 Fractural Property

Fracture energy or work of fracture is a measure of indirect surface energy for the cementitious materials [164]. The test was carried out in accordance with the recommendation of RILEM 50-FMC/198 Technical Committee [165]. As shown in Figure 3.5a, Instron 5500R closed-loop testing machine with a maximum capacity of 250 kN was used to apply the load while the displacement was measured simultaneously by using a linear variable displacement transducer (LVDT) at the mid-span. Figure 3.5b shows the notched beam sample in which the effective cross section was reduced to 42 x 70 mm via a diamond saw to accommodate large aggregates in more abundance so that the notch to depth ratios (a/W) being 0.4. According to RILEM [165], the fracture energy, GF, of a single edge notched beam is calculated under three point bending as:

$$G_F = \frac{W_o + mg\delta_s \frac{S}{U}}{B(W-a)} \tag{3.1}$$

Where W_o is the area under the load - deflection curve; m is the mass of the beam; g is the acceleration due to gravity; δ_s is the specified deflection of the beam, while S, U, B, W, and a are span, length, width, depth, and notch depth of the beam, respectively. For each mixture, at least three specimens were tested at 28 days.

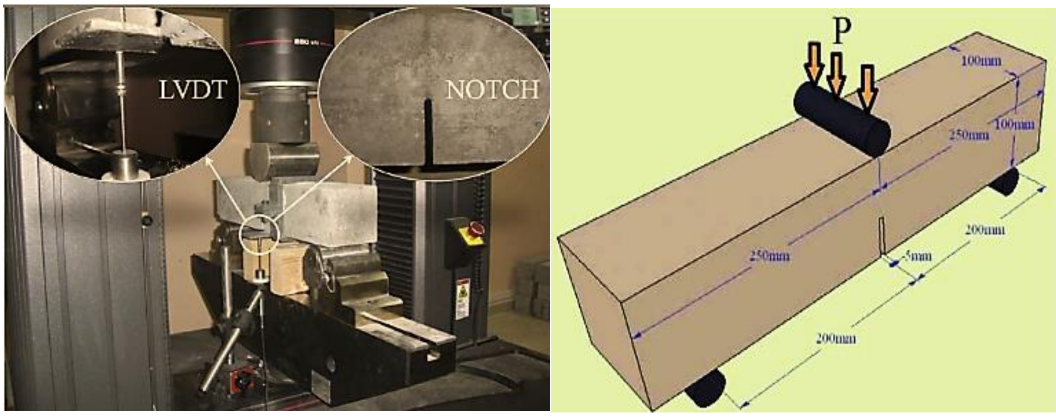

Figure 3.5. Beam under three point bending

In according to the literature, the net flexural strength, f_{flex}, was calculated via Eq. (3.2) by assuming no notch sensitivity. All the beams were loaded at a constant rate of 0.02 mm/min.

$$f_{flex} = \frac{3P_{max}S}{2B(W-a)^2} \tag{3.2}$$

where the P_{max} being the ultimate load by assuming no notch sensitivity [166, 167].

The characteristic length (l_{ch}) as a measure of ductility was computed using Eq. (3.3) as a function of the modulus of elasticity (E), fracture energy (G_F), and splitting tensile strength (f_{st}) [168].

$$l_{ch} = \frac{EG_F}{f_{st}^2} \tag{3.3}$$

3.2.3.4 Physical Property

In order to monitor the drying shrinkage, four 70x70x280 mm prisms were used with respect to ASTM C 157 [169] (Figure 3.6). As soon as the prisms were demolded, the gage length was fixed by gluing the reference pins on the face of each specimen. The change in gauge length was measured via a dial gauge extensometer, which had a gauge length of 200 mm and strains sensitivity of 0.002 (see Figure 3.7). Measurements were taken at every 24 h for the first three weeks and then three times a week. Meanwhile, weight loss was measured on the identical prism.

Figure 3.6. Drying shrinkage prism

Like the dry shrinkage, unless, before concrete casting, inside of the molds were covered with two layers of thin plastic sheets. After keeping the molds under a polyethylene sheet for about four hr setting, the stainless steel studs were fixed on the samples using a thin layer of adhesive, and the sidewalls were de-molded.

Figure 3.7. Length change measuring device

Thereafter, each specimen was resealed using another layer of plastic sheet and two layers of aluminum foil using adhesive tape (Figure 3.3). The measurements were taken over a 200 mm gage length by a dial gauge extensometer with an accuracy of 0.002 strain [170]. Autogenous shrinkage of the concretes was measured on four 70x70x280 mm prisms.

The restrained shrinkage caused by cracking of UHPFRC implemented by ring specimens, the ring mold dimensions are presented in Figure 3.8. The concrete was directed to an internal force made by the restraining internal steel cylinder. The value of the radial pressure was 20% of the maximum hoop stress. While the variance between the values of the tensile hoop pressure on the external and internal sides of the concrete was reached 10%. Therefore, it can be expected that the concrete collar was in essence exposed to a uniaxial, uniform tensile pressure due to inner restrained via the mold steel ring. A uniform shrinkage along the width of the specimen can be presumed because the thickness of the sample (35mm) was equal to a quarter of its width (140mm) [171-174]. In this study, three ring samples used to conclude the shrinkage made cracking of UHPFRCs manufactured. Restrained shrinkage samples cured for 4 hours in the same way of dry and autogenous shrinkages prisms, and then the outside steel ring has been demolded. For allowing the dry shrinkage is drying only from the outside peripheral surface, the highest surface of the concrete ring sealed using silicon elastic. Then, all specimens faced to drying in a room at a temperature of 23 ± 2°C and relative humidity of 50 ± 5%, as per ASTM C157 [169] for 60 days. A special microscope was used to measure the crack widt mens [172, 173]. The average of 3 readings was monitored: the two centers and bottom halves and the middle of the ring. The readings performed after cracking for every 24 hours at the first seven days, then each 48 hours.

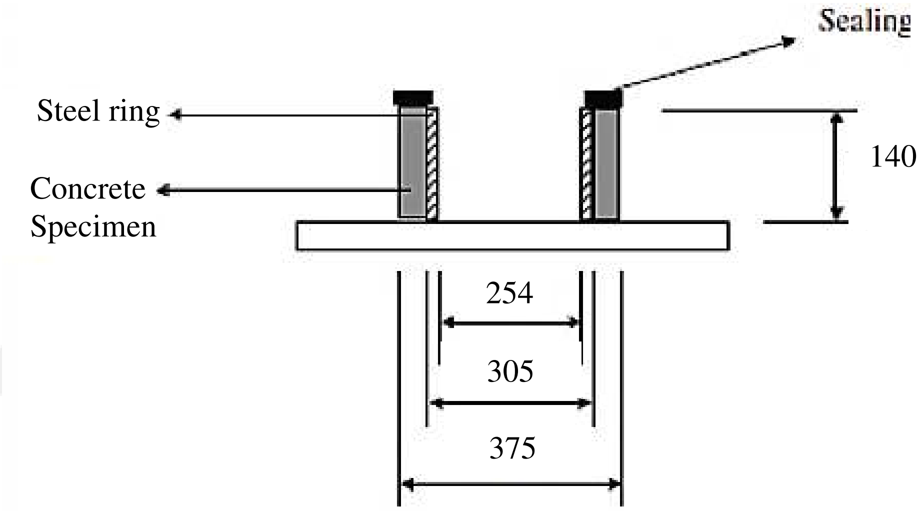

Figure 3.8. Restrained shrinkage dimension of ring specimen (in mm)

3.3 Numerical Analysis

3.3.1 Methodology of Applications of UHPFRCs into CFST columns

The type of loading application as shown in Figure 3.9, was used in whole 50 mm experimental cube samples, where the concrete and steel tube are loaded at the same time. In which; t is the wall thickness of the steel tube, D is the external diameter, and L is the length of the CFST column. On the other hand, Table 3.5 illustrates the key investigation parameters of fiber contents, testing age, measured specimen dimensions of circular concrete pilled steel tube (CFST) columns, and relatively short length of specimens (L/D) were used to guarantee that they would be short columns with a small slenderness effect and would not fail in overall buckling. The conversion relations between different dimensions of compressive strength regulated in Table 3.6 that proposed by the researchers [175-177].

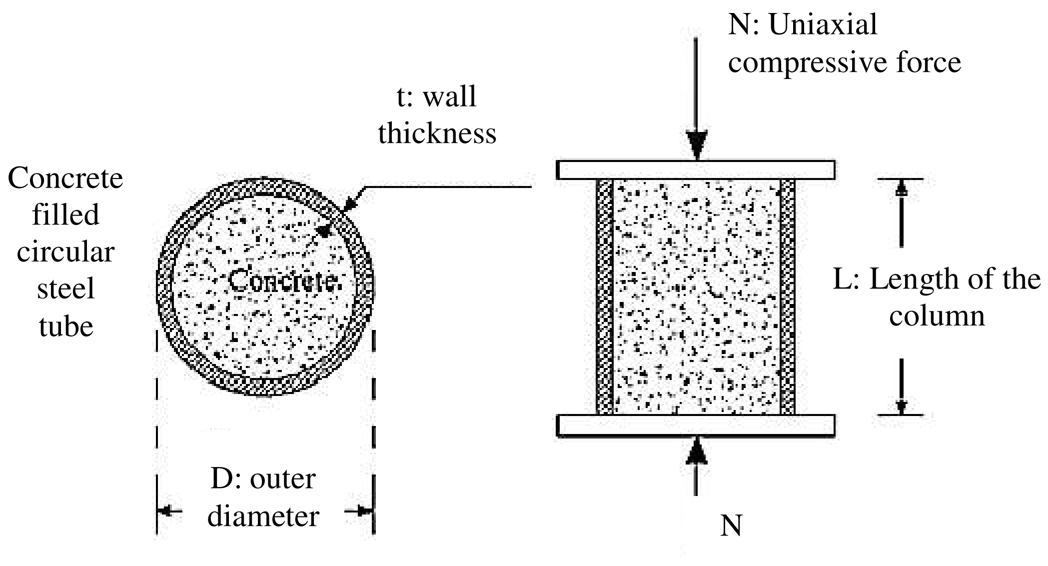

Figure 3.9. Illustration of load applied to the circular CFST columns

Table 3.5. Fiber contents, testing age, and measured specimen dimensions of circular CFST short columns

Fiber amount (%)	0, 0.25, 0.5, 0.75, 1, 1.5, and 2
Testing age (days)	7, 28, 56, 90, and 180
D (mm)	90, 180, and 270
t (mm)	3
f_y (MPa)	300, 450, and 600
L/D ratio	2.5

Table 3.6. Transformation factors for various type and size of specimens for compressive strength

References	Specimen type and size	Conversion factor
Skazlic et al. [175]	Cylinder, (70x 140/100 x200)	1.05–1.15
	Cylinder, (150 x 300/100 x 200)	0.85–0.95
Graybeal and Davis [176]	Cylinder 76/cube 100	1
	Cylinder 76/cube 71	0.94
	Cylinder 76/cube 51	0.96
	Cylinder 76/cylinder 102	1.01
Kazemi and Lubell [177]	Cube, (50/100)	1.09
	Cube 50/cylinder 100	1.14
	Cube 50/cylinder 50	1.09

3.3.2 Axial Capacity of CFST Short Column Formulas

A brief calculation of the axial capacity of CFST short columns using the methods described in the international codes is presented as follows. In whole design calculations, the material partial and resistance factors are set to one.

3.3.2.1 Eurocode 4

The Eurocode 4 (EC4) [178] determines the resistant capacity of a circular CFST short column by adding the contribution of the concrete core and steel tube with the consideration of confinement effect. Because the hoop stresses decrease the effective yield stress of the steel, the strength of the steel tube is also reduced by dint of n_a. In addition, due to higher strength once a triaxial state of stress occurs, the strength of the concrete is raised via coefficient n_c. The axial load capacity is calculated by Eq. 3.4.

$$N_u = \left(1 + n_c \frac{t}{D} \frac{f_y}{f_{c-,150}}\right) f_{c-} + n_a f_y A_s \tag{3.4}$$

In which

$$n_c = 4.9 - 18.5\gamma^{-} + 17\gamma^{-2} \qquad (n_c \geq 0) \tag{3.5a}$$

$$n_a = 0.25(3 + 2\gamma^{-}) \quad (n_a \leq 1.0) \tag{3.5b}$$

$$\lambda^{-} = \sqrt{\frac{N_{pIR}}{N_{cr}}} \tag{3.5c}$$

$$N_{pIR} = f_y A_s + f_{c-} A_c \tag{3.5d}$$

$$N_{cr} = \frac{\pi^2 (EI)_{eff2}}{l^2} \tag{3.5e}$$

$$(EI)_{eff2} = E_s I_s + K_e E_{c2} I_c \tag{3.5f}$$

$$E_{c2} = 22000\ [(f_c + 8)/10]^{0.3} \tag{3.5g}$$

Where, n_a is the coefficient of confinement for the steel tube, n_c is the coefficient of confinement for the concrete, *l* is buckling length of the CFST column, λ^{-} is relative slenderness, K_e is a correction factor which is equal to 0.6, $(EI)_{eff2}$ is the effective flexural stiffness for calculation of relative slenderness, and E_{c2} is elastic modulus of concrete.

Essentially, when $\lambda^{-} = 0$, the zero length strength (the sectional capacity), N_o can be shortened as:

$$N_o = \left(1 + 4.9 \frac{t}{D} \frac{f_y}{f_{c-,150}}\right) f_{c-,150} A_c + 0.75 f_y A_s \tag{3.6}$$

3.3.2.2 American Concrete Institute (ACI)

The ACI 318 [179] used the following method for calculating the ultimate axial capacity (N_u) of the circular CFST for short columns. This specification has not taken into account the interaction between the concrete core and steel tube nor the concrete confinement. The equation for the axial capacity of a circular CFST short column, N_u (ACI=AS), is given as:

$$\mathrm{N_u} = 0.85 f_C^{-} A_c + f_y A_s \tag{3.7}$$

Where; A_s is the cross-sectional area of the steel tube and A_c is the cross-sectional area of the concrete.

3.3.2.3 American Institute of Steel Construction (AISC)

For the circular CFST short columns, the AISC [180] allows for an increase of the usable concrete stress to account for the beneficial effects of the restraining hoop action arising from transverse confinement. This is accomplished by increasing the multiplier of the first term of Eq. (3.7) from 0.85 to 0.95. Therefore, the cross-sectional strength, $P_{o,\ AISC}$ is given by;

$$\mathrm{P_o} = 0.95 f_C^{-}\ A_c + \ f_y A_s \tag{3.8}$$

In reality, P_o; AISC is the nominal, zero length strength (i.e., the plastic capacity of the section). Therefore, the nominal axial capacity of a circular CFT stub column, N_{AISC} included with length effects is computed by;

$$N_u = P_o \left[0.658^{\left(\frac{P_o}{P_e}\right)} \right] \quad (P_e \geq 0.44\ P_o) \tag{3.9}$$

Where P_e is the elastic buckling load. According to AISC [180], P_e is given by;

$$P_e = \frac{\pi^2 (EI)_{eff1}}{(K_A L_A)^2} \tag{3.10a}$$

In which

$$(EI)_{eff1} = E_s I_s + C_3 E_{c1} I_c \tag{3.10b}$$

$$C_3 = 0.6 + 2\left(\frac{A_s}{A_c + A_s}\right) \leq 0.9 \tag{3.10c}$$

K_A = the effective length factor; L_A = laterally unbraced length of the column; I_s and I_c = moment of inertia of steel tube and concrete core, respectively; E_{c1} = the modulus of elasticity of concrete = 4730 (f′c, 150)$^{1/2}$ MPa (normal weight concrete); and $(EI)_{eff1}$ = effective stiffness of composite section.

3.3.2.4 Architectural Institute of Japan (AIJ)

According to AIJ [181, 182], the ultimate compressive strength of an axially loaded circular CFST short column, N_{AIJ} is calculated by Eq. (3.11).

$$N_u = 0.85 f_{c-,100} A_c + (1.0 + n) f_y A_s \quad (l_k/D \le 4) \tag{3.11}$$

Where l_k = effective length of a CFST column; and n = the confinement factor = 0.27.

According to Eq. (3.11), the improvement of load carrying capacity due to the composite action is denoted by the confinement factor n, which is independent of the strength of the materials and the dimensions of the columns.

3.3.2.5 Chinese Code DL/T

The Chinese code [183] for axially loaded concrete filled steel circular columns treats the composite section as one material with the corresponding nominal yielding strength of f_{scy} and a total area of A_{sc}. A confinement factor (ξ) is presented to define the composite action between the filled concrete and the steel tube. The equation of axial load capacity of circular CFST columns is specified by:

$$N_u = f_{scy} A_{sc} \tag{3.12}$$

In which

$$A_{sc} = A_s + A_c \tag{3.13a}$$

$$f_{scy} = (1.212 + B\xi + C\xi^2) f_{ck} \tag{3.13b}$$

$$B = 0.1759 \frac{f_y}{235} + 0.974 \tag{3.13c}$$

$$C = -0.1038 \frac{f_{ck}}{20} + 0.0309 \tag{3.13d}$$

$$\xi = \frac{A_s f_y}{A_c f_{ck}} \tag{3.13e}$$

$$f_{ck} = 0.67 f_{cu,150} \tag{3.13f}$$

Where ξ the confinement factor; A_{sc} = the area of composite section; f_{scy} = the "nominal yielding strength" of the composite section; and f_{ck} = the characteristic concrete strength.

CHAPTER 4

4.1 RESULTS AND DISCUSSION ON EXPERIMENTAL STUDY

4.1.1 Analysis of Mechanical Behavior

4.1.1.1 Compressive Strength

Effects of fiber type on the compressive strength of the UHPCs reinforced with micro steel, hooked steel, and micro glass fibers are presented in Figure 4.1a, b, and c, respectively. Moreover, Figure 4.1d presents the percent increase in the 28-day compressive strength of the concretes. It was observed that the compressive strength of concretes continuously grown in the case of steel fiber reinforced UHPCs while the strength increment ended at 1.5% of glass fibers, irrespective of the testing age. In addition, the growth of compressive strength after 56 days seemed to be quite limited as there was little enhancement at 90 and 180 days, irrespective of fiber types. Such phenomenon was possibly because of the acceleration of chemical reactions due to 20% silica fume used. Beyond 1.5% of micro glass fiber, compressive strength began to decrease so that adding 2% of micro glass fibers lessened the 180-day compressive strength by about 3%. Finally, the test results suggested an order of micro steel fiber, hooked steel fiber, and micro glass fiber considering their beneficial effects on the compressive strength. Therefore, micro steel fibers seemed to be more preferable than hooked steel fibers and micro glass fibers. Indeed, UHPCs with 2% of micro steel fibers had the highest compressive strength of 182 MPa at 180 days which reduced to 177 MPa for 2% hooked fiber reinforced UHPC and to 172 MPa for 1.5% of micro glass fiber reinforced UHPC. The preference micro steel fibers over the others are probably more regular and systematic distribution of such fibers within the concrete as seen in Figure 4.2a, b, and c. Similarly, Yoo and Yoon [34] reported that the compressive strength was higher by about 15% when the fibers are incorporated. In their study, the highest compressive strength was obtained for the concretes with 30 mm long twisted steel fibers. A similar finding was observed in the study of Yu et al. [184] in that the use of 2% micro steel fibers (0.16 mm diameter and 6 mm long) increased the compressive strength from 99 to 120.8 MPa indicating a strength enhancement by as much as 22%.

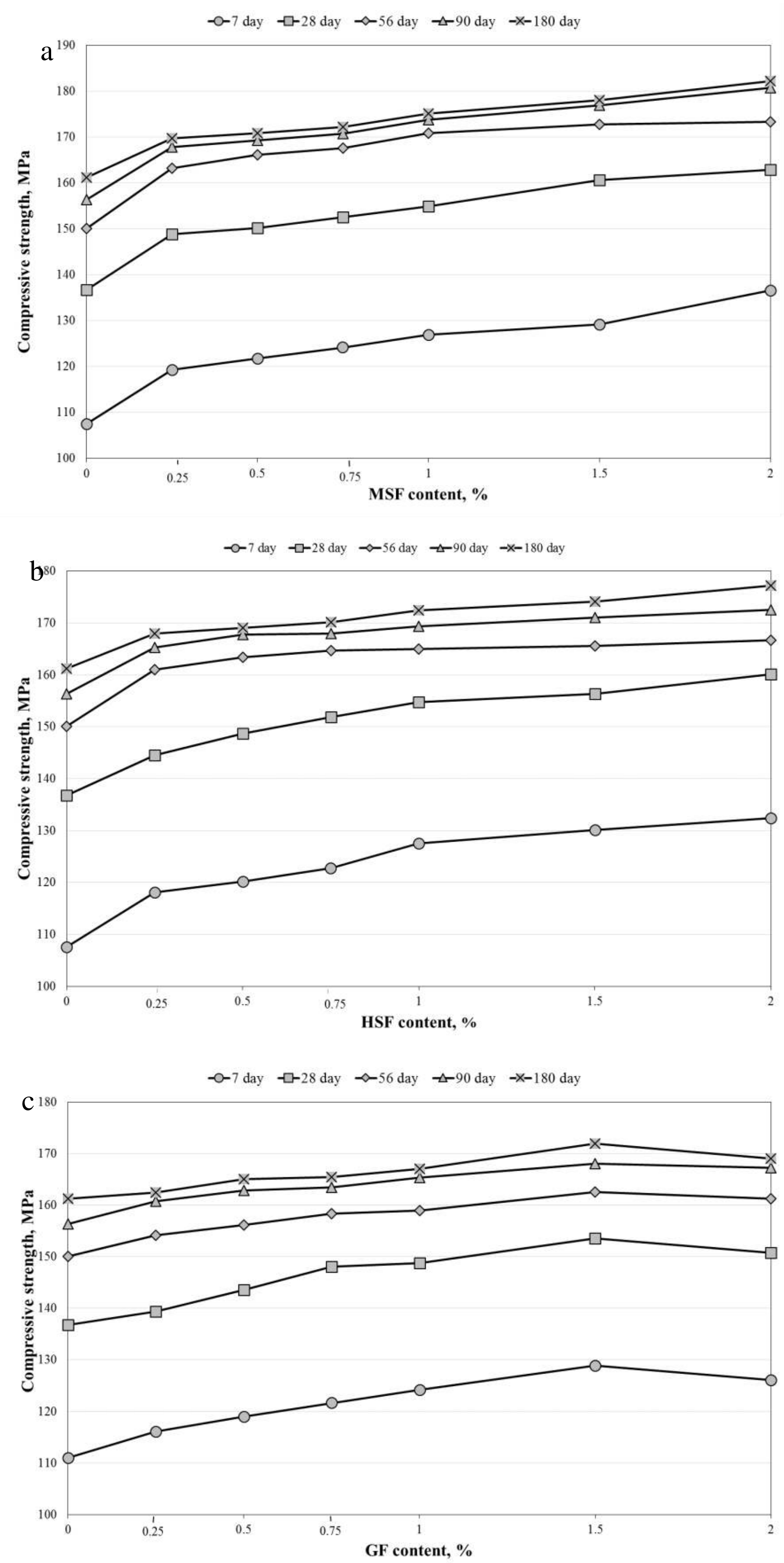

7 day
28 day
56 day
90 day
180 day
a
Compressive strength, MPa
MSF content, %
b
Compressive strength, MPa
HSF content, %
c
Compressive strength, MPa
GF content, %

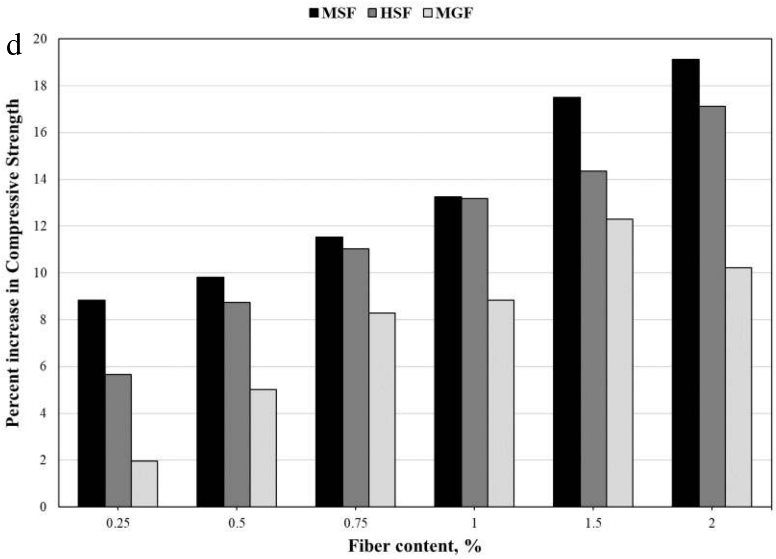

Figure 4.1. Compressive strength development vs fiber content: (a) MSF, (b) HSF, (c) MGF, and (d) Percent increase in 28-day strength

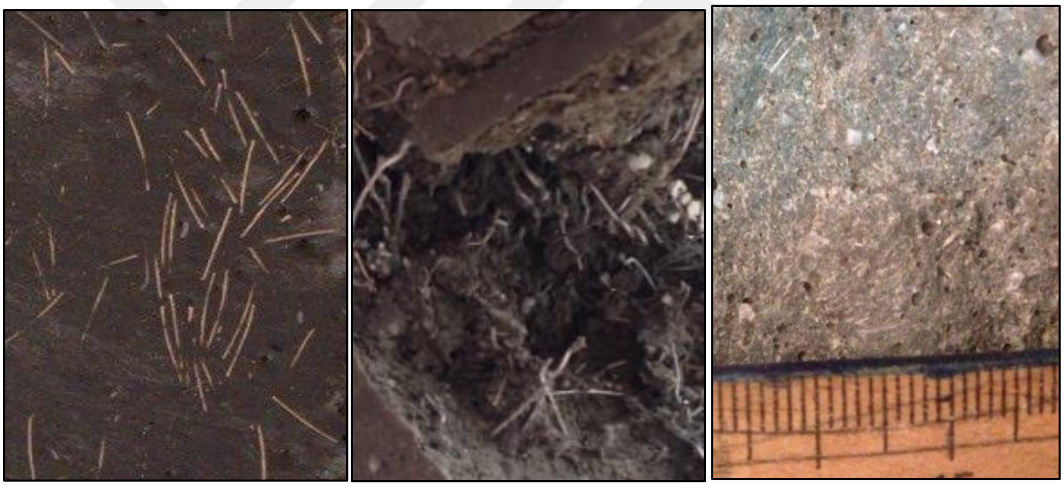

(a) Micro Steel Fiber (b) Hooked Steel Fiber (c) Micro Glass Fiber

Figure 4.2. Fiber distribution within UHPCs

Effects of fiber type and cubic size effects on the compressive strength of UHPCs reinforced with micro steel, hooked steel, and micro glass fibers at 90 days are presented in Figure 4.3 for 50 and 100 mm^3 cubes. Among the UHPFR concretes it was observed that compressive strength continuously increased for the steel fibers. Unless at 2 % of micro glass fiber the compressive strength decreased by about 1-2% for the both size groups. However, the 2% UHP micro steel fiber reinforced concretes showed the highest value of compressive strength, irrespective of the specimen size. This may be attributed to the huge number of micro steel fibers restricted micro before converting to macrocracks. The reduction in compressive strength of 2% can be attributed to; the dispersion of the cementations particles by micro glass fiber more than an optimized volume (1.5%) and to the higher volume of voids that effect on the strength of concrete [185].

Regardless of fiber types, UHPFRC made with small size specimens showed higher strength results than their corresponded bigger sizes. For example, the compressive strength of 50mm^3 results greater than same concrete but with 10mm^3 cube dimensions by 11% for the UHPC contained 2% of micro steel fibers, i.e. MSF2 mixture. In addition to the present study on increasing strengths of UHPFRC by decreasing size, other researchers like Dehestani et al. [186] increased the compressive strength of self-compaction concrete (SCC) from 51.3 to 80.1 MPa by reducing the height of cylinder from 100mm to 25mm. Whereas, Hamad [187] improved the 28-days compressive strength of normal concrete by 27.5% when the cube sizes decreased from 150mm^3 to 50mm^3. Those findings agree with Griffith Theory [188], which indicated that the failure of the specimen would be in the zone of cracking. Decreasing in the section area of specimen accompanied by declining stresses then the failure delayed [75].

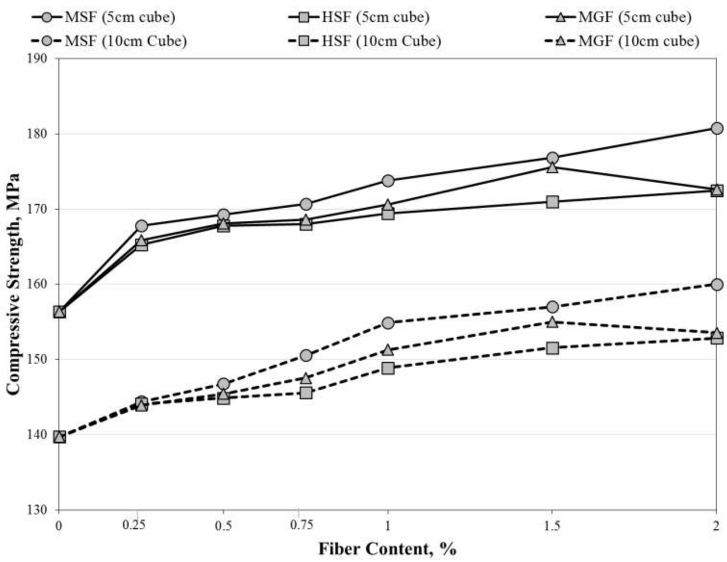

Figure 4.3. Compressive strength vs. fiber content at 90 days with different cube sizes

4.1.1.2 Splitting Tensile Strength

The tensile strength of concrete is necessary to determine the load as being responsible for cracking in members because concrete is very weak in tension due to its brittle nature. The splitting test is the simplest indirect way of measuring the tensile strength of concrete. The load values are monitored till the crack on the sample has been detected although there would be further increased in the load due to bridging effect of the fibers in the concrete [189].

Influence of fiber type and fiber volume fractions on the splitting tensile strength at 28 days is presented in Figure 4.4a. Moreover, the percent increase in the strength values is depicted in Figure 4.4b. In general, the addition of the fibers improves the splitting tensile strength of the concretes. This is because the fibers can bridge tensile cracks then retarding the propagation, and transmitting stress across a crack as well as restricting crack growth [190]. Using 0.25, 0.5, 0.75, 1, 1.5 and 2% of micro and hooked steel fibers seemed to enhance the splitting tensile strength by 3.97, 6.92, 12.06, 13.57, 15.97, and 16.79% for the former and 2.42, 5.47, 8.05, 9.84, 12.06 and 12.45% for the latter group of concretes, respectively. Furthermore, considering the concrete group reinforced with glass fibers, splitting tensile strength increased up to 1.5% of fiber volume, thereafter strength started to decrease. Nevertheless, the concretes with 0.25, 0.5, 0.75, 1, 1.5 and 2% of the glass fiber had greater strength by about 2, 4, 6, 7, 10, and 8%, respectively, compared to that of the plain concrete.

The greater tensile strength of the concretes reinforced with micro steel fiber is attributed to the mechanism of fiber orientation. Owing to its quite smaller aspect ratio than the hooked steel fiber and its higher density than the glass fiber, micro steel fibers have a propensity to align in the stream direction and better orientation [191]. The superior tensile strength of the concretes with micro steel fibers was also explained by Yu et al. [184]. Short fibers can bridge micro-cracks more efficiently, because they are very thin and their number in concrete is much higher than that of the long steel fibers, for the same fiber volume.

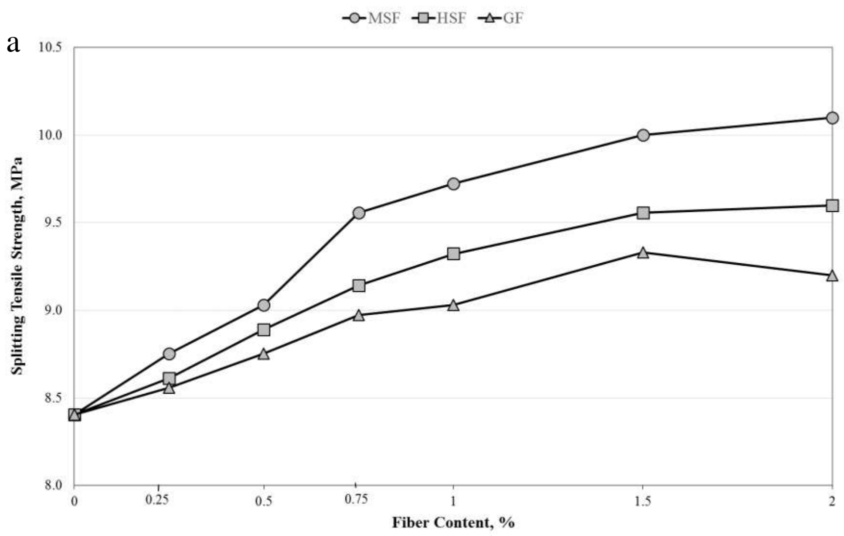

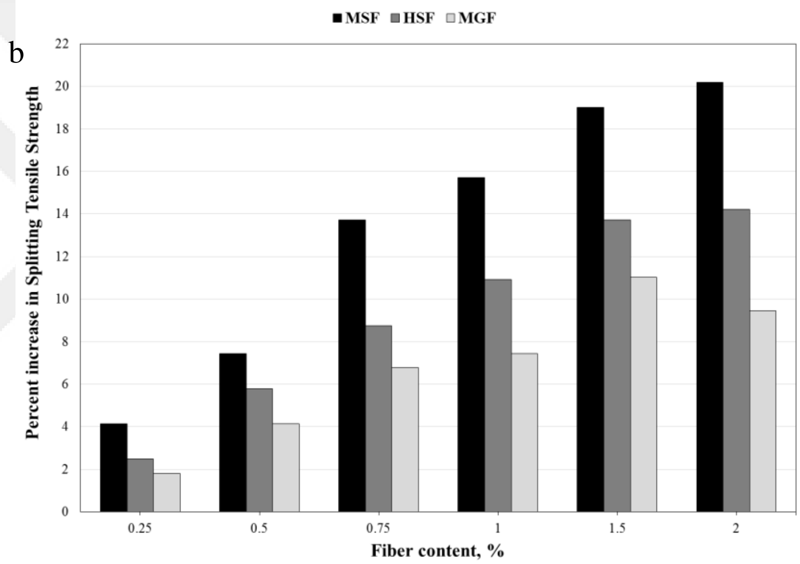

Figure 4.4. a) Splitting tensile strength of UHPFRCs vs. fiber content and b) percent increase in the tensile strength

4.1.1.3 Elastic Modulus

The static elastic moduli of UHPCs at 28 days with different fiber types and contents are demonstrated in Figure 4 5. The behavior herein was considered similar to that seen in the compressive strength. It was observed in Figure 4.5 that the effect of using fibers was to increase the elastic modulus of UHPC. The increasing tendency continued and reached the maximum when the mixtures contained 2% of micro or hooked steel fibers. The rise in the modulus at this fiber content was 12.56 and 9.54% for the former and the latter, respectively when compared to the reference concrete. However, in the case of concrete with glass fibers, the maximum was achieved at

1.5% fiber volume accounting for a 7.41% enhancement. Again, at 2% glass fiber content static elastic modulus began to decrease.

In this study, it is observed that the glass fibers have dismantled during mixing with the other concrete constituents to form fibers with varying lengths as shown in Figure 4.6. However, it seems like there is a demand point for these particles to distribute inside UHPC, after that dismantled glass fibers may work as a lubrication region to cause a slippage between the aggregate over each other.

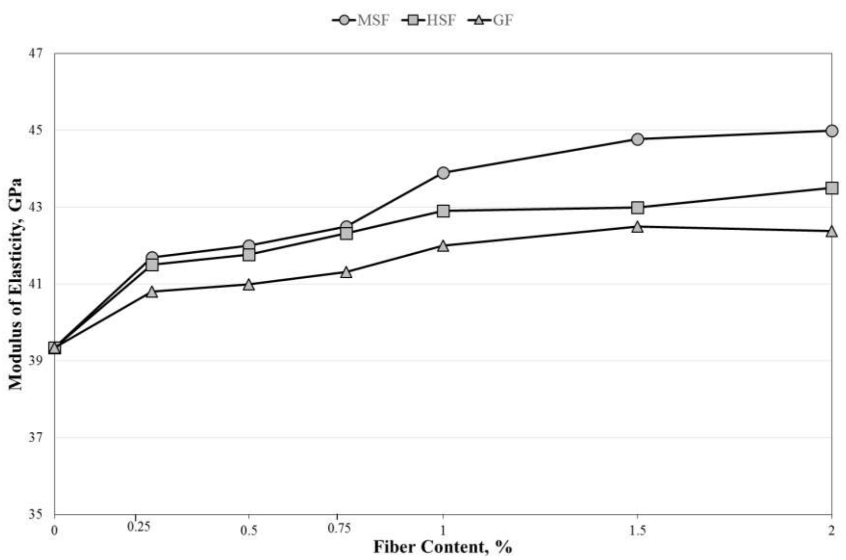

Figure 4.5. Elastic moduli of UHPFRCs vs. fiber content

Figure 4.6. Capillary micro glass fiber within UHPC before and after addition

4.1.2 Analysis of Fracture Behavior

4.1.2.1 Modulus of Rupture Under Three-Point Bending

The flexural strength or modulus of rupture of UHPCs reinforced with micro steel, hooked steel, and micro glass fibers under three-point bending are presented in Figure 4.7a. Also, the percent increase in the strength values at 28 days are depicted in Figure 4.7b. The results of this study well agreed on the previous research on enhancing the flexural strength of UHPCs as fibers were used especially at higher volume fractions [192, 193]. After cracking of the matrix, the fibers carry the load until the interfacial bond between the fibers and the matrix has lost. Arresting the crack by the fibers prevent the sudden failure, thus resulting in increasing the load carrying capacity [194, 195]. Moreover, increased fiber volume in the vicinity of the crack may lead to much more effective stress transfer across the crack [196]. Regarding the effect of fiber type on the flexural strength, unlike compressive and splitting tensile strengths, hooked steel fiber seemed to be more effective on this concrete property than the micro steel and micro glass fibers. Also, the micro steel fibers were least favorable on enhancing the flexural strength. Indeed, regardless of fiber volume, the maximum net flexural strength of the concretes were 14.2, 10.8, and 8.2 MPa for the hooked steel, micro glass, and micro steel fibers, respectively. As the fibers have been used, the rise in the flexural strength is well explained in Figure 4.8 considering the crack arresting mechanisms of the fibers, especially macro cracks by hooked steel fibers and micro cracks by micro steel or glass fibers. Moreover, despite the same working mechanism for stopping micro cracks seen in Figure 4.8, the performance of glass fiber was superior, compared to micro steel fiber, probably owing to the varying fiber length of the former (see Figure 4.6) by which more cracks would be arrested. The high performance of hooked fibers over the micro steel and glass fibers is attributed to the fact that the hooked steel fibers can bridge cracks and retard their propagation that could change the fracture behavior of concrete from brittle to plastic and then considerably raise the ultimate flexural strength of UHPFRC [197].

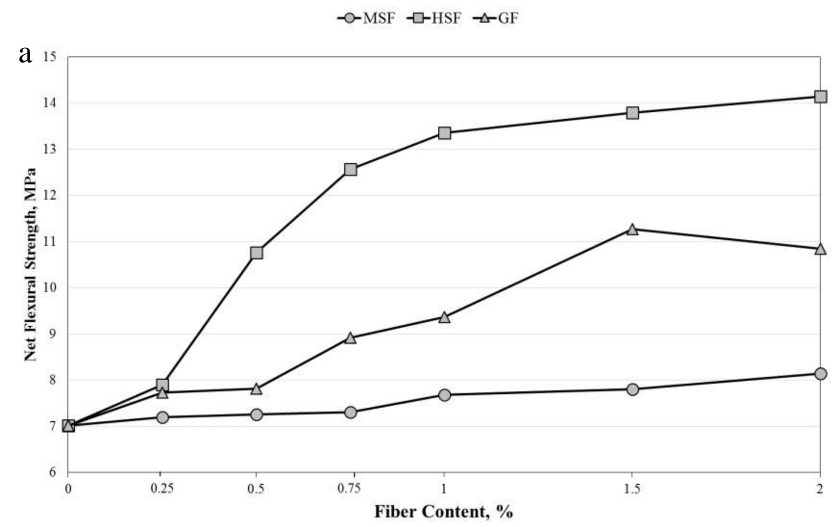

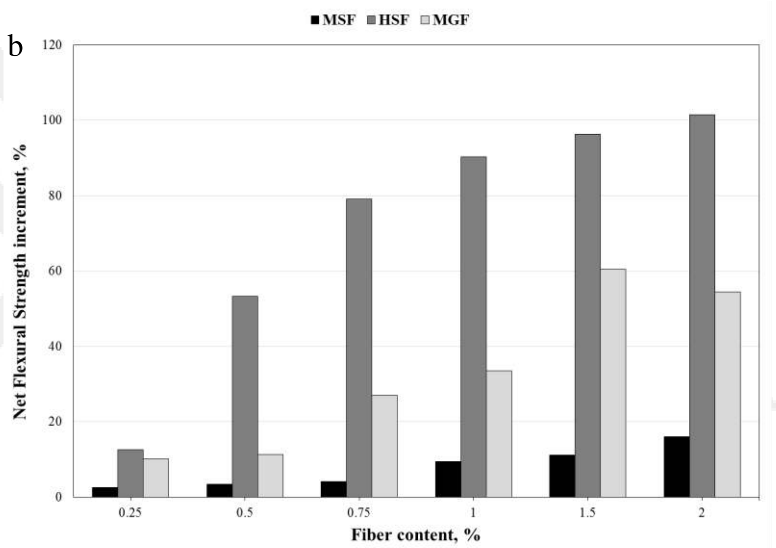

Figure 4.7. a) Flexural strength of UHPFRCs vs. fiber content and b) percent increase in the flexural strength

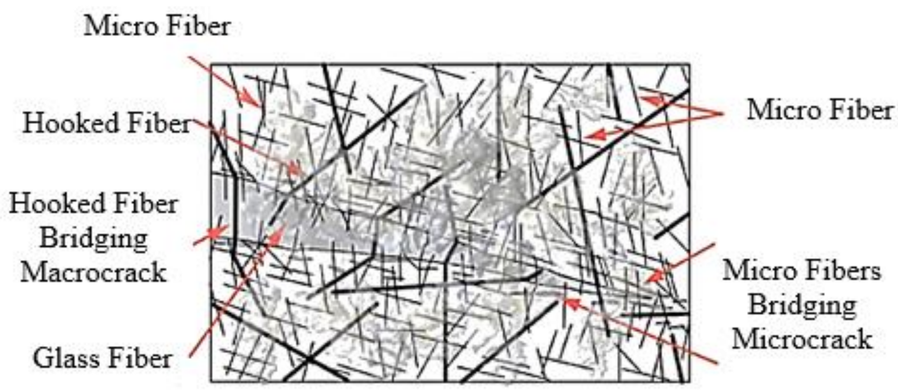

Figure 4.8. Effect of hooked fiber, microfiber, and glass fibers on UHPCs

4.1.2.2 Fracture Energy

In the present work as shown in Figure 4.9, the total fracture energy of UHPC at 28 days depends on two critical parameters, namely fiber type and fiber volume fraction. It was noticed that the UHPC with hooked steel fibers gave the highest fracture energy followed by micro steel and micro glass fibers, respectively. Precisely, adding 2% of micro steel, hooked steel and micro glass fibers to plain UHPCs led to enhancement by as high as 101, 601, and 50 order of the fracture energy that the plain concrete has, respectively. The remarkable superior performance of hooked steel fiber is attributed to its nature with hooked ends as well as bigger diameter and length. So, they can catch the sides of macrocracks and increase the energy required to fracture the beams. It is also important to notice that the load quickly drops after reaching the peak load in the case of short fibers. This should be attributed to the fact that the short steel fibers are less effective in bridging the macro-cracks and cannot provide a stable post-peak response. As the micro-cracks grow and merge into larger macro-cracks, the long steel fibers become more and more active in crack bridging. In this way, primarily the ductility and partly the flexural strength associated with the fracture energy can be improved. Long fibers can, therefore, provide a stable post-peak response [184].

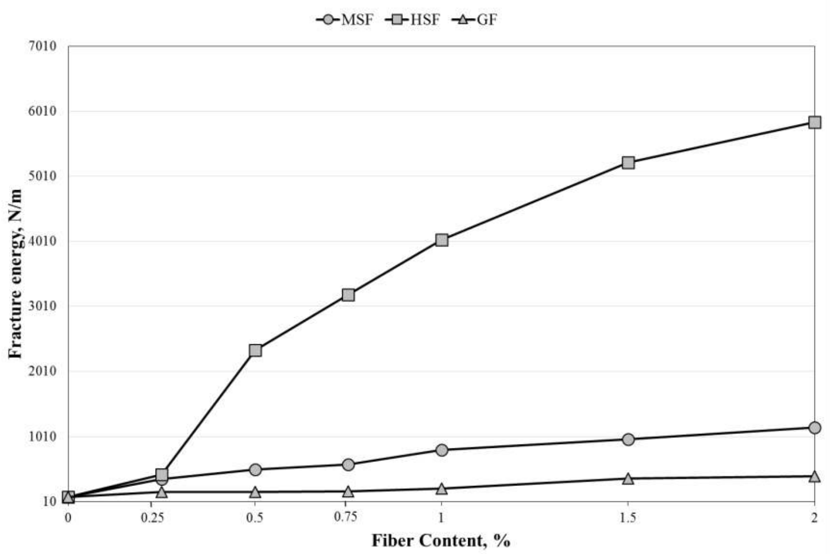

Figure 4.9. Fracture energy vs. fiber content of UHPFRCs

To evaluate the brittleness of UHPC, the characteristic length (l_{ch}) computed via Eq. (3.3) is a proper parameter because of the smaller the l_{ch}, the further brittleness the material. Fracture energy, modulus of elasticity, and tensile strength influenced the characteristic length of UHPCs as the two prior being direct whereas the latter being inversely proportional to this value. The variation in the characteristic length of UHPCs reinforced with micro steel, hooked steel, and micro glass fibers is presented in Figure 4.10 which well agreed on the tendency seen in the fracture energy. Consistent with the increase in the fracture energy at 28 days as seen in Figure 4.9, adding 2% of micro steel, hooked steel, and micro glass fibers let to higher characteristic length by as high as 47, 280 and 20 times, respectively compared to the reference concrete. Indeed, by adding micro steel, hooked steel, and micro glass fibers the maximum characteristic length was recorded as 469, 2790, and 200 mm, respectively. Particularly, the concretes with hooked steel fibers experienced a strain hardening behavior leading to substantial ductility.

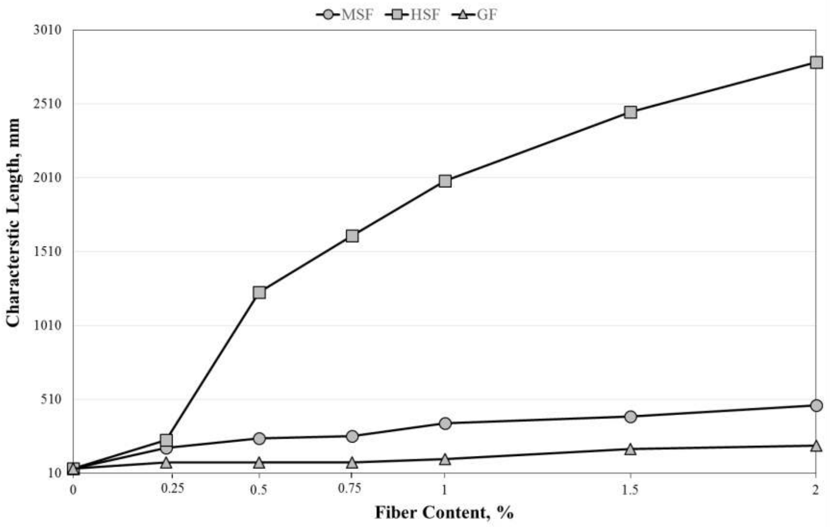

Figure 4.10. Characteristic length vs. fiber content of UHPFRCs

4.1.2.3 Load–Displacement Curves

The typical load–deflection curves for the plain concrete (no fiber) can be mainly divided into elastic section and strain softening section as shown in Figure 4.11. Whereas adding fibers brought strain hardening section to concrete (see Figure 4.12). The load-displacement curves for the notched UHPC beams with 0, 0.25, 0.5, 0.75, 1.0, 1.5, and 2% of micro steel, hooked steel, and micro glass fibers are shown in Figures 4.13-4.15, which covering the pre-peak, post-peak, peak load, area underneath the curve, maximum displacement phases. It can be noted that the general shapes of curves due to hooked steel fibers are entirely different from the others by extending more displacement against applied loads. While micro steel fibers were different by showing zigzagged curves at the post peaked region. On the other hand, it can also be noted that the fiber reinforcement index which is a function of a number of fibers available for a given concrete area is more for low modulus glass fibers compared to steel fibers, regardless of their sizes. This possibly reveals that, upon crack propagation, the stress-balancing occurs at 95% of the ultimate load due to matrix cracking and further instability after peak load resulting to a great crack width could not possibly be bridged by a low modulus of micro glass fibers. This behavior of micro glass fiber are eventually seen as a sudden drop in a load-displacement curve which exactly like a magnification of plain UHPC, i.e. control mixture, as clearly noticed in Figure 4.15. In addition, due to dismantling properties of glass fibers (see Figure 4.6), the visual and failure pattern of the specimens of plain and 2% glass reinforced UHPC were the same or little different, as illustrated in Figure 4.16.

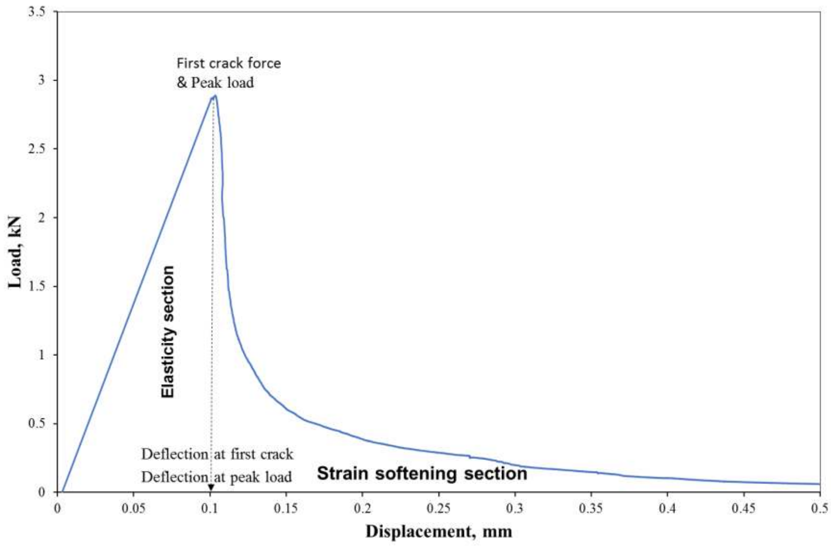

Figure 4.11. Typical load vs. displacement curve for the plain UHPC

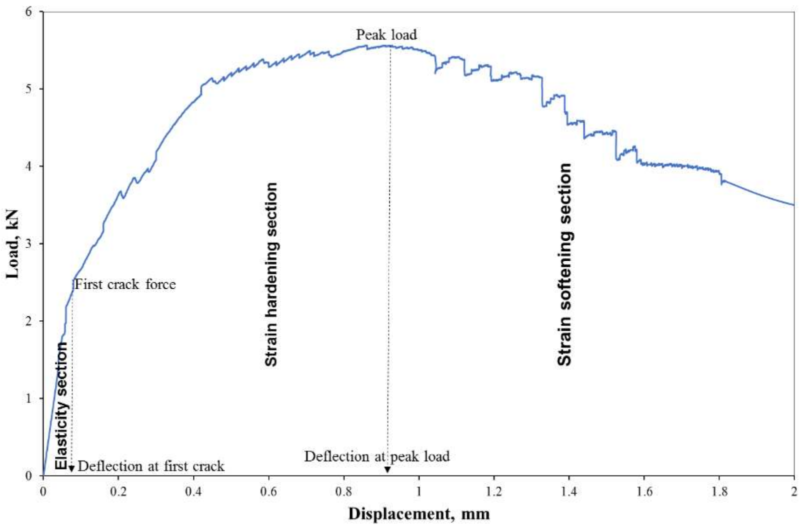

Figure 4.12. Typical load vs. displacement curve for UHPFRC

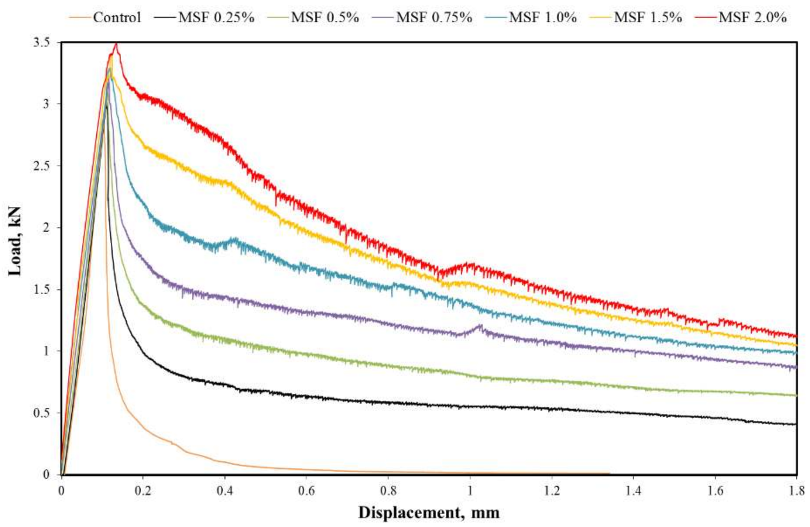

Figure 4.13. Load vs. displacement curves of UHPC with respect to MSF contents

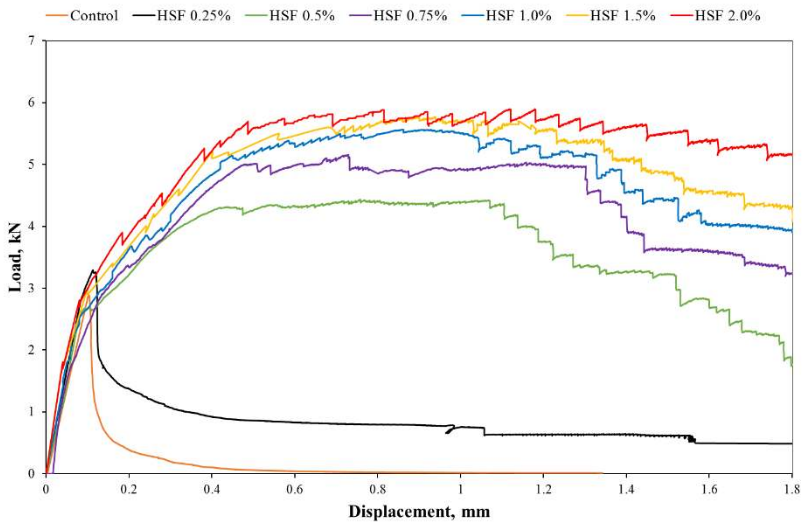

Figure 4.14. Load vs. displacement curves of UHPC with respect to HSF contents

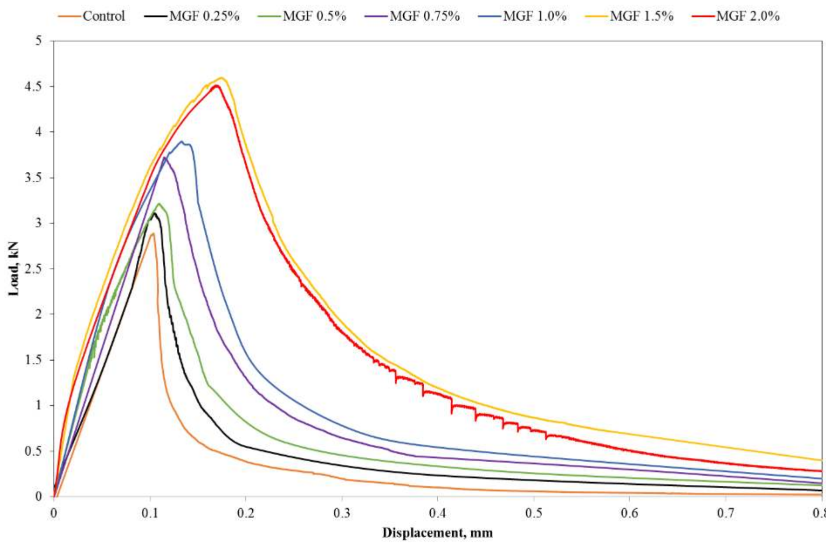

Figure 4.15. Load vs. displacement curves of UHPC with respect to MGF contents

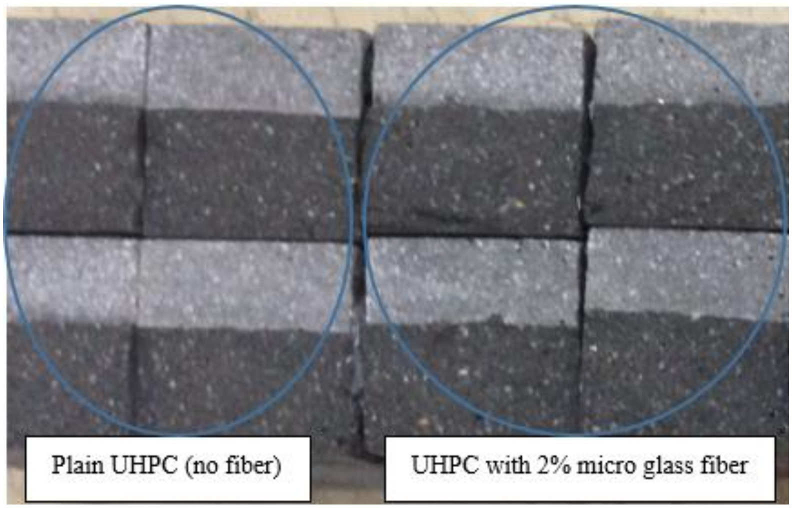

Figure 4.16. Failed plain and reinforced UHPC beam specimens

4.1.2.4 Absolute Toughness

Absolute toughness as defined by the total energy absorbed before complete separation of the specimen is given by the area under the load-deflection curve. Toughness or energy absorption of concrete is increased considerably by the addition of fibers. The toughness is calculated as the area under the load-deflection curve [198]. Table 4.1 presents the area underneath the load-displacement curve (toughness), as well as peak load of the notched UHPC beams with 0, 0.25, 0.5, 0.75, 1, 1.5, and 2% of micro steel, hooked steel, and micro glass fibers. Absolute toughness and cracking behavior of UHPFRC is primarily influenced by the type and the dosage of fiber although there is a clear enhancement of the volume content of fibers increase. These also presented in Figures 4.13, 4.14, and 4.15, as a number of fibers increased from 0% to 2%, all series shows an increasing trend in toughness. Additionally, other authors showed favorable effects on both tensile strength and strain capacity via incorporating fibers to concrete [29]. Additionally, among different UHPFRCs (see Table 4.1), the mixture containing 2% long hooked steel showed the highest toughness value of 17141 N.m. This may be due to most notably the longer fibers proved to be efficient in bridging all cracks, i.e. micro and macro cracks, that resulting to a great area under the load-deformation curve and significantly yielding a higher toughness value. In addition, macro fibers made a high bond strength and a longer length that increased stress transfer performance even after initiating the first crack, but, microfibers (micro steel and micro glass fibers) can’t work well for bridging crack surfaces on the macro level. Furthermore, it can be justified that the fiber matrix is better enhanced in the case of long hooked fibers which showed synergistic interaction in the high strength matrix. This can be stated from the fundamental mechanics that the fiber matrix interface is influenced by the longer length of fiber due to that there is a corresponding crack bridging stress as shown in Figure 4.8. Also, the crack bridging stress is a function of a number of fibers available at the crack front and dependent on the fiber modulus.

On the other hand, Lawler et al. [199] studied the effect of the micro steel fibers with the diameter less than 0.022 mm and macro steel fibers using the diameter over 0.5 mm. They stated that a concrete reinforced by microfibers presented higher toughness compared with concrete which reinforced by macro fibers. They concerned these behaviors to the delay of macrocracks formation due to microfibers, which directs the higher toughness of concrete.

4.1.2.5 Strain Hardening Section (Prepeak Region)

From the beginning of the test until the moment when the first crack appears, the linear section part of the curve can be observed. After the first crack appears, the strain hardening section starts, and some small cracks generate in the tested beam. In this process, the fibers in concrete will mainly endure the load and limit the growth of the generated cracks, until the peak load appears. Subsequently, the fibers pulled, and the slope of the pre peak region of the curve faced to some extent, related to fiber type and content. Among the mixtures as demonstrated from Figures 4.13-4.15, UHFRC with hooked steel fibers has highest strain hardening part, while microfibers have limited or less effect on the strain hardening region. This may because of macro fibers has a higher aspect ratio and tensile strength than micro steel and micro glass fibers, respectively, which resulted in superior load-displacement properties [200].

Table 4.1. Absolute toughness and peak load of UHPC

Fiber Type	Fiber Content (%)	Area under the curve (N.m) "W_o"	Peak load (kN)
Control	0	201.2	2.9
Micro steel fiber group	0.25	1005.9	3.0
	0.50	1425.3	3.0
	0.75	1656.9	3.0
	1	2325.8	3.2
	1.50	2790.5	3.2
	2	3319.6	3.4
Hooked steel fiber group	0.25	1200.1	3.3
	0.50	6839.7	4.4
	0.75	9341.5	5.2
	1	11807.2	5.5
	1.50	15297.3	5.7
	2	17141.0	5.8
Micro glass fiber group	0.25	438.2	3.1
	0.50	455.9	3.2
	0.75	480.7	3.7
	1	590.6	3.9
	1.50	1036.7	4.6
	2	1143.7	4.5

4.1.2.6 Peak Load

At the beginning of the bending test, the plain UHPC matrix can withstand the amount of load called first crack load (Figure 4.11), but the fibers inside UHPCs would become more active and sustain the rest of the force named as peak load (Figure 4.12). However, when the fibers and UHPC matrix could not stand more applied load, the first crack appeared and the maximum load simultaneously reduced. The further load above first crack force is may attribute to the potential energy due to fibers that imparted in delay fracturing the beam [201]. Subsequently, the fibers pulled out and the slope of the pre-peak region as well as the post-peak of the curve exposed to an extent. It was observed from Table 4.11 that the peak load of mixtures continuously increased with increasing fiber content. For instance; adding 2% of micro steel, hooked steel, and micro glass fibers improved the peak load of plain UHPC (Control) by 17.2, 100, and 55.2%, respectively. Thus, hooked steel fiber seems to be more preferable than glass and micro steel fibers.

The reason for promising results with the concretes containing micro glass fiber compared to the micro steel fiber may be attributed the dismantled nature of glass fibers as they have marked higher aspect ratio than micro steel fibers in addition to more improvement of ITZ by glass fibers.

4.1.2.7 Strain Softening Section (Post Peak Region)

After the peak load, the softening phase began and its slope continuously changed as more fibers were pulled out or fractured, along with a drop in the load carrying capacity. The tickling sound was detected during the softening phase due to pulling out of fibers or fracturing. It was observed that the length of the softening phase for the tested specimens made with the short fibers, i.e. micro steel and micro glass fibers, was smaller and exhibited a steeper drop in load carrying capacity since short fibers can easily debond from the matrix because of their smaller embedment length. Conversely, UHPFRC mixes incorporating long fibers (namely; hooked steel fibers) had more improved strain-softening (post-peak) behavior. Furthermore, the load-displacement curve for segments incorporating long fibers exhibited a relatively steadier load drop after reaching peak load, unlike the steeper load drop for segments made with short fibers. This is due to the increase in the energy required for de-bonding longer steel fibers.

Moreover, increasing the fiber content resulted in taller post-peak load, regardless of the fiber length. This can be attributed to the fact that at higher fiber content fibers are more closely spaced. Thus, they can better inhibit the coalescence of microcracks into macro-cracks. This delay of macrocrack propagation increases the load carrying capacity and the associated ultimate strain, as reported in the previous studies [23, 26]. Therefore, the mixed with fibers offered remarkably long tails especially this observed with hooked steel then followed by each of micro steel and micro glass fibers, respectively. Moreover, the improvements of plain UHPC that reinforced by each of micro steel, hooked steel, and micro glass fibers can be explained like; First, the tail of load displacement curve is cut at displacement that are 10, 20, and 2 times larger than the maximum displacement for Control UHPC by adding 2% of MSF, HSF, and MGF, correspondingly, whereas, 10 to 20 times recorded by the study of Vandewalle [202]. These can be attributed to the two reasons. Firstly, the micro steel fibers can efficiently bridge the micro-cracks, whereas as the micro-cracks grow and turn into to macro-cracks, the hooked steel fibers will take all activity in bridging the cracks. However, as the crack width increases, micro steel fibers become less active because they were pulled out, as illustrated in Figure 4.17. Secondly, hooked long steel fibers are always well oriented between the two borders of molds during casting of concrete as displayed in Figure 4.18. Therefore, such fibers are located in the direction parallel to the direction of the loading to enhance the shape of load-displacement curve as reported in the literature [184]. Wille et al. [27] prepared an investigational study on the performance of UHPC mixtures incorporated by four different types of steel fibers. They established that deformed steel fibers enhanced post-cracking strains more than smooth steel fibers.

Figure 4.17. Failure state in MSF reinforced UHPC after fracture energy test

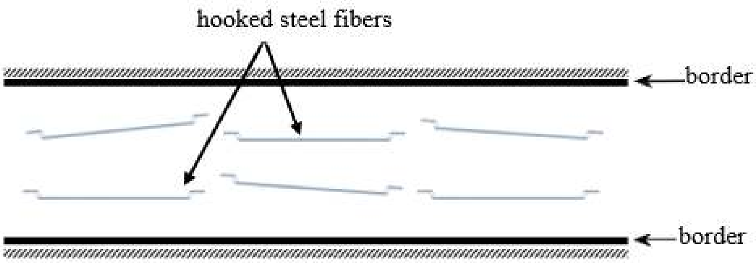

Figure 4.18. Orientation of hooked steel fibers between the mold walls

4.1.3 Analysis of Physical Behavior

4.1.3.1 Shrinkage Deformation

Though the drying shrinkage strains were comparable for the early ages of the drying period, a clear distinction observed at the later periods for UHPC with a different amount of MSF, HSF, and MGF content as shown in Figures 4.19, 4.20, and 4.21, respectively. As seen in Figures, up to 2 weeks, the drying shrinkage developments of UHPFRCs were extremely steep and near to each other, regardless of fibers size and content. At later ages, the micro steel fibers yielded lower shrinkage in comparison to the specimens with HSF and MGF, irrespective of the different age. For example, at 60 days, the drying shrinkages of MSF2, HSF2, and MGF2 were approximately 24, 19, and 16.5%, correspondingly, lower than that of the plain UHPC (control). However, maximum shrinkage strains at 60 days were achieved at the control of about 570.1 micro-strains, whereas the lowest of about 431.2 micro-strains was reached in MSF2. The effect of using higher fiber addition level almost worked like shrinkage reducer or compensator. This may relate to the mix design composition shown in Table 3.5 that more fiber addition directly effects on the reducing of aggregate weight or it can suggest fibers as an aggregate replacer. Thus, the replacer (fibers) have superior properties over quartz aggregate, consequently, the interfacial transition zone (ITZ) improved, and the shrinking of concrete will reduce.

The findings of the present study agree with the others. For example, Garas et al. [203] showed that there is a drop in free shrinkage by approximately 50% with adding 2% of steel fibers to UHPC mixes. Moreover, Swamy and Stavrides [204] stated that the drying shrinkage reduced by 20% and delayed the formation of the first crack by the presence of recycled polymer fibers obtained from end-of-life tires.

The weight losses with respect to drying time of UHPC mixtures reinforced with MSF, HSF, and MGF are shown in Figures 4.22, 4.23, and 4.24, respectively. Although the differences in weight loss were some kind of insignificant at the early ages of the drying period, a distinction was made as weight loss increased with the drying time. It can be seen that the addition of fibers, in general, decreased the weight loss of UHPCs for different percentage ratios. For example, in the case of using 2% of MSF, HSF, and MGF, the reduction in weight loss approximately lower than control mixture (most weight loss mixture) by 40, 30.4, and 48 %, correspondingly. The reason of fewer loss of weight with the contribution of fibers may be related to replacing quartz aggregate by higher property of material like fibers (see Table 3.5), irrespective of their types and sizes. Furthermore, this conflict between the glass fiber and steel fibers related to the former has superior decreasing weight loss and later have preferred of drying shrinkage improvement was explained by Wiegrink et al. [174] that some other factors may interfere to this intimate relation.

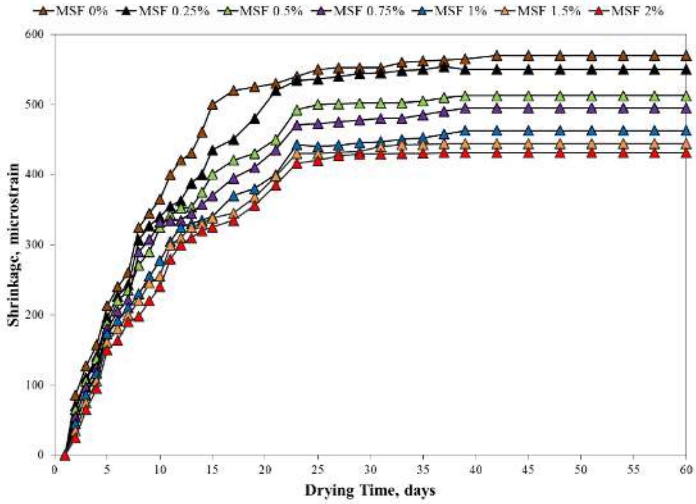

Figure 4.19. Drying shrinkage deformation for UHPCs with different volume of MSFs

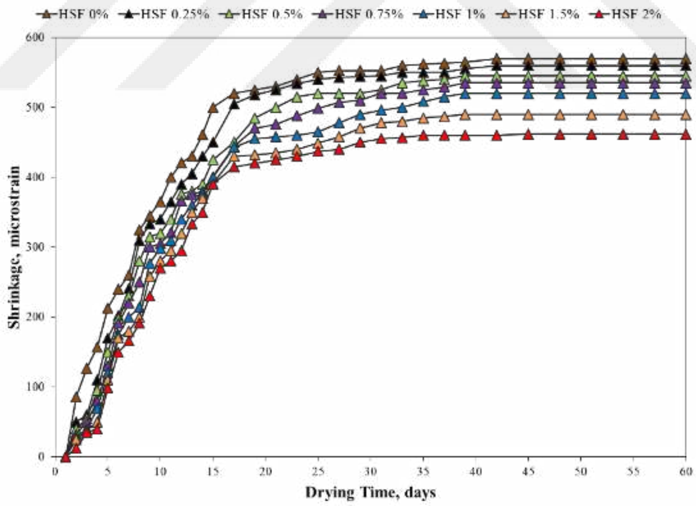

Figure 4.20. Drying shrinkage deformation for UHPCs with different volume of HSFs

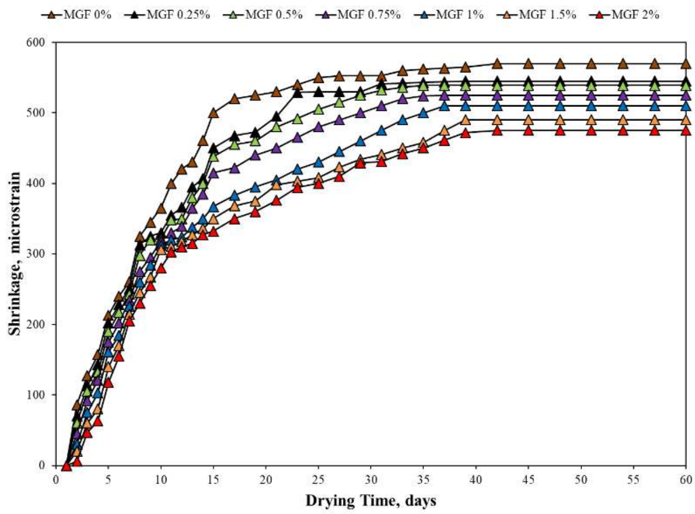

Figure 4.21. Drying shrinkage deformation for UHPCs with different volume of MGFs

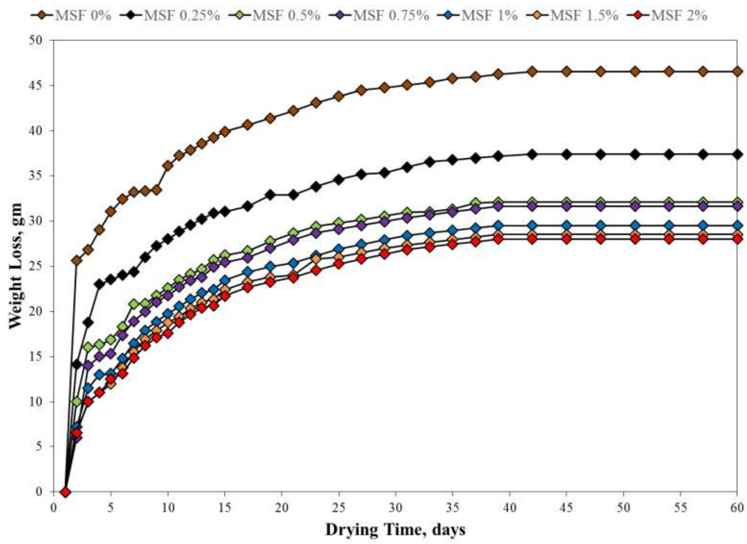

Figure 4.22. Weight loss for UHPCs with MSFs

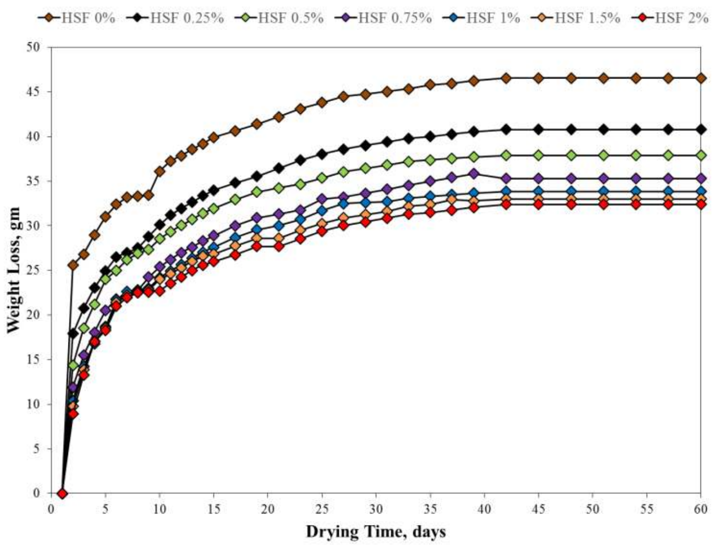

Figure 4.23. Weight loss for UHPCs with HSFs

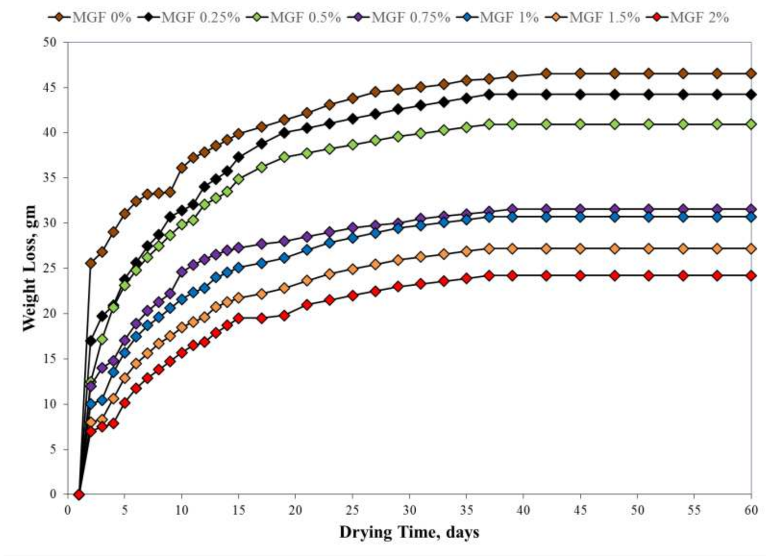

Figure 4.24. Weight loss for UHPCs with MGFs

Autogenous Deformation follows the decrease of relative humidity in the cement paste. Therefore, self-desiccation shrinkage becomes the main constituent of autogenous deformation after a certain time [170]. Thus, autogenous shrinkage has been defined as the bulk deformation of cementitious material without any weight loss when cement hydrates in a closed isothermal system not subjected to external forces [205]. The measurement of autogenous shrinkage starts with the initial setting time because this type of shrinkage usually used for the prediction of cracking so that the reduction of volume in the fresh state (before initial set) is excluded [206]. The typical autogenous shrinkage of UHPCs with different volume amounts of MSF, HSF, and MGF are displayed in Figures 4.25, 4.26, and 4.27 respectively. The maximum autogenous shrinkage was laid at 377.3 microstrains for the control mixture and the lowest autogenous shrinkage "267.3 microstrains" was measured in the UHPC having 2% MSF. However, when UHPC contained 2% of MSF, HSF, and MGF, autogenous shrinkage was mitigated by 29.1, 27, and 25.5 %, respectively, lower than that of the plain UHPC.

Some other researchers worked on decreasing autogenous shrinkage by adding fibers. Farhat et al. [207] suggested that the incorporating fibers to concrete caused a decline in autogenous deformation and increase in tensile strength of large beams. Garas et al. 2008 [203] also showed an improvement of autogenous shrinkage by about 42% through adding 2% of steel fibers to UHPC.

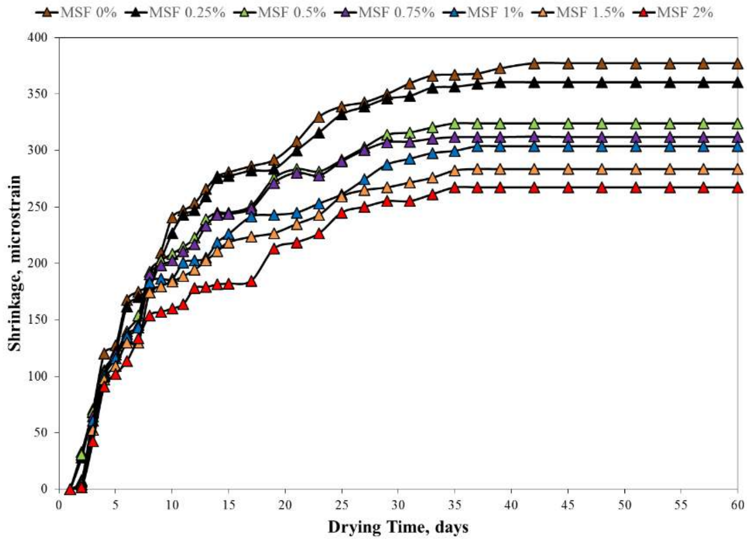

Figure 4.25. Autogenous shrinkage deformation for UHPCs with MSFs

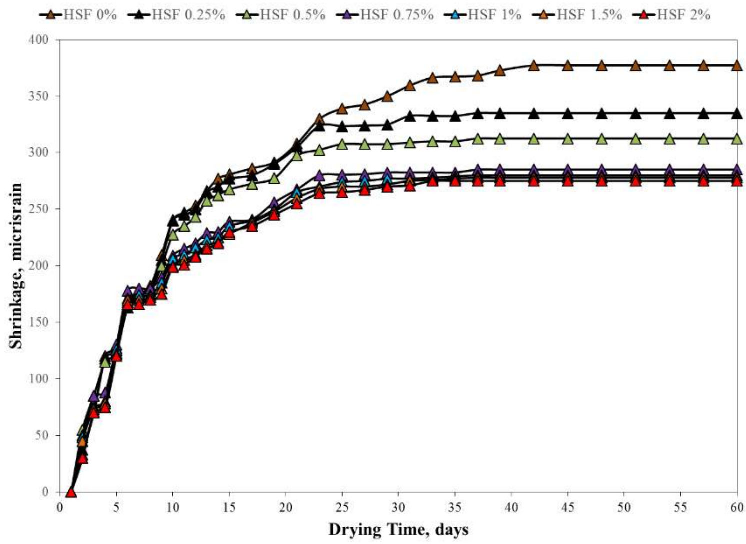

Figure 4.26. Autogenous shrinkage deformation for UHPCs with HSFs

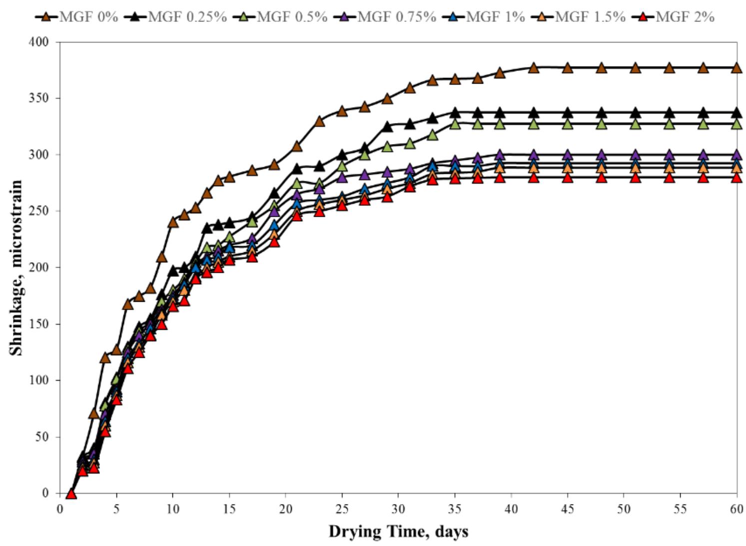

Figure 4.27. Autogenous shrinkage deformation for UHPCs with MGFs

4.1.3.2 Shrinkage Cracking and Crack Width Propagation

The time of starting crack of restrained shrinkage concrete influenced by many important factors like; tensile strength, free shrinkage strain, creep strain of the concrete, and modulus of elasticity. For instance, where stress relaxation mechanism caused by tensile creep, the free shrinkage causes stresses in concrete. The crack of will begins when tensile stress that made by restrained of free shrinkage exceeds its tensile strength of concrete. There was a clear effect of fiber types on the cracking of restrained shrinkage performance of UHPCs. As it is seen in Figures 4.28, 4.29, and 4.30, the initial cracking of the specimen was observed at third day for the control concrete; however, cracking of MSF2, HSF2, and MGF2 was observed on the 13th, 12th, and 10th days, respectively. The authors of the present study analyzed the starting cracking date of concretes such as; the plain UHPC (control mixture) resisted the tensile stress and free shrinkage up to 3 days. Whereas, 2% of each of MS, HS, and MG of fibers withstood with the named factors to stop micro cracks for 10 (13-3), 9 (12-3), and 7 (10-3) days. In addition to the cracking time, the fiber types also affected the final crack and width related to the situation in the final shrinkage. Although the cracking time prolonged, the crack opening for UHPCs with fiber was quicker on the first day, regardless of fiber sizes and types. The smallest crack width (0.11mm) was detected for HSF2 mixture, irrespective of drying time, but the supreme crack propagation (0.36 mm) at the end of 50 days was observed for MGF2 mixture. Moreover, as a best group for restrained shrinkage reduction, the addition of 0.25, 0.5, 0.75, 1, 1.5, and 2% of HSF provided 59, 70, 79, 82, 86, and 89% reduction in the crack width, respectively, comparing with mixture of control (0% fiber) at the end of 50 days drying period.

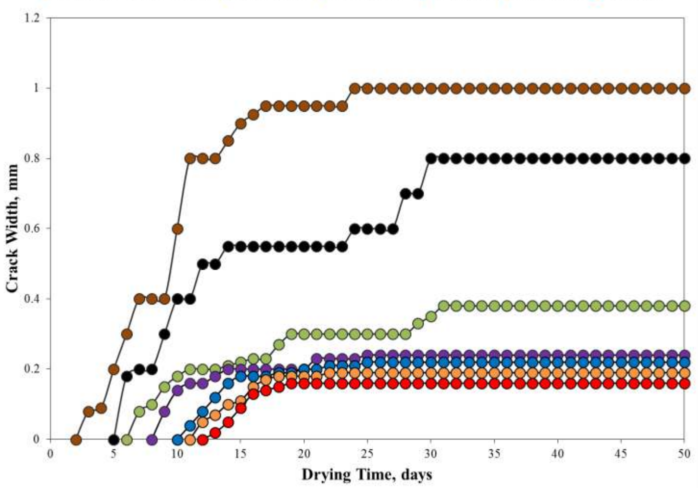

Figure 4.28. Restrained shrinkage cracking for UHPCs with MSFs

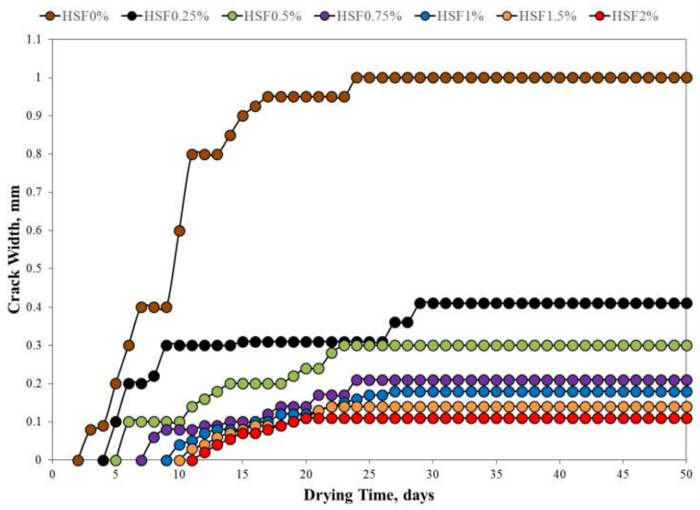

Figure 4.29. Restrained shrinkage cracking for UHPCs with HSFs

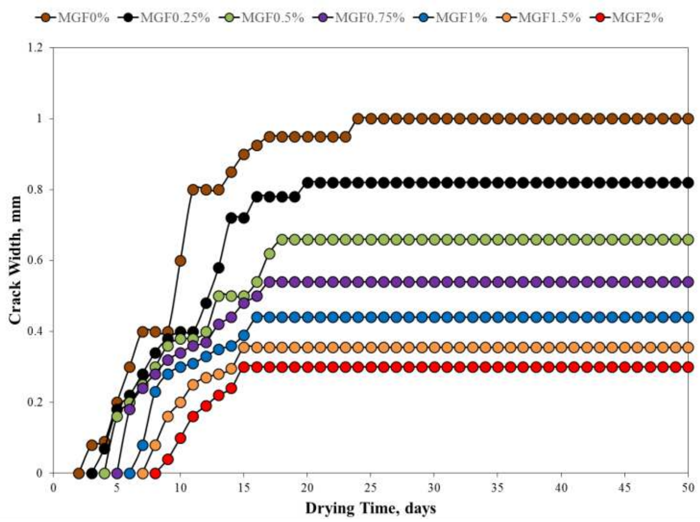

Figure 4.30. Restrained shrinkage cracking for UHPCs with MGFs

4.2 RESULTS AND DISCUSSION ON NUMERICAL ANALYSIS

4.2.1 Axial Capacity of CFST Short Column Infilled with UHPFRC

4.2.1.1 Eurocode 4

Effects of fiber types on the axial load carrying capacity (N_u) of CFST made with UHPCs reinforced by; MSF, HSF, and MGF are presented; in Figures 4.31-4.33, 4.34-4.36, and 4.37-4.39, respectively, which categorized according to change of yield strength and D/t of UHPFRC. Eurocode 4 is the only code that treats the effects of long-term loading separately. It was observed that the ultimate axial load of concretes continuously increased in the case of steel fiber reinforced UHPCs while the axial load increment limited at 1.5% volume of micro glass fibers, irrespective to testing age. However, the growth of the results after 56 days seemed to be quite limited as there was little enhancement at 90 and 180 days, regardless of fiber types. Indeed, at 180 days age of UHPC incorporated with 2% MSF, 2% HSF, 1.5% MGF, which gives the highest concrete compressive strength, the maximum axial load capacity of 9868, 9660, and 9443 kN was recorded, respectively. On the other hand, with any increase in diameter and yield strength of the steel tube, the axial load capacity of the columns infilled with UHPFRC directly improved. The mixture in this study a superior concrete of UHPC containing 2% of MSF, with 180 days, D/t = 90 and fy= 600. Finally, the results of using this code suggested an order of micro steel fiber, hooked steel fiber, and micro glass fiber plus the greater column diameter and yield strength of the steel tube considering their beneficial effects on the axial load capacity.

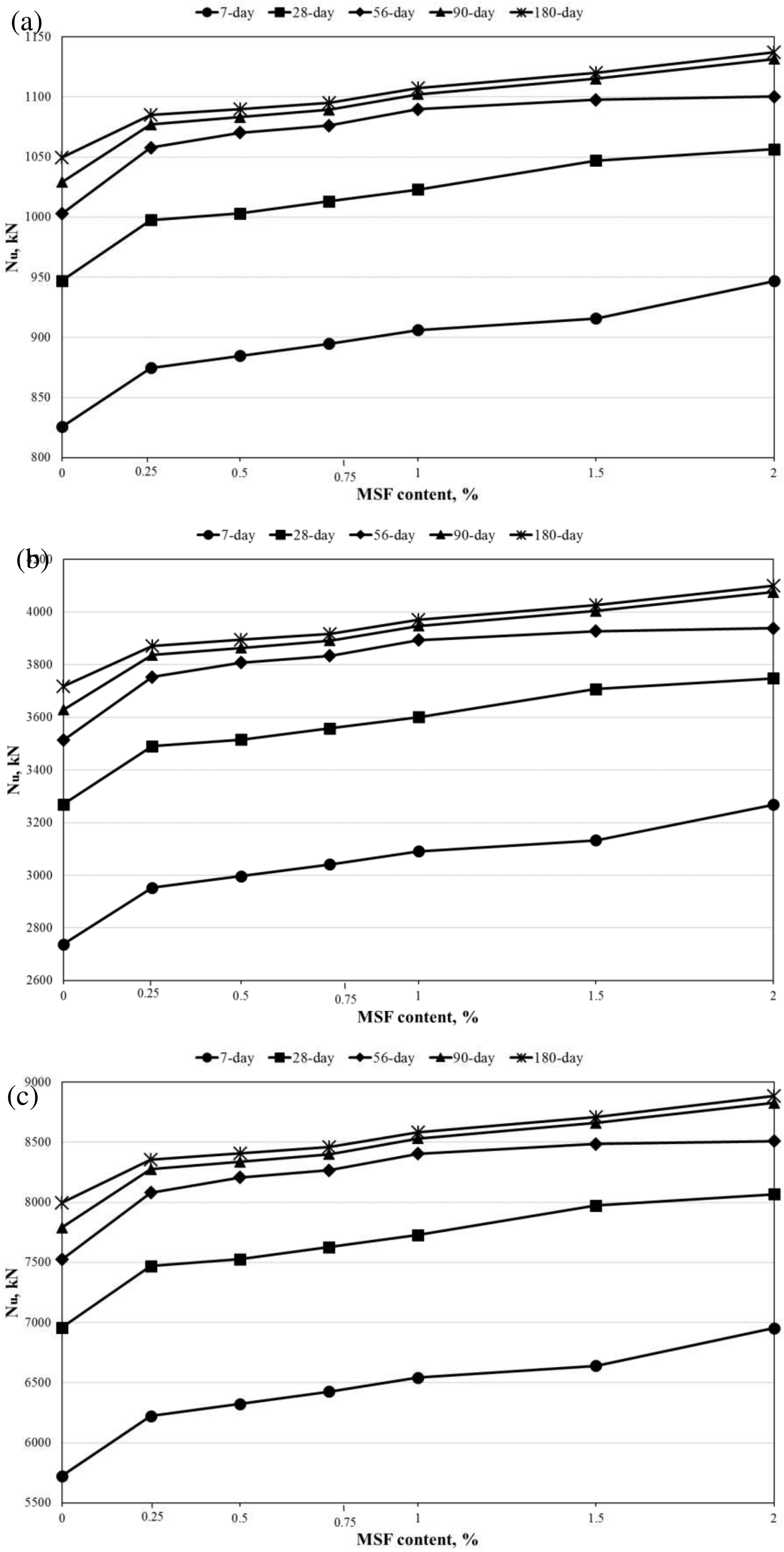

Figure 4.31. Calculated axial load capacity of CFST columns having UHPC with MSF via EC4 equation for steel tube yield strength of 300 MPa: a) D/t=30, b) D/t=60, and c) D/t=90

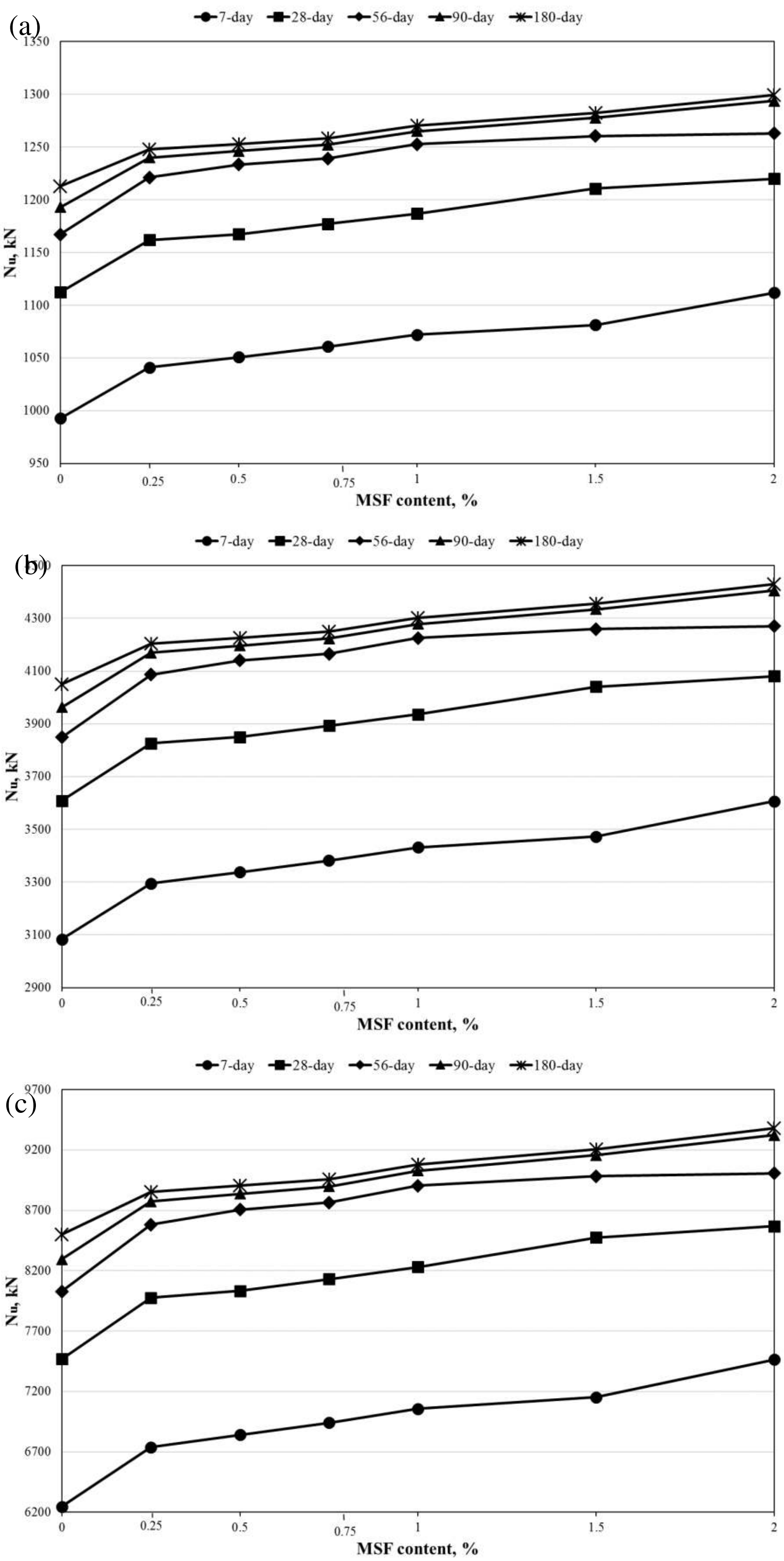

Figure 4.32. Calculated axial load capacity of CFST columns having UHPC with MSF via EC4 equation for steel tube yield strength of 450 MPa: a) D/t=30, b) D/t=60, and c) D/t=90

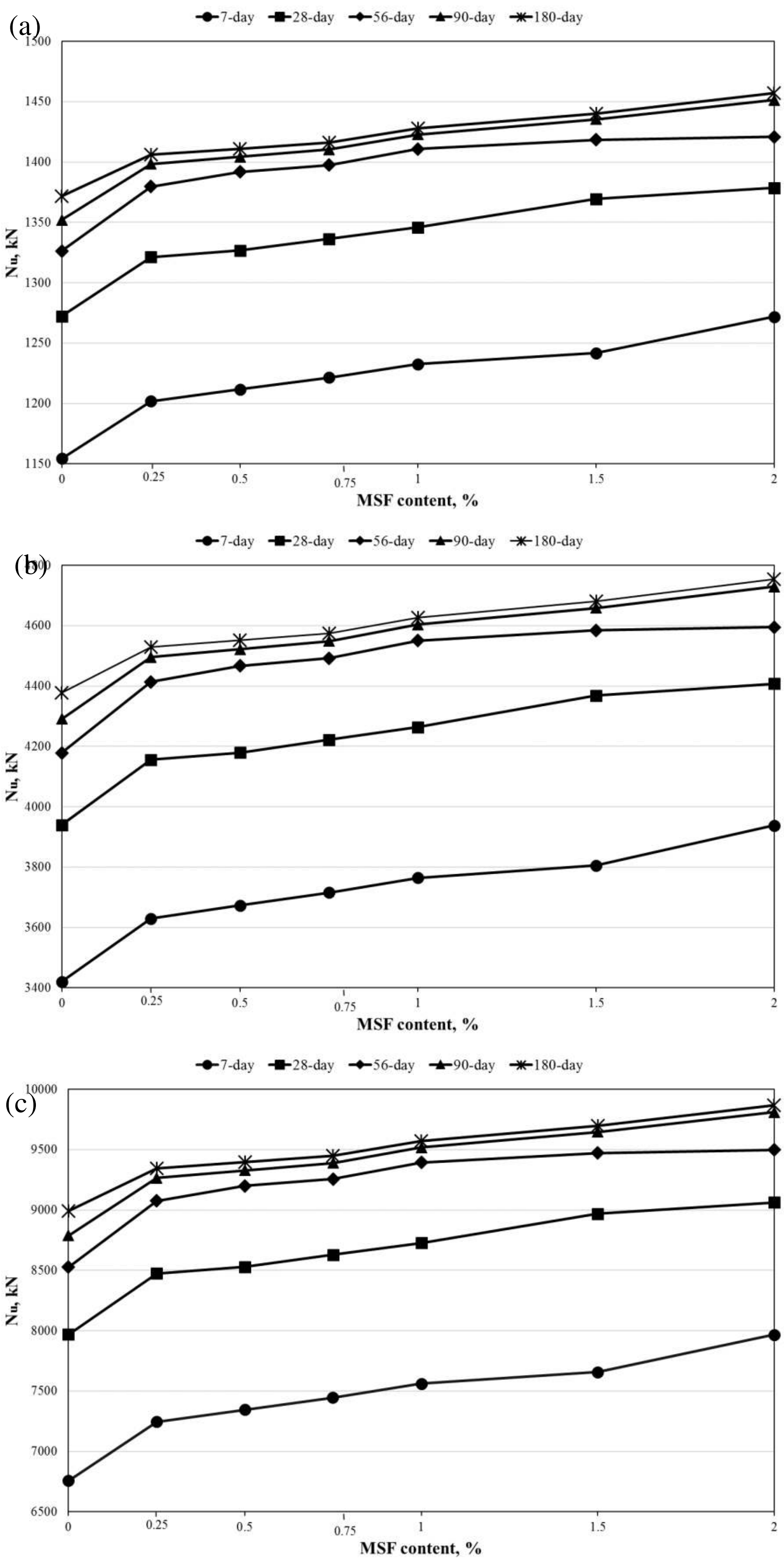

Figure 4.33. Calculated axial load capacity of CFST columns having UHPC with MSF via EC4 equation for steel tube yield strength of 600 MPa: a) D/t=30, b) D/t=60, and c) D/t=90

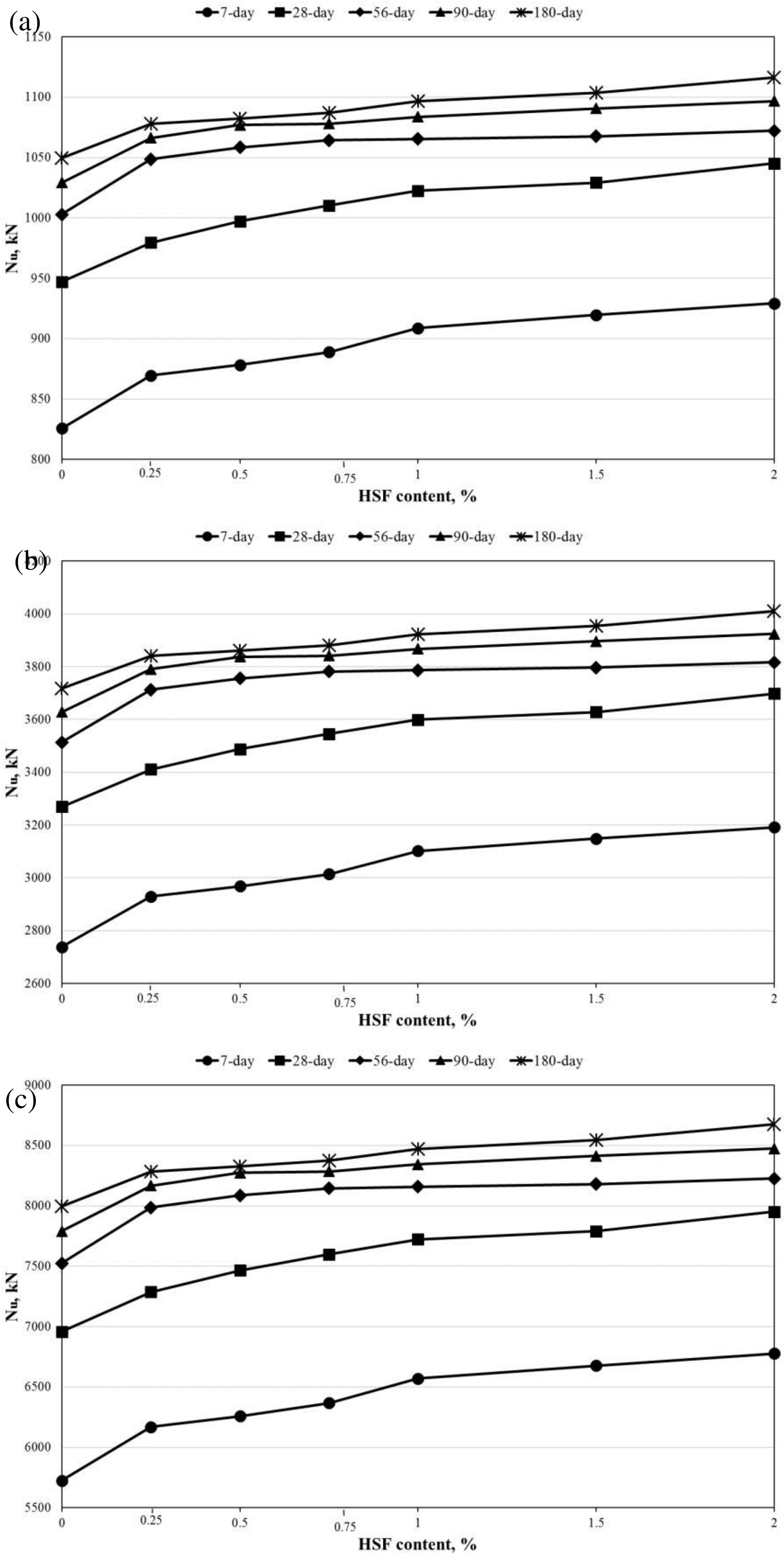

Figure 4.34. Calculated axial load capacity of CFST columns having UHPC with HSF via EC4 equation for steel tube yield strength of 300 MPa: a) D/t=30, b) D/t=60, and c) D/t=90

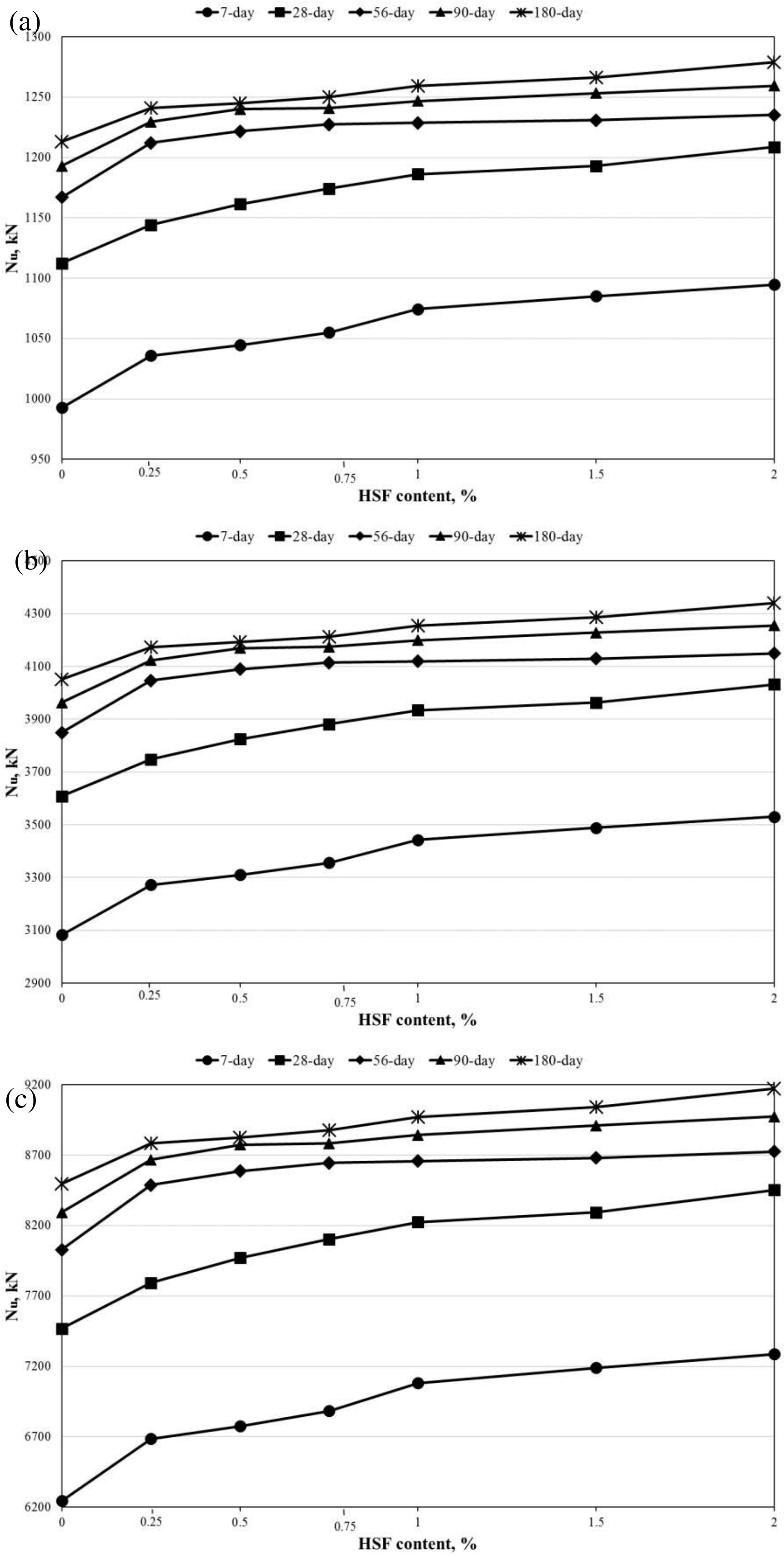

Figure 4.35. Calculated axial load capacity of CFST columns having UHPC with HSF via EC4 equation for steel tube yield strength of 450 MPa: a) D/t=30, b) D/t=60, and c) D/t=90

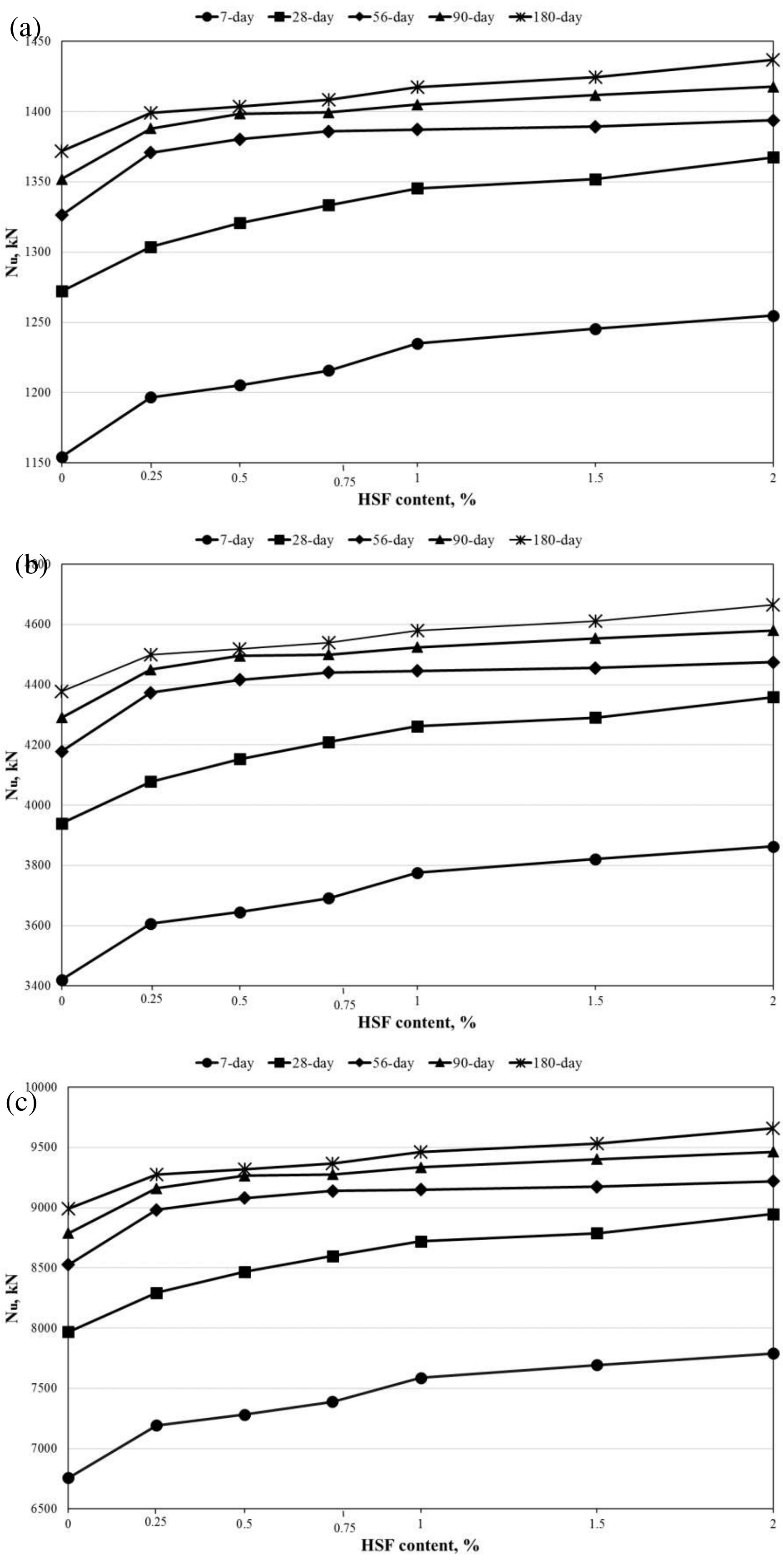

Figure 4.36. Calculated axial load capacity of CFST columns having UHPC with HSF via EC4 equation for steel tube yield strength of 600 MPa: a) D/t=30, b) D/t=60, and c) D/t=90

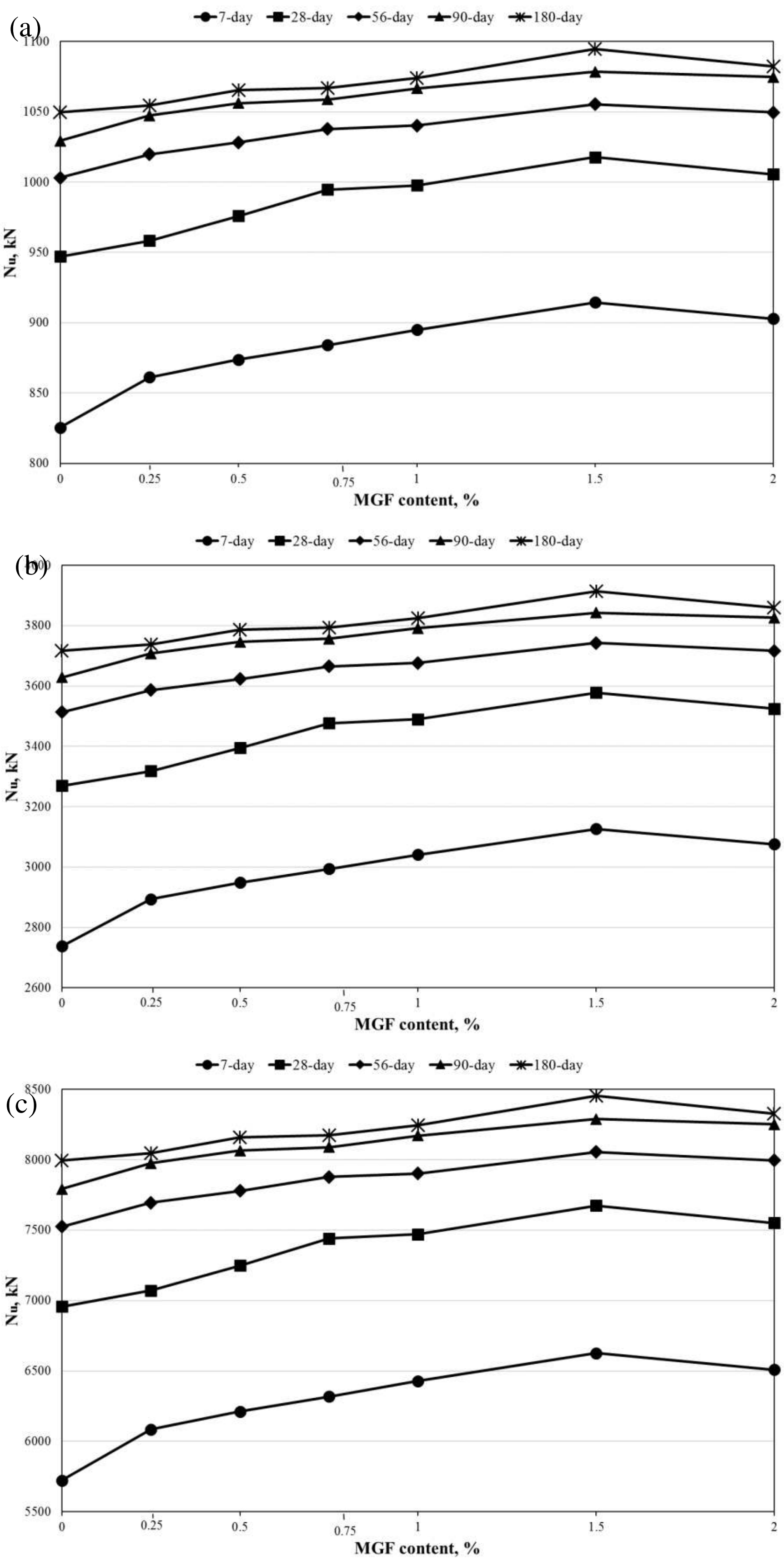

Figure 4.37. Calculated axial load capacity of CFST columns having UHPC with MGF via EC4 equation for steel tube yield strength of 300 MPa: a) D/t=30, b) D/t=60, and c) D/t=90

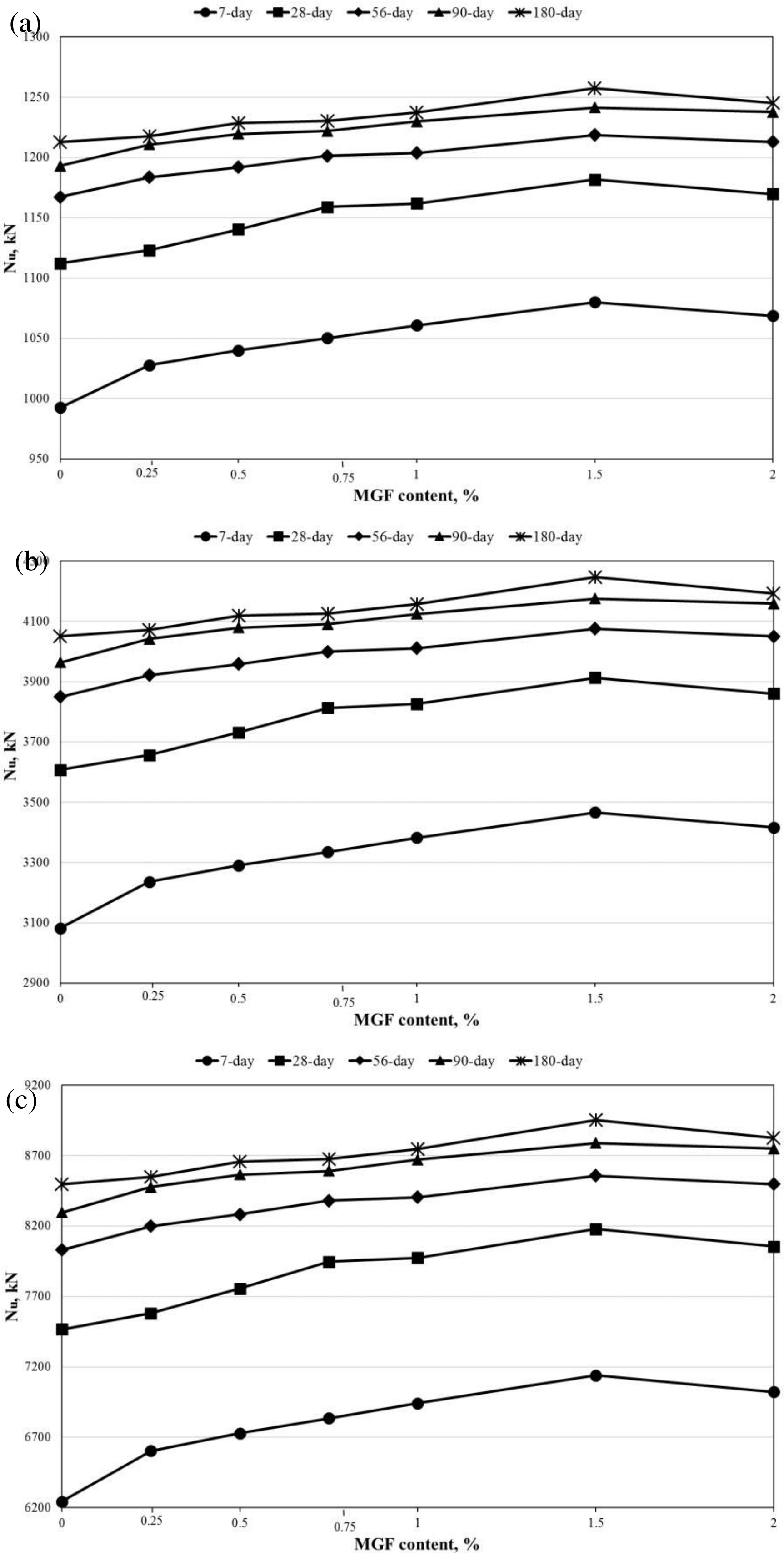

Figure 4.38. Calculated axial load capacity of CFST columns having UHPC with MGF via EC4 equation for steel tube yield strength of 450 MPa: a) D/t=30, b) D/t=60, and c) D/t=90

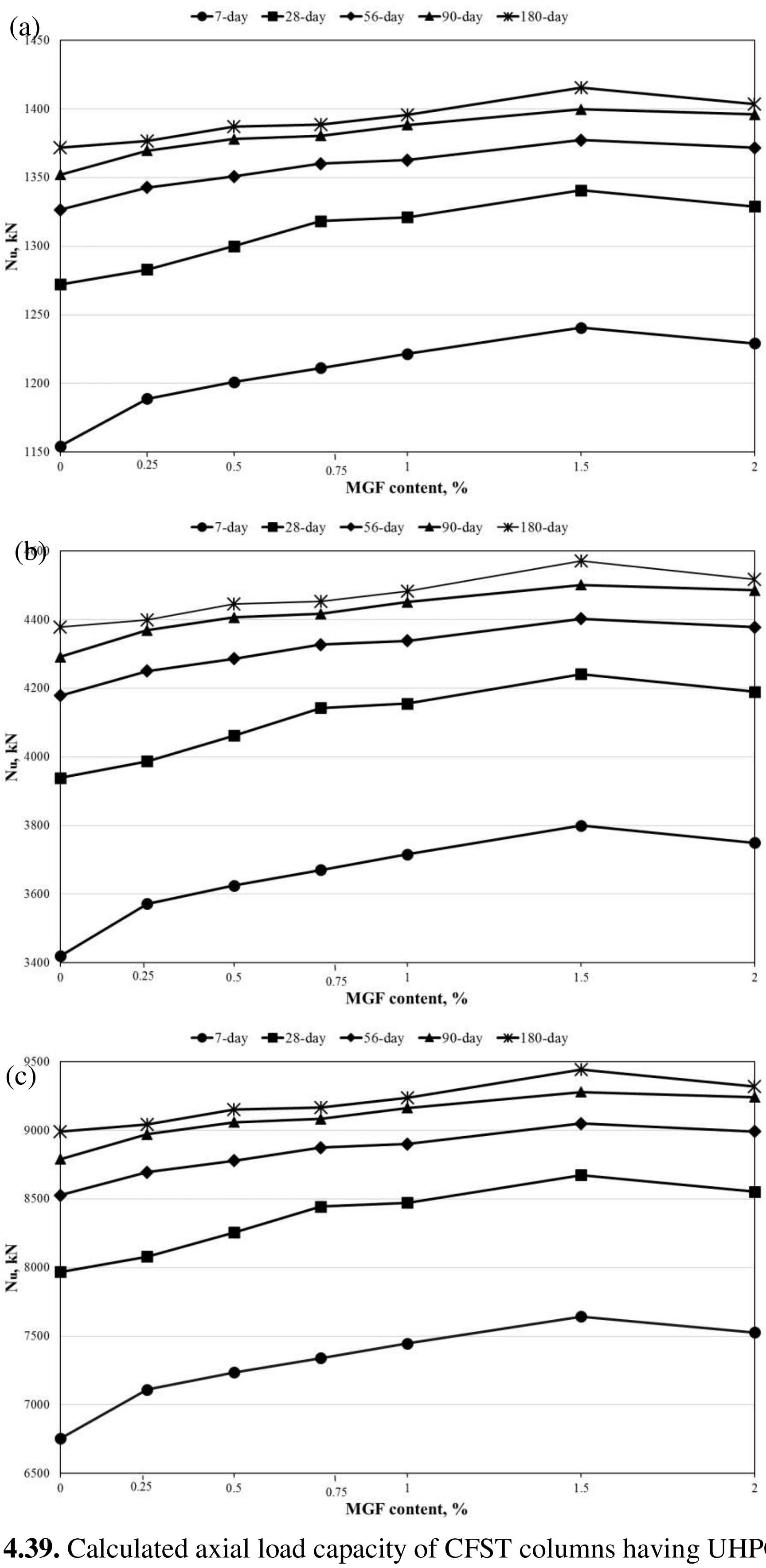

Figure 4.39. Calculated axial load capacity of CFST columns having UHPC with MGF via EC4 equation for steel tube yield strength of 600 MPa: a) D/t=30, b) D/t=60, and c) D/t=90

4.2.1.2 American Concrete Institute (ACI)

Effects of fiber type, diameter and the yield strength of steel column on the axial load capacity of CFST filled with UHPCs reinforced with different volume of micro steel, hooked steel, and micro glass fibers are illustrated in Figures 4.40-4.42, 4.43-4.45, and 4.46-4.48, respectively. It was observed that as the volume of fibers increased from 0 to 2%, D/t increased from 30 to 90 mm, and Fy from 300 to 600 MPa all series showed growing trend in the capacity of CFST section in all ages. The enlarging tendency of the hypothetical ultimate load carrying capacity of CFST sections filled with UHPFRC continued and reached the maximum when the mixture contained 2% of micro steel or hooked steel fiber, D/t=90, and fy=600 MPa at 180 days that recorded 8203 and 8021 kN when it was 7435 kN at 0% of fiber content. However, in the case of micro glass fibers with D/t= 90 and Fy= 600 MPa at 180 days the maximum result was 7829.3 kN achieved at 1.5% then the axial load capacity began to decrease to 7721.4 kN at 2% fiber, this decline entire for all cases of MGF content.

In addition to the present study on increasing axial load capacity of ultra-high performance fiber reinforced concrete incorporated with circular concrete filled steel tubular (UHPFRC-CFST) by increasing diameter of steel tube, other researchers like Kalingarani et al. [208] with increasing D/t from 13.25 to 21.14 increased the axial load capacity of CFST filled with normal concrete from 155.15 to 350.19 kN for M20 grade and from 163.8 to 381. 86 kN for M30 grade of concrete using the equation of the ACI code.

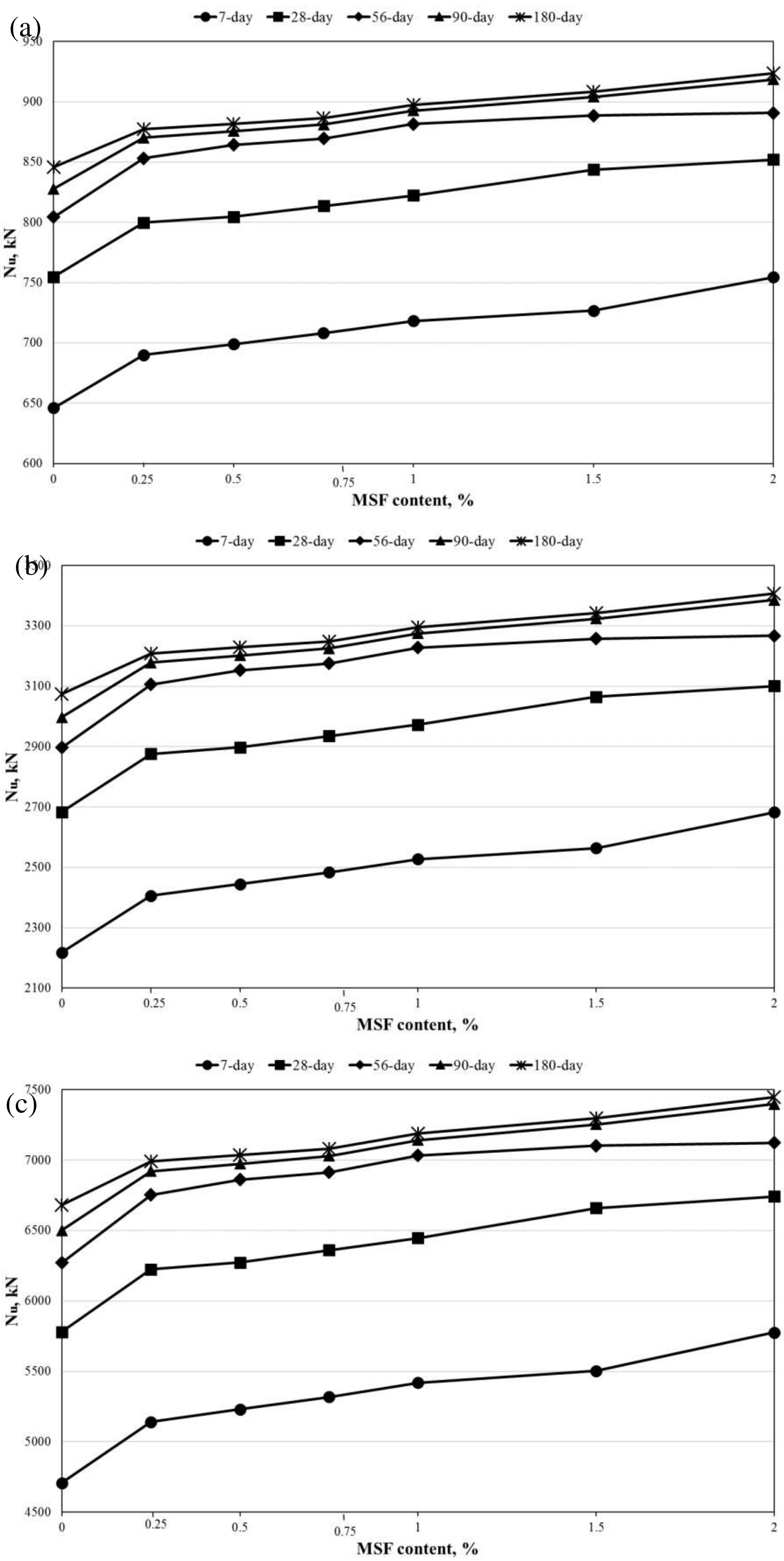

Figure 4.40. Calculated axial load capacity of CFST columns having UHPC with MSF via ACI equation for steel tube yield strength of 300 MPa: a) D/t=30, b) D/t=60, and c) D/t=90

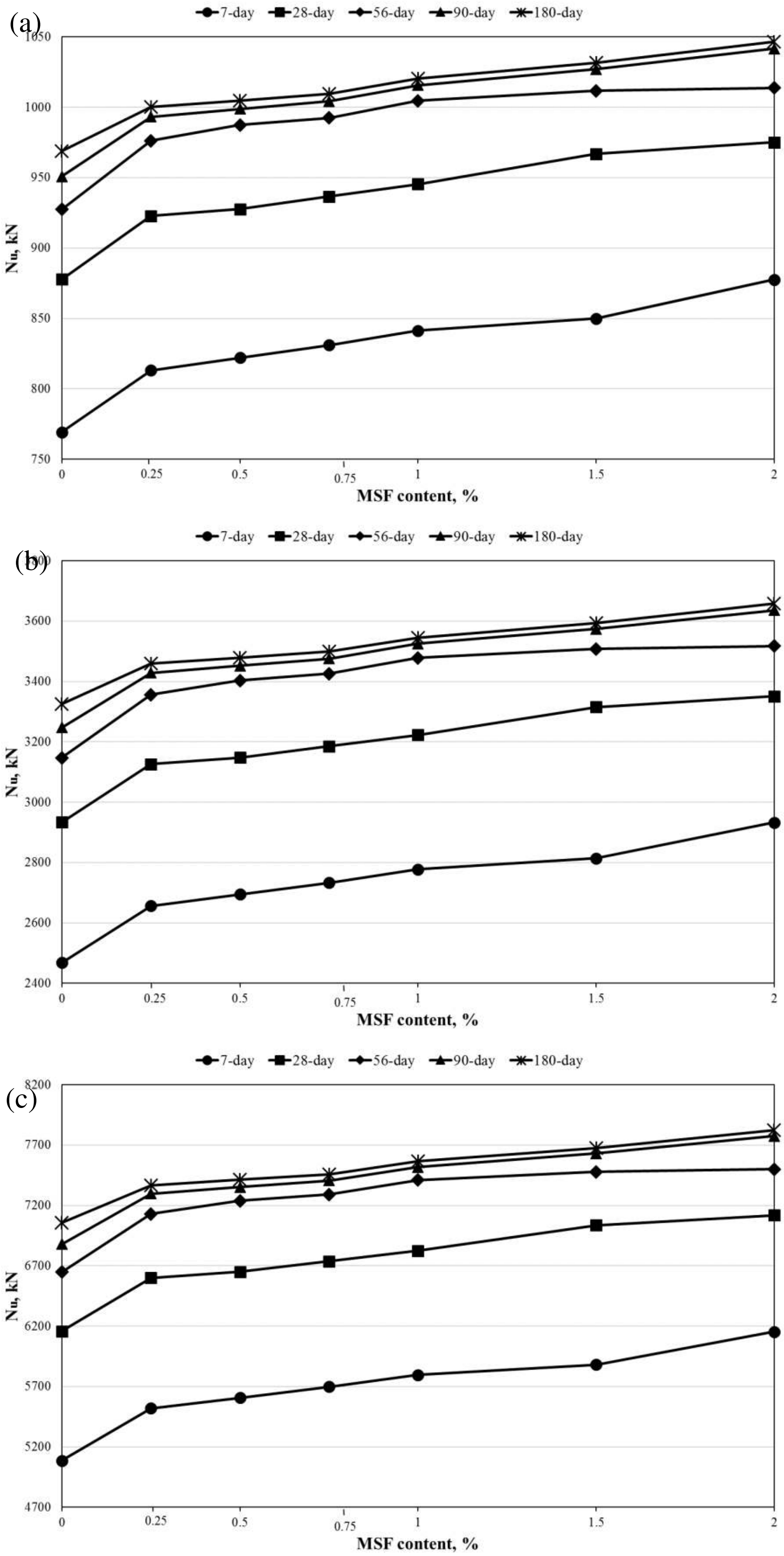

Figure 4.41. Calculated axial load capacity of CFST columns having UHPC with MSF via ACI equation for steel tube yield strength of 450 MPa: a) D/t=30, b) D/t=60, and c) D/t=90

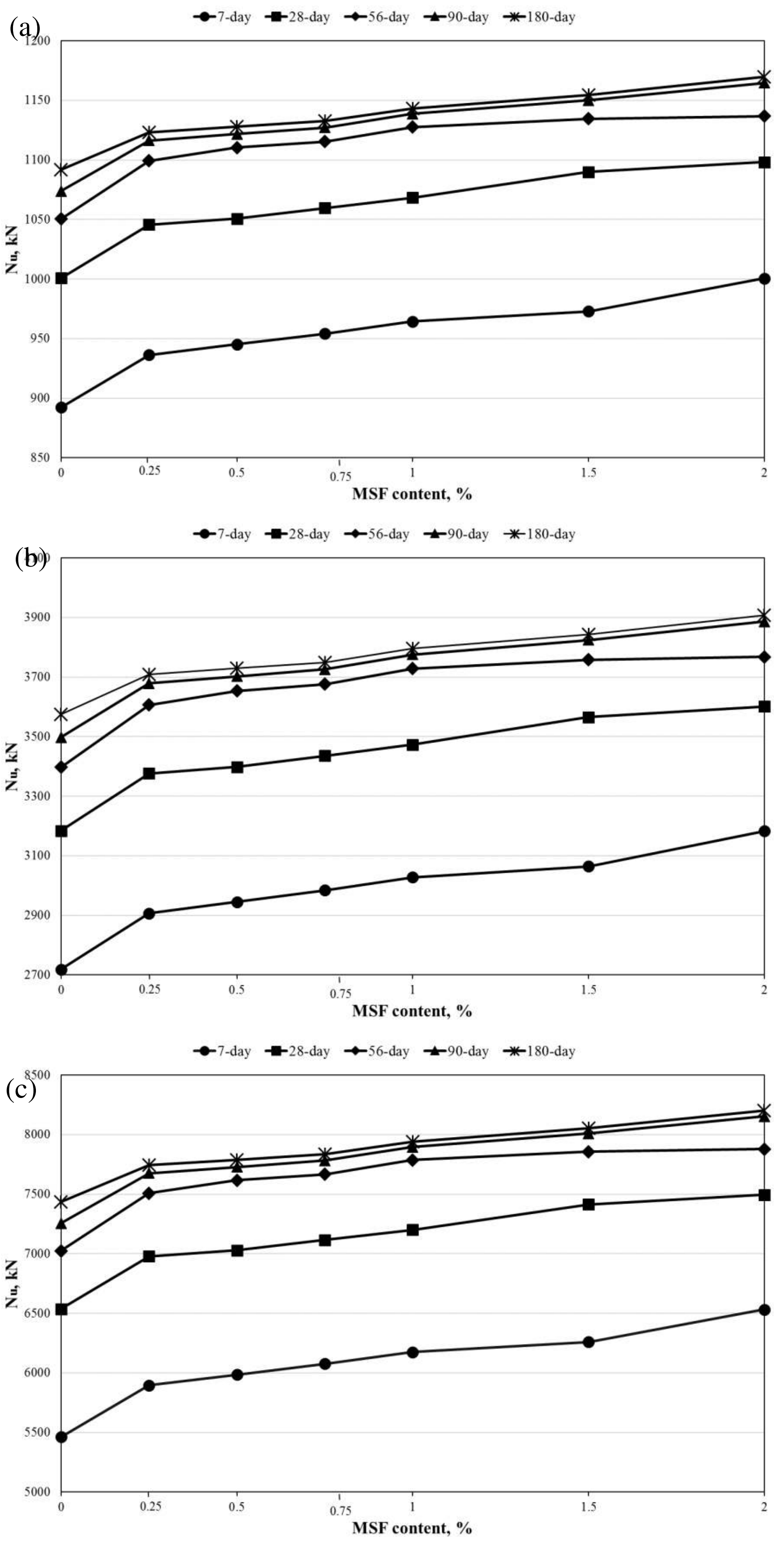

Figure 4.42. Calculated axial load capacity of CFST columns having UHPC with MSF via ACI equation for steel tube yield strength of 600 MPa: a) D/t=30, b) D/t=60, and c) D/t=90

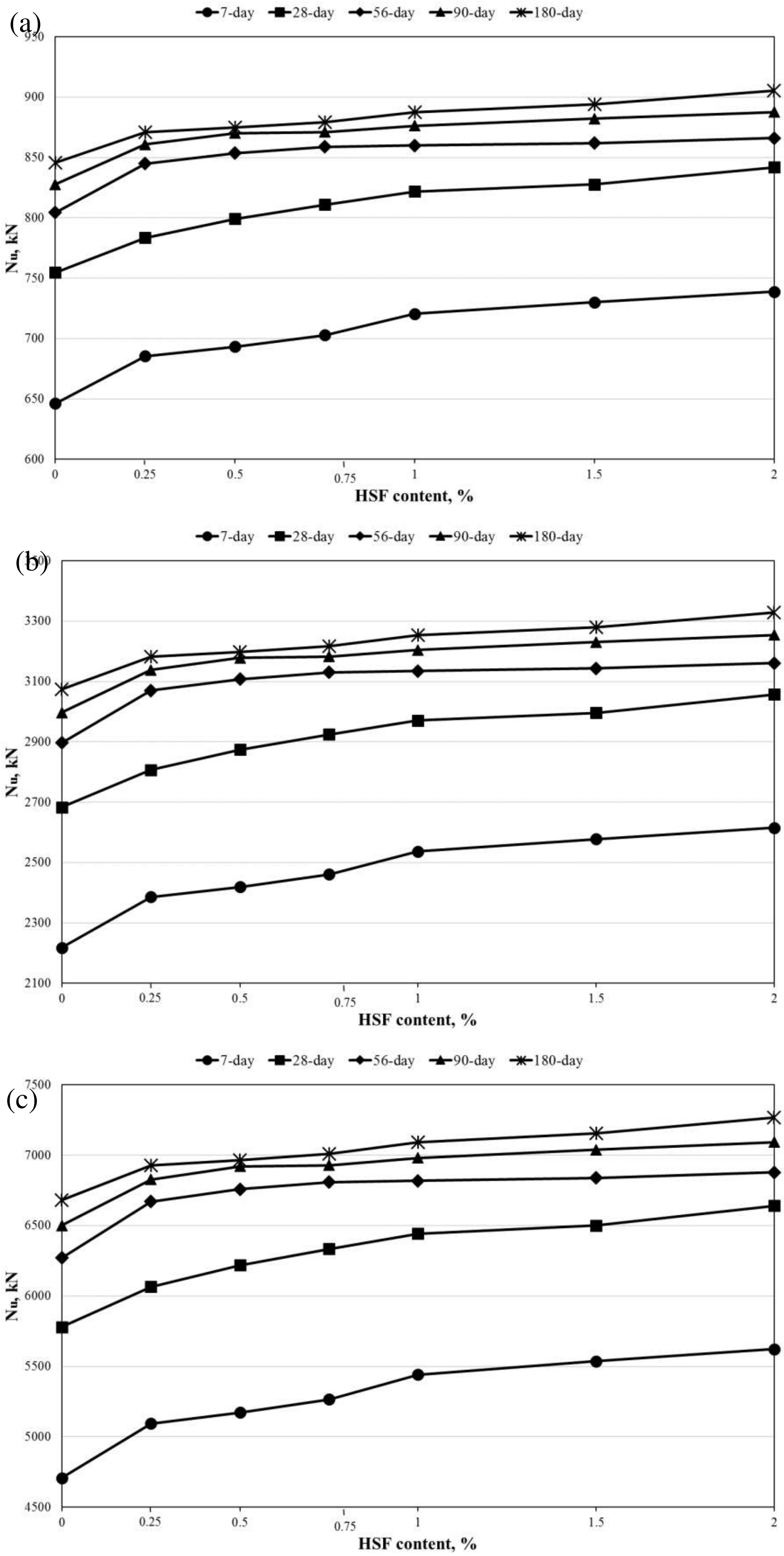

Figure 4.43. Calculated axial load capacity of CFST columns having UHPC with HSF via ACI equation for steel tube yield strength of 300 MPa: a) D/t=30, b) D/t=60, and c) D/t=90

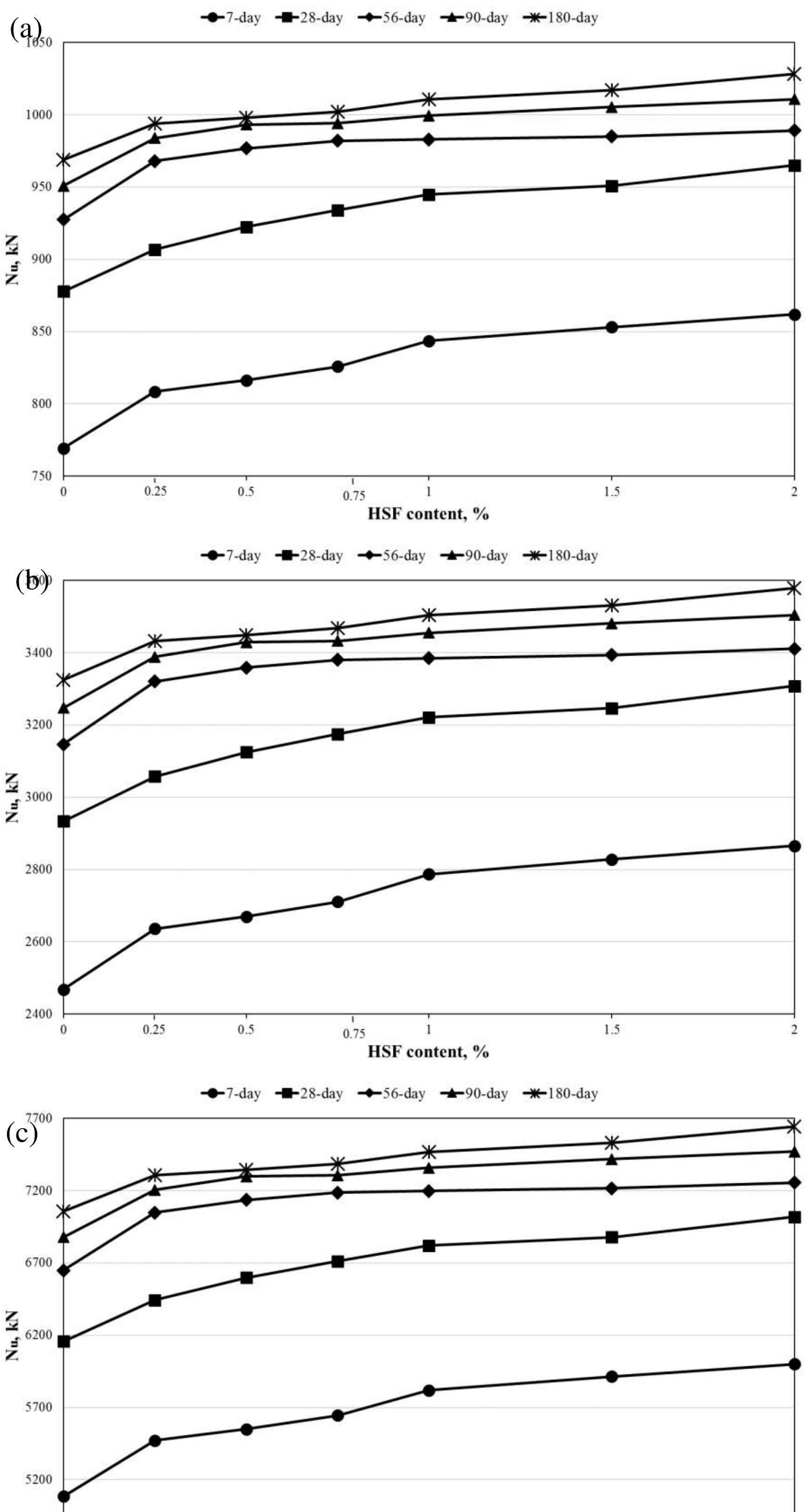

Figure 4.44. Calculated axial load capacity of CFST columns having UHPC with HSF via ACI equation for steel tube yield strength of 450 MPa: a) D/t=30, b) D/t=60, and c) D/t=90

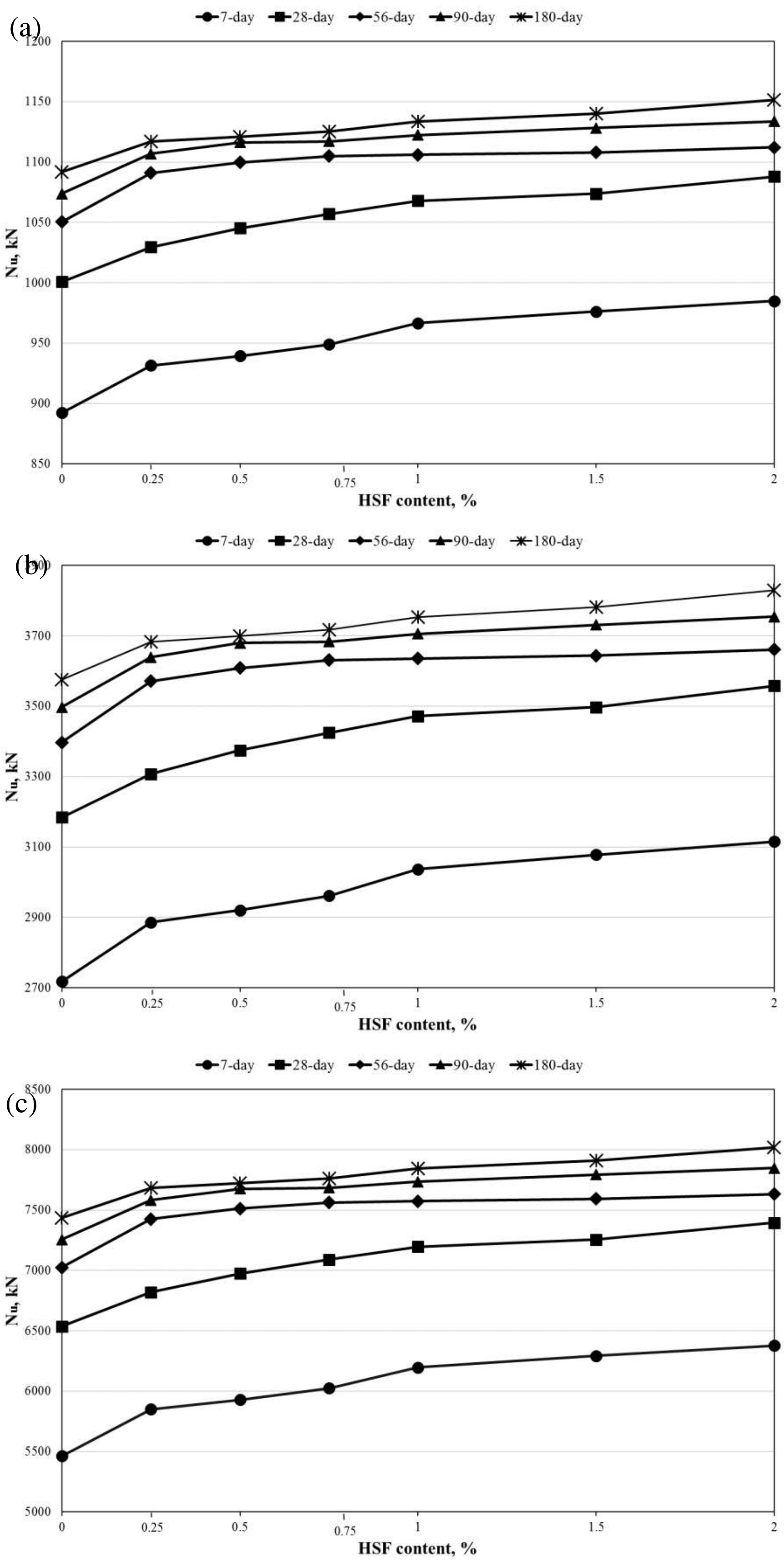

Figure 4.45. Calculated axial load capacity of CFST columns having UHPC with HSF via ACI equation for steel tube yield strength of 600 MPa: a) D/t=30, b) D/t=60, and c) D/t=90

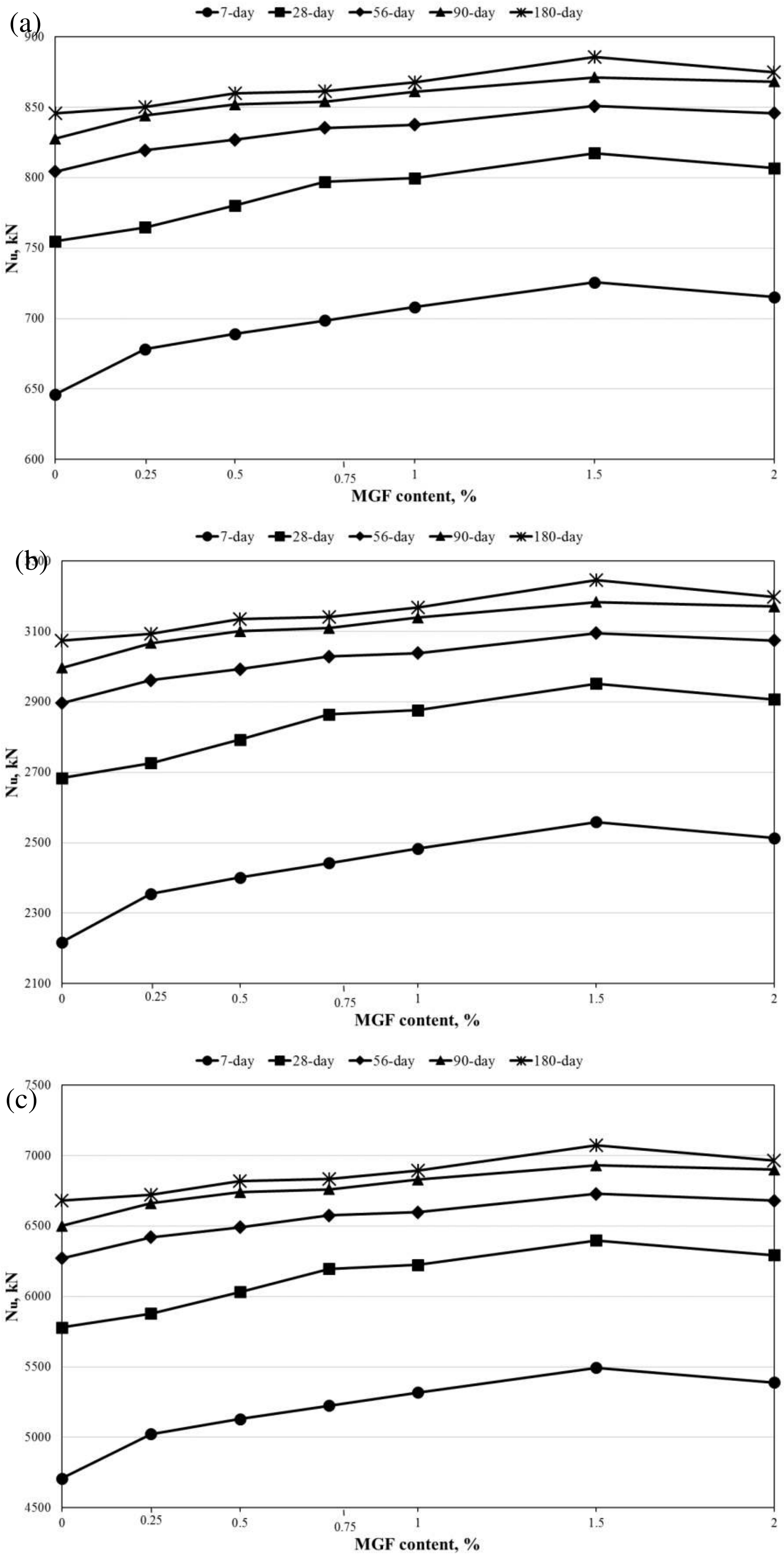

Figure 4.46. Calculated axial load capacity of CFST columns having UHPC with MGF via ACI equation for steel tube yield strength of 300 MPa: a) D/t=30, b) D/t=60, and c) D/t=90

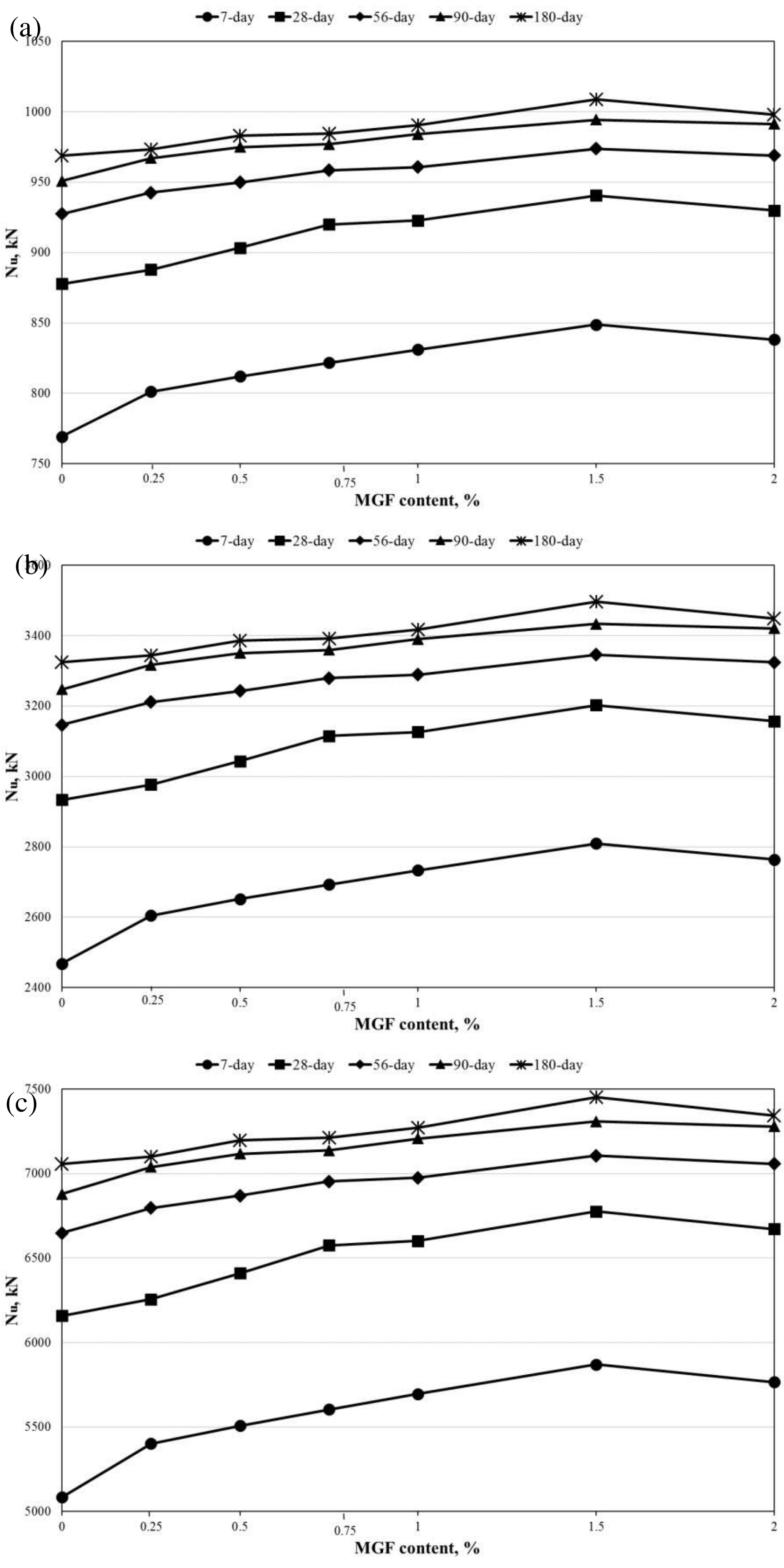

Figure 4.47. Calculated axial load capacity of CFST columns having UHPC with MGF via ACI equation for steel tube yield strength of 450 MPa: a) D/t=30, b) D/t=60, and c) D/t=90

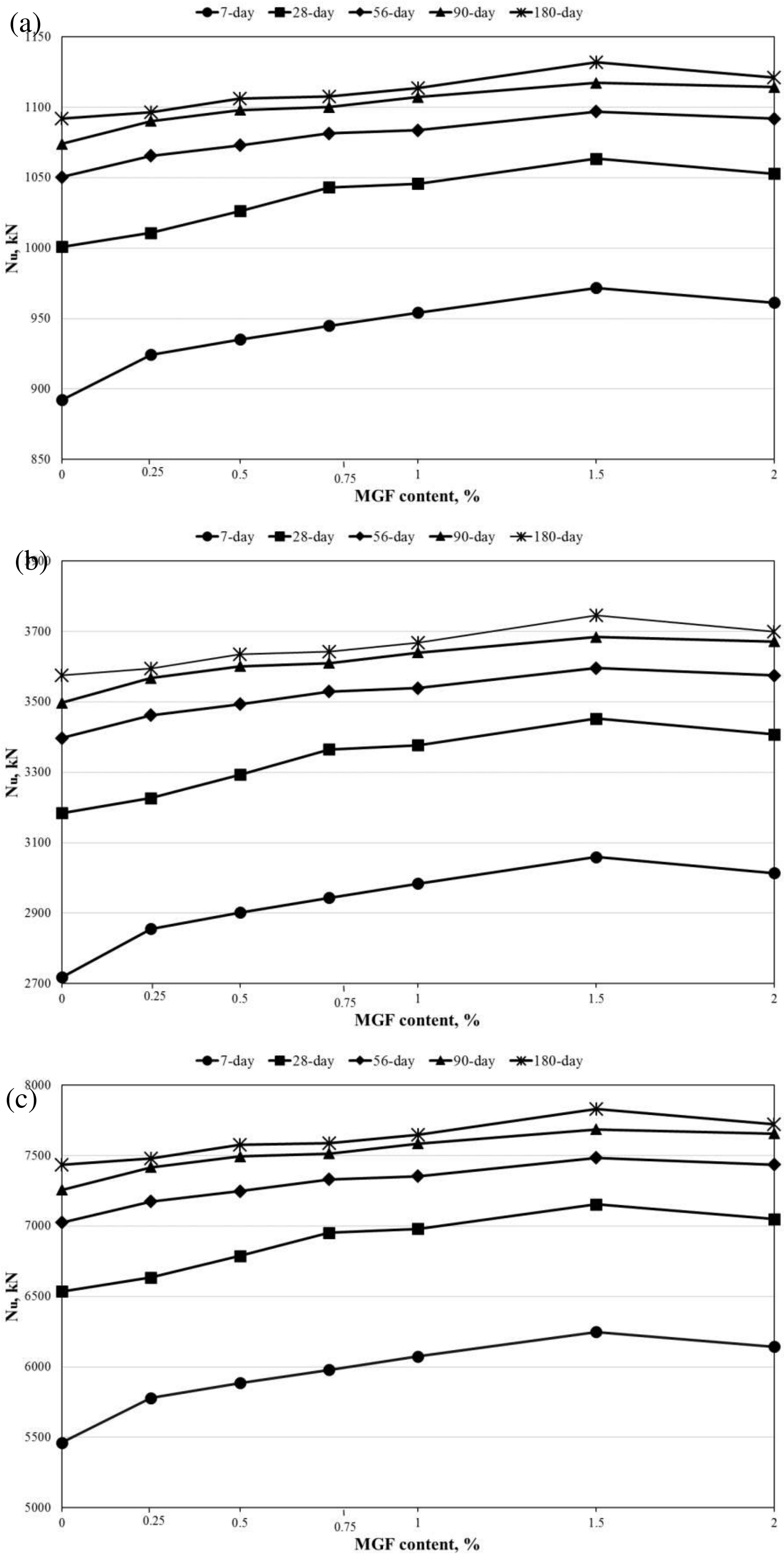

Figure 4.48. Calculated axial load capacity of CFST columns having UHPC with MGF via ACI equation for steel tube yield strength of 600 MPa: a) D/t=30, b) D/t=60, and c) D/t=90

4.2.1.3 American Institute of Steel Construction (AISC)

Influence of yield strength and the diameter of steel column on the theoretical axial load capacity of CFST filled with UHPC reinforced with different fiber concentrations from 0 to 2% of MSF, HSF, and MGF types according to the AISC code are illustrated in Figures 4.49-4.51, 4.52-4.54, and 4.55-4.57, respectively. By setting D/t= 30, 60, and 90 and three values of 300, 450 and 600 MPa of fy has been taken. Compared to the plain concrete, the addition of 0.25, 0.5, 0.75, 1, 1.5 and 2% of different volume of fibers to UHPC at 180 days with D/t= 90 and Fy= 600 MPa seemed to enhance the ultimate load capacity by; 4.23, 4.84, 5.47, 6.92, 8.43, and 10.47% for the MSF, 3.38, 3.9, 4.49, 5.62, 6.48, and 8.0% for HSF, and by about 0.6, 2.0, 2.1, 2.95, 5.41, and 3.91% for MGF.

It can be noted from figures that the rates of enhancement of axial load capacity of CFST columns were lowered with increasing the age of UHPFRC. For example, when the ages of concrete were reached 90 days, there were insignificant grow of the results for the other next 90 days (at the age of 180 days) which not exceed 5% of the total enhancement gained. This may be due to completion whole chemical reactions that restrict the growth of the strength of concrete. On the other hand, all the results positively affected with increasing fiber volumes for micro steel and hooked steel fibers even the concentration got hold of 2%. In contrast, during incorporating of micro glass fibers, there was enhancement up to 1.5% then began to drop slowly. This may be because of that the huge numbers of 2% lightweight micro glass fibers disrupted the other UHPC constituents.

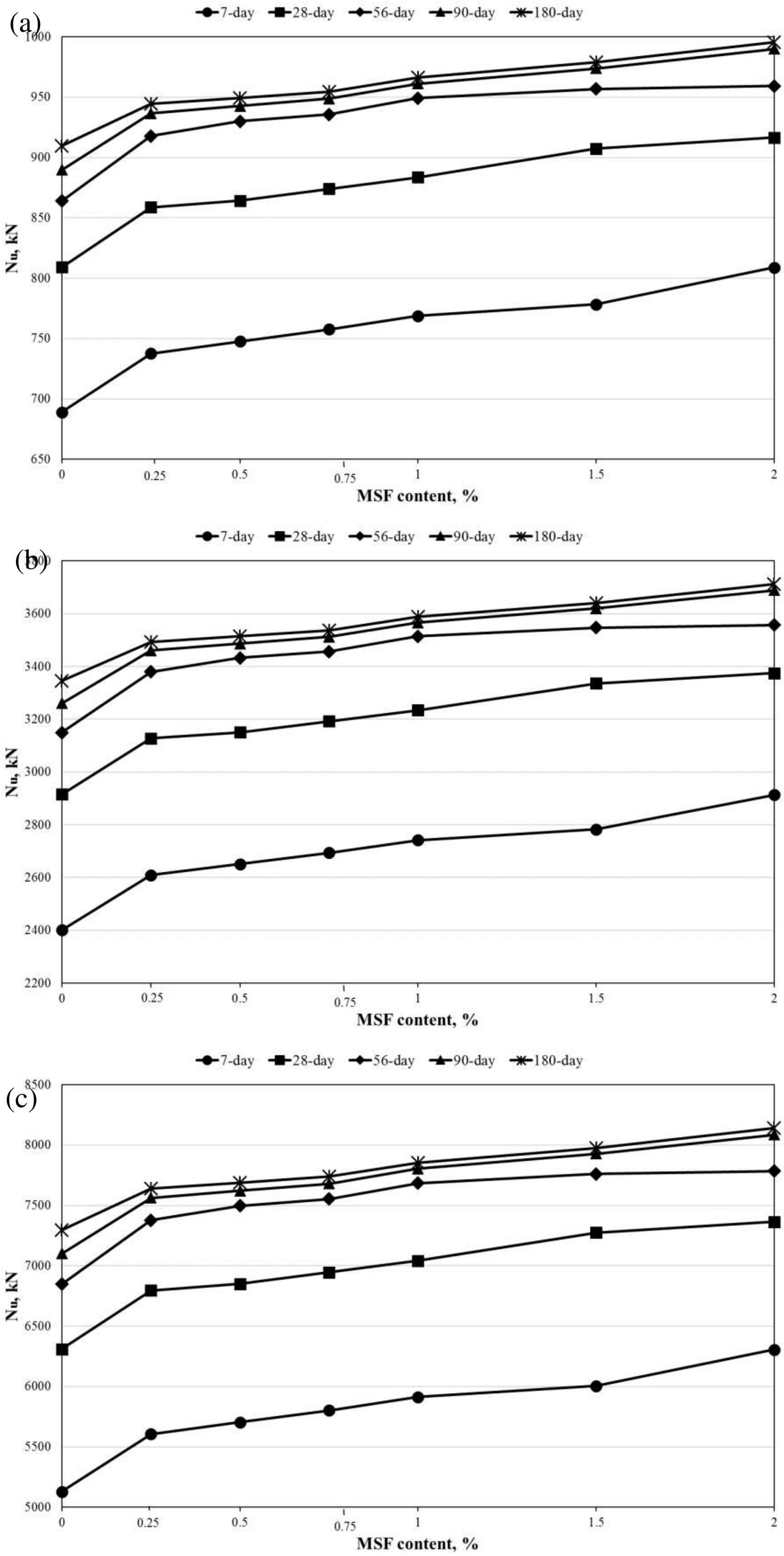

Figure 4.49. Calculated axial load capacity of CFST columns having UHPC with MSF via AISC equation for steel tube yield strength of 300 MPa: a) D/t=30, b) D/t=60, and c) D/t=90

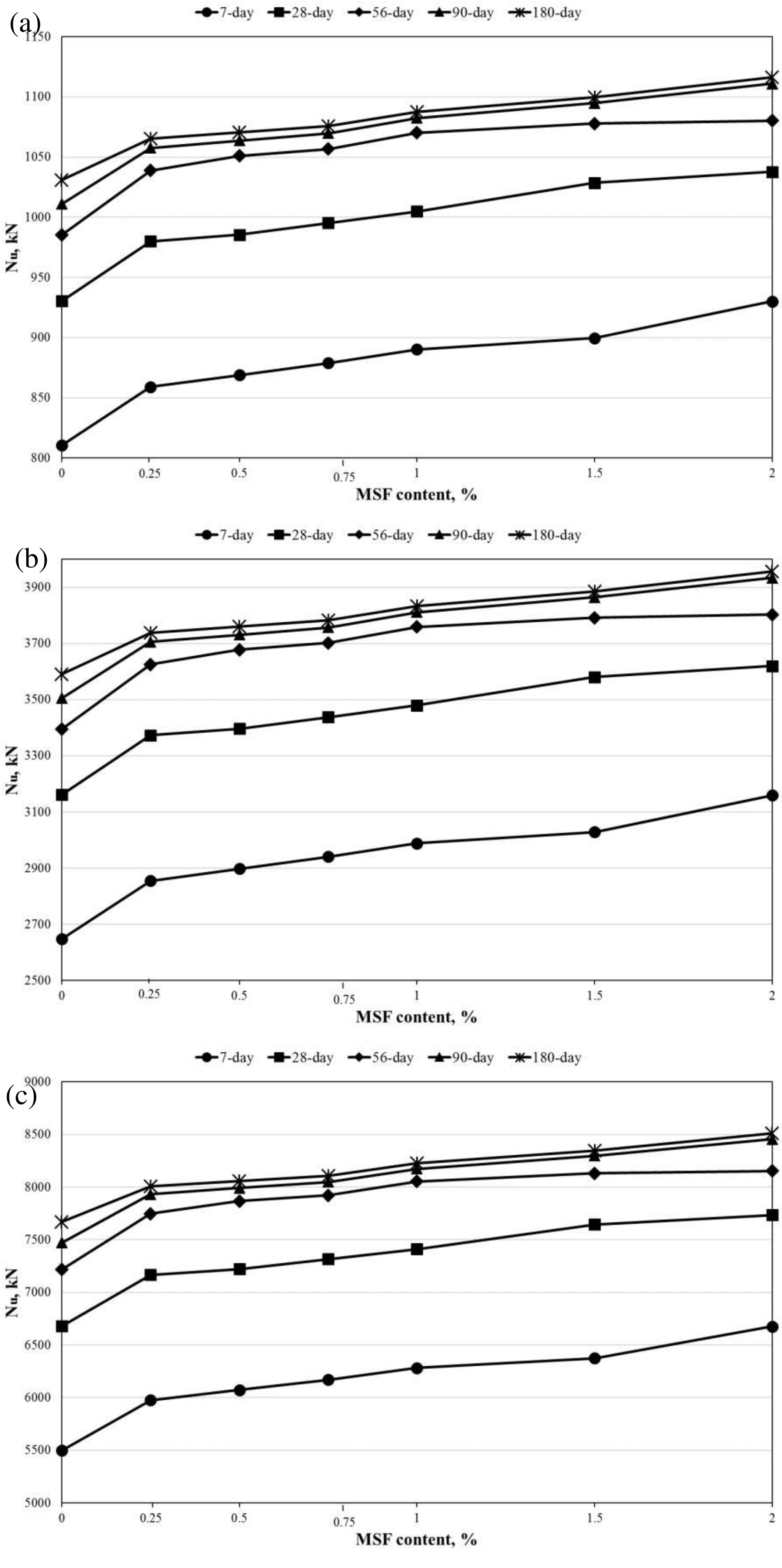

Figure 4.50. Calculated axial load capacity of CFST columns having UHPC with MSF via AISC equation for steel tube yield strength of 450 MPa: a) D/t=30, b) D/t=60, and c) D/t=90

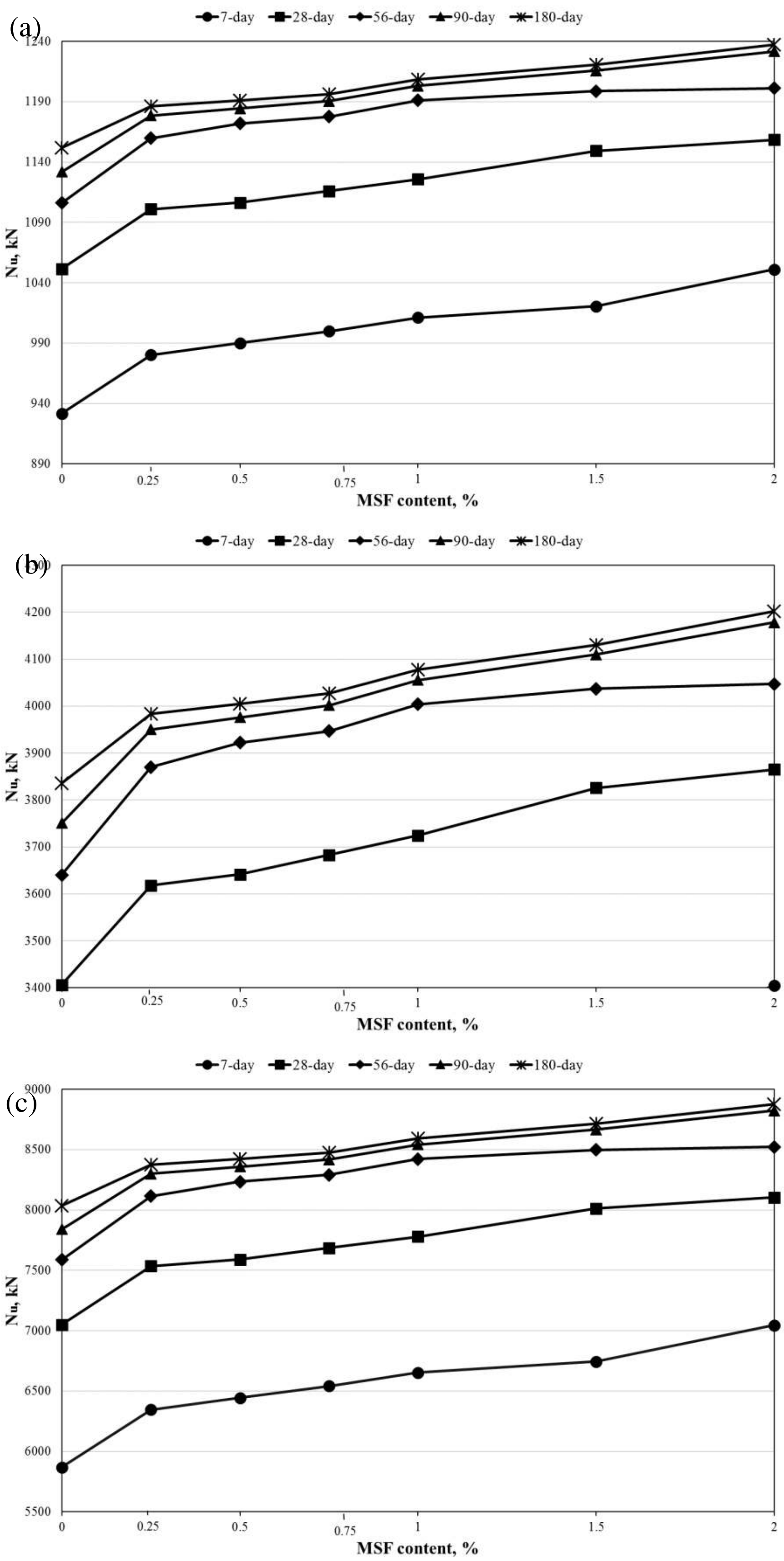

Figure 4.51. Calculated axial load capacity of CFST columns having UHPC with MSF via AISC equation for steel tube yield strength of 600 MPa: a) D/t=30, b) D/t=60, and c) D/t=90

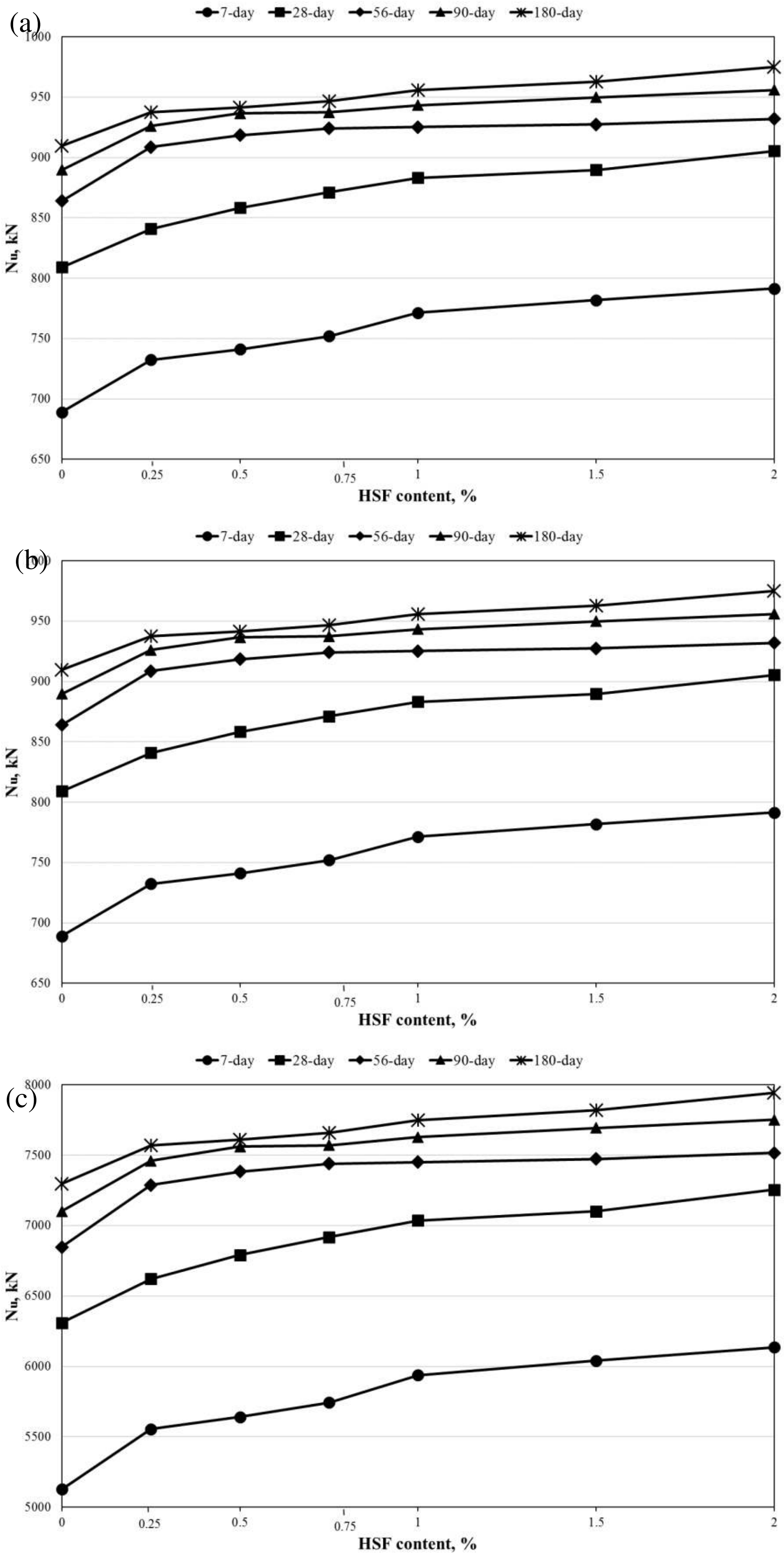

Figure 4.52. Calculated axial load capacity of CFST columns having UHPC with HSF via AISC equation for steel tube yield strength of 300 MPa: a) D/t=30, b) D/t=60, and c) D/t=90

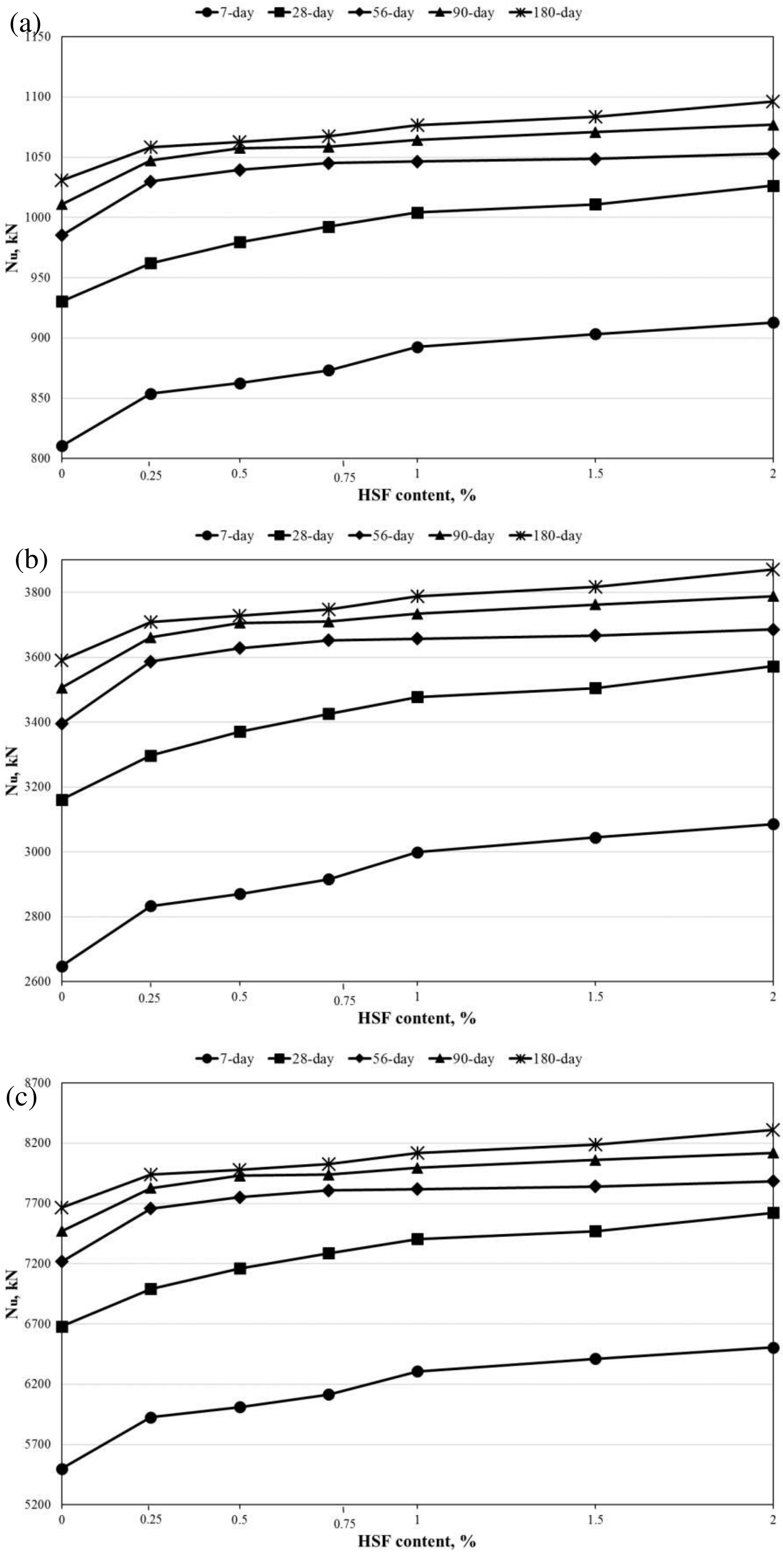

Figure 4.53. Calculated axial load capacity of CFST columns having UHPC with HSF via AISC equation for steel tube yield strength of 450 MPa: a) D/t=30, b) D/t=60, and c) D/t=90

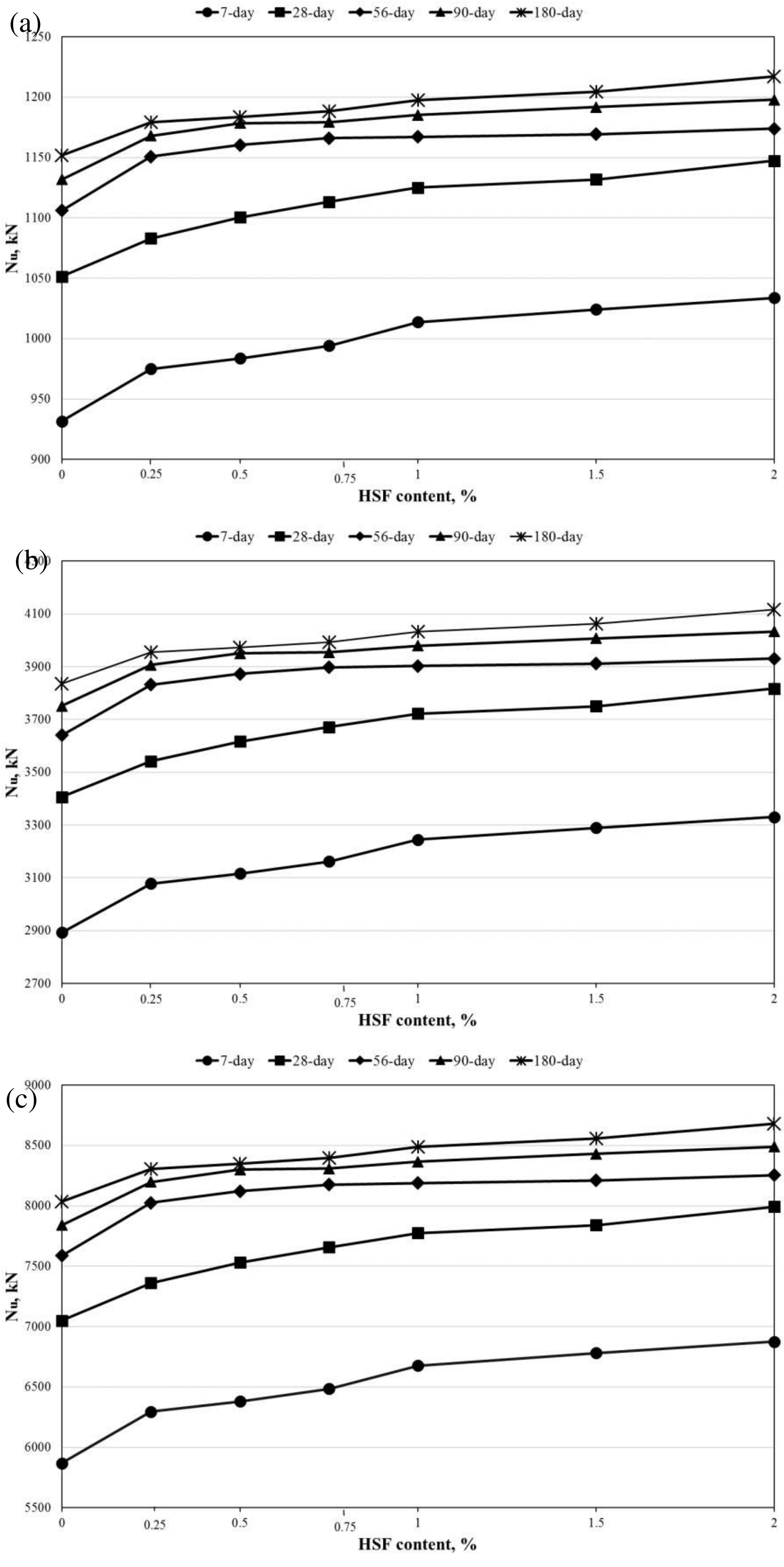

Figure 4.54. Calculated axial load capacity of CFST columns having UHPC with HSF via AISC equation for steel tube yield strength of 600 MPa: a) D/t=30, b) D/t=60, and c) D/t=90

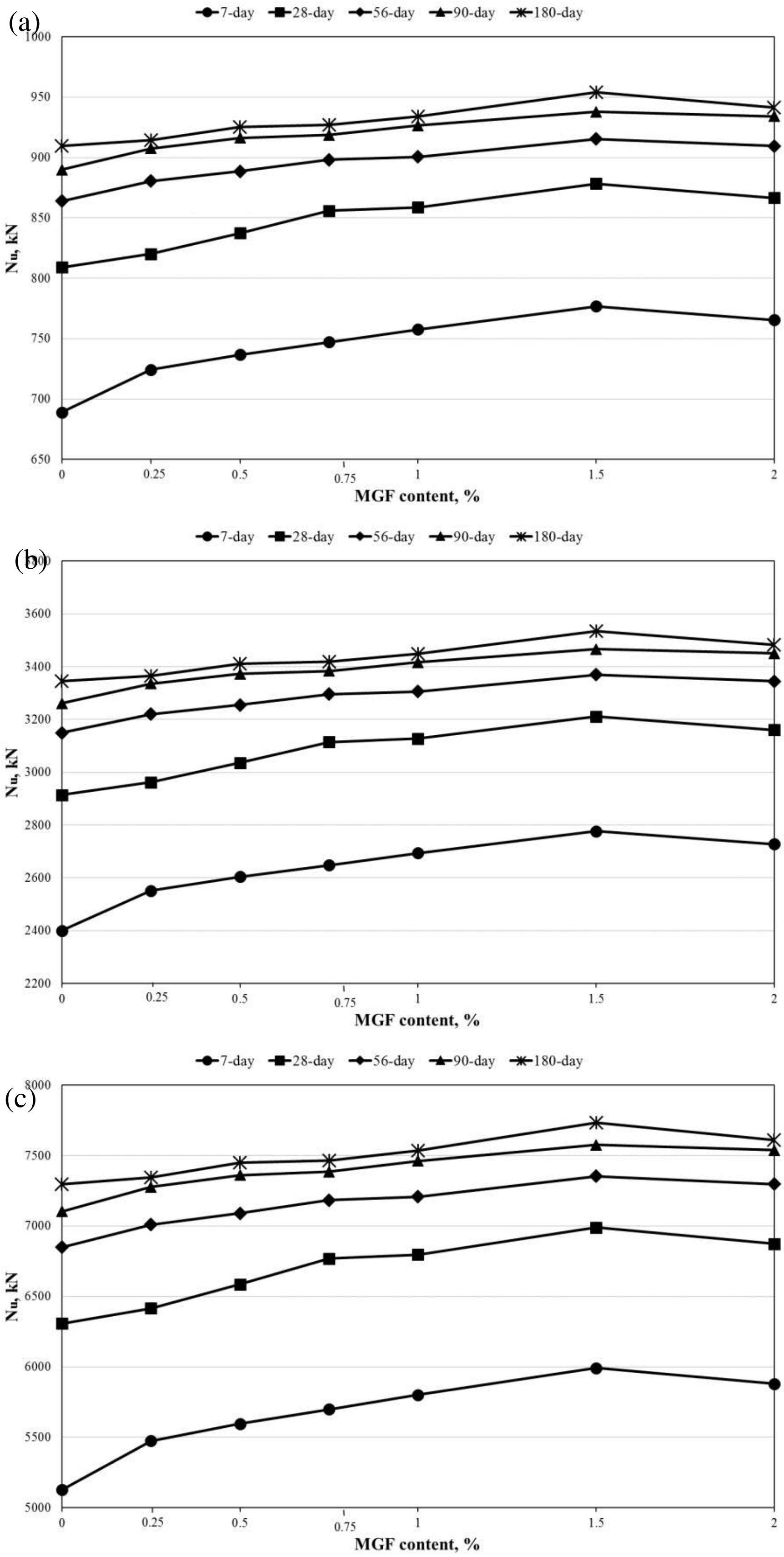

Figure 4.55. Calculated axial load capacity of CFST columns having UHPC with MGF via AISC equation for steel tube yield strength of 300 MPa: a) D/t=30, b) D/t=60, and c) D/t=90

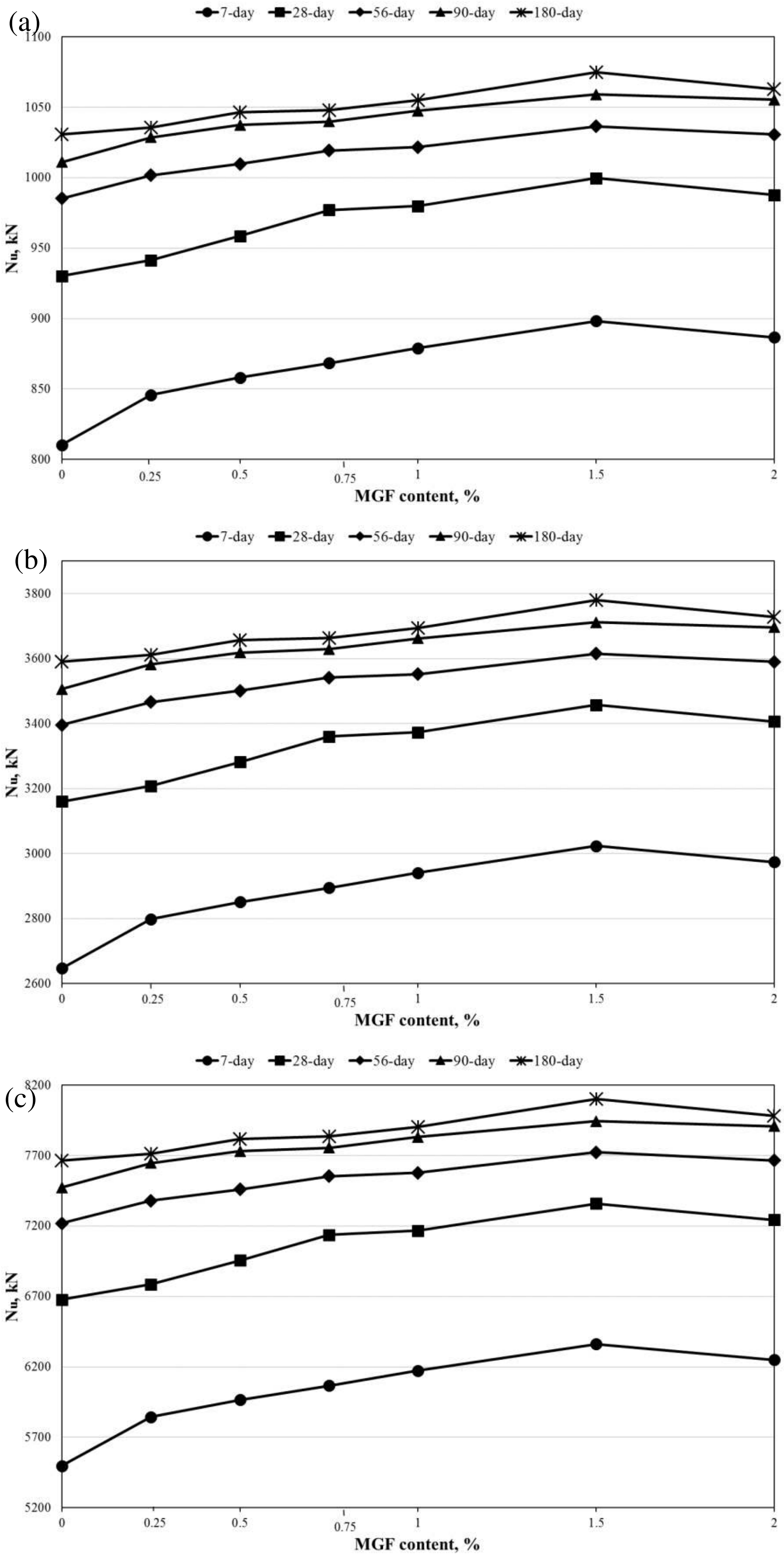

Figure 4.56. Calculated axial load capacity of CFST columns having UHPC with MGF via AISC equation for steel tube yield strength of 450 MPa: a) D/t=30, b) D/t=60, and c) D/t=90

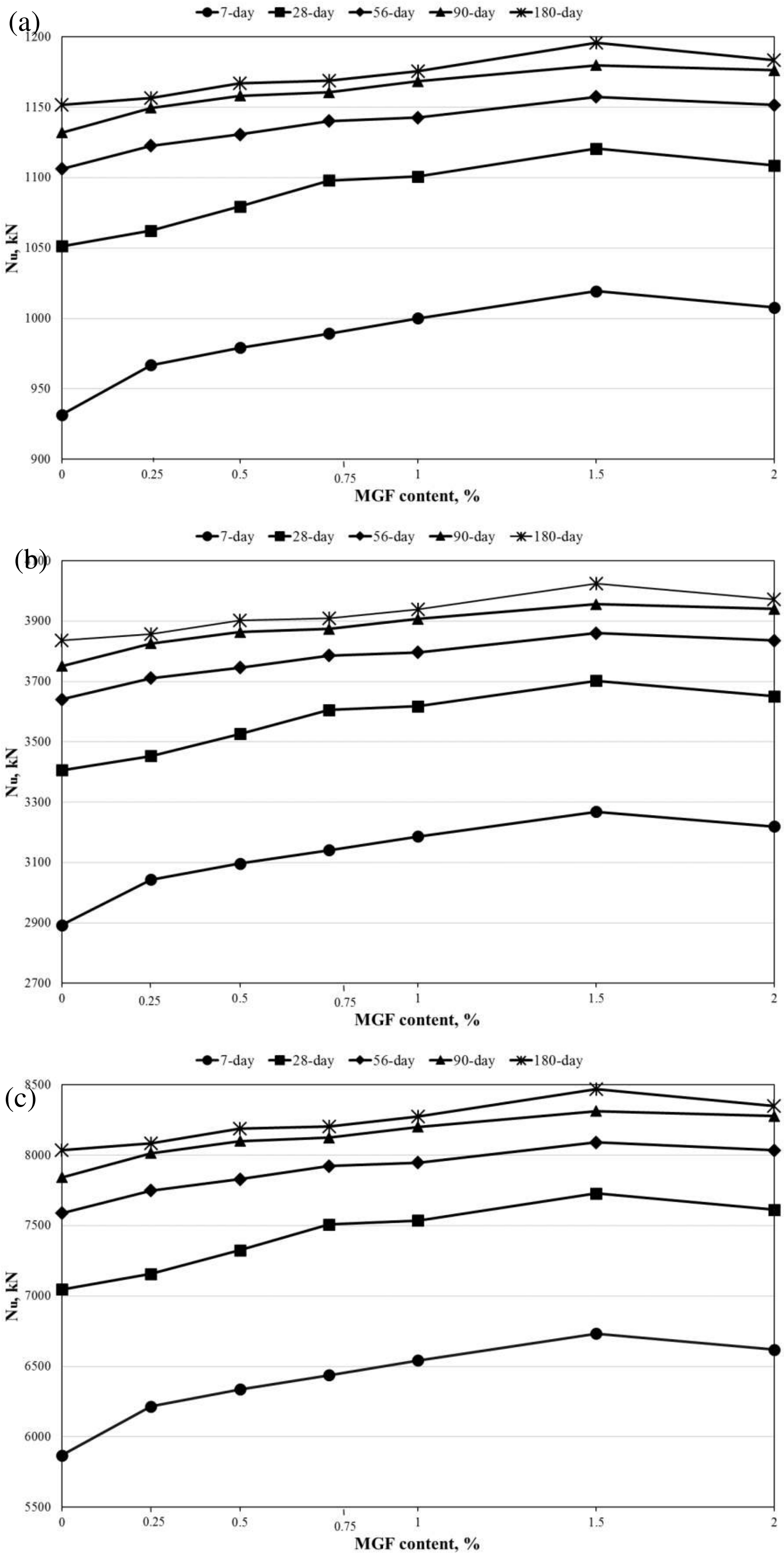

Figure 4.57. Calculated axial load capacity of CFST columns having UHPC with MGF via AISC equation for steel tube yield strength of 600 MPa: a) D/t=30, b) D/t=60, and c) D/t=90

4.2.1.4 Architectural Institute of Japan (AIJ)

The theoretical ultimate load carrying capacity of CFST filled with UHPCs with different D/t ratios, and yield strength incorporated with various volumes from 0-2% of MSF, HSF, and MGF fiber types are demonstrated in Figures of 4.58-4.60, 4.61-4.63, and 4.64-4.66, correspondingly. The behavior herein was considered similar to that seen in the previous codes. As it is seen from Figure 4.58a that the minimum ultimate load carrying capacity was observed for seven days of testing age when D/t ratio is set as 30 and yield stress is 300 MPa, specifically of the plain concrete was 757.1 kN that increased to 877.4 kN at 2% of micro steel fiber. However, in Figure 4.61a for the UHPCs with the hooked steel fiber group the minimum ultimate load carrying capacity reached 860 kN at 2%.

On the other hand, for the UHPCs reinforced with micro glass the maximum results of the ultimate load carrying capacity about 845.5 kN is linked to 1.5 % then decreased to 833.7 kN for 2% of fiber concentration. The test results recommended using micro steel fiber, hooked steel fiber, and micro glass fiber considering their beneficial effects on the ultimate load carrying capacity. Therefore, micro steel fibers seemed to be preferable than hooked steel fiber then micro glass fibers. Actually, UHPCs with 2% of MSF, D/t =90, and Fy= 600 MPa had the highest axial load capacity of 9354.5 kN at 180 days, which reduced to 9152.3 kN for 2% hooked fiber and to 8939.4 kN for 1.5% of micro glass fibers. This may be concerned to rigidity and large amounts of micro steel pieces that made an intimate relationship with the other concrete constituents.

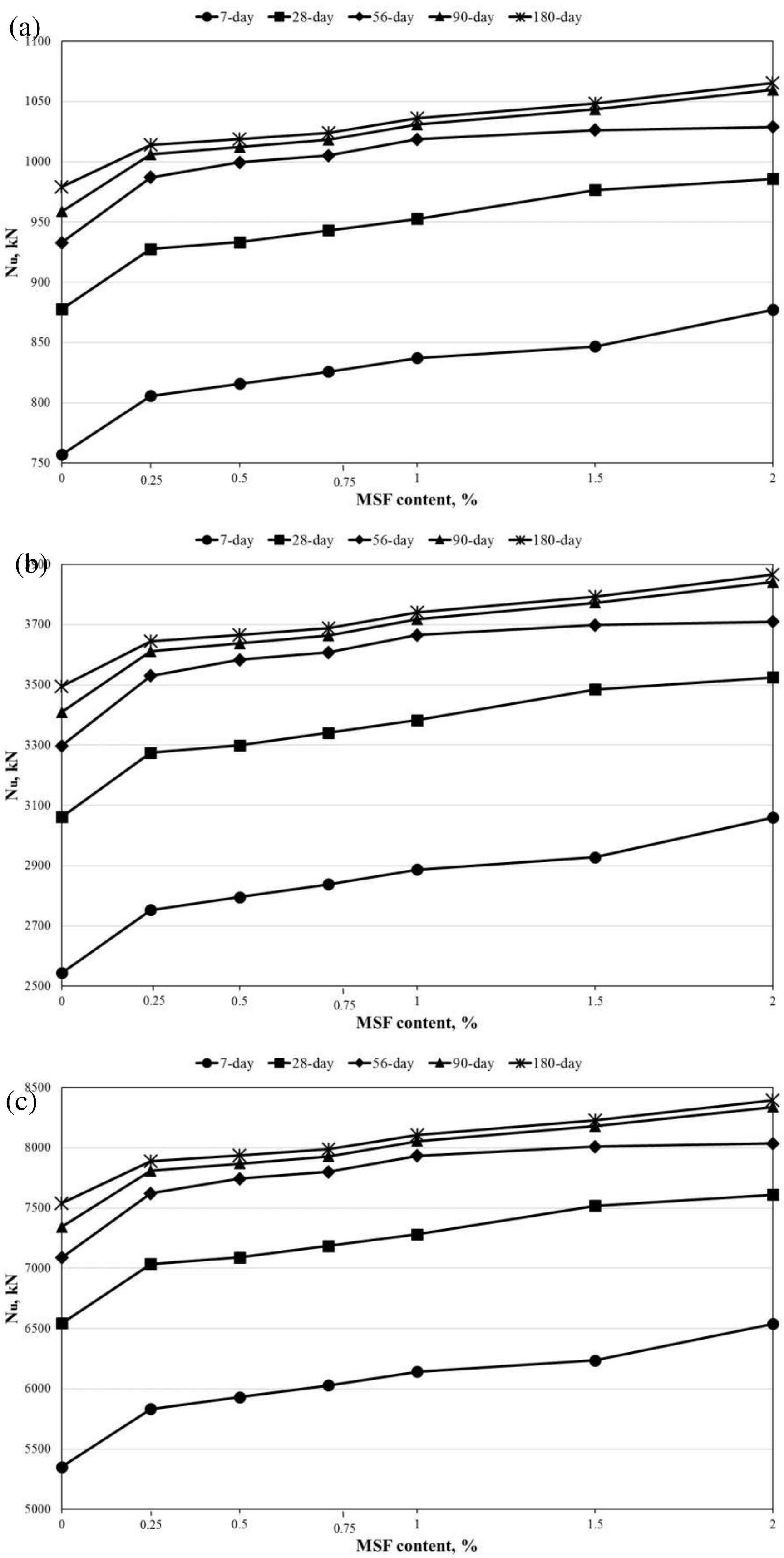

Figure 4.58. Calculated axial load capacity of CFST columns having UHPC with MSF via AIJ equation for steel tube yield strength of 300 MPa: a) D/t=30, b) D/t=60, and c) D/t=90

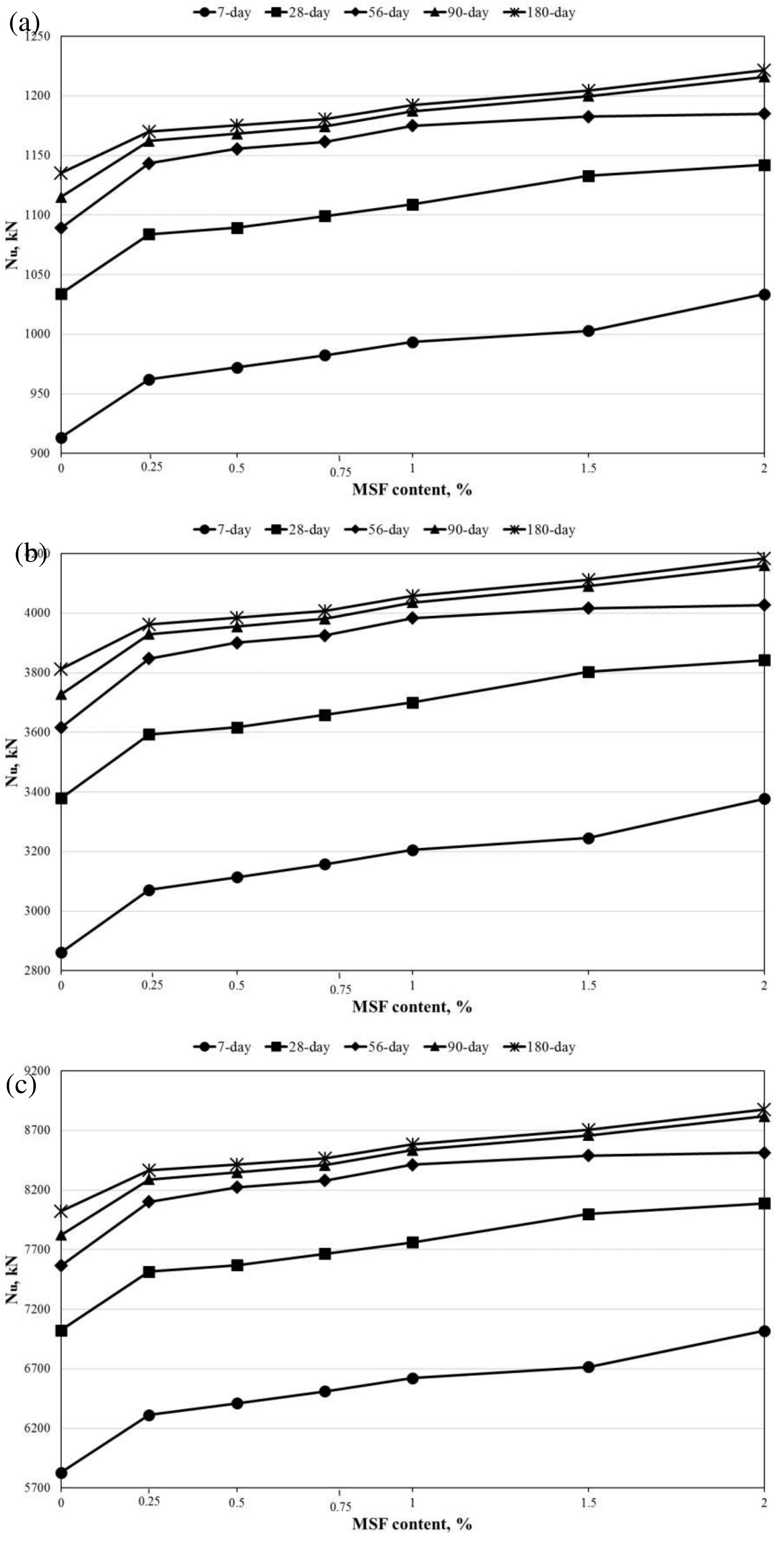

Figure 4.59. Calculated axial load capacity of CFST columns having UHPC with MSF via AIJ equation for steel tube yield strength of 450 MPa: a) D/t=30, b) D/t=60, and c) D/t=90

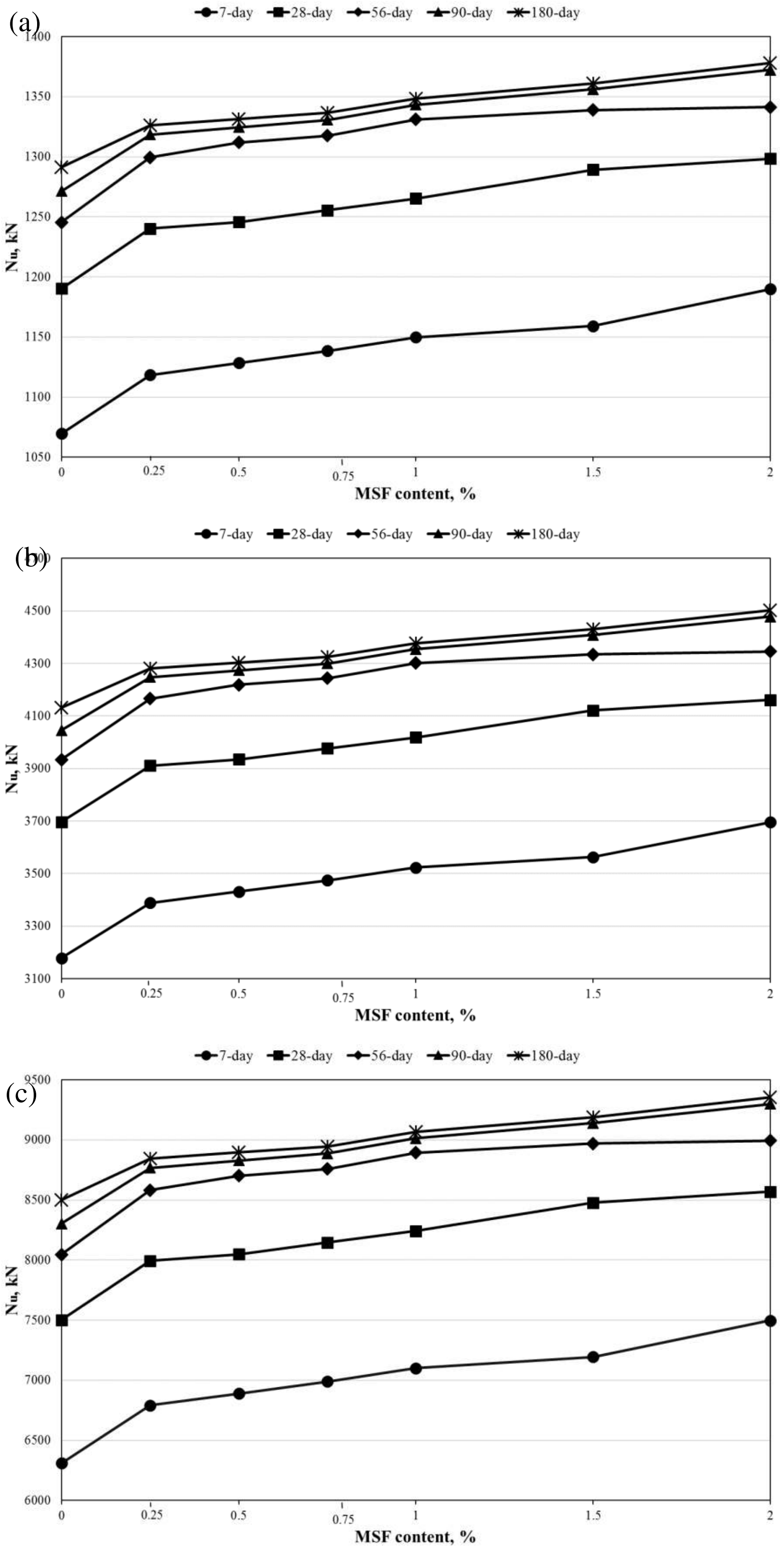

Figure 4.60. Calculated axial load capacity of CFST columns having UHPC with MSF via AIJ equation for steel tube yield strength of 600 MPa: a) D/t=30, b) D/t=60, and c) D/t=90

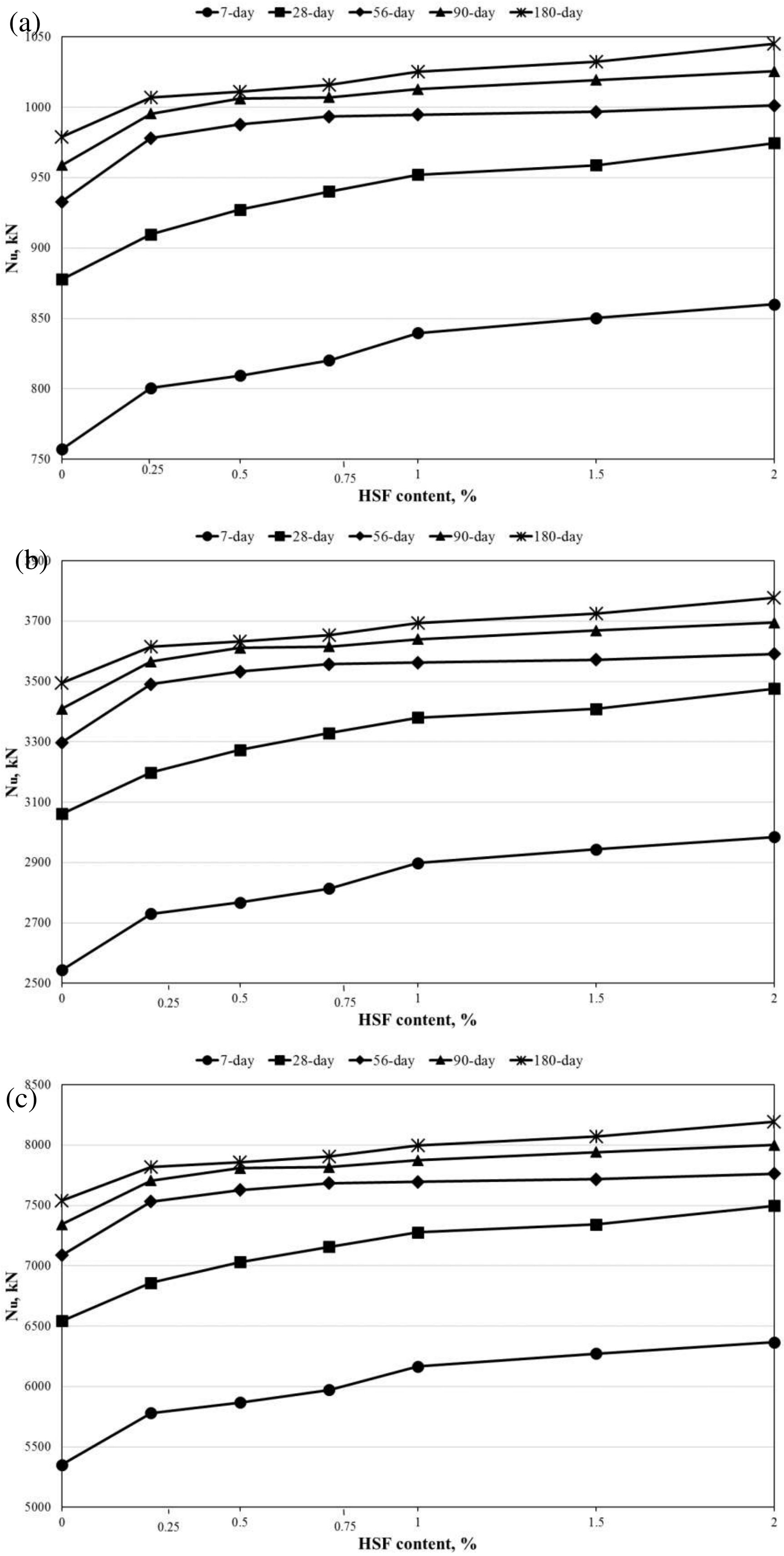

Figure 4.61. Calculated axial load capacity of CFST columns having UHPC with HSF via AIJ equation for steel tube yield strength of 300 MPa: a) D/t=30, b) D/t=60, and c) D/t=90

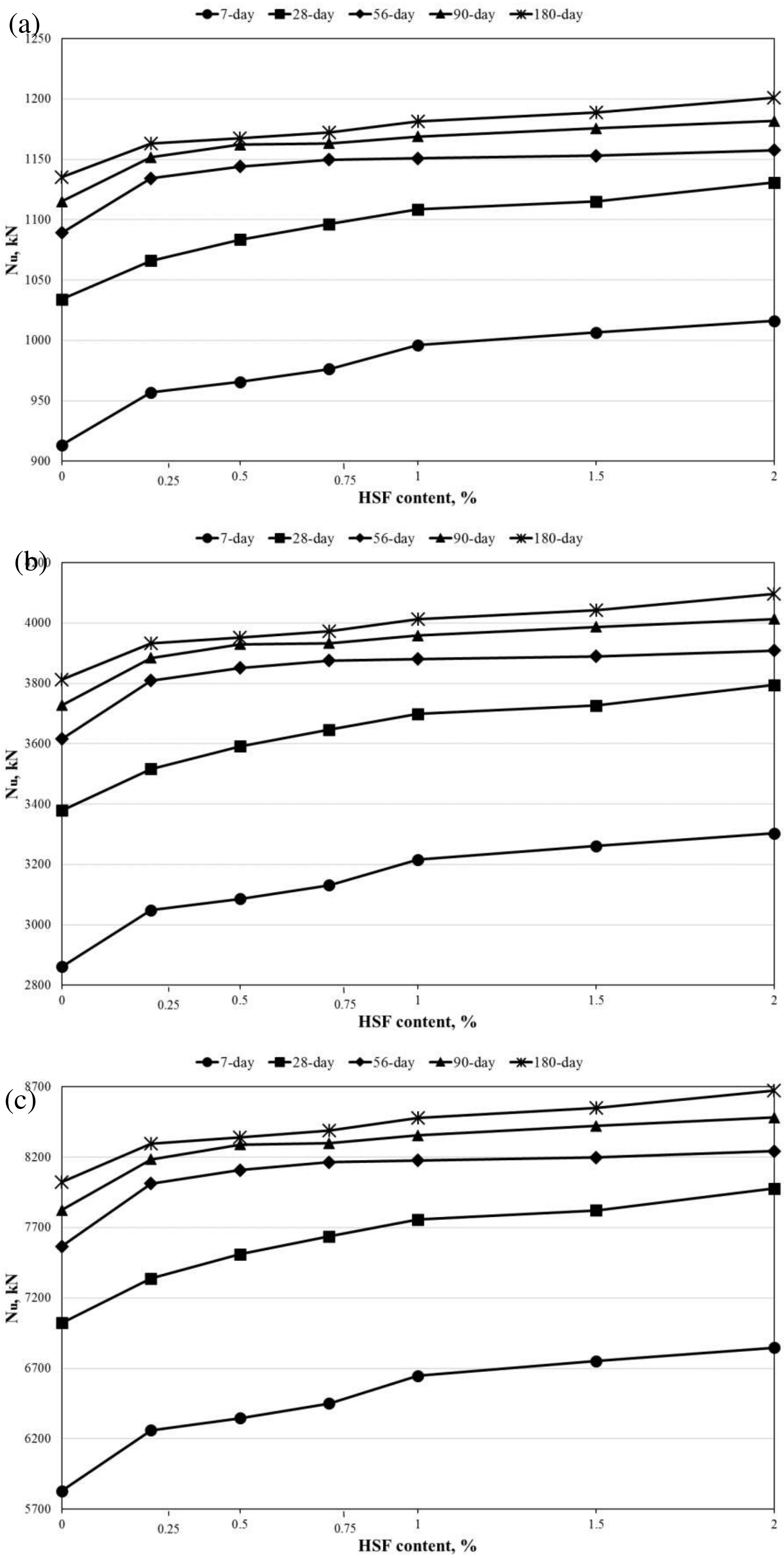

Figure 4.62. Calculated axial load capacity of CFST columns having UHPC with HSF via AIJ equation for steel tube yield strength of 450 MPa: a) D/t=30, b) D/t=60, and c) D/t=90

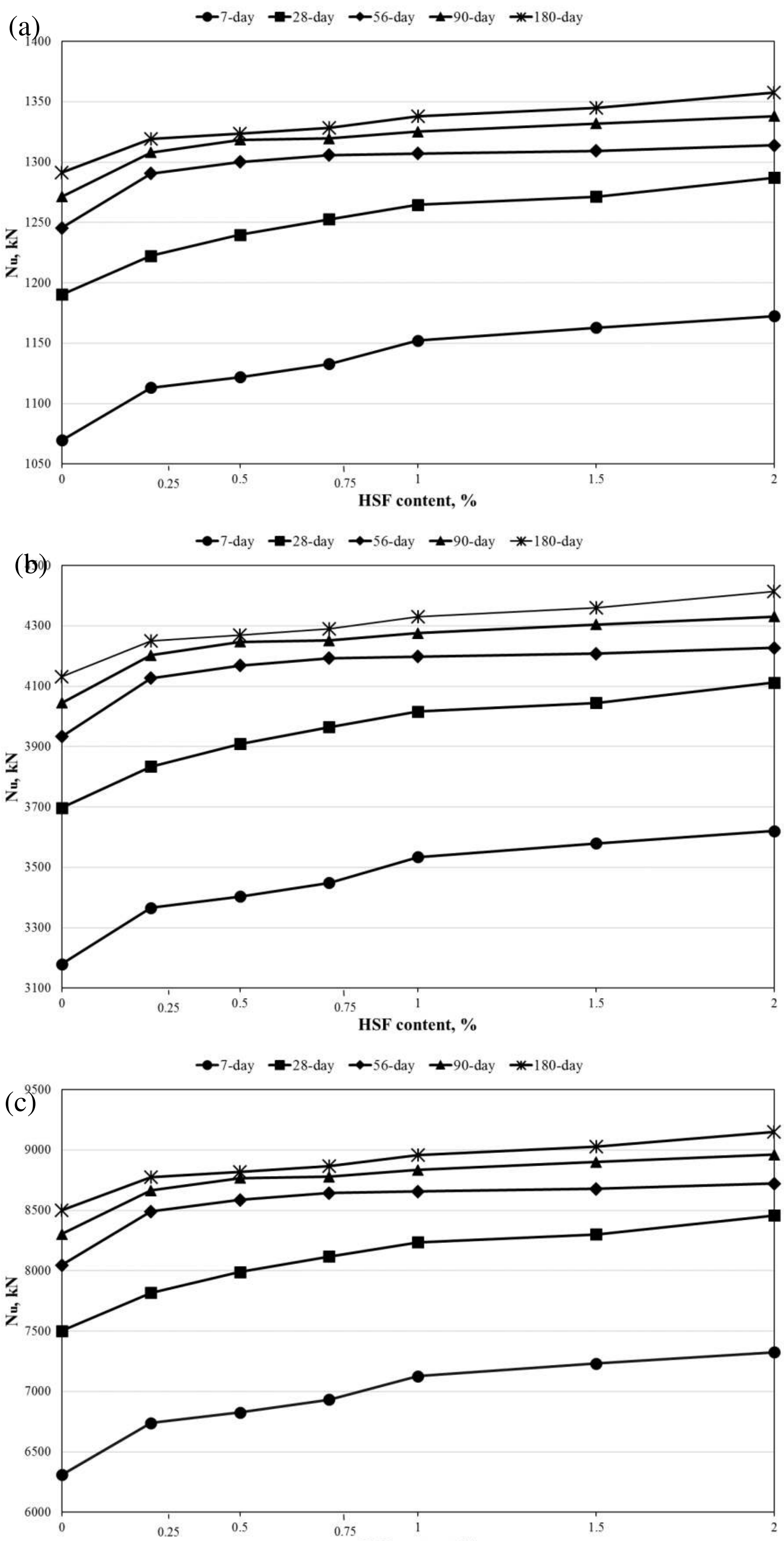

Figure 4.63. Calculated axial load capacity of CFST columns having UHPC with HSF via AIJ equation for steel tube yield strength of 600 MPa: a) D/t=30, b) D/t=60, and c) D/t=90

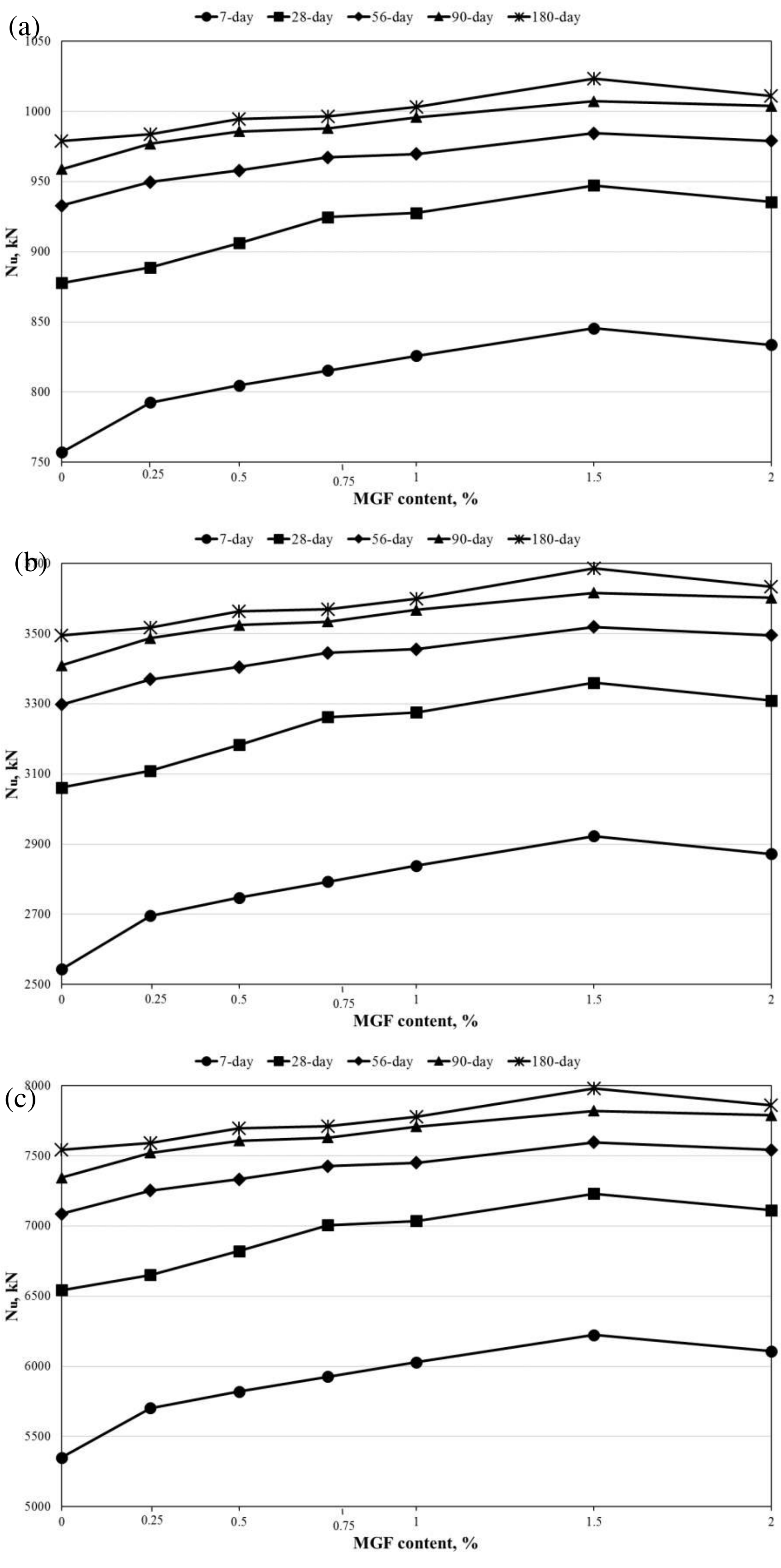

Figure 4.64. Calculated axial load capacity of CFST columns having UHPC with MGF via AIJ equation for steel tube yield strength of 300 MPa: a) D/t=30, b) D/t=60, and c) D/t=90

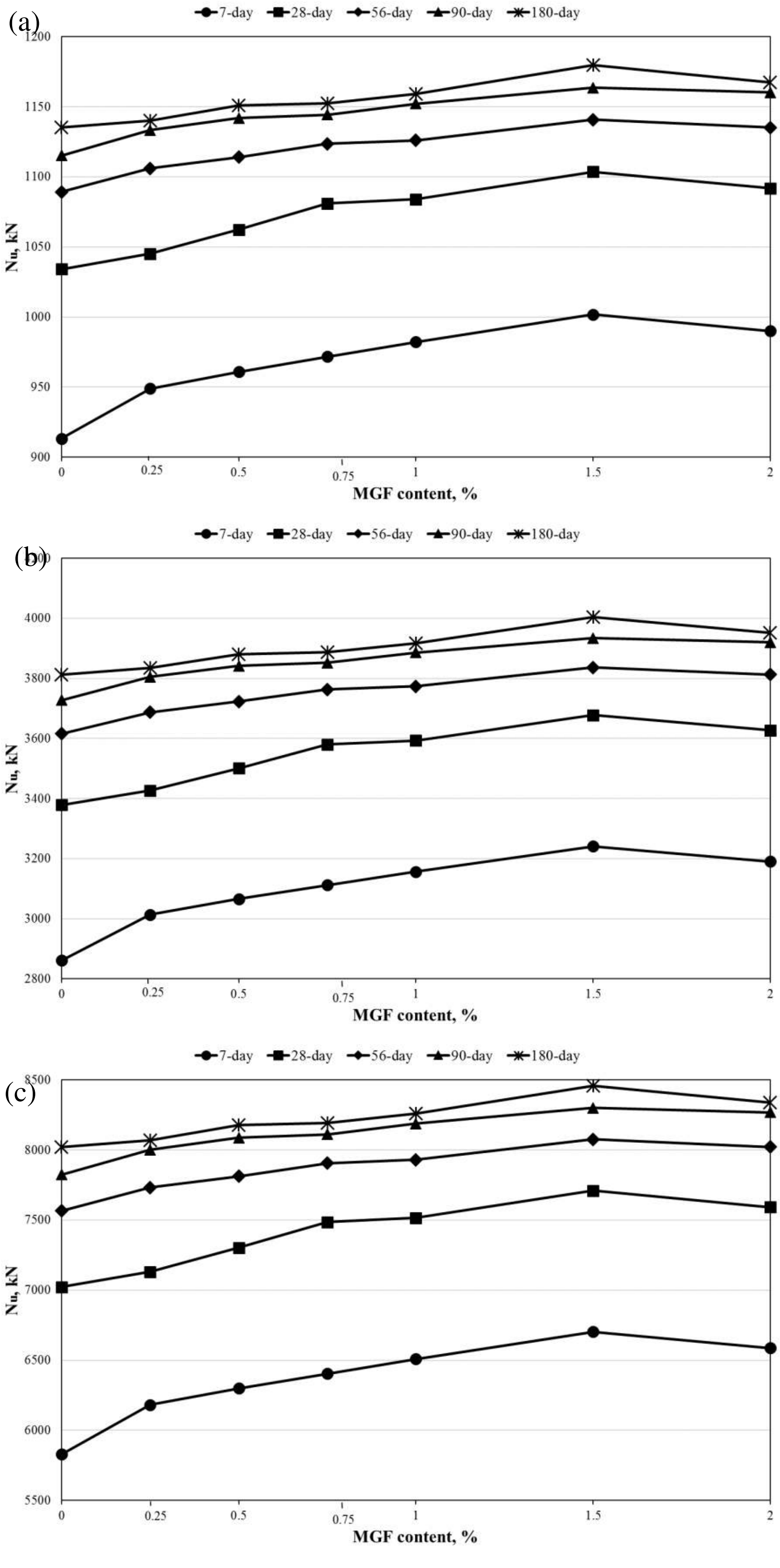

Figure 4.65. Calculated axial load capacity of CFST columns having UHPC with MGF via AIJ equation for steel tube yield strength of 450 MPa: a) D/t=30, b) D/t=60, and c) D/t=90

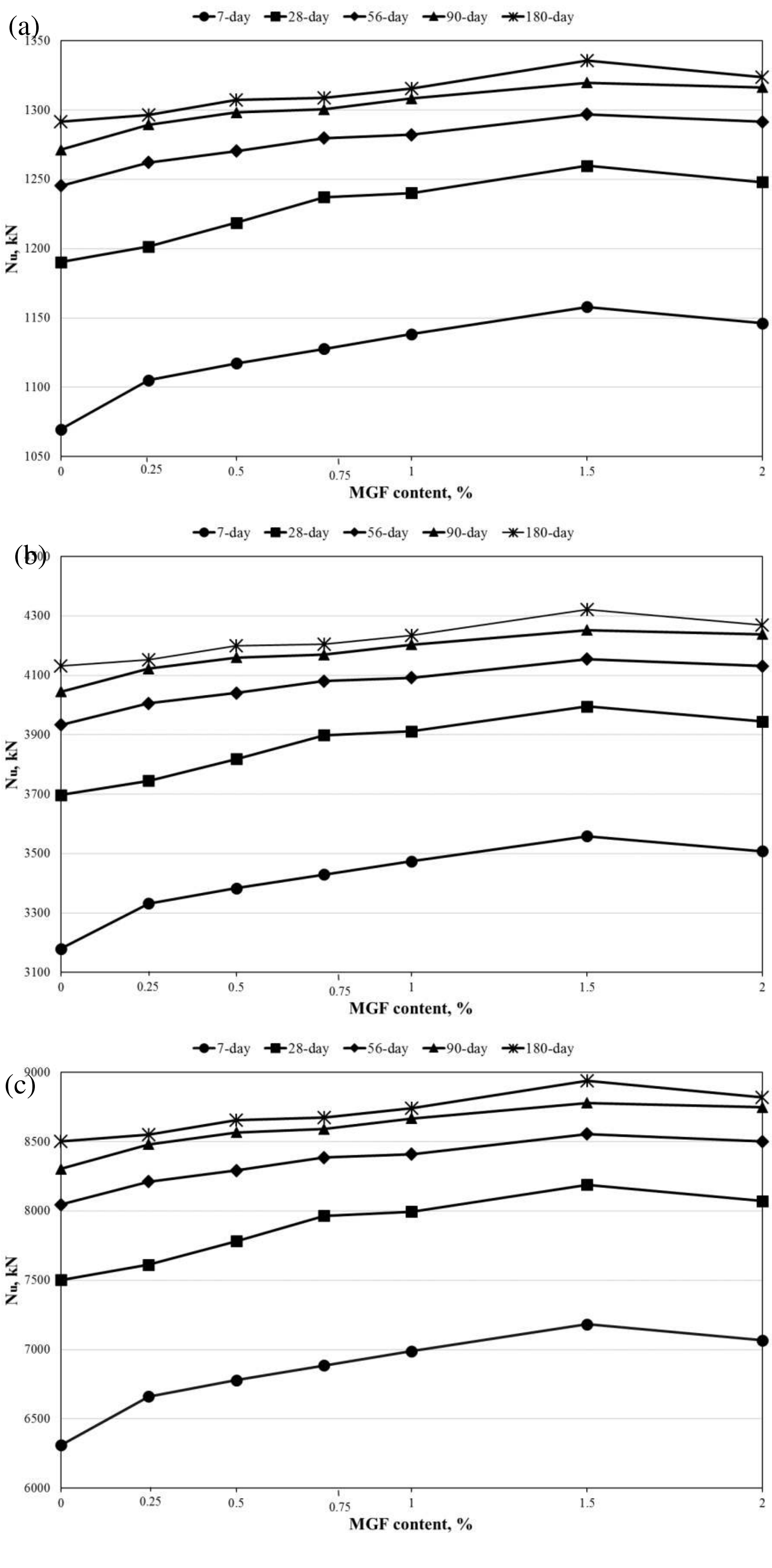

Figure 4.66. Calculated axial load capacity of CFST columns having UHPC with MGF via AIJ equation for steel tube yield strength of 600 MPa: a) D/t=30, b) D/t=60, and c) D/t=90

4.2.1.5 Chinese code (DL/T)

Effects of fiber type on the ultimate axial load capacity of the CFST filled with UHPCs reinforced with micro steel, hooked steel, and micro glass fibers are presented in Figures 4.67-4.69, 4.70-4.72, and 4.73-4.75, respectively. Regardless of the testing age, it was observed that the ultimate axial load capacity of CFST continuously increased in the case of steel fibers whereas the augmentation ended at 1.5% of micro glass fibers. Afar 1.5% of micro glass fiber, axial load capacity started to decrease but the value still higher than 1% of all cases. Moreover, the growth of the results after 56 days appeared to be quite restricted as there was little improvement observed at 90 and 180 days, irrespective of fiber types. Such phenomenon was perhaps due to the quickening of finishing chemical reactions because of a constant amount of silica fume used for all the mixtures which equal to 20% of total binder content.

Finally, the test results recommended an order of micro steel fiber, hooked steel fiber, and micro glass fiber seeing their beneficial effects on the axial load capacity. Consequently, MSF appeared to be more desirable than HSF then MGF. Actually, UHPCs with 2% of MSF had the maximum axial load capacity of 9400.9 kN at 180 days, fy=600MPa, and D/t=90 which lowered to 9202.2 kN for 2% HSF reinforced UHPC and to 8992.3 kN for 1.5% of MGF reinforced UHPC. The favorite MSF over the others is maybe due to that huge number of micro steel fibers per any percentage amount distributed regularly and intimately inside concrete with an assistant of their rigidity and size, as seen in Figure 4.2 a, b, and c.

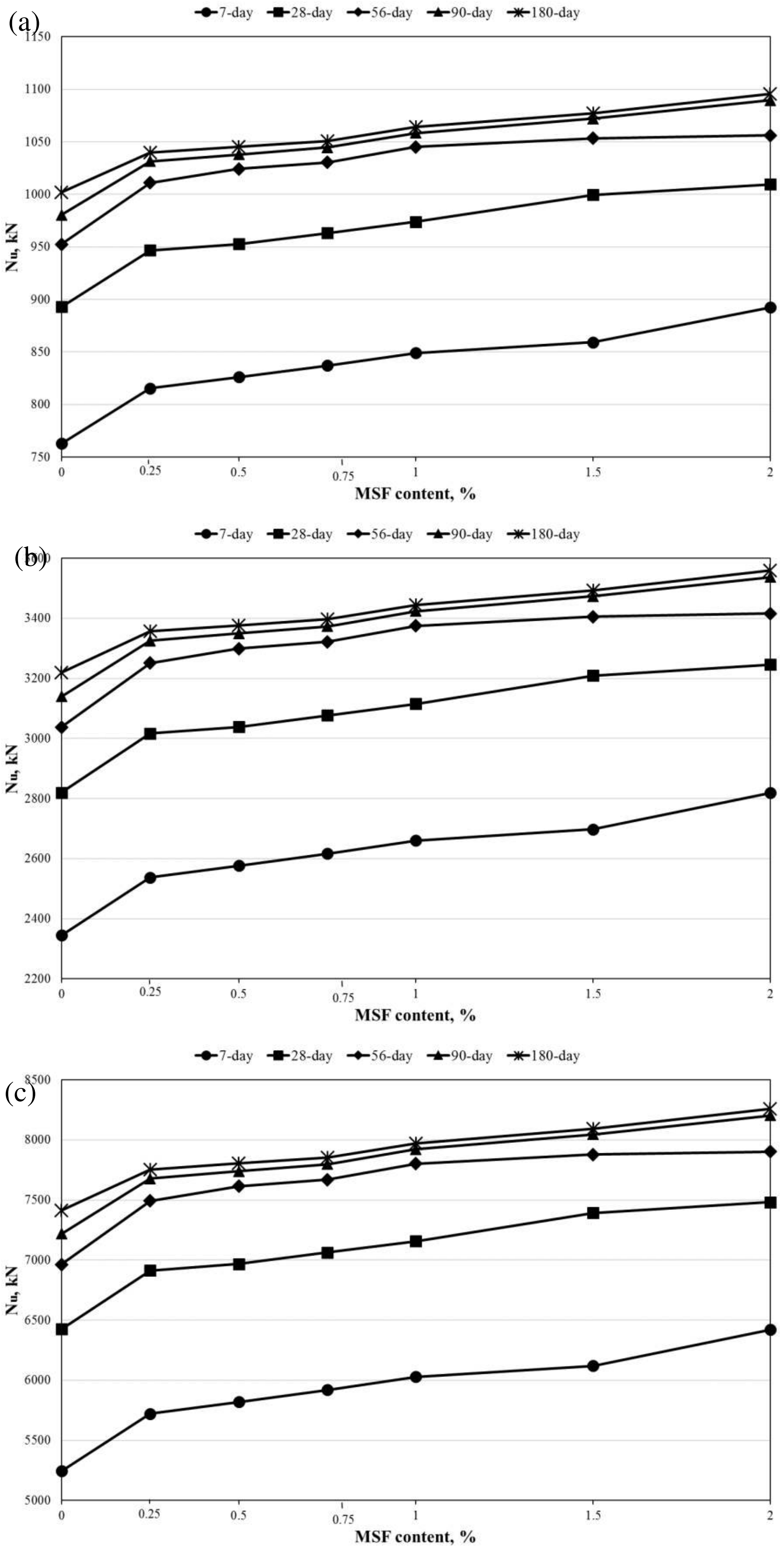

Figure 4.67. Calculated axial load capacity of CFST columns having UHPC with MSF via DL/T equation for steel tube yield strength of 300 MPa: a) D/t=30, b) D/t=60, and c) D/t=90

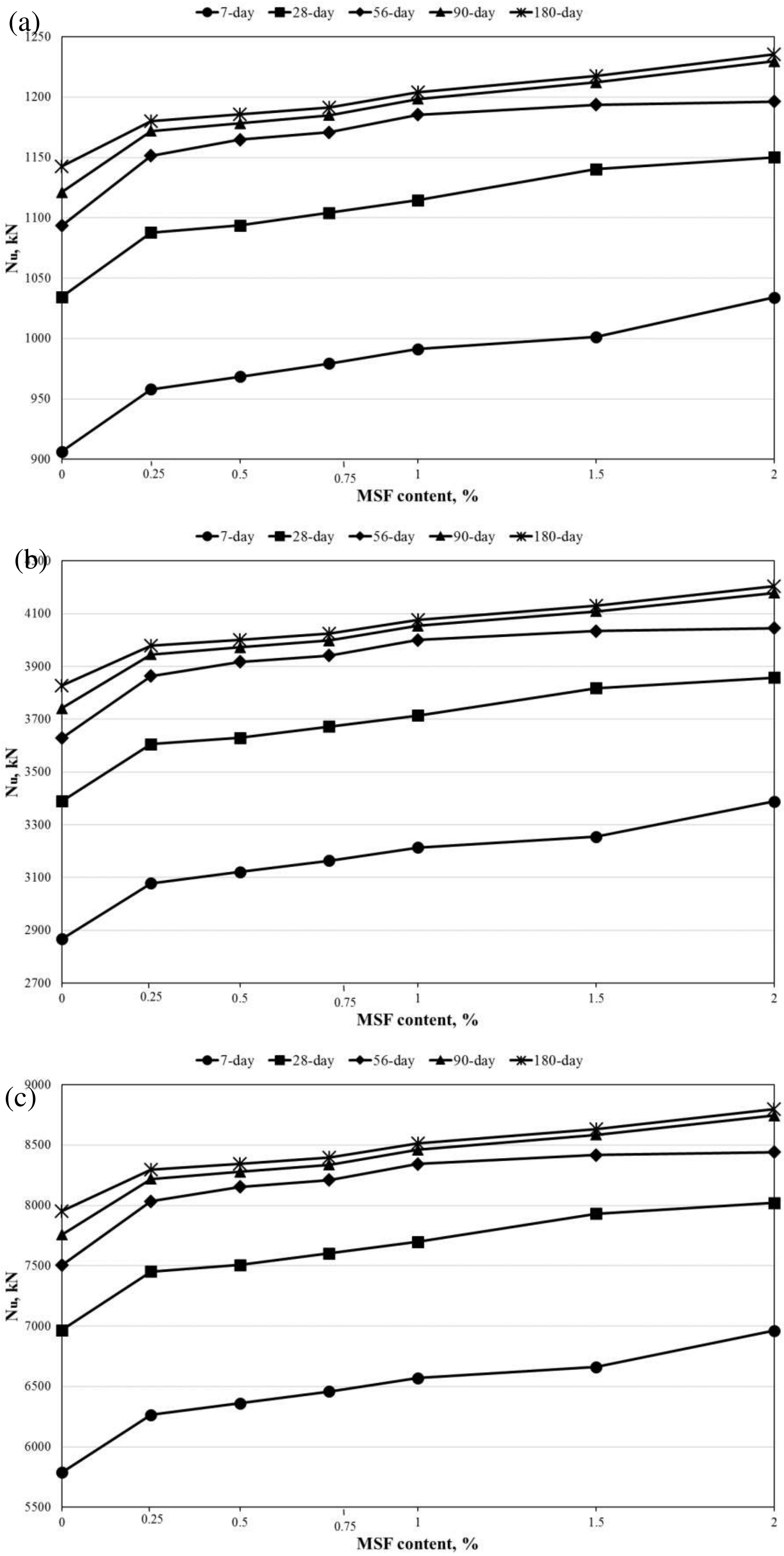

Figure 4.68. Calculated axial load capacity of CFST columns having UHPC with MSF via DL/T equation for steel tube yield strength of 450 MPa: a) D/t=30, b) D/t=60, and c) D/t=90

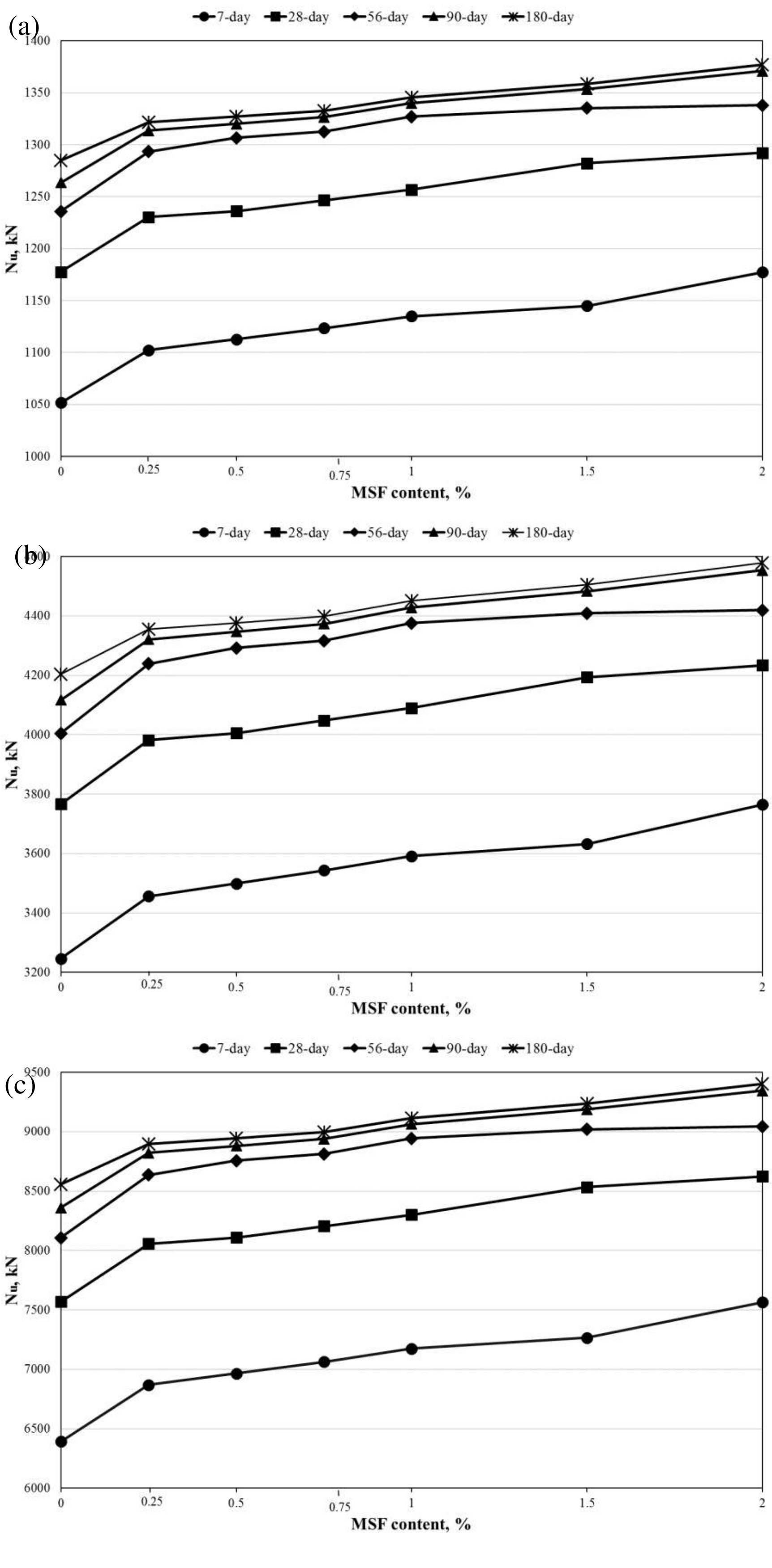

Figure 4.69. Calculated axial load capacity of CFST columns having UHPC with MSF via DL/T equation for steel tube yield strength of 600 MPa: a) D/t=30, b) D/t=60, and c) D/t=90

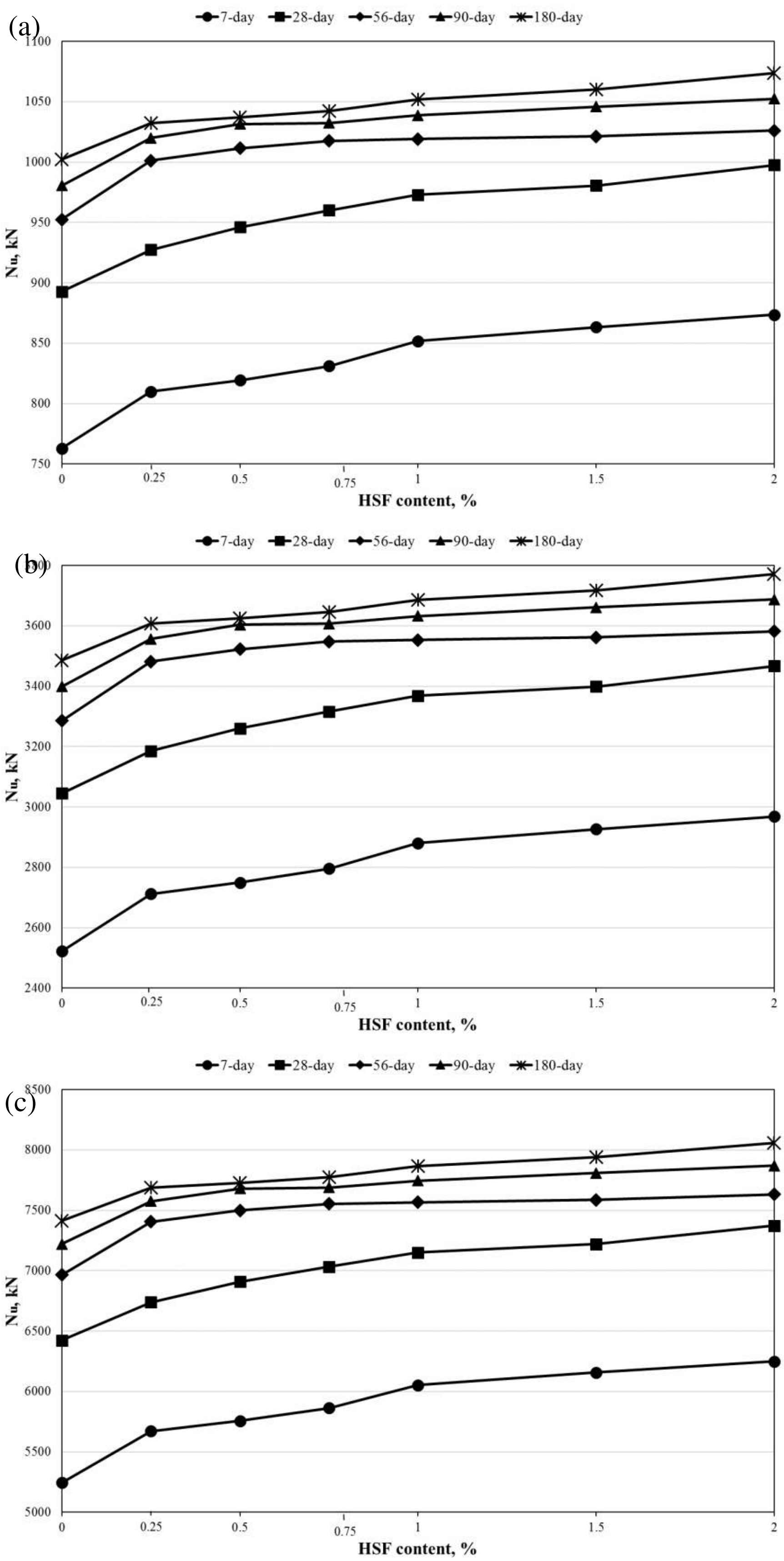

Figure 4.70. Calculated axial load capacity of CFST columns having UHPC with MSF via DL/T equation for steel tube yield strength of 300 MPa: a) D/t=30, b) D/t=60, and c) D/t=90

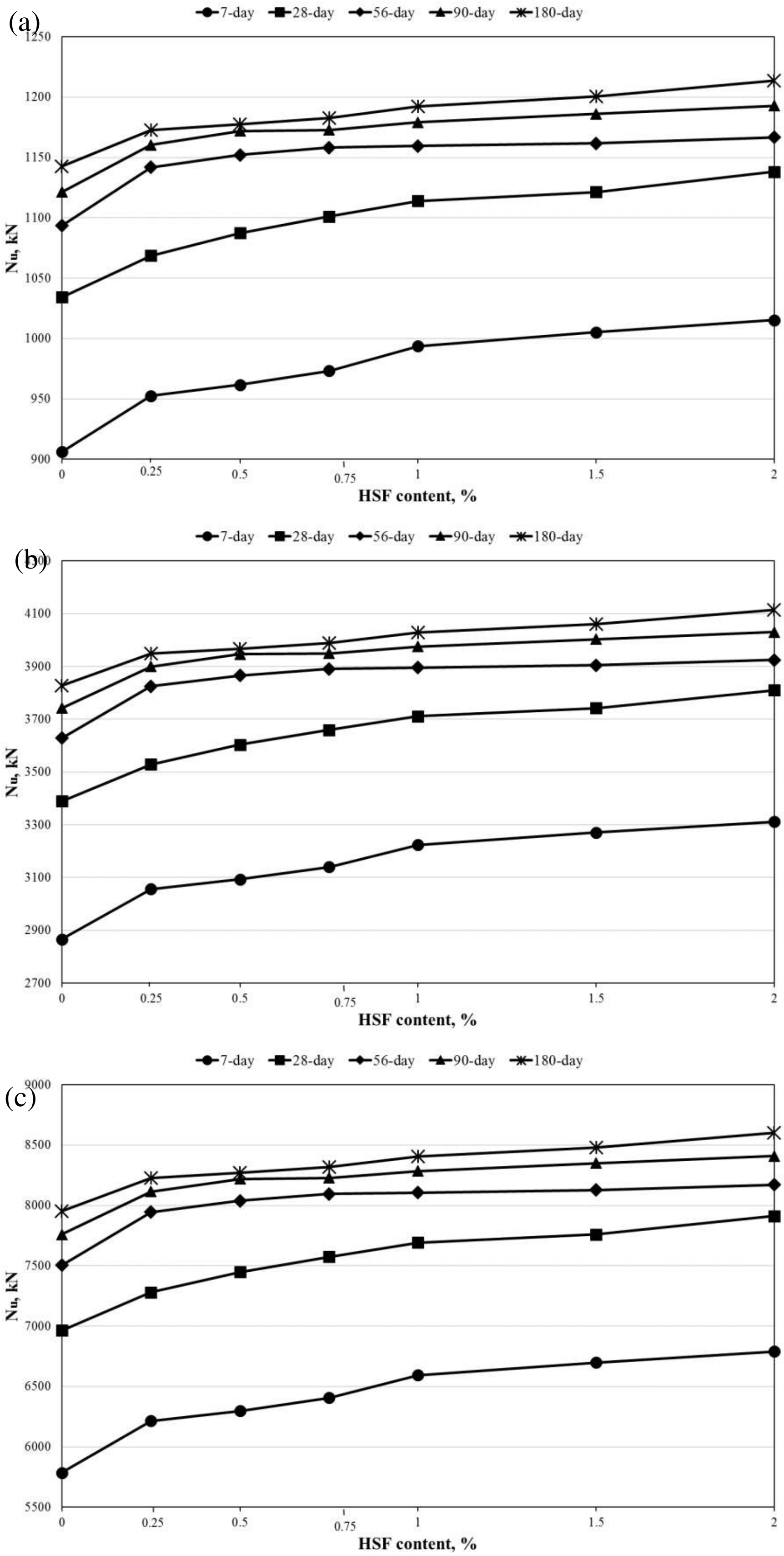

Figure 4.71. Calculated axial load capacity of CFST columns having UHPC with MSF via DL/T equation for steel tube yield strength of 450 MPa: a) D/t=30, b) D/t=60, and c) D/t=90

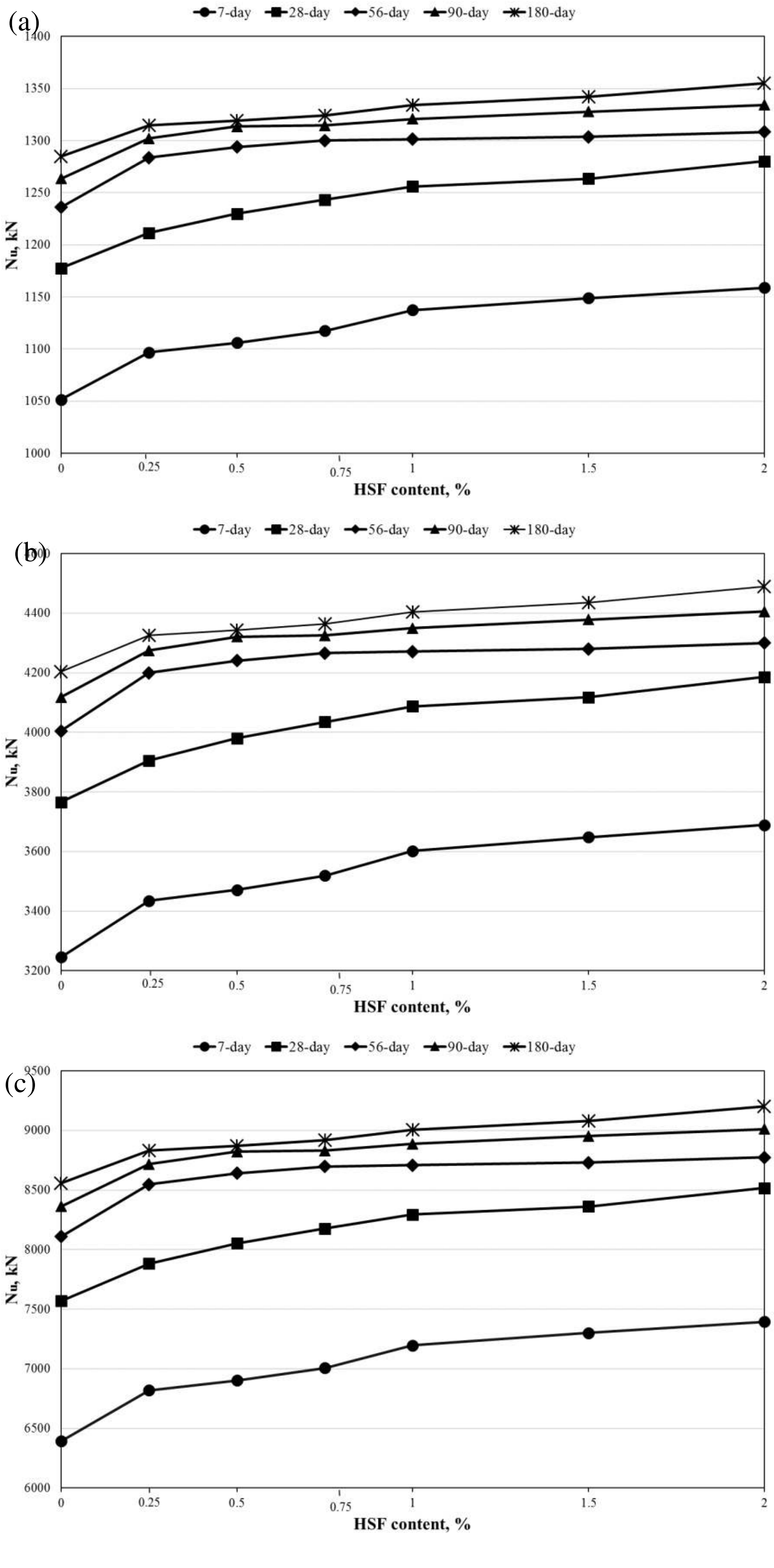

Figure 4.72. Calculated axial load capacity of CFST columns having UHPC with MSF via DL/T equation for steel tube yield strength of 600 MPa: a) D/t=30, b) D/t=60, and c) D/t=90

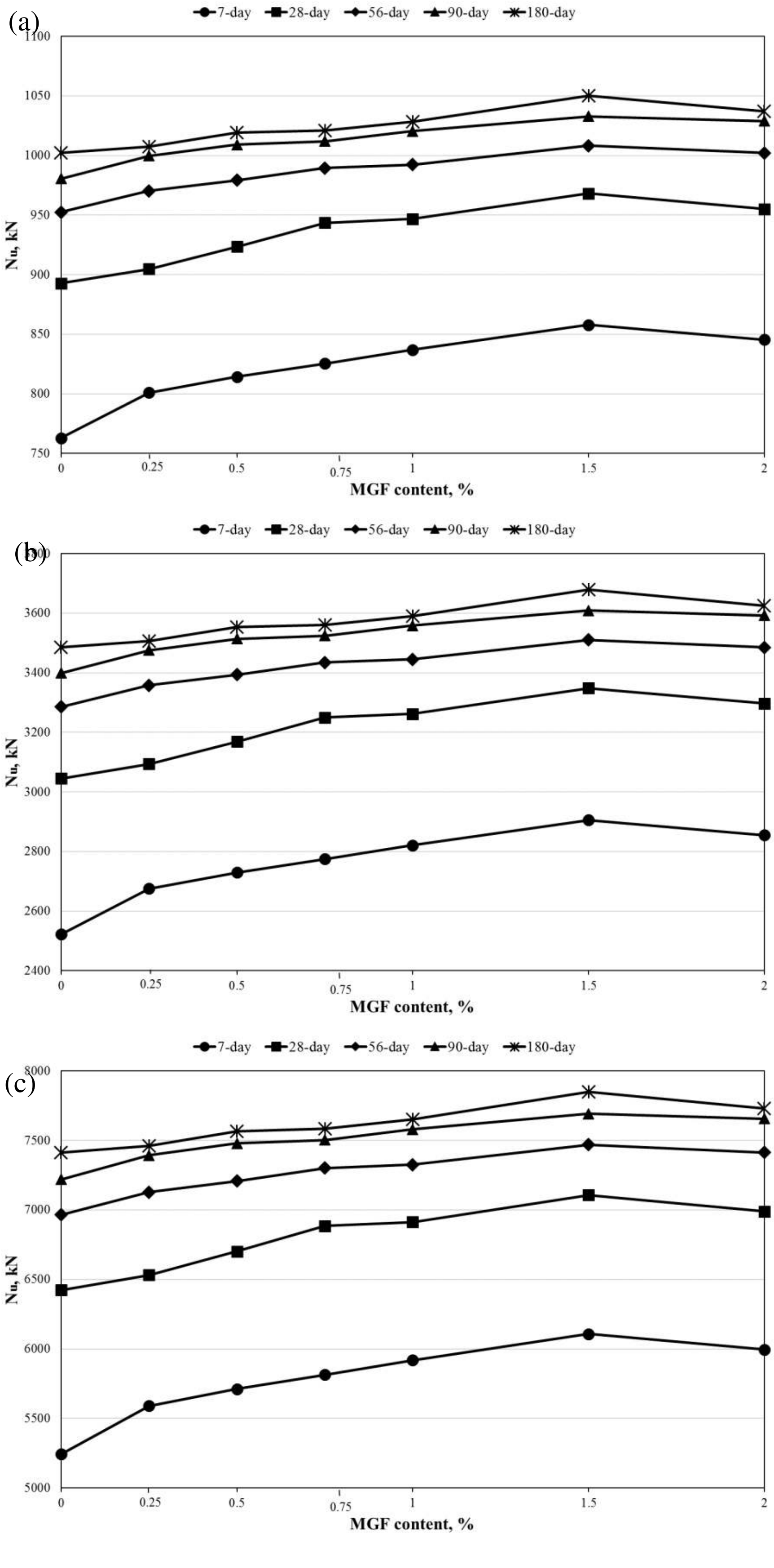

Figure 4.73. Calculated axial load capacity of CFST columns having UHPC with MGF via DL/T equation for steel tube yield strength of 300 MPa: a) D/t=30, b) D/t=60, and c) D/t=90

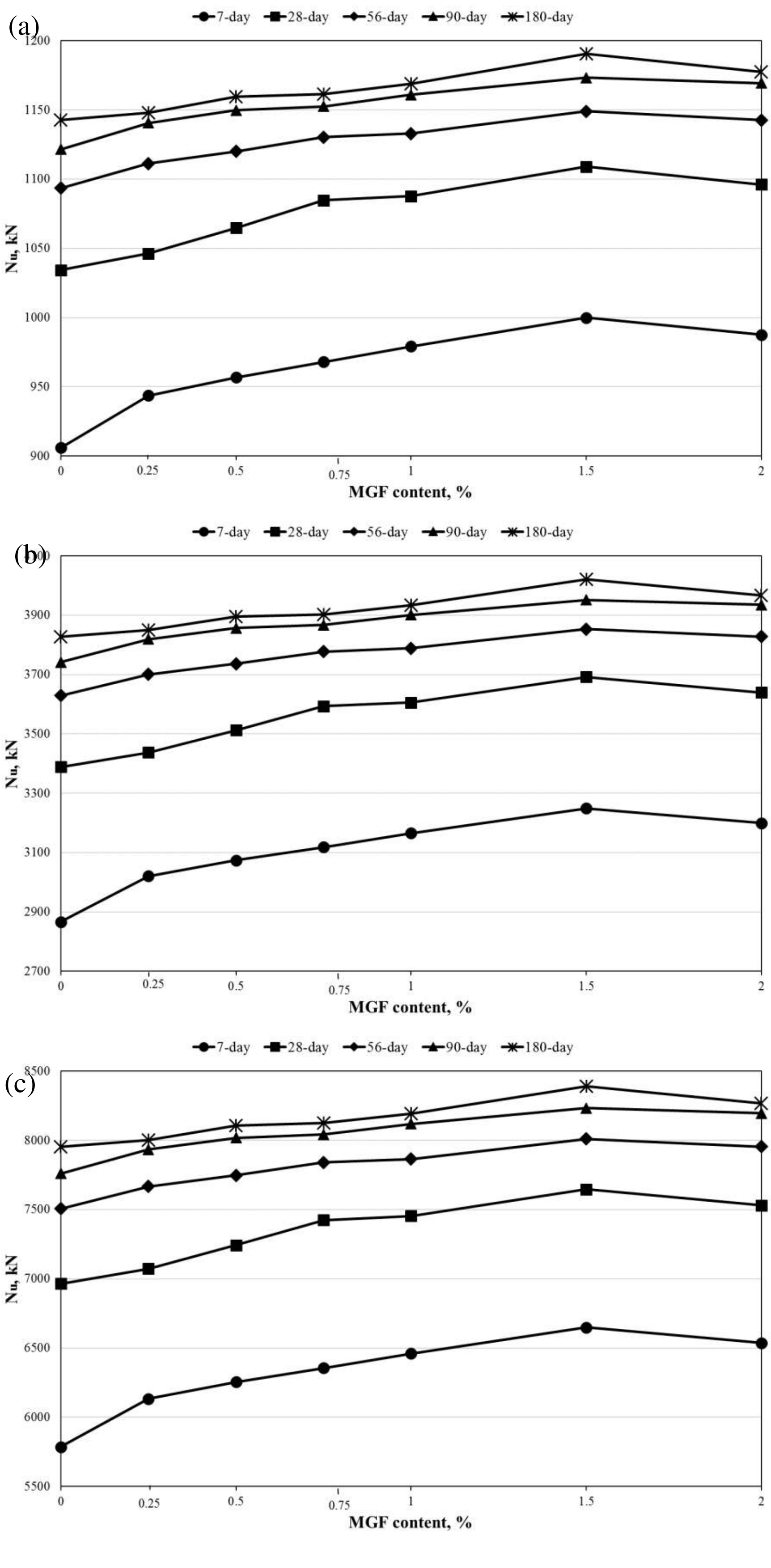

Figure 4.74. Calculated axial load capacity of CFST columns having UHPC with MGF via DL/T equation for steel tube yield strength of 450 MPa: a) D/t=30, b) D/t=60, and c) D/t=90

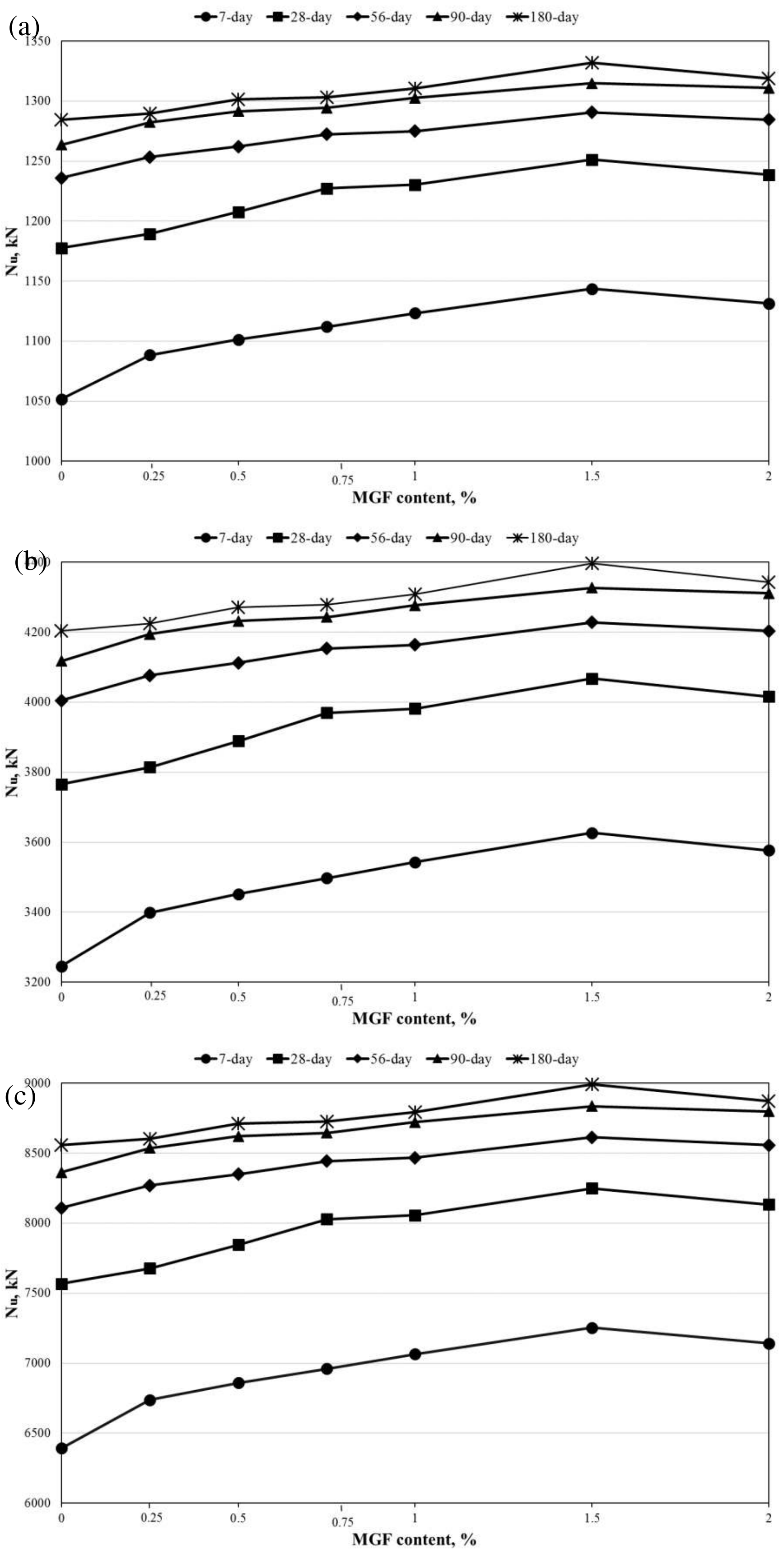

Figure 4.75. Calculated axial load capacity of CFST columns having UHPC with MGF via DL/T equation for steel tube yield strength of 600 MPa: a) D/t=30, b) D/t=60, and c) D/t=90

4.2.2 Comparative Analysis of Numerical Study

4.2.2.1 Comparison of the Eurocode 4 with the other Design Codes Based on Testing Ages and Fiber Type

The performances of the different types of fibers and development of the axial load capacity of the calculated equation codes at the time were evaluated through the Figures of 4.76-4.85. However, to show more precise results about the critical points of maximum and minimum points Table 4.2 is drawn. According to the table, the author can decide to use appropriate properties to develop the axial capacity from a specific age and keep away from the other characteristics. For example, the highest developments of the results from 28 to 90 caught when the fiber volume was =0.25%, D/t=90, and fy=300 for all fiber types. Thus, a high concentration of fibers and high yield strength is not a condition of significant development of the axial capacity of UHPFRC, but it seems like the diameter per plate thickness played an important role because the lowest D/t resulted from lowest growth and vice versa.

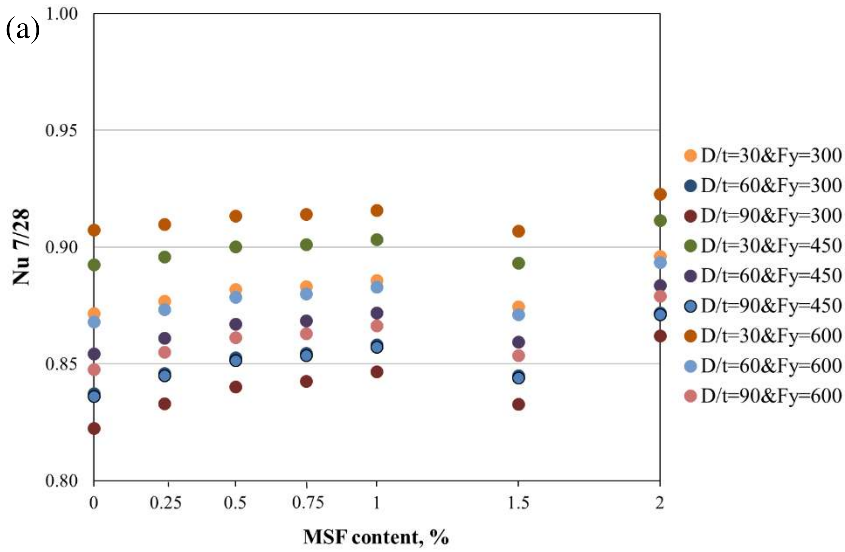

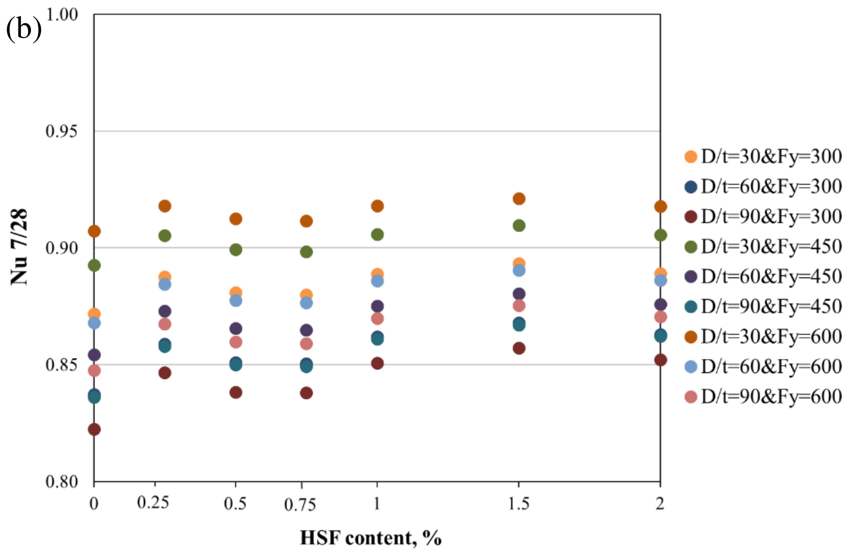

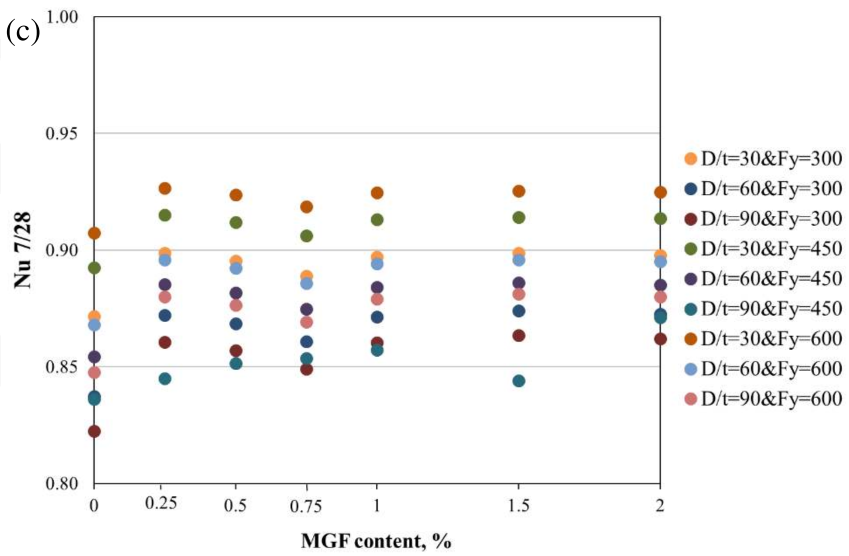

Figure 4.76. Column strength variation of 7-day vs. 28-day according to Eurocode 4 for UHPC with a) MSF, b) HSF, and c) MGF

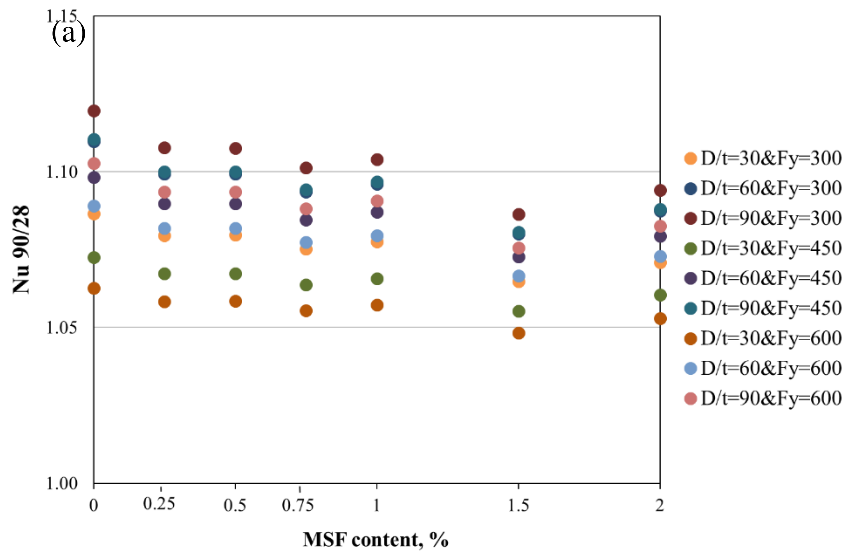

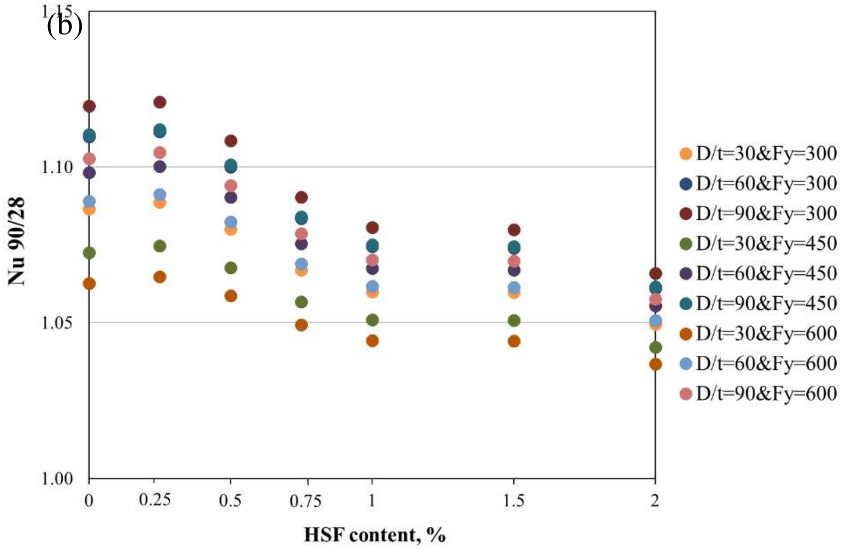

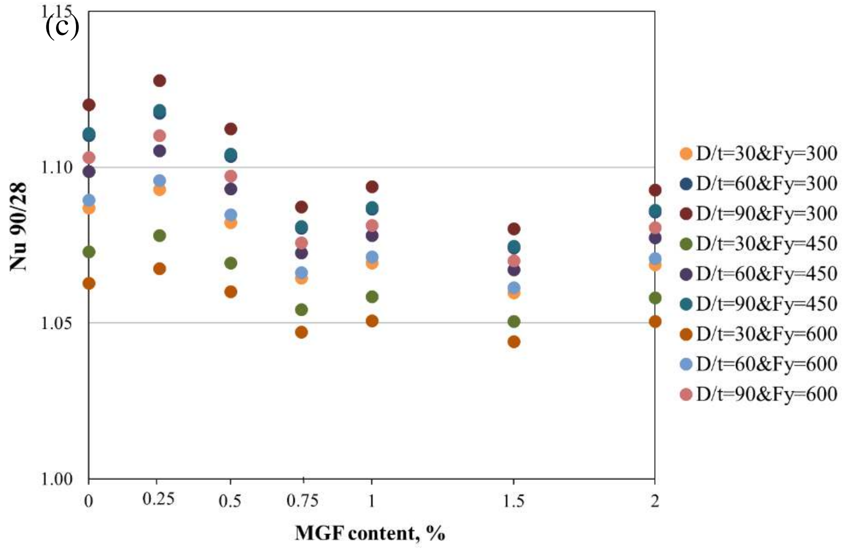

Figure 4.77. Column strength variation of 28-day vs. 90-day according to Eurocode 4 for UHPC with a) MSF, b) HSF, and c) MGF

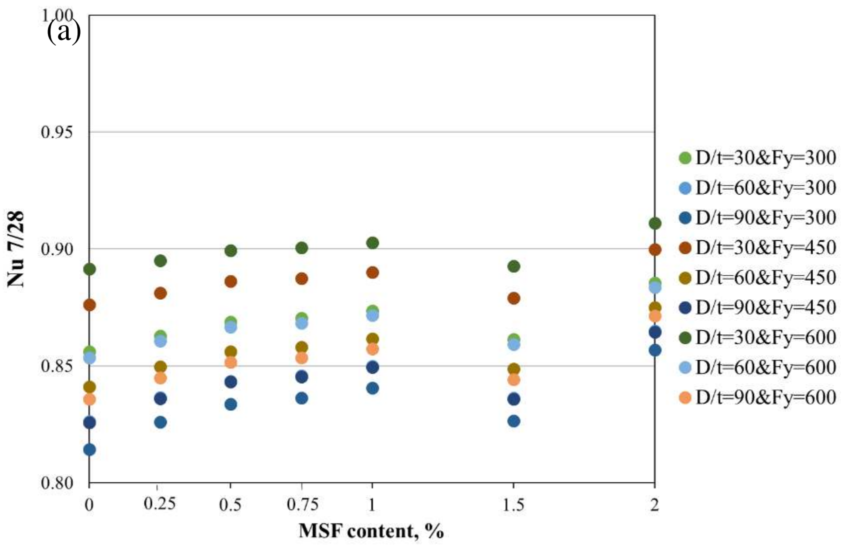

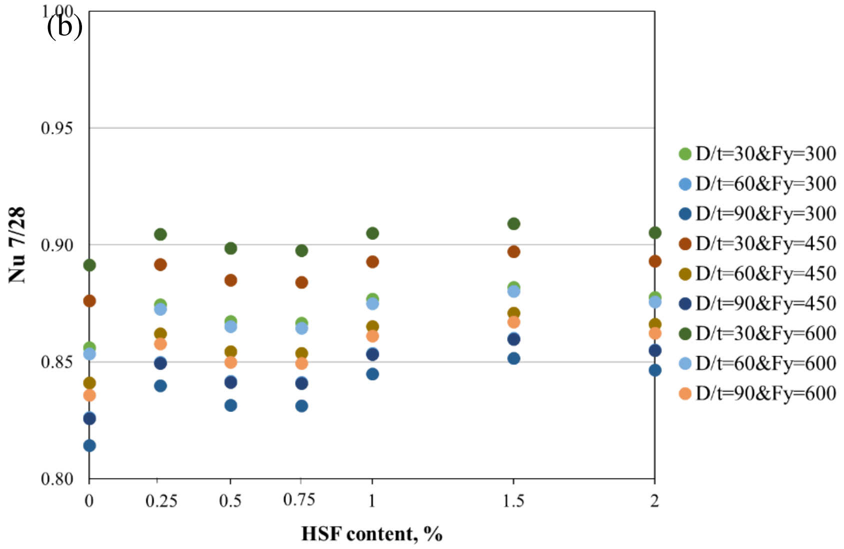

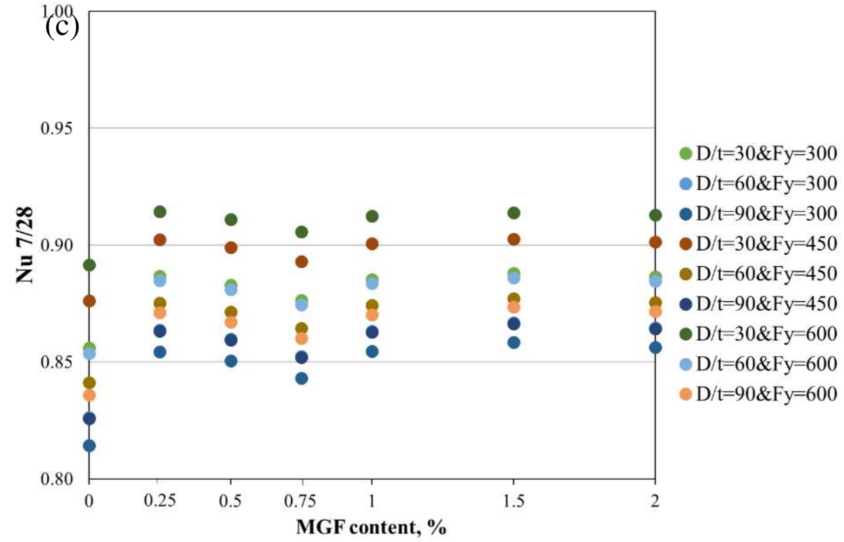

Figure 4.78. Column strength variation of 7-day vs. 28-day according to ACI for UHPC with a) MSF, b) HSF, and c) MGF

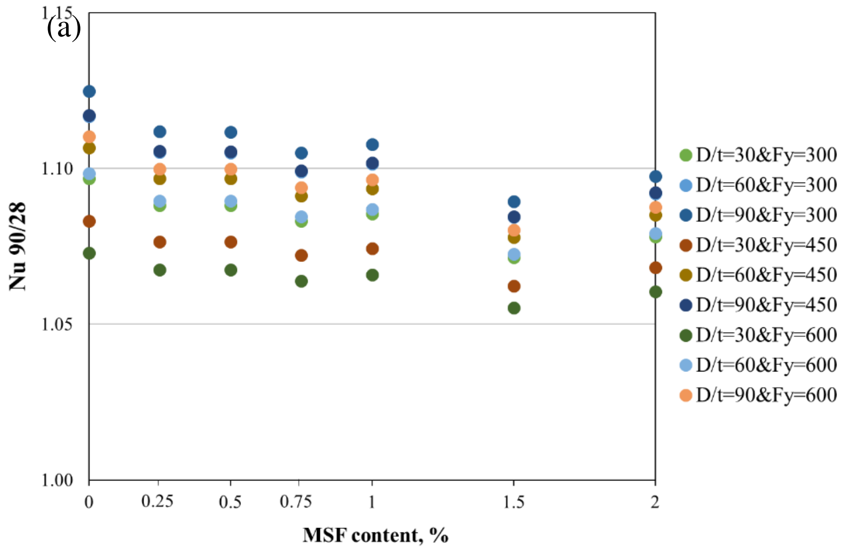

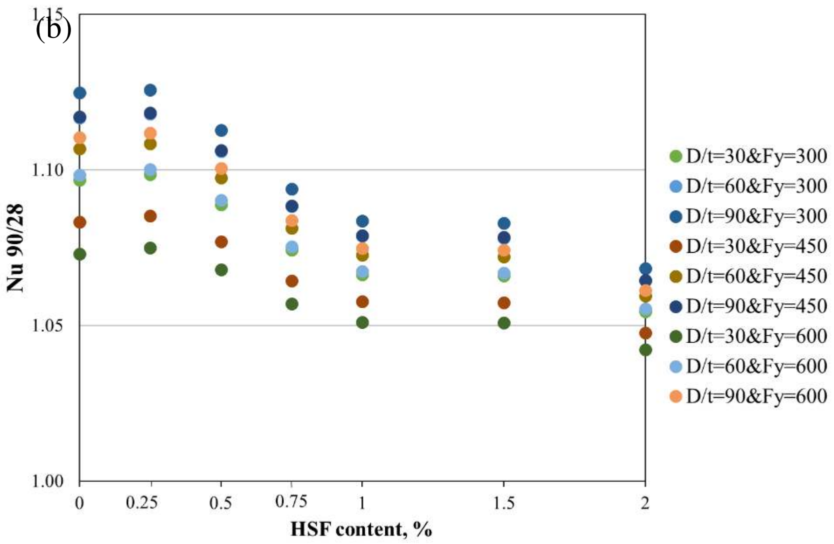

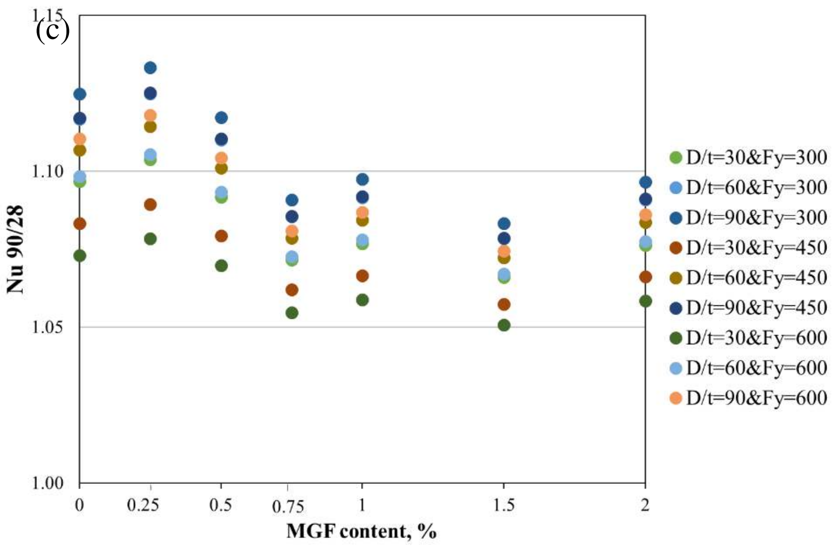

Figure 4.79. Column strength variation of 28-day vs. 90-day according to ACI for UHPC with a) MSF, b) HSF, and c) MGF

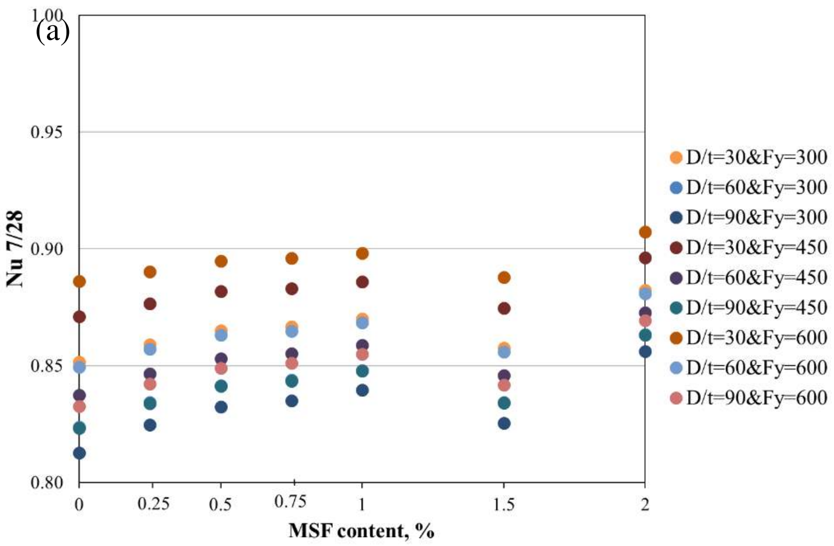

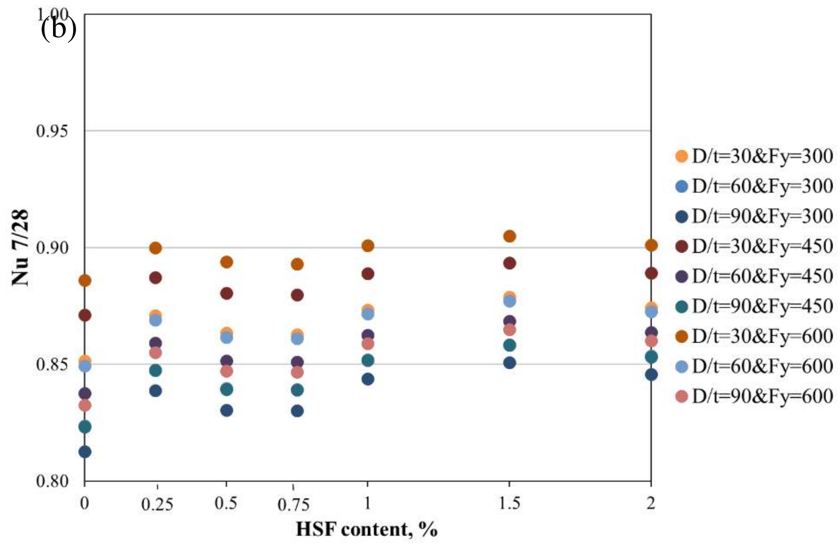

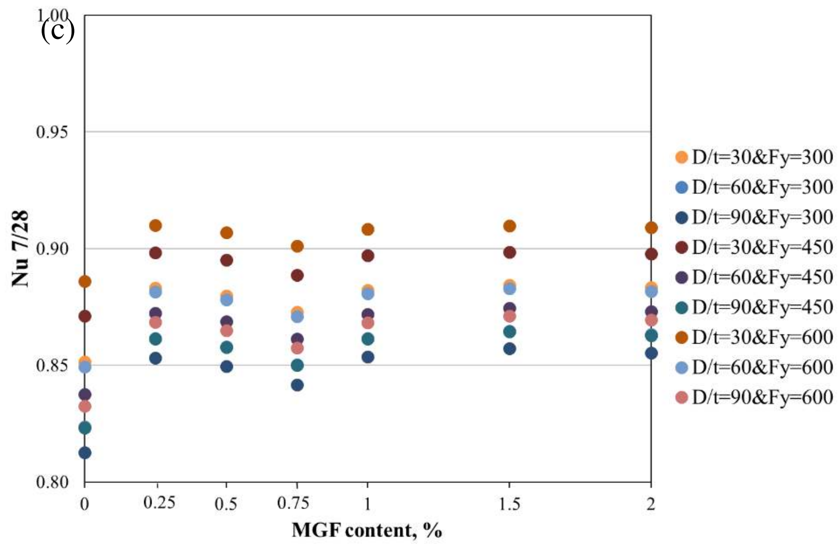

Figure 4.80. Column strength variation of 7-day vs. 28-day according to AISC for UHPC with a) MSF, b) HSF, and c) MGF

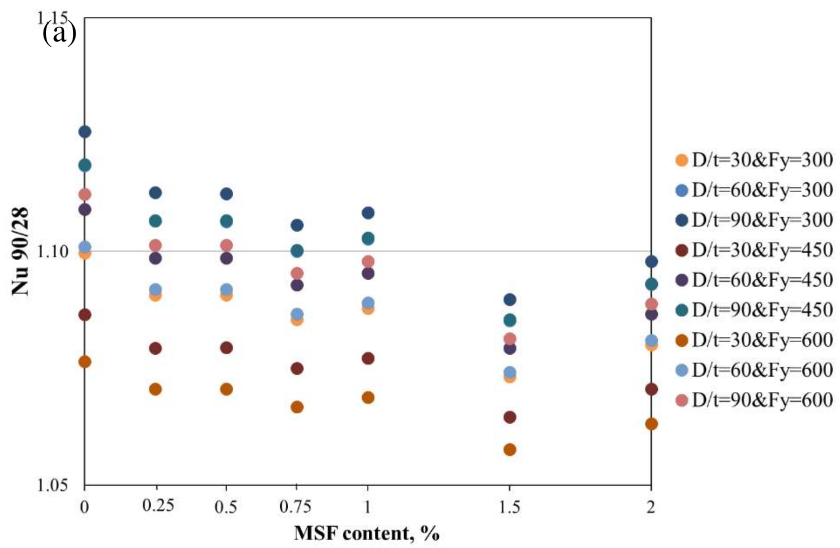

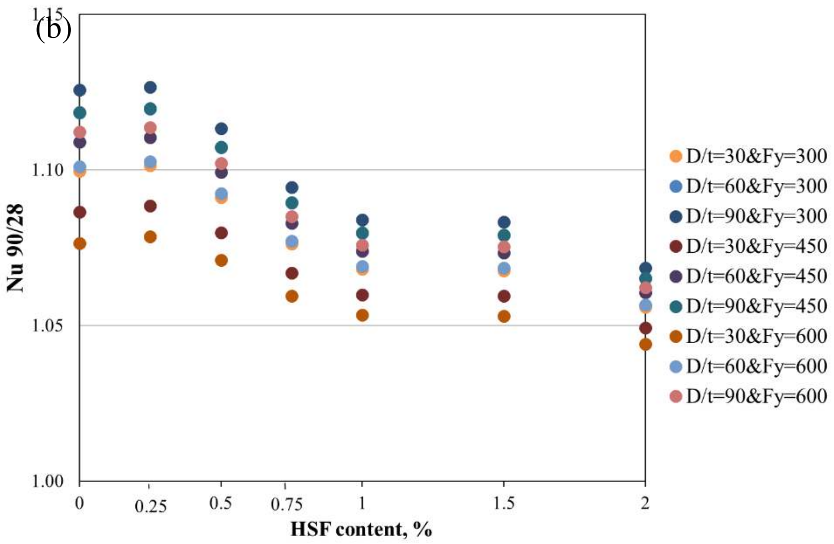

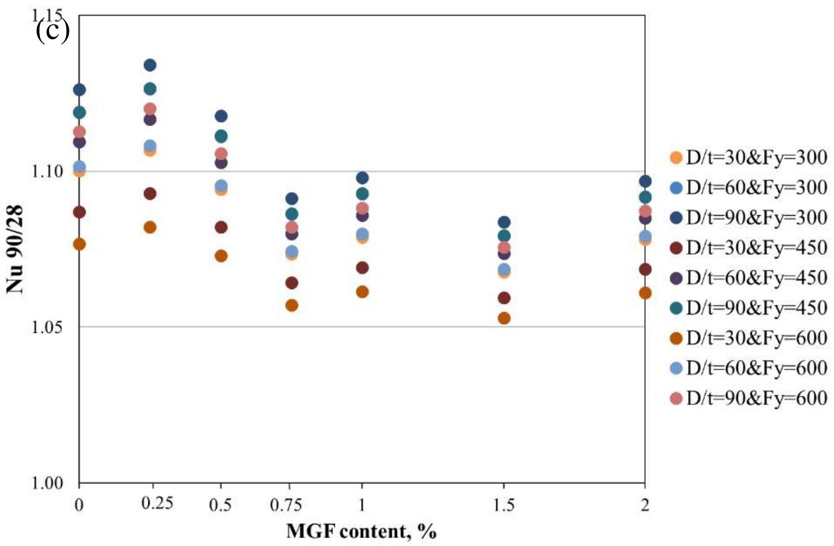

Figure 4.81. Column strength variation of 28-day vs. 90-day according to AISC for UHPC with a) MSF, b) HSF, and c) MGF

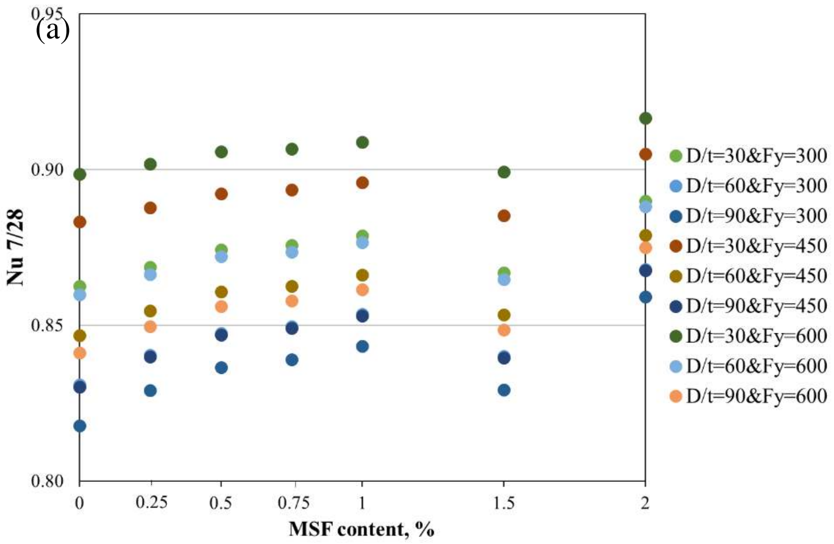

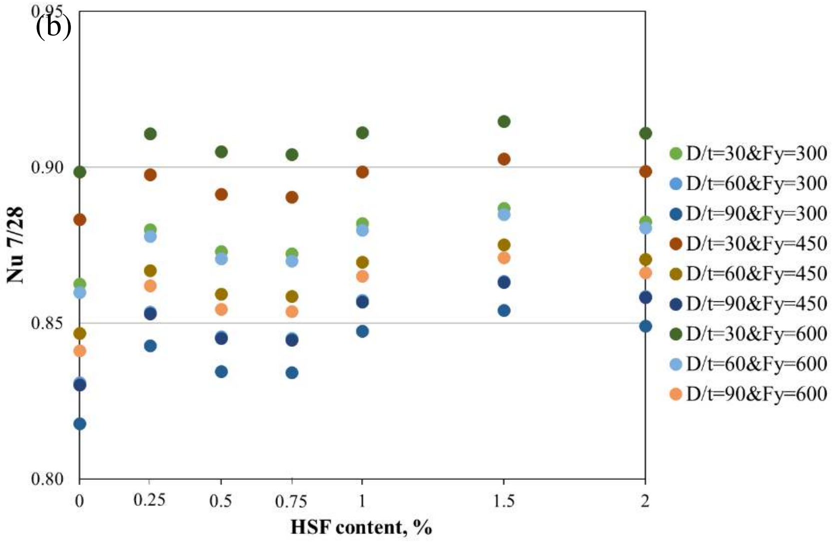

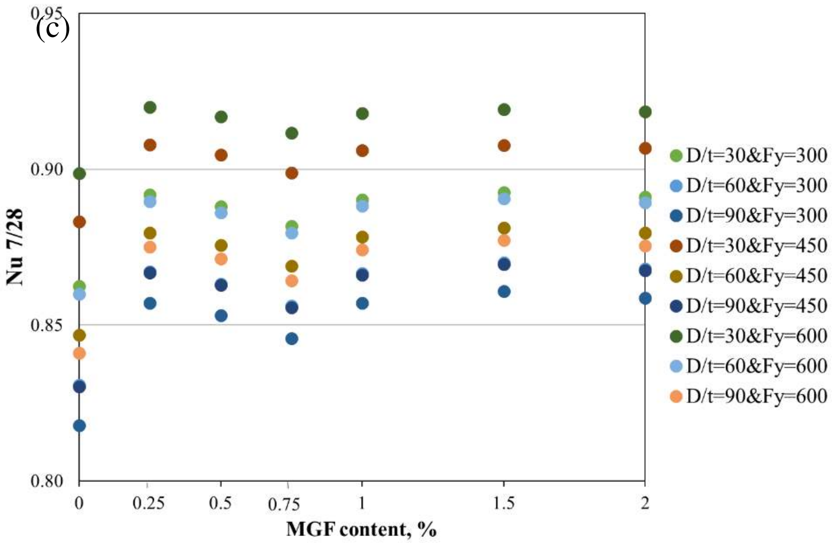

Figure 4.82. Column strength variation of 7-day vs. 28-day according to AIJ for UHPC with a) MSF, b) HSF, and c) MGF

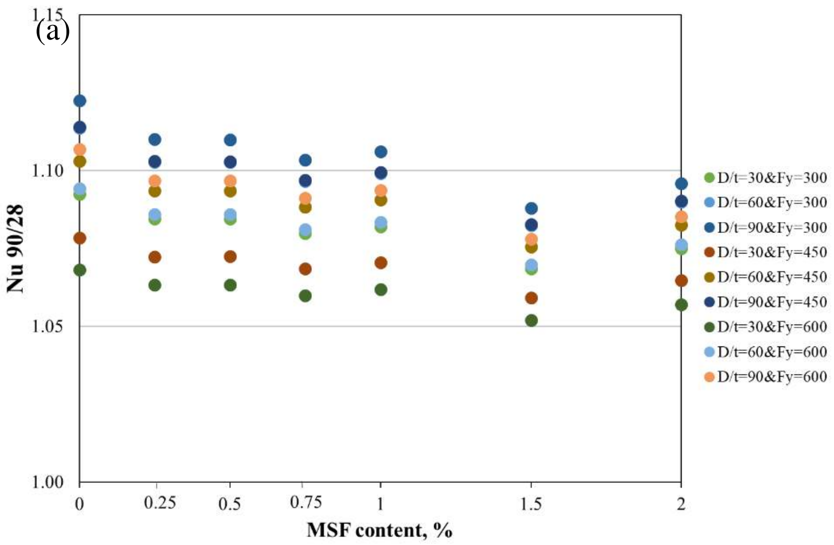

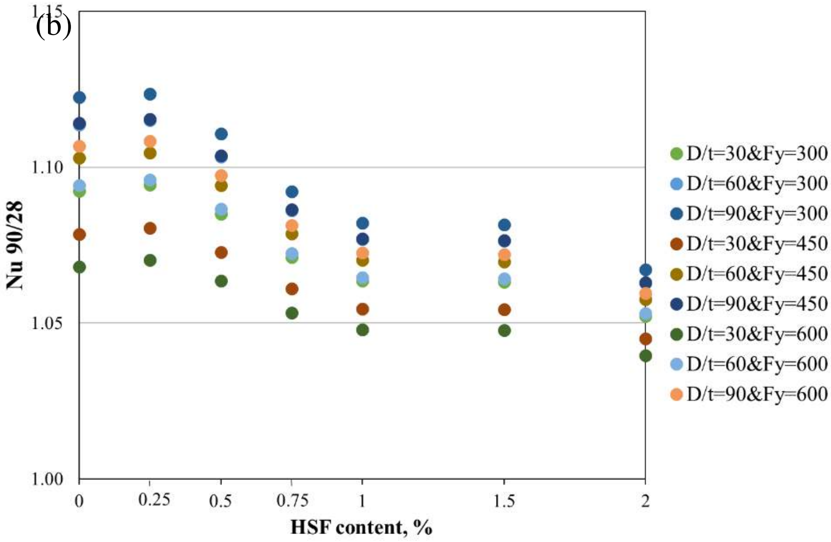

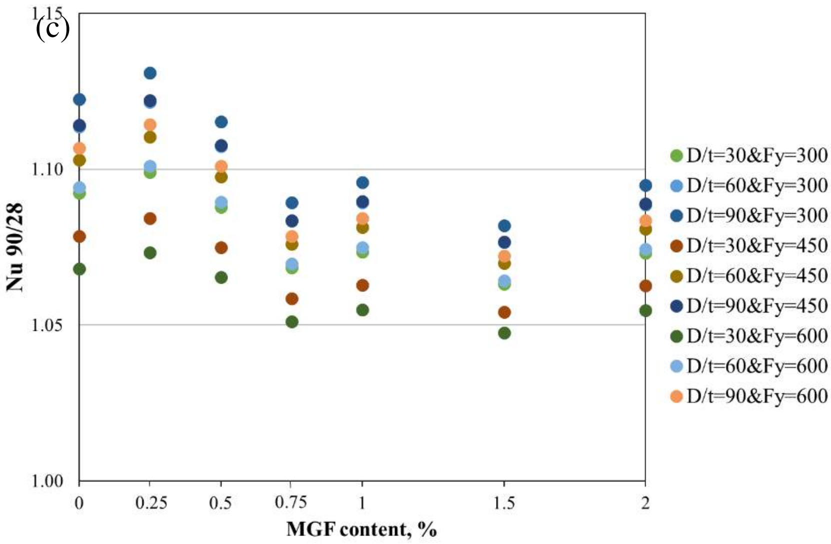

Figure 4.83. Column strength variation of 28-day vs. 90-day according to AIJ for UHPC with a) MSF, b) HSF, and c) MGF

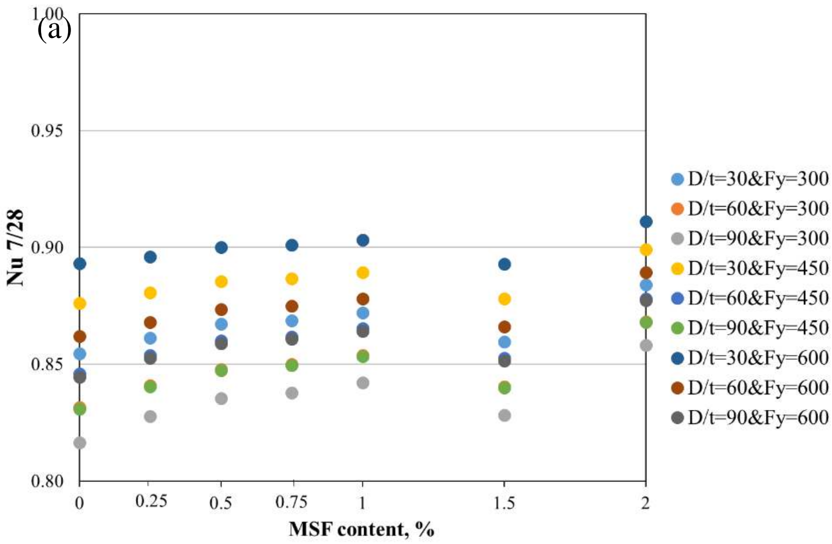

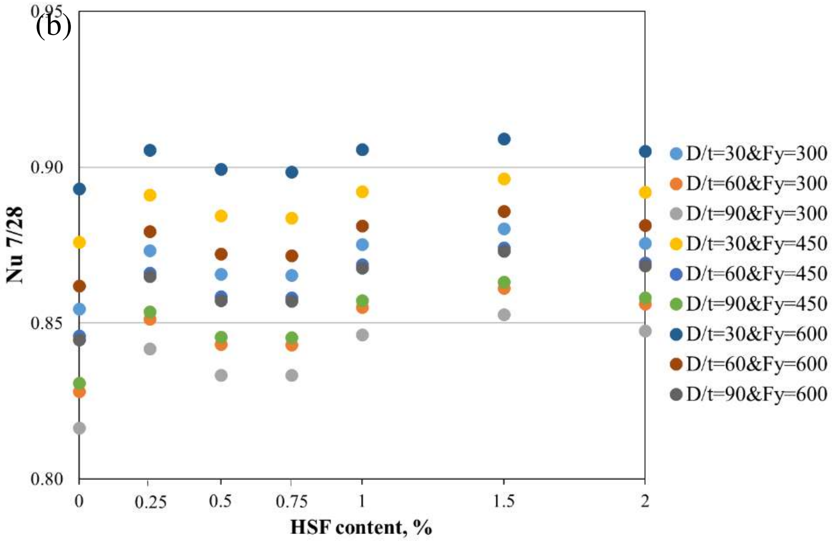

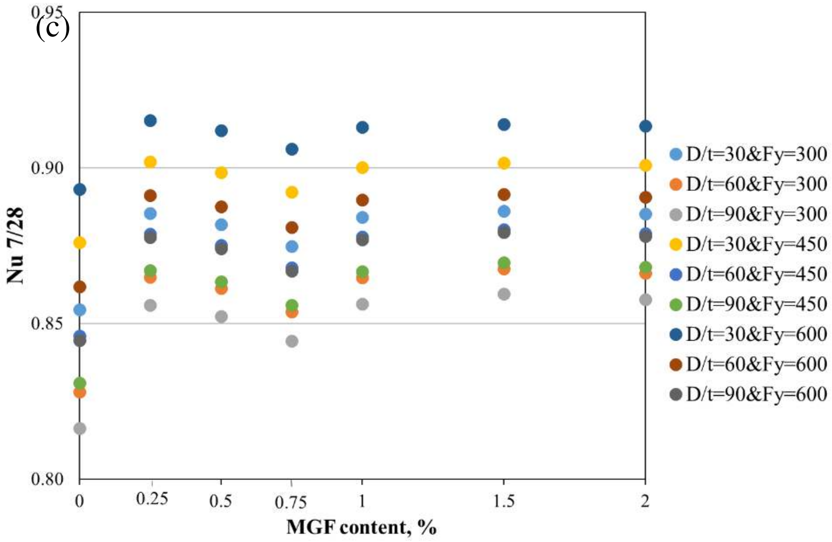

Figure 4.84. Column strength variation of 7-day vs. 28-day according to DL/T for UHPC with a) MSF, b) HSF, and c) MGF

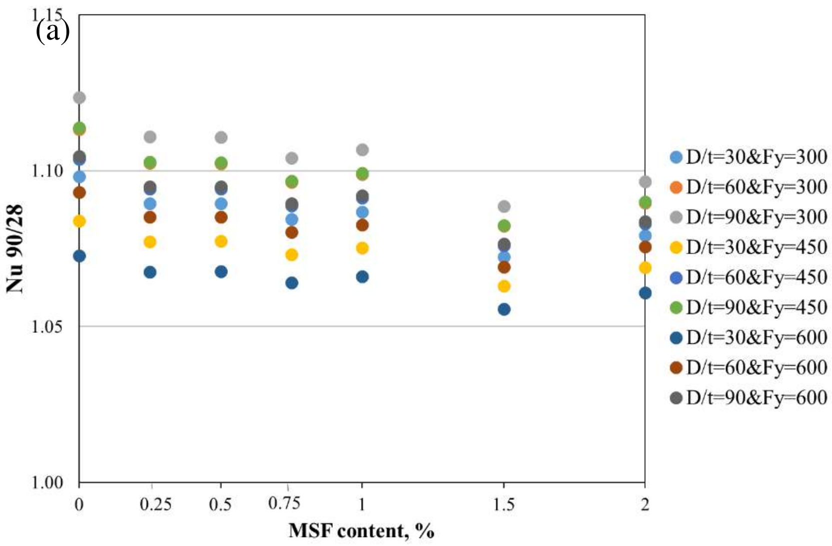

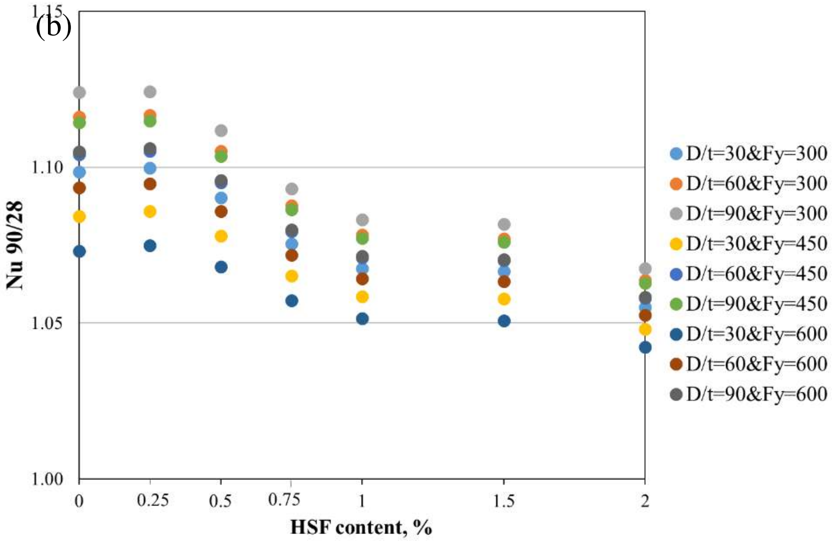

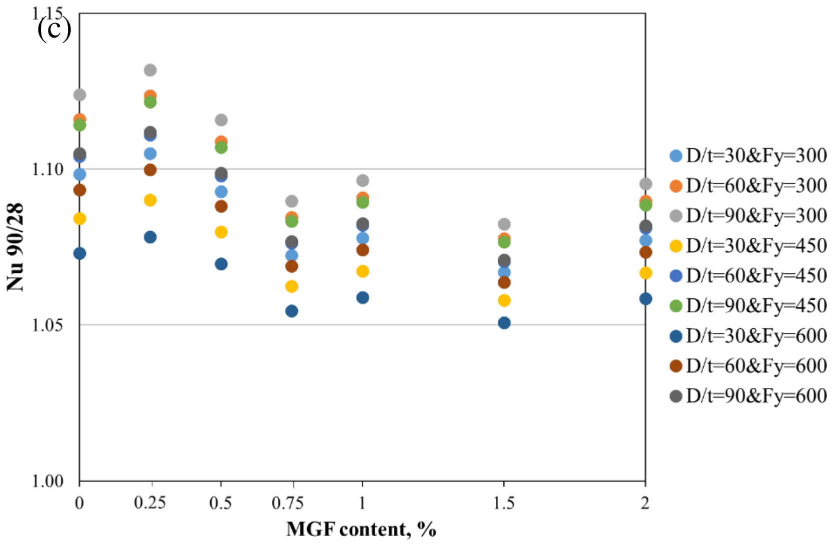

Figure 4.85. Column strength variation of 28-day vs. 90-day according to DL/T for UHPC with a) MSF, b) HSF, and c) MGF

Table 4.2. Developments of axial load capacity for different testing ages

Codes	Fiber Types	Nu7/Nu28								Nu90/Nu28							
		Lowest development				Highest development				Lowest development				Highest development			
		Fiber vol. (%)	D/t	fy (MPa)	Nu7/Nu28 ratio	Fiber vol. (%)	D/t	fy (MPa)	Nu7/Nu28 value	Fiber vol. (%)	D/t	fy (MPa)	Nu90/Nu28 value	Fiber vol. (%)	D/t	fy (MPa)	Nu90/Nu28 value
EC4	MSF	2	30	600	0.923	1.5	90	300	0.833	1.5	30	600	1.048	0.25	90	300	1.108
	HSF	1.5	30	600	0.921	0.75	90	300	0.838	2	30	600	1.037	0.25	90	300	1.121
	MGF	0.25	30	600	0.927	0.75	90	300	0.849	1.5	30	600	1.044	0.25	90	300	1.128
ACI	MSF	2	30	600	0.911	0.25	90	300	0.826	1.5	30	600	1.055	0.25	90	300	1.112
	HSF	1.5	30	600	0.909	0.75	90	300	0.831	2	30	600	1.042	0.25	90	300	1.126
	MGF	0.25	30	600	0.914	0.75	90	300	0.843	1.5	30	600	1.051	0.25	90	300	1.133
AISC	MSF	2	30	600	0.907	0.25	90	300	0.825	1.5	30	600	1.058	0.25	90	300	1.113
	HSF	1.5	30	600	0.905	0.75	90	300	0.830	2	30	600	1.044	0.25	90	300	1.127
	MGF	0.25	30	600	0.910	0.75	90	300	0.842	1.5	30	600	1.053	0.25	90	300	1.134
AIJ	MSF	2	30	600	0.916	0.25	90	300	0.829	1.5	30	600	1.052	0.25	90	300	1.110
	HSF	1.5	30	600	0.915	0.75	90	300	0.834	2	30	600	1.040	0.25	90	300	1.124
	MGF	0.25	30	600	0.920	0.75	90	300	0.846	1.5	30	600	1.048	0.25	90	300	1.131
DL/T	MSF	2	30	600	0.911	0.25	90	300	0.828	1.5	30	600	1.056	0.25	90	300	1.111
	HSF	1.5	30	600	0.909	0.75	90	300	0.833	2	30	600	1.042	0.25	90	300	1.124
	MGF	0.25	30	600	0.915	0.75	90	300	0.844	1.5	30	600	1.051	0.25	90	300	1.132

4.2.2.2 Comparison of Design Codes with Eurocode4 Based On Fiber Type and D/t Ratio

Effects of micro steel, hooked steel, and micro glass fibers on the axial load capacity of UHPCs are presented in Tables 4.3, 4.4, and 4.5with respect to D/t with three values of 30, 60, and 90. From tables mentioned above, all codes trying to approach to EC4 with increasing D/t ratio from 30 to 60. Whereas the increment ratio from 60 to 90 of D/t faced some disparity. On the other hand, from the analyzing of the tables it's noticed that the fibers will not play any role in closing the codes with each other, irrespective of the different D/t ratio.

Table 4.3. Variation of the normalized Nu values of EC4 and the other codes with D/t ratio of CFST column sections for UHPC with MSF

fy (MPa)	D/t=30				D/t=60				D/t=90			
	Nu (ACI/ EC4)	Nu (AISC/ EC4)	Nu (AIJ/ EC4)	Nu (DL/T/ EC4)	Nu (ACI/ EC4)	Nu (AISC/ EC4)	Nu (AIJ/ EC4)	Nu (DL/T/ EC4)	Nu (ACI/ EC4)	Nu (AISC/ EC4)	Nu (AIJ/ EC4)	Nu (DL/T/ EC4)
300	0.783	0.835	0.917	0.924	0.810	0.877	0.929	0.856	0.822	0.896	0.935	0.916
300	0.789	0.843	0.921	0.932	0.815	0.884	0.932	0.859	0.826	0.901	0.937	0.920
300	0.790	0.845	0.922	0.934	0.816	0.885	0.933	0.860	0.827	0.902	0.938	0.920
300	0.791	0.847	0.923	0.935	0.817	0.886	0.933	0.860	0.828	0.903	0.938	0.921
300	0.793	0.848	0.924	0.937	0.818	0.887	0.934	0.861	0.828	0.904	0.939	0.921
300	0.794	0.850	0.924	0.938	0.818	0.888	0.935	0.861	0.829	0.904	0.939	0.922
300	0.797	0.854	0.927	0.943	0.821	0.891	0.936	0.862	0.831	0.907	0.940	0.923
300	0.797	0.854	0.927	0.943	0.821	0.892	0.936	0.862	0.831	0.907	0.940	0.923
300	0.802	0.861	0.930	0.949	0.824	0.896	0.938	0.864	0.833	0.910	0.942	0.925
300	0.802	0.861	0.930	0.950	0.824	0.896	0.939	0.865	0.833	0.910	0.942	0.926
300	0.803	0.863	0.931	0.951	0.825	0.897	0.939	0.865	0.834	0.911	0.942	0.926
300	0.804	0.864	0.931	0.952	0.826	0.898	0.939	0.865	0.834	0.911	0.942	0.926
300	0.806	0.867	0.933	0.955	0.827	0.900	0.940	0.866	0.835	0.912	0.943	0.927
300	0.806	0.868	0.933	0.956	0.827	0.900	0.941	0.866	0.836	0.913	0.943	0.927
300	0.802	0.861	0.930	0.950	0.824	0.896	0.939	0.864	0.833	0.910	0.942	0.926
300	0.807	0.868	0.933	0.956	0.827	0.900	0.941	0.866	0.836	0.913	0.943	0.927
300	0.808	0.869	0.934	0.957	0.828	0.901	0.941	0.866	0.836	0.914	0.944	0.928
300	0.808	0.870	0.934	0.958	0.828	0.902	0.941	0.867	0.836	0.914	0.944	0.928
300	0.809	0.871	0.935	0.959	0.829	0.903	0.942	0.867	0.837	0.914	0.944	0.928
300	0.809	0.872	0.935	0.960	0.829	0.903	0.942	0.867	0.837	0.915	0.944	0.929
300	0.810	0.872	0.935	0.960	0.830	0.903	0.942	0.867	0.837	0.915	0.944	0.929

Table 4.3 continued

300	0.804	0.865	0.932	0.953	0.826	0.898	0.940	0.865	0.834	0.912	0.943	0.926
300	0.808	0.870	0.934	0.958	0.828	0.902	0.941	0.867	0.836	0.914	0.944	0.928
300	0.808	0.870	0.934	0.958	0.829	0.902	0.941	0.867	0.836	0.914	0.944	0.928
300	0.809	0.871	0.935	0.959	0.829	0.903	0.942	0.867	0.837	0.914	0.944	0.928
300	0.810	0.872	0.935	0.960	0.830	0.903	0.942	0.867	0.837	0.915	0.944	0.929
300	0.811	0.873	0.936	0.961	0.830	0.904	0.942	0.868	0.838	0.915	0.944	0.929
300	0.812	0.875	0.937	0.963	0.831	0.905	0.943	0.868	0.838	0.916	0.945	0.929
300	0.806	0.867	0.933	0.955	0.827	0.900	0.940	0.866	0.835	0.913	0.943	0.927
300	0.809	0.870	0.934	0.958	0.829	0.902	0.941	0.867	0.837	0.914	0.944	0.928
300	0.809	0.871	0.935	0.959	0.829	0.903	0.942	0.867	0.837	0.914	0.944	0.928
300	0.809	0.871	0.935	0.959	0.829	0.903	0.942	0.867	0.837	0.915	0.944	0.928
300	0.810	0.873	0.935	0.961	0.830	0.904	0.942	0.867	0.837	0.915	0.944	0.929
300	0.811	0.874	0.936	0.962	0.830	0.904	0.942	0.868	0.838	0.916	0.945	0.929
300	0.812	0.875	0.937	0.963	0.831	0.905	0.943	0.868	0.838	0.916	0.945	0.930
450	0.775	0.816	0.920	0.913	0.800	0.859	0.928	0.930	0.814	0.881	0.934	0.927
450	0.781	0.825	0.924	0.920	0.806	0.866	0.932	0.934	0.819	0.887	0.937	0.930
450	0.782	0.827	0.925	0.922	0.807	0.868	0.933	0.935	0.820	0.888	0.937	0.930
450	0.783	0.828	0.926	0.923	0.808	0.869	0.933	0.936	0.821	0.889	0.938	0.931
450	0.785	0.830	0.927	0.925	0.809	0.871	0.934	0.937	0.822	0.890	0.938	0.931
450	0.786	0.832	0.927	0.926	0.810	0.872	0.935	0.937	0.822	0.891	0.939	0.931
450	0.789	0.836	0.930	0.930	0.813	0.876	0.936	0.939	0.824	0.894	0.940	0.933
450	0.789	0.837	0.930	0.930	0.813	0.876	0.936	0.939	0.825	0.894	0.940	0.933
450	0.794	0.843	0.933	0.936	0.817	0.881	0.939	0.942	0.828	0.899	0.942	0.935
450	0.795	0.844	0.933	0.937	0.817	0.882	0.939	0.943	0.828	0.899	0.942	0.935
450	0.796	0.845	0.934	0.938	0.818	0.883	0.940	0.943	0.829	0.900	0.943	0.935

Table 4.3 continued

450	0.796	0.847	0.934	0.939	0.819	0.884	0.940	0.944	0.829	0.900	0.943	0.935
450	0.799	0.850	0.936	0.942	0.821	0.886	0.941	0.945	0.830	0.902	0.944	0.936
450	0.799	0.851	0.936	0.943	0.821	0.887	0.942	0.945	0.831	0.903	0.944	0.936
450	0.795	0.844	0.933	0.937	0.817	0.882	0.939	0.943	0.828	0.899	0.942	0.935
450	0.799	0.851	0.936	0.943	0.821	0.887	0.942	0.945	0.831	0.903	0.944	0.936
450	0.8	0.852	0.937	0.944	0.822	0.888	0.942	0.946	0.831	0.903	0.944	0.937
450	0.801	0.853	0.937	0.945	0.822	0.889	0.942	0.946	0.832	0.904	0.945	0.937
450	0.802	0.854	0.938	0.946	0.823	0.890	0.943	0.947	0.832	0.905	0.945	0.937
450	0.803	0.855	0.938	0.947	0.824	0.890	0.943	0.947	0.833	0.905	0.945	0.937
450	0.803	0.855	0.938	0.947	0.824	0.891	0.943	0.947	0.833	0.905	0.945	0.937
450	0.797	0.847	0.935	0.940	0.819	0.885	0.940	0.944	0.829	0.901	0.943	0.935
450	0.801	0.853	0.937	0.945	0.822	0.889	0.942	0.946	0.832	0.904	0.945	0.937
450	0.801	0.854	0.938	0.946	0.823	0.889	0.943	0.947	0.832	0.904	0.945	0.937
450	0.802	0.854	0.938	0.946	0.823	0.890	0.943	0.947	0.832	0.905	0.945	0.937
450	0.803	0.856	0.939	0.948	0.824	0.891	0.943	0.947	0.833	0.905	0.945	0.937
450	0.804	0.857	0.939	0.949	0.825	0.892	0.944	0.948	0.833	0.906	0.946	0.938
450	0.805	0.859	0.940	0.950	0.825	0.893	0.944	0.948	0.834	0.907	0.946	0.938
450	0.799	0.850	0.936	0.942	0.821	0.886	0.941	0.945	0.830	0.902	0.944	0.936
450	0.802	0.854	0.938	0.946	0.823	0.889	0.943	0.947	0.832	0.904	0.945	0.937
450	0.802	0.854	0.938	0.946	0.823	0.890	0.943	0.947	0.832	0.905	0.945	0.937
450	0.802	0.855	0.938	0.947	0.823	0.890	0.943	0.947	0.833	0.905	0.945	0.937
450	0.803	0.856	0.939	0.948	0.824	0.891	0.943	0.948	0.833	0.906	0.945	0.937
450	0.804	0.858	0.939	0.949	0.825	0.892	0.944	0.948	0.834	0.906	0.946	0.938
450	0.805	0.859	0.940	0.951	0.826	0.893	0.944	0.949	0.834	0.907	0.946	0.938
600	0.773	0.807	0.927	0.911	0.795	0.846	0.930	0.949	0.808	0.869	0.934	0.946

Table 4.3 continued

600	0.779	0.815	0.931	0.917	0.801	0.854	0.934	0.952	0.814	0.876	0.937	0.948
600	0.78	0.817	0.931	0.918	0.802	0.856	0.934	0.953	0.815	0.877	0.938	0.948
600	0.781	0.819	0.932	0.920	0.803	0.857	0.935	0.953	0.816	0.878	0.938	0.948
600	0.782	0.820	0.933	0.921	0.804	0.859	0.936	0.954	0.817	0.880	0.939	0.949
600	0.783	0.822	0.933	0.922	0.805	0.860	0.936	0.954	0.817	0.881	0.940	0.949
600	0.787	0.826	0.936	0.926	0.808	0.865	0.938	0.956	0.820	0.884	0.941	0.950
600	0.787	0.826	0.936	0.926	0.808	0.865	0.938	0.956	0.820	0.884	0.941	0.950
600	0.792	0.833	0.939	0.931	0.813	0.871	0.941	0.958	0.824	0.889	0.943	0.951
600	0.792	0.834	0.939	0.932	0.813	0.871	0.941	0.958	0.824	0.890	0.944	0.951
600	0.793	0.835	0.940	0.933	0.814	0.872	0.942	0.959	0.825	0.891	0.944	0.951
600	0.794	0.836	0.940	0.934	0.815	0.873	0.942	0.959	0.825	0.892	0.944	0.951
600	0.796	0.839	0.941	0.936	0.816	0.876	0.943	0.960	0.827	0.893	0.945	0.952
600	0.797	0.840	0.942	0.937	0.817	0.877	0.944	0.960	0.827	0.894	0.946	0.952
600	0.792	0.834	0.939	0.932	0.813	0.871	0.941	0.958	0.824	0.890	0.944	0.951
600	0.797	0.841	0.942	0.937	0.817	0.877	0.944	0.960	0.827	0.894	0.946	0.952
600	0.798	0.842	0.943	0.939	0.818	0.878	0.944	0.961	0.828	0.895	0.946	0.952
600	0.798	0.843	0.943	0.939	0.818	0.879	0.945	0.961	0.828	0.896	0.946	0.952
600	0.799	0.844	0.944	0.941	0.819	0.880	0.945	0.962	0.829	0.897	0.947	0.952
600	0.8	0.845	0.944	0.941	0.820	0.881	0.946	0.962	0.829	0.897	0.947	0.952
600	0.8	0.845	0.944	0.942	0.820	0.881	0.946	0.962	0.829	0.897	0.947	0.952
600	0.794	0.837	0.940	0.935	0.815	0.874	0.943	0.959	0.826	0.892	0.945	0.951
600	0.798	0.843	0.943	0.939	0.818	0.879	0.945	0.961	0.828	0.896	0.946	0.952
600	0.799	0.843	0.943	0.940	0.819	0.879	0.945	0.961	0.829	0.896	0.946	0.952
600	0.799	0.844	0.943	0.940	0.819	0.880	0.945	0.962	0.829	0.897	0.947	0.952
600	0.8	0.846	0.944	0.942	0.820	0.881	0.946	0.962	0.830	0.897	0.947	0.952

Table 4.3 continued

600	0.801	0.847	0.945	0.943	0.821	0.882	0.946	0.962	0.830	0.898	0.947	0.952
600	0.802	0.849	0.945	0.944	0.822	0.883	0.947	0.963	0.831	0.899	0.948	0.953
600	0.796	0.840	0.942	0.937	0.817	0.876	0.944	0.960	0.827	0.894	0.945	0.952
600	0.799	0.844	0.943	0.940	0.819	0.879	0.945	0.961	0.829	0.896	0.946	0.952
600	0.799	0.844	0.944	0.941	0.819	0.880	0.945	0.962	0.829	0.897	0.947	0.952
600	0.8	0.845	0.944	0.941	0.820	0.880	0.945	0.962	0.829	0.897	0.947	0.952
600	0.801	0.846	0.944	0.942	0.820	0.881	0.946	0.962	0.830	0.898	0.947	0.952
600	0.802	0.847	0.945	0.943	0.821	0.882	0.946	0.962	0.830	0.899	0.947	0.952
600	0.803	0.849	0.946	0.945	0.822	0.884	0.947	0.963	0.831	0.900	0.948	0.953

Table 4.4. Variation of the normalized Nu values of EC4 and the other codes with D/t ratio of CFST column sections for UHPC with HSF

fy (MPa)	D/t=30				D/t=60				D/t=90			
	Nu (ACI/ EC4)	Nu (AISC/ EC4)	Nu (AIJ/ EC4)	Nu (DL/T/ EC4)	Nu (ACI/ EC4)	Nu (AISC/ EC4)	Nu (AIJ/ EC4)	Nu (DL/T/ EC4)	Nu (ACI/ EC4)	Nu (AISC/ EC4)	Nu (AIJ/ EC4)	Nu (DL/T/ EC4)
300	0.783	0.835	0.917	0.924	0.810	0.877	0.929	0.921	0.822	0.896	0.935	0.916
300	0.788	0.842	0.921	0.932	0.814	0.883	0.932	0.926	0.826	0.900	0.937	0.919
300	0.789	0.844	0.922	0.933	0.815	0.884	0.932	0.926	0.826	0.901	0.937	0.920
300	0.791	0.846	0.922	0.935	0.816	0.885	0.933	0.927	0.827	0.902	0.938	0.921
300	0.793	0.849	0.924	0.937	0.818	0.888	0.934	0.929	0.828	0.904	0.939	0.921
300	0.794	0.850	0.925	0.939	0.819	0.889	0.935	0.930	0.829	0.905	0.939	0.922
300	0.795	0.852	0.925	0.940	0.819	0.890	0.935	0.930	0.830	0.905	0.940	0.922
300	0.797	0.854	0.927	0.942	0.821	0.892	0.936	0.931	0.831	0.907	0.940	0.923

Table 4.4 continued

300	0.800	0.859	0.929	0.947	0.823	0.894	0.938	0.934	0.832	0.909	0.941	0.925
300	0.802	0.861	0.930	0.949	0.824	0.896	0.938	0.935	0.833	0.910	0.942	0.925
300	0.803	0.862	0.931	0.950	0.825	0.897	0.939	0.935	0.834	0.911	0.942	0.926
300	0.804	0.864	0.931	0.952	0.826	0.898	0.939	0.936	0.834	0.911	0.942	0.926
300	0.804	0.865	0.932	0.953	0.826	0.898	0.940	0.937	0.834	0.912	0.943	0.927
300	0.806	0.866	0.932	0.955	0.827	0.900	0.940	0.938	0.835	0.912	0.943	0.927
300	0.802	0.861	0.930	0.950	0.824	0.896	0.939	0.935	0.833	0.910	0.942	0.926
300	0.806	0.867	0.933	0.955	0.827	0.900	0.940	0.938	0.835	0.913	0.943	0.927
300	0.807	0.868	0.933	0.956	0.827	0.901	0.941	0.938	0.836	0.913	0.943	0.927
300	0.807	0.868	0.933	0.956	0.828	0.901	0.941	0.938	0.836	0.913	0.943	0.928
300	0.807	0.868	0.934	0.956	0.828	0.901	0.941	0.938	0.836	0.913	0.943	0.928
300	0.807	0.869	0.934	0.957	0.828	0.901	0.941	0.938	0.836	0.913	0.943	0.927
300	0.808	0.869	0.934	0.957	0.828	0.901	0.941	0.939	0.836	0.914	0.944	0.928
300	0.804	0.865	0.932	0.953	0.826	0.898	0.940	0.937	0.834	0.912	0.943	0.927
300	0.807	0.869	0.934	0.956	0.828	0.901	0.941	0.938	0.836	0.913	0.943	0.928
300	0.808	0.870	0.934	0.958	0.828	0.902	0.941	0.939	0.836	0.914	0.944	0.928
300	0.808	0.870	0.934	0.958	0.828	0.902	0.941	0.939	0.836	0.914	0.944	0.928
300	0.808	0.870	0.934	0.958	0.829	0.902	0.941	0.939	0.837	0.914	0.944	0.928
300	0.809	0.871	0.935	0.959	0.829	0.903	0.942	0.940	0.837	0.914	0.944	0.928
300	0.809	0.872	0.935	0.960	0.829	0.903	0.942	0.940	0.837	0.915	0.944	0.929
300	0.806	0.867	0.933	0.955	0.827	0.900	0.940	0.938	0.835	0.913	0.943	0.927
300	0.808	0.870	0.934	0.958	0.828	0.902	0.941	0.939	0.836	0.914	0.944	0.928
300	0.808	0.870	0.934	0.958	0.829	0.902	0.941	0.939	0.836	0.914	0.944	0.928
300	0.809	0.871	0.935	0.959	0.829	0.902	0.941	0.940	0.837	0.914	0.944	0.928
300	0.809	0.872	0.935	0.959	0.829	0.903	0.942	0.940	0.837	0.915	0.944	0.928

Table 4.4 continued

300	0.810	0.872	0.935	0.960	0.830	0.903	0.942	0.940	0.837	0.915	0.944	0.929
300	0.811	0.873	0.936	0.962	0.830	0.904	0.942	0.941	0.838	0.915	0.944	0.929
450	0.7748	0.816	0.920	0.913	0.800	0.859	0.928	0.930	0.814	0.881	0.934	0.927
450	0.7805	0.824	0.924	0.920	0.806	0.866	0.931	0.934	0.818	0.886	0.936	0.929
450	0.7815	0.826	0.925	0.921	0.806	0.867	0.932	0.935	0.819	0.887	0.937	0.930
450	0.7828	0.828	0.925	0.922	0.808	0.869	0.933	0.936	0.820	0.888	0.937	0.930
450	0.7851	0.831	0.927	0.925	0.810	0.871	0.934	0.937	0.822	0.891	0.938	0.931
450	0.7863	0.832	0.928	0.926	0.811	0.873	0.935	0.938	0.823	0.892	0.939	0.932
450	0.7873	0.834	0.928	0.928	0.811	0.874	0.935	0.938	0.823	0.893	0.939	0.932
450	0.7892	0.837	0.930	0.930	0.813	0.876	0.936	0.939	0.825	0.894	0.940	0.933
450	0.7925	0.841	0.932	0.934	0.816	0.880	0.938	0.941	0.827	0.897	0.942	0.934
450	0.7941	0.843	0.933	0.936	0.817	0.881	0.939	0.942	0.828	0.898	0.942	0.935
450	0.7953	0.845	0.934	0.938	0.818	0.883	0.940	0.943	0.828	0.899	0.943	0.935
450	0.7964	0.847	0.934	0.939	0.819	0.884	0.940	0.943	0.829	0.900	0.943	0.935
450	0.797	0.847	0.935	0.940	0.819	0.885	0.940	0.944	0.829	0.901	0.943	0.936
450	0.7984	0.849	0.936	0.942	0.820	0.886	0.941	0.945	0.830	0.902	0.944	0.936
450	0.7947	0.844	0.933	0.937	0.817	0.882	0.939	0.943	0.828	0.899	0.942	0.935
450	0.7987	0.850	0.936	0.942	0.821	0.886	0.941	0.945	0.830	0.902	0.944	0.936
450	0.7995	0.851	0.936	0.943	0.821	0.887	0.942	0.945	0.831	0.903	0.944	0.936
450	0.8	0.852	0.937	0.944	0.822	0.888	0.942	0.946	0.831	0.903	0.944	0.936
450	0.8001	0.852	0.937	0.944	0.822	0.888	0.942	0.946	0.831	0.903	0.944	0.936
450	0.8003	0.852	0.937	0.944	0.822	0.888	0.942	0.946	0.831	0.903	0.944	0.936
450	0.8006	0.852	0.937	0.944	0.822	0.888	0.942	0.946	0.832	0.904	0.945	0.936
450	0.797	0.847	0.935	0.940	0.819	0.885	0.940	0.944	0.829	0.901	0.943	0.936
450	0.8001	0.852	0.937	0.944	0.822	0.888	0.942	0.946	0.831	0.903	0.944	0.936

Table 4.4 continued

450	0.801	0.853	0.937	0.945	0.822	0.889	0.942	0.946	0.832	0.904	0.945	0.937
450	0.8011	0.853	0.937	0.945	0.822	0.889	0.942	0.946	0.832	0.904	0.945	0.937
450	0.8015	0.854	0.938	0.946	0.823	0.889	0.943	0.947	0.832	0.904	0.945	0.937
450	0.8021	0.854	0.938	0.946	0.823	0.890	0.943	0.947	0.832	0.905	0.945	0.937
450	0.8025	0.855	0.938	0.947	0.824	0.890	0.943	0.947	0.833	0.905	0.945	0.937
450	0.7988	0.850	0.936	0.942	0.821	0.886	0.941	0.945	0.830	0.902	0.944	0.936
450	0.8011	0.853	0.937	0.945	0.822	0.889	0.942	0.946	0.832	0.904	0.945	0.937
450	0.8014	0.854	0.938	0.946	0.823	0.889	0.943	0.946	0.832	0.904	0.945	0.937
450	0.8018	0.854	0.938	0.946	0.823	0.890	0.943	0.947	0.832	0.904	0.945	0.937
450	0.8025	0.855	0.938	0.947	0.824	0.890	0.943	0.947	0.833	0.905	0.945	0.937
450	0.8031	0.856	0.939	0.948	0.824	0.891	0.943	0.948	0.833	0.905	0.945	0.938
450	0.804	0.857	0.939	0.949	0.825	0.892	0.944	0.948	0.833	0.906	0.946	0.938
600	0.7729	0.807	0.927	0.911	0.795	0.846	0.930	0.949	0.808	0.869	0.934	0.946
600	0.7783	0.815	0.930	0.917	0.800	0.854	0.933	0.952	0.813	0.875	0.937	0.948
600	0.7793	0.816	0.931	0.918	0.801	0.855	0.934	0.952	0.814	0.876	0.937	0.948
600	0.7805	0.818	0.932	0.919	0.802	0.857	0.935	0.953	0.815	0.878	0.938	0.949
600	0.7827	0.821	0.933	0.921	0.804	0.859	0.936	0.954	0.817	0.880	0.939	0.949
600	0.7839	0.822	0.934	0.922	0.806	0.861	0.937	0.955	0.818	0.881	0.940	0.949
600	0.7849	0.824	0.934	0.923	0.807	0.862	0.937	0.955	0.819	0.882	0.940	0.949
600	0.7867	0.826	0.936	0.926	0.808	0.865	0.938	0.956	0.820	0.884	0.941	0.950
600	0.7899	0.831	0.938	0.929	0.811	0.869	0.940	0.958	0.822	0.888	0.943	0.951
600	0.7915	0.833	0.939	0.931	0.813	0.871	0.941	0.958	0.824	0.889	0.943	0.951
600	0.7927	0.835	0.939	0.932	0.814	0.872	0.942	0.959	0.824	0.890	0.944	0.951
600	0.7937	0.836	0.940	0.934	0.815	0.873	0.942	0.959	0.825	0.891	0.944	0.951
600	0.7943	0.837	0.940	0.935	0.815	0.874	0.943	0.960	0.826	0.892	0.945	0.952

Table 4.4 continued

600	0.7957	0.839	0.941	0.936	0.816	0.876	0.943	0.960	0.827	0.893	0.945	0.952
600	0.792	0.834	0.939	0.932	0.813	0.871	0.941	0.959	0.824	0.890	0.944	0.951
600	0.796	0.840	0.941	0.937	0.816	0.876	0.944	0.960	0.827	0.894	0.945	0.952
600	0.7968	0.841	0.942	0.937	0.817	0.877	0.944	0.960	0.827	0.894	0.946	0.952
600	0.7973	0.841	0.942	0.938	0.818	0.878	0.944	0.961	0.828	0.895	0.946	0.952
600	0.7974	0.841	0.942	0.938	0.818	0.878	0.944	0.961	0.828	0.895	0.946	0.952
600	0.7975	0.842	0.942	0.938	0.818	0.878	0.944	0.961	0.828	0.895	0.946	0.952
600	0.7979	0.842	0.943	0.939	0.818	0.878	0.945	0.961	0.828	0.895	0.946	0.952
600	0.7943	0.837	0.940	0.935	0.815	0.874	0.943	0.960	0.826	0.892	0.945	0.951
600	0.7974	0.842	0.942	0.938	0.818	0.878	0.944	0.961	0.828	0.895	0.946	0.952
600	0.7983	0.843	0.943	0.939	0.818	0.879	0.945	0.961	0.828	0.896	0.946	0.952
600	0.7984	0.843	0.943	0.939	0.818	0.879	0.945	0.961	0.828	0.896	0.946	0.952
600	0.7988	0.844	0.943	0.940	0.819	0.879	0.945	0.961	0.829	0.896	0.946	0.952
600	0.7993	0.844	0.944	0.941	0.819	0.880	0.945	0.962	0.829	0.897	0.947	0.952
600	0.7998	0.845	0.944	0.941	0.820	0.881	0.946	0.962	0.829	0.897	0.947	0.952
600	0.7961	0.840	0.942	0.937	0.817	0.876	0.944	0.960	0.827	0.894	0.945	0.952
600	0.7983	0.843	0.943	0.939	0.818	0.879	0.945	0.961	0.828	0.896	0.946	0.952
600	0.7987	0.843	0.943	0.940	0.819	0.879	0.945	0.961	0.829	0.896	0.946	0.952
600	0.7991	0.844	0.943	0.940	0.819	0.880	0.945	0.962	0.829	0.896	0.947	0.952
600	0.7998	0.845	0.944	0.941	0.820	0.880	0.946	0.962	0.829	0.897	0.947	0.952
600	0.8004	0.846	0.944	0.942	0.820	0.881	0.946	0.962	0.830	0.898	0.947	0.952
600	0.8013	0.847	0.945	0.943	0.821	0.882	0.946	0.962	0.830	0.898	0.947	0.953

Table 4.5. Variation of the normalized Nu values of EC4 and the other codes with D/t ratio of CFST column sections for UHPC with MGF

fy (MPa)	D/t=30				D/t=60				D/t=90			
	Nu (ACI/ EC4)	Nu (AISC/ EC4)	Nu (AIJ/ EC4)	Nu (DL/T/ EC4)	Nu (ACI/ EC4)	Nu (AISC/ EC4)	Nu (AIJ/ EC4)	Nu (DL/T/ EC4)	Nu (ACI/ EC4)	Nu (AISC/ EC4)	Nu (AIJ/ EC4)	Nu (DL/T/ EC4)
300	0.783	0.835	0.917	0.924	0.810	0.877	0.929	0.921	0.823	0.896	0.935	0.916
300	0.787	0.841	0.920	0.930	0.814	0.882	0.932	0.925	0.826	0.900	0.937	0.919
300	0.789	0.843	0.921	0.932	0.814	0.883	0.932	0.926	0.826	0.901	0.937	0.920
300	0.790	0.845	0.922	0.934	0.816	0.885	0.933	0.927	0.827	0.902	0.938	0.920
300	0.791	0.847	0.923	0.935	0.816	0.886	0.933	0.928	0.827	0.903	0.938	0.921
300	0.794	0.850	0.925	0.938	0.818	0.888	0.935	0.929	0.829	0.904	0.939	0.922
300	0.792	0.848	0.923	0.936	0.817	0.887	0.934	0.928	0.828	0.903	0.938	0.921
300	0.797	0.854	0.927	0.943	0.821	0.891	0.936	0.932	0.831	0.907	0.940	0.923
300	0.798	0.856	0.928	0.944	0.822	0.893	0.937	0.932	0.831	0.907	0.941	0.924
300	0.800	0.858	0.929	0.946	0.823	0.894	0.937	0.933	0.832	0.909	0.941	0.925
300	0.801	0.860	0.930	0.949	0.824	0.896	0.938	0.935	0.833	0.910	0.942	0.925
300	0.802	0.861	0.930	0.949	0.824	0.896	0.938	0.935	0.833	0.910	0.942	0.925
300	0.803	0.863	0.931	0.951	0.825	0.898	0.939	0.936	0.834	0.911	0.942	0.926
300	0.802	0.862	0.930	0.950	0.825	0.897	0.939	0.935	0.834	0.910	0.942	0.926
300	0.802	0.861	0.930	0.950	0.824	0.896	0.938	0.935	0.833	0.910	0.942	0.926
300	0.804	0.863	0.931	0.952	0.826	0.898	0.939	0.936	0.834	0.911	0.943	0.926
300	0.804	0.864	0.932	0.952	0.826	0.898	0.940	0.937	0.835	0.911	0.943	0.926
300	0.805	0.865	0.932	0.954	0.826	0.899	0.940	0.937	0.835	0.912	0.943	0.927
300	0.805	0.866	0.932	0.954	0.826	0.899	0.940	0.937	0.835	0.912	0.943	0.927
300	0.806	0.867	0.933	0.955	0.827	0.900	0.940	0.938	0.835	0.913	0.943	0.927
300	0.806	0.867	0.933	0.955	0.827	0.900	0.940	0.938	0.835	0.913	0.943	0.927

Table 4.5 continued

300	0.804	0.865	0.932	0.953	0.826	0.898	0.939	0.937	0.834	0.912	0.942	0.927
300	0.806	0.867	0.933	0.955	0.827	0.900	0.940	0.938	0.835	0.912	0.943	0.927
300	0.807	0.867	0.933	0.956	0.828	0.900	0.941	0.938	0.836	0.913	0.943	0.927
300	0.807	0.868	0.933	0.956	0.828	0.901	0.941	0.938	0.836	0.913	0.943	0.927
300	0.807	0.869	0.934	0.957	0.828	0.901	0.941	0.938	0.836	0.913	0.944	0.928
300	0.808	0.870	0.934	0.958	0.828	0.902	0.941	0.939	0.836	0.914	0.944	0.928
300	0.808	0.869	0.934	0.957	0.829	0.902	0.941	0.939	0.836	0.914	0.944	0.928
300	0.806	0.867	0.933	0.955	0.827	0.900	0.940	0.938	0.835	0.913	0.943	0.927
300	0.806	0.867	0.933	0.955	0.827	0.900	0.941	0.938	0.836	0.913	0.943	0.927
300	0.807	0.868	0.934	0.956	0.828	0.901	0.941	0.938	0.836	0.913	0.944	0.928
300	0.807	0.869	0.934	0.957	0.828	0.901	0.941	0.938	0.836	0.913	0.944	0.928
300	0.808	0.869	0.934	0.957	0.828	0.902	0.941	0.939	0.836	0.914	0.943	0.928
300	0.809	0.871	0.935	0.959	0.829	0.903	0.941	0.940	0.837	0.915	0.944	0.928
300	0.808	0.870	0.934	0.958	0.829	0.902	0.941	0.939	0.837	0.914	0.944	0.928
450	0.775	0.816	0.920	0.913	0.801	0.859	0.928	0.930	0.814	0.881	0.934	0.927
450	0.780	0.823	0.923	0.918	0.805	0.864	0.931	0.933	0.818	0.885	0.936	0.929
450	0.781	0.825	0.924	0.920	0.806	0.866	0.932	0.934	0.819	0.887	0.936	0.929
450	0.782	0.827	0.925	0.922	0.807	0.868	0.933	0.935	0.820	0.888	0.937	0.930
450	0.783	0.829	0.926	0.923	0.808	0.869	0.933	0.936	0.821	0.889	0.938	0.931
450	0.786	0.832	0.927	0.926	0.810	0.872	0.935	0.937	0.822	0.891	0.939	0.931
450	0.784	0.830	0.926	0.924	0.809	0.870	0.934	0.936	0.821	0.890	0.938	0.931
450	0.789	0.836	0.930	0.930	0.813	0.876	0.937	0.939	0.825	0.894	0.940	0.933
450	0.790	0.838	0.931	0.931	0.814	0.877	0.937	0.940	0.825	0.895	0.941	0.933
450	0.792	0.841	0.932	0.934	0.815	0.879	0.938	0.941	0.826	0.897	0.941	0.934
450	0.794	0.843	0.933	0.936	0.817	0.881	0.939	0.942	0.827	0.898	0.942	0.934

Table 4.5 continued

450	0.794	0.843	0.933	0.936	0.817	0.881	0.939	0.942	0.828	0.899	0.942	0.935
450	0.796	0.846	0.934	0.939	0.818	0.883	0.940	0.943	0.829	0.900	0.943	0.935
450	0.795	0.844	0.933	0.937	0.818	0.882	0.940	0.943	0.828	0.899	0.943	0.935
450	0.795	0.844	0.933	0.937	0.817	0.882	0.939	0.943	0.828	0.899	0.942	0.935
450	0.796	0.846	0.934	0.939	0.819	0.884	0.940	0.944	0.829	0.900	0.943	0.935
450	0.797	0.847	0.935	0.940	0.819	0.884	0.941	0.944	0.829	0.901	0.943	0.935
450	0.798	0.848	0.935	0.941	0.820	0.885	0.941	0.944	0.830	0.901	0.943	0.936
450	0.798	0.849	0.935	0.941	0.820	0.886	0.941	0.945	0.830	0.902	0.944	0.936
450	0.799	0.850	0.936	0.943	0.821	0.887	0.941	0.945	0.830	0.903	0.944	0.936
450	0.799	0.850	0.936	0.942	0.821	0.886	0.941	0.945	0.831	0.902	0.944	0.936
450	0.797	0.847	0.935	0.940	0.819	0.885	0.940	0.944	0.829	0.901	0.943	0.935
450	0.799	0.850	0.936	0.942	0.821	0.886	0.941	0.945	0.830	0.902	0.944	0.936
450	0.799	0.851	0.936	0.943	0.821	0.887	0.942	0.945	0.831	0.903	0.944	0.936
450	0.800	0.851	0.936	0.943	0.821	0.887	0.942	0.945	0.831	0.903	0.944	0.936
450	0.800	0.852	0.937	0.944	0.822	0.888	0.942	0.946	0.831	0.903	0.944	0.936
450	0.801	0.853	0.937	0.945	0.822	0.889	0.942	0.946	0.832	0.904	0.944	0.937
450	0.801	0.853	0.937	0.945	0.822	0.888	0.943	0.946	0.832	0.904	0.945	0.937
450	0.799	0.850	0.936	0.942	0.821	0.886	0.941	0.945	0.831	0.902	0.944	0.936
450	0.799	0.850	0.936	0.943	0.821	0.887	0.942	0.945	0.831	0.902	0.944	0.936
450	0.800	0.852	0.937	0.944	0.822	0.888	0.942	0.946	0.831	0.903	0.944	0.936
450	0.800	0.852	0.937	0.944	0.822	0.888	0.942	0.946	0.831	0.903	0.944	0.936
450	0.801	0.853	0.937	0.945	0.822	0.888	0.942	0.946	0.831	0.904	0.944	0.937
450	0.802	0.855	0.938	0.947	0.823	0.890	0.943	0.947	0.832	0.905	0.945	0.937
450	0.801	0.854	0.938	0.946	0.823	0.889	0.943	0.946	0.832	0.904	0.945	0.937
600	0.773	0.807	0.927	0.911	0.795	0.846	0.930	0.949	0.809	0.869	0.934	0.946

Table 4.5 continued

600	0.777	0.813	0.930	0.916	0.799	0.852	0.933	0.951	0.813	0.874	0.937	0.947
600	0.779	0.815	0.930	0.917	0.800	0.854	0.933	0.952	0.813	0.876	0.937	0.948
600	0.780	0.817	0.931	0.918	0.802	0.856	0.934	0.953	0.815	0.877	0.938	0.948
600	0.781	0.819	0.932	0.920	0.803	0.857	0.935	0.953	0.816	0.878	0.938	0.948
600	0.783	0.822	0.934	0.922	0.805	0.860	0.937	0.954	0.818	0.881	0.940	0.949
600	0.782	0.820	0.933	0.921	0.804	0.859	0.936	0.954	0.816	0.879	0.939	0.949
600	0.787	0.826	0.936	0.926	0.808	0.865	0.939	0.956	0.820	0.884	0.941	0.950
600	0.788	0.828	0.936	0.927	0.809	0.866	0.939	0.957	0.821	0.886	0.942	0.950
600	0.789	0.830	0.937	0.929	0.811	0.868	0.940	0.957	0.822	0.887	0.943	0.950
600	0.791	0.833	0.938	0.931	0.812	0.870	0.941	0.958	0.823	0.889	0.943	0.951
600	0.792	0.833	0.939	0.931	0.813	0.871	0.941	0.958	0.824	0.889	0.944	0.951
600	0.793	0.836	0.940	0.933	0.814	0.873	0.942	0.959	0.825	0.891	0.944	0.951
600	0.792	0.834	0.939	0.932	0.813	0.872	0.942	0.959	0.824	0.890	0.944	0.951
600	0.792	0.834	0.939	0.932	0.813	0.871	0.941	0.958	0.824	0.890	0.944	0.951
600	0.794	0.836	0.940	0.934	0.814	0.873	0.942	0.959	0.825	0.891	0.944	0.951
600	0.794	0.837	0.940	0.934	0.815	0.874	0.943	0.959	0.826	0.892	0.945	0.951
600	0.795	0.838	0.941	0.935	0.816	0.875	0.943	0.960	0.826	0.893	0.945	0.951
600	0.795	0.839	0.941	0.936	0.816	0.875	0.943	0.960	0.826	0.893	0.945	0.951
600	0.796	0.840	0.942	0.937	0.817	0.877	0.944	0.960	0.827	0.894	0.945	0.952
600	0.796	0.840	0.942	0.937	0.817	0.876	0.944	0.960	0.827	0.894	0.945	0.952
600	0.794	0.837	0.940	0.935	0.815	0.874	0.943	0.959	0.825	0.892	0.944	0.951
600	0.796	0.839	0.942	0.936	0.817	0.876	0.944	0.960	0.827	0.893	0.945	0.952
600	0.797	0.840	0.942	0.937	0.817	0.877	0.944	0.960	0.827	0.894	0.946	0.952
600	0.797	0.841	0.942	0.938	0.817	0.877	0.944	0.960	0.827	0.894	0.946	0.952
600	0.797	0.842	0.942	0.938	0.818	0.878	0.944	0.961	0.828	0.895	0.946	0.952

Table 4.5 continued

600	0.798	0.843	0.943	0.939	0.818	0.879	0.945	0.961	0.828	0.896	0.946	0.952
600	0.798	0.843	0.943	0.939	0.818	0.879	0.945	0.961	0.828	0.896	0.946	0.952
600	0.796	0.840	0.942	0.937	0.817	0.876	0.944	0.960	0.827	0.894	0.945	0.952
600	0.797	0.840	0.942	0.937	0.817	0.877	0.944	0.960	0.827	0.894	0.946	0.952
600	0.797	0.841	0.942	0.938	0.818	0.878	0.944	0.961	0.828	0.895	0.946	0.952
600	0.798	0.842	0.942	0.938	0.818	0.878	0.944	0.961	0.828	0.895	0.946	0.952
600	0.798	0.842	0.943	0.939	0.818	0.878	0.944	0.961	0.828	0.895	0.946	0.952
600	0.800	0.845	0.944	0.941	0.819	0.880	0.945	0.962	0.829	0.897	0.947	0.952
600	0.799	0.843	0.943	0.940	0.819	0.879	0.945	0.961	0.829	0.896	0.946	0.952

4.2.2.3 Comparison of Eurocode 4 with the Other Design Codes Based on Infill UHPFRC Compressive Strength

The range of the ratio of the axial load capacity of codes per EC4 versus the compressive strength of UHPC reinforced with MSF, HSF, and MGFs were illustrated in Figures 4.86, 4.87, and 4.88. Generally, with any increase in the compressive strength value, the codes go closer to each other, regardless of fiber types and concentration. To be more perceive about the results Table 4.6 has been drawn, which exact value of compressive strength and the other properties mentioned. MSF had been superior on approaching the other codes to EC4 then followed by HSF and MGF. The maximum available values of each curing date (180 days), cylindrical compressive strength, fiber concentration of 2% (unless 1.5% for MGF) gave the best results for near all codes to EC4. Nevertheless, the behaviors of D/t and fy were various, as 90 of D/t for the ACI, AISC, and AIJ codes gave the greatest results for all types of fibers, the asset value compared to DL/T was different by giving 30, 60, and 60 of D/t for MSF, HSF, and MGF, respectively. On the other hand, the values of fy were some disparity comparing to the other properties of effecting on approaching the codes to EC4.

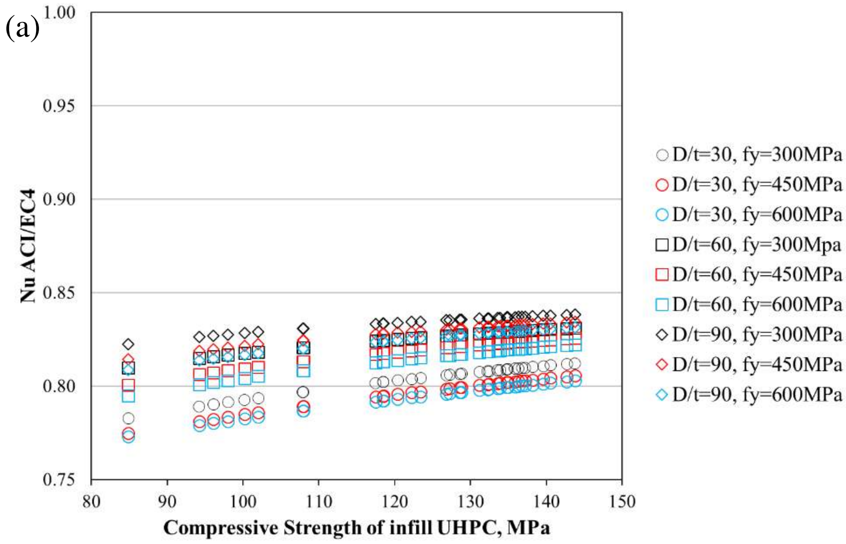

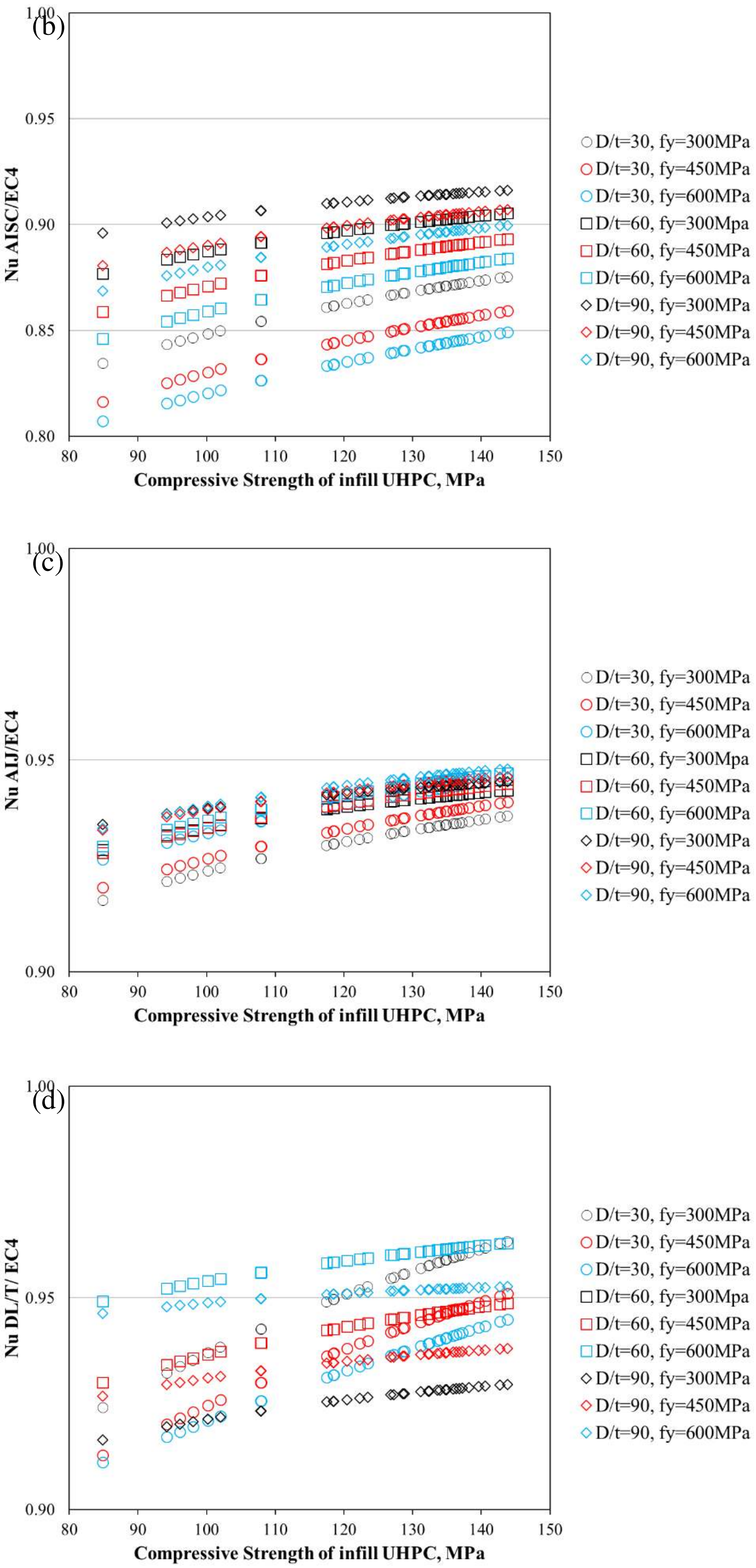

Figure 4.86. Variation of the normalized Nu values of EC4 and the other codes with infill UHPC strength of CFST column sections for MSF

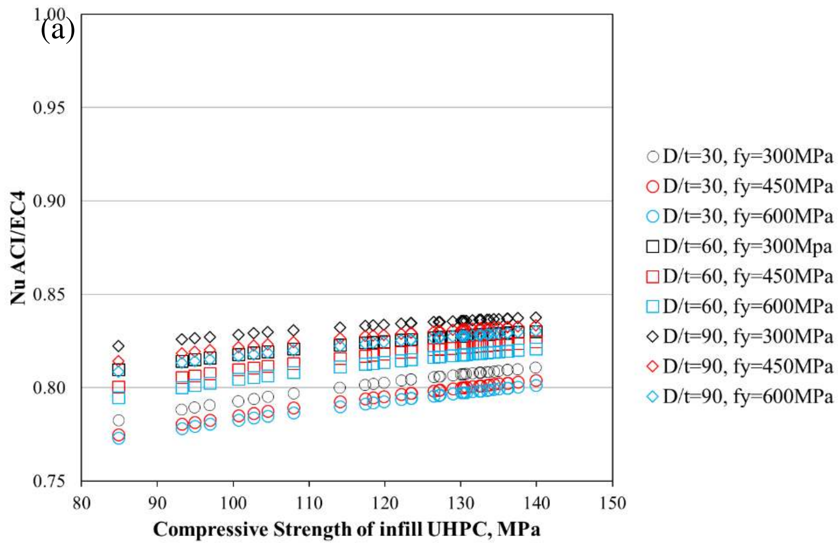
(a)
Nu ACI/EC4
1.00
0.95
0.90
0.85
0.80
0.75
80 90 100 110 120 130 140 150
Compressive Strength of infill UHPC, MPa
D/t=30, fy=300MPa
D/t=30, fy=450MPa
D/t=30, fy=600MPa
D/t=60, fy=300Mpa
D/t=60, fy=450MPa
D/t=60, fy=600MPa
D/t=90, fy=300MPa
D/t=90, fy=450MPa
D/t=90, fy=600MPa

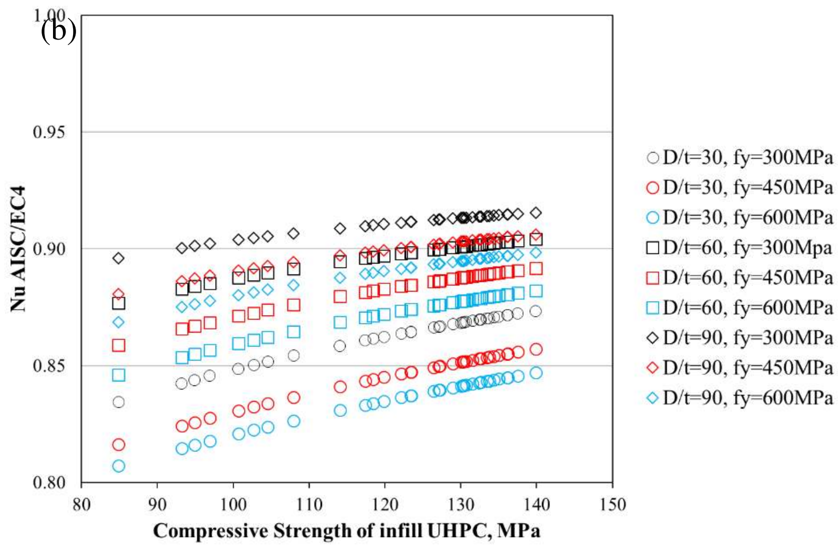
(b)
Nu AISC/EC4
1.00
0.95
0.90
0.85
0.80
80 90 100 110 120 130 140 150
Compressive Strength of infill UHPC, MPa
D/t=30, fy=300MPa
D/t=30, fy=450MPa
D/t=30, fy=600MPa
D/t=60, fy=300Mpa
D/t=60, fy=450MPa
D/t=60, fy=600MPa
D/t=90, fy=300MPa
D/t=90, fy=450MPa
D/t=90, fy=600MPa

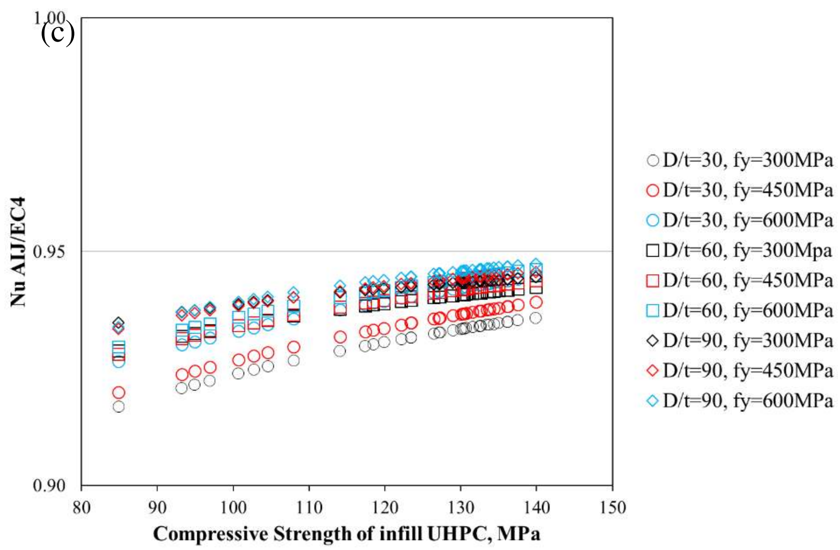
(c)
Nu AIJ/EC4
1.00
0.95
0.90
80 90 100 110 120 130 140 150
Compressive Strength of infill UHPC, MPa
D/t=30, fy=300MPa
D/t=30, fy=450MPa
D/t=30, fy=600MPa
D/t=60, fy=300Mpa
D/t=60, fy=450MPa
D/t=60, fy=600MPa
D/t=90, fy=300MPa
D/t=90, fy=450MPa
D/t=90, fy=600MPa

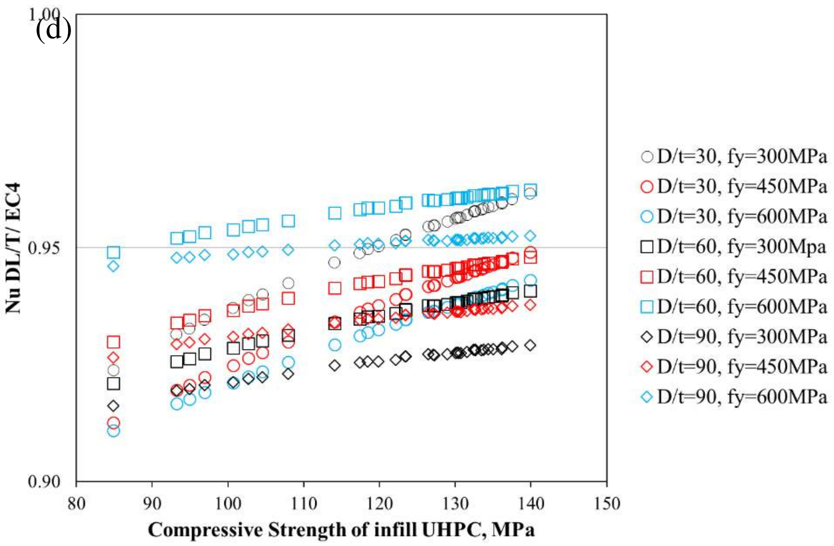

Figure 4.87. Variation of the normalized Nu values of EC4 and the other codes with infill UHPC strength of CFST column sections for HSF

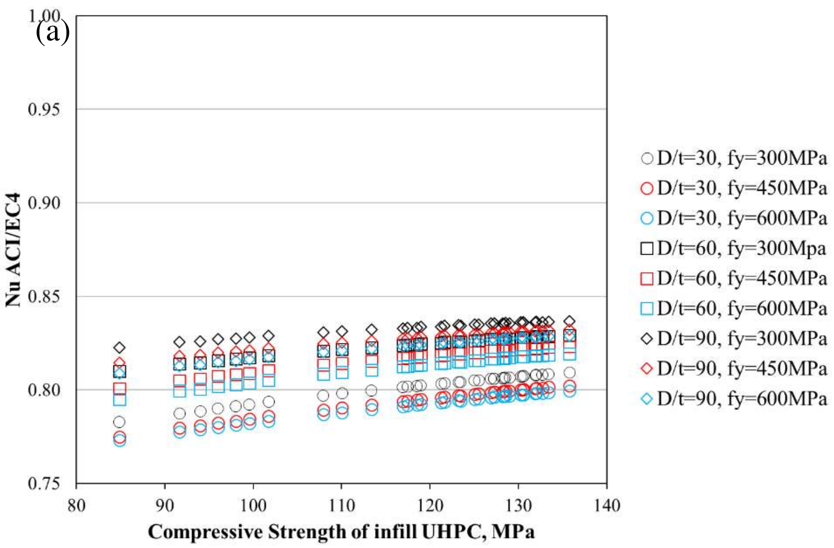

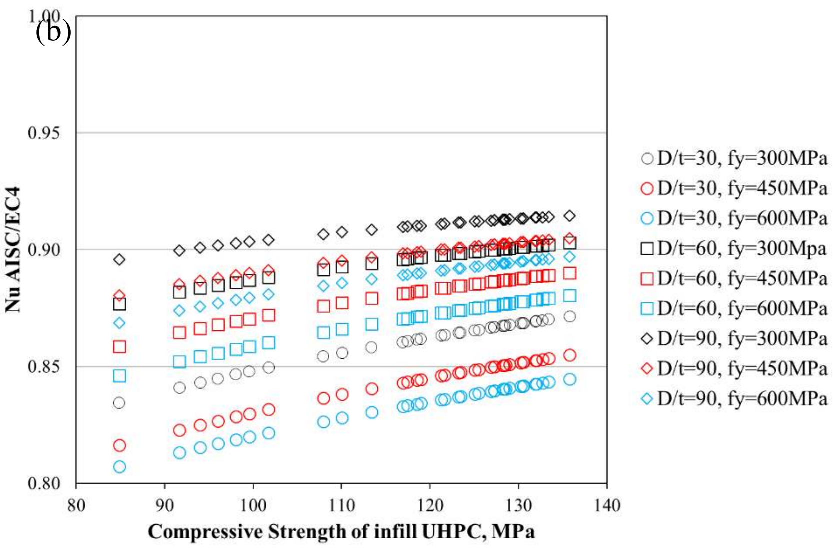

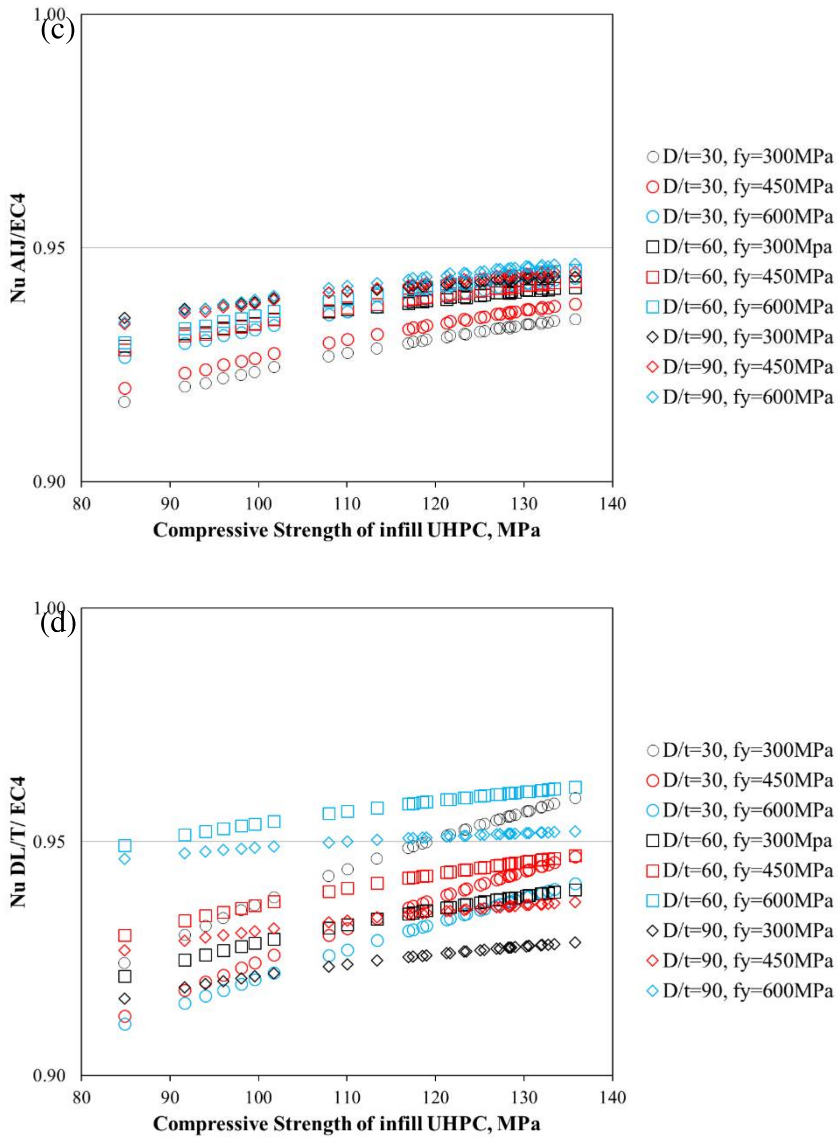

Figure 4.88. Variation of the normalized Nu values of EC4 and the other codes with infill UHPC strength of CFST column sections for MGF

Table 4.6. Role of the compressive strength, fibers, and steel tube properties in comparison of codes

X-Code/EC4	Fiber Types	Nearest Point to 1						Farther Point to 1					
		Fiber vol. (%)	D/t	fy (MPa)	Age (days)	Cylinder Compressive strength 150X300mm (MPa)	X Code /EC4 ratio	Fiber vol. (%)	D/t	fy (MPa)	Age (days)	Cylinder Compressive strength 150X300mm (MPa)	X Code /EC4 ratio
ACI/EC4	MSF	2	90	300	180	143.8	0.8382	0.25	30	600	7	94.2	0.7789
	HSF	2	90	300	180	139.9	0.8376	0.25	30	600	7	93.2	0.7783
	MGF	1.5	90	300	180	135.8	0.8367	0.25	30	600	7	91.7	0.7775
AISC/EC4	MSF	2	90	300	180	143.8	0.9162	0.25	30	600	7	94.2	0.8155
	HSF	2	90	300	180	139.9	0.9154	0.25	30	600	7	93.2	0.8146
	MGF	1.5	90	300	180	135.8	0.9146	0.25	30	600	7	91.7	0.8132
AIJ/EC4	MSF	2	90	600	180	143.8	0.9479	0.25	30	300	7	94.2	0.9213
	HSF	2	90	600	180	139.9	0.9474	0.25	30	300	7	93.2	0.9208
	MGF	1.5	90	600	180	135.8	0.9466	0.25	30	300	7	91.7	0.9204
DL/T/EC4	MSF	2	30	450	180	143.8	0.9633	0.25	60	300	7	94.2	0.8592
	HSF	2	60	600	180	139.9	0.9625	0.25	30	600	7	93.2	0.9166
	MGF	1.5	60	600	180	135.8	0.9617	0.25	30	600	7	91.7	0.9155

4.2.2.4 Comparison of Eurocode 4 with the Other Design Codes Based on Correlation Equations

To examine the effectiveness of the existing formulation codes, Euro Code (EC4) was used as a reference to compare the results of the other codes. Thus, Figures 4.89, 4.90, and 4.91 has been drawn all data which shown the scatter EC4 versus the other codes for MSF, HSF, and MGF, respectively. From above-mentioned figures, it is clear that AIJ and DL/T so near to EC4 results showing nearly bisector line (y=1.06x) followed by of AISC (y=1.1x) then ACI (y=1.2x), Irrespective of fiber types and volumes. This behavior may have related to numbers of parameters and factors. For example, ACI code depended on four elements on the calculation of axial strength for composite columns, but EC4, AISC, AIJ, and DL/T based on many other factors (see equations in Section 3.2). On the other hand, for demonstrating the effect of fibers and their directions on the approaching codes with each other, plain and different types of fibers were drawn in Figures (4.89, 4.90, and 4.91)a and both (Plain+Fibers) together were demonstrated in Figures (4.89, 4.90, and 4.91)b. While MSF and HSF groups were supported to approach different codes with each other, MGF group played an adverse role; even these effects were little in both cases. This may attribute to some mechanical properties of glass fibers that affected on the calculation of axial load capacity like compressive strength which the increments limited after addition of 1.5% of micro glass fibers (Section 4.1.1). The findings of present work agree with the study of Güneyisi et al. [143] that the axial load capacity of EC4, AIJ, and DL/T codes are near to each other compared ACI code results.

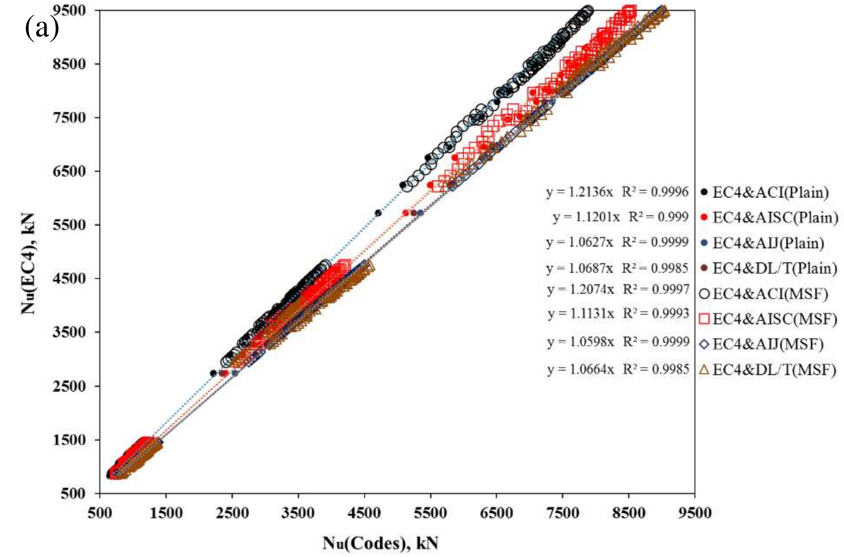

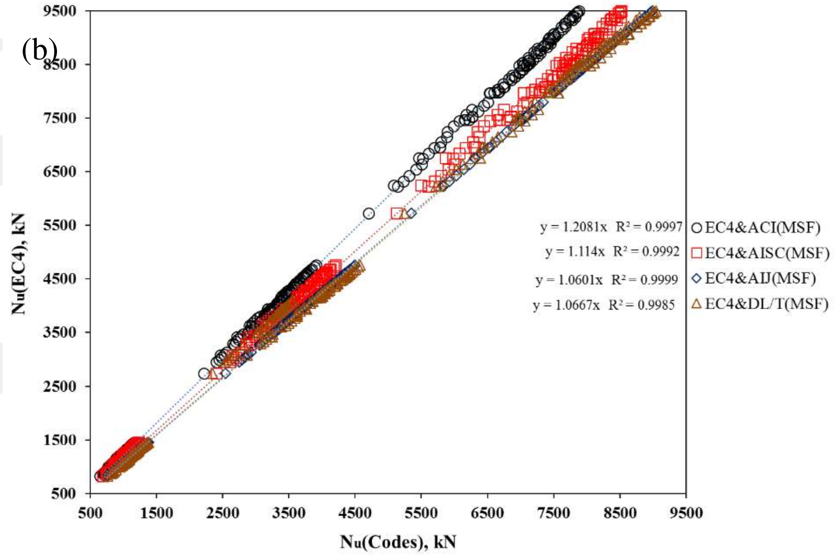

Figure 4.89. Equations of correlation of the normalized Nu values of EC4 and the other codes for CFST column sections with MSF

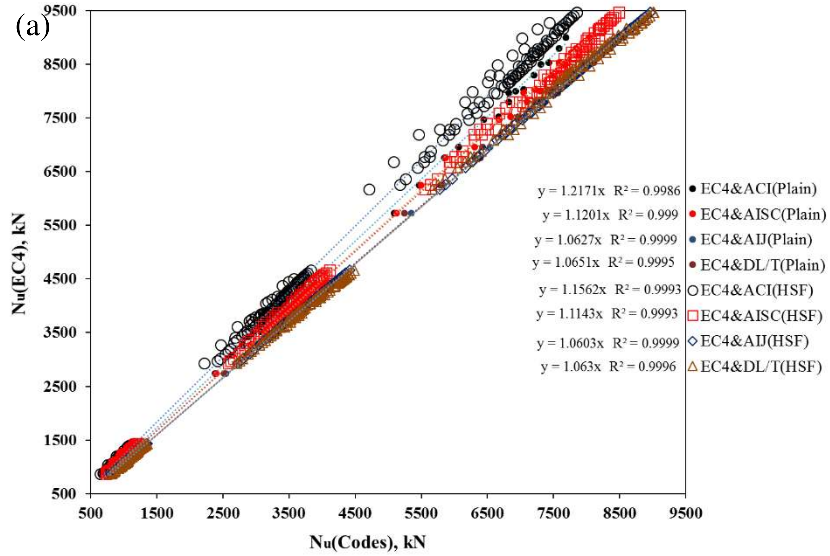

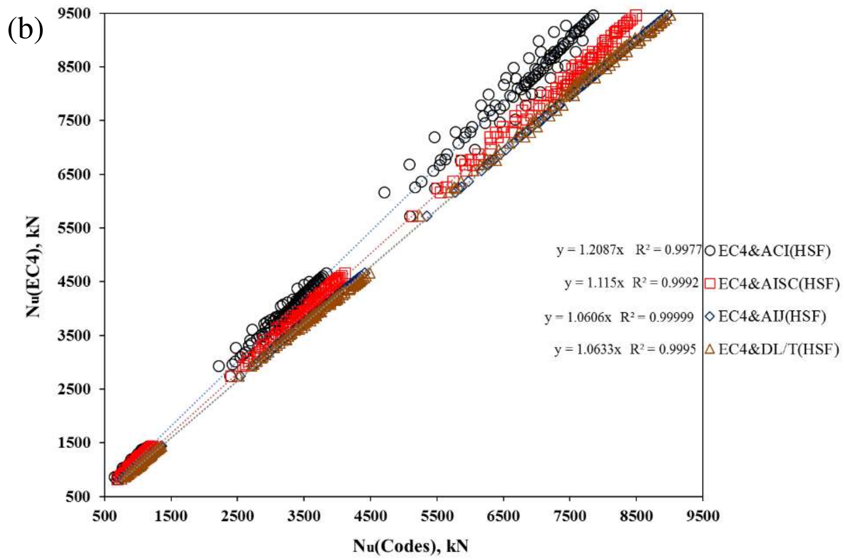

Figure 4.90. Equations of correlation of the normalized Nu values of EC4 and the other codes for CFST column sections with HSF

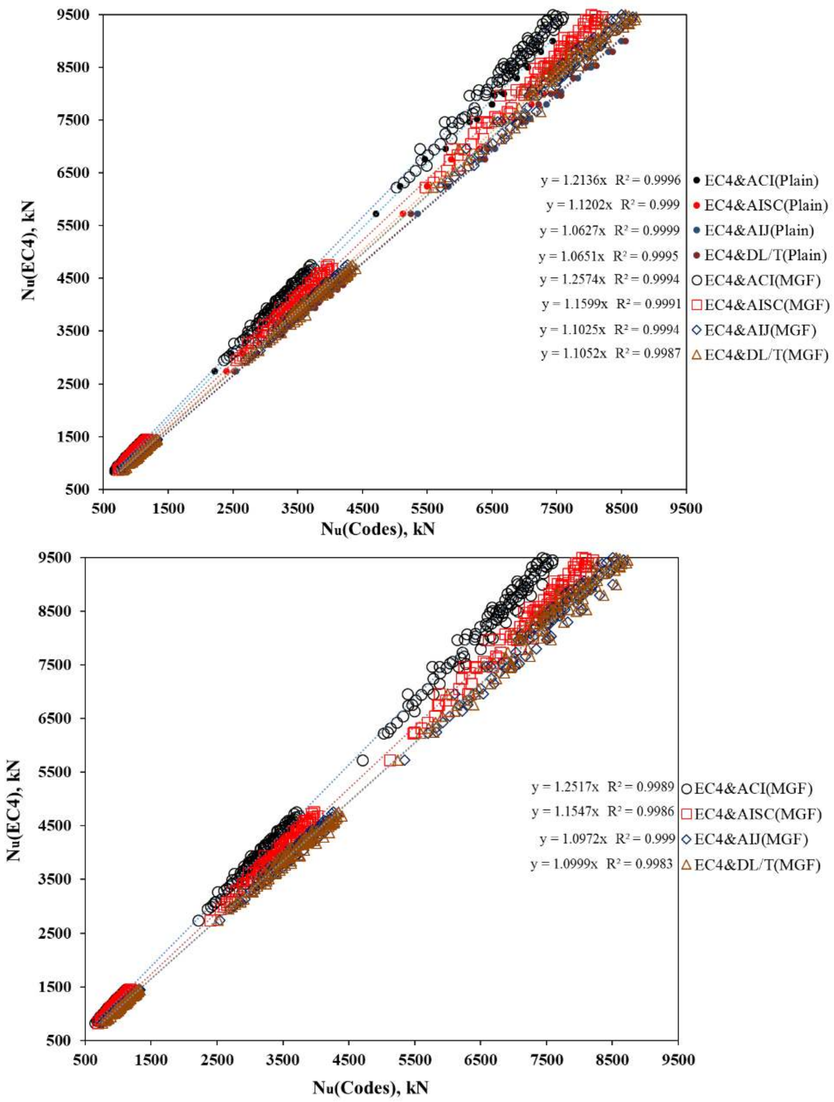

Figure 4.91. Equations of correlation of the normalized Nu values of EC4 and the other codes for CFST column sections with MGF

CHAPTER 5

CONCLUSIONS

The following conclusions were drawn based on the findings of this study:

1. It was observed that the fiber reinforcement continuously improved the mechanical, fracture, physical behaviors of UHPC, irrespective of the fiber type. However, the strength values began to decrease after 1.5% volume with the presence of micro glass fibers.

2. Concerning to the compressive strength of UHPCs, the reinforcing with micro steel fibers appeared to be more favorable than others. Test results also showed that UHPFRC made with small size specimens illustrated higher strength results than their corresponded bigger sizes.

3. In general, the addition of the fibers provided higher splitting tensile strength, irrespective of the fiber type. However, this beneficial effect was more pronounced for micro steel fibers owing to the mechanism of fiber orientation.

4. Unlike compressive and splitting tensile strengths, hooked steel fibers appeared to be much more effective on flexural strength than the others. Arresting the crack by the hooked fibers prevents the sudden failure, thus resulting in higher the load carrying capacity.

5. Despite the same working mechanism for stopping micro cracks, the performance of glass fiber was superior on flexural strength improvement, compared to micro steel fiber, probably owing to the varying fiber length of the former which more cracks would be arrested.

6. The excellent performance of hooked fibers over the micro steel and glass fibers is attributed to the fact that the hooked steel fibers can bridge cracks and retard their propagation that could change the fracture behavior of concrete from brittle to plastic and then considerably raise the ultimate flexural strength of UHPFRC.

5. UHPC with hooked steel fibers had the highest fracture energy followed by micro steel and micro glass fibers, respectively. As a measure of ductility which consistent with the fracture energy, the characteristic length also significantly increased with fiber reinforcement especially for concretes with the hooked steel fibers.

6. It can be noted that the general shapes of load-displacement curves due to hooked steel fibers are entirely different from the others by extending more displacement against applied loads. While micro steel fibers were different by showing zigzagged curves at the post peaked region.

7. The mixture containing 2% long hooked steel showed the highest toughness value. In addition, macro fibers made a high bond strength and a longer length that increased stress transfer performance even after initiating the first crack, but, microfibers cannot work well for bridging crack surfaces on the macro level.

8. The tail of load displacement curve is cut at displacement that are 10, 20, and 2 times larger than the maximum displacement for control UHPC by adding 2% of MSF, HSF, and MGF, correspondingly.

9. The hooked steel fibers yielded lower shrinkage in comparison to MSF and MGF. Also, the effect of using higher fiber addition level almost worked like shrinkage reducer or compensator.

10. It was observed that the ultimate axial load of CFST composite columns continuously increased in the case of steel fiber reinforced UHPCs while the axial load increment limited at 1.5% volume of micro glass fibers, irrespective to testing age.

11. When the testing ages of concrete were reached 90 days, there were insignificant grow of the results for the other next 90 days (at the age of 180 days) which not exceed 5% of the total enhancement gained.

12. The favorite MSF over the others on increasing axial load strength of CFST column may be due to that huge number of micro steel fibers per any percentage amount distributed regularly and intimately inside concrete with an assistant of their rigidity and size

13. High concentration of fibers and high yield strength is not a condition of significant development of the axial capacity of the steel tube infilled with UHPFRC, but it seems like the diameter per wall thickness played an important role because the lowest D/t resulted from lowest growth and vice versa.

14. From the analyzing of the figures, it's noticed that the fibers will not play any role in closing the codes with each other, irrespective of the different D/t ratio, but with any increase of the compressive strength value, the codes go closer to each other, regardless of fiber types and concentration.

15. It is concluded from this study that AIJ and DL/T so near to EC4 results showing nearly bisector line (y=1.06x) followed by of AISC (y=1.1x) then ACI (y=1.2x), Irrespective of fiber types and volumes. This behavior may have related to numbers of parameters and factors. For example, ACI code depended on four elements on the calculation of axial strength for composite columns, but EC4, AISC, AIJ, and DL/T codes based on many other factors.

16. While MSF and HSF groups were supported to approach different codes with each other, MGF group played an adverse role. This may attribute to some mechanical properties of glass fibers that affected on the calculation of axial load capacity like compressive strength which the increments limited after addition of 1.5% of micro glass fibers.

REFERENCES

[1]. Zhao, S. and Sun, W. (2014). Nano-mechanical behavior of a green ultra-high performance concrete. *Construction and Building Materials*. **63**: p. 150-160.

[2]. Ahlborn T.M., Peuse, E.J., and Misson, D.L. (2008), Ultra-high-performance-concrete for michigan bridges material performance–phase I. *Michigan Tech Transportation Institute*. p. 931-1295.

[3]. Richard, P. and Cheyrezy, M.H. (1994). Reactive powder concretes with high ductility and 200-800 MPa compressive strength. *Special Publication*. **144**: p. 507-518.

[4]. Coppola, L. (1996). Innovative cementitious materials. from HPC to RPC. part II. The effect of cement and silica fume type on the compressive strength of reactive powder concrete. *L'Industria Italiana del Cemento*. **707**: p. 112-125.

[5]. Long, G., Wang X., and Xie, Y. (2002). Very-high-performance concrete with ultrafine powders. *Cement and Concrete Research*. **32**(4): p. 601-605.

[6]. Bonneau, O., et al. (1996). Reactive powder concretes: from theory to practice. *Concrete International*. **18**(4): p. 47-49.

[7]. Roux, N., Andrade, C., and Sanjuan, M. (1996). Experimental study of durability of reactive powder concretes. *Journal of Materials in Civil Engineering*. **8**(1): p. 1-6.

[8]. Graybeal, B.A. (2006), Material property characterization of ultra-high performance concrete.

[9]. de Larrard, F. and Sedran, T. (1994). Optimization of ultra-high-performance concrete by the use of a packing model. *Cement and Concrete Research*. **24**(6): p. 997-1009.

[10]. Richard, P. and Cheyrezy, M. (1995). Composition of reactive powder concretes. *Cement and concrete research*. **25**(7): p. 1501-1511.

[11]. Habel, K. (2006). Development of the mechanical properties of an ultra-high performance fiber reinforced concrete (UHPFRC). *Cement and Concrete Research*. **36**(7): p. 1362-1370.

[12]. Nguyen, D.L. (2014). Size and geometry dependent tensile behavior of ultra-high-performance fiber-reinforced concrete. *Composites Part B: Engineering*. **58**: p. 279-292.

[13]. Hannant, D. (1987). Fiber cement and fiber concrete. *A Wiley Interscience Publication*.

[14]. Balaguru, P.N. and Shah, S.P. (1992), Fiber-reinforced cement composites. 1992.

[15]. Banthia, N. and Nandakumar, N. (2003). Crack growth resistance of hybrid fiber reinforced cement composites. *Cement and Concrete Composites*. **25**(1): p. 3-9.

[16]. Won, J.-P. (2012). Flexural behaviour of amorphous micro-steel fibre-reinforced cement composites. *Composite Structures*. **94**(4): p. 1443-1449.

[17]. Pyo, S. (2015). Strain rate dependent properties of ultra high performance fiber reinforced concrete (UHP-FRC) under tension. *Cement and Concrete Composites*. **56**: p. 15-24.

[18]. Yazıcı, Ş., İnan, G., and Tabak, V. (2007). Effect of aspect ratio and volume fraction of steel fiber on the mechanical properties of SFRC. *Construction and Building Materials*. **21**(6): p. 1250-1253.

[19]. Bentur, A. (1989). Fiber-reinforced cementitious materials. *Material science of concrete*: p. 223-285.

[20]. Bentur, A. and Mindess, S. (2006), Fibre reinforced cementitious composites. 2006: *CRC Press*.

[21]. Kim, H.S. and Shin, Y.S. (2011). Flexural behavior of reinforced concrete (RC) beams retrofitted with hybrid fiber reinforced polymers (FRPs) under sustaining loads. *Composite structures*. **93**(2): p. 802-811.

[22]. Yap, S.P. (2014). Flexural toughness characteristics of steel–polypropylene hybrid fibre-reinforced oil palm shell concrete. *Materials & Design*. **57**: p. 652-659.

[23]. Kang, S.-T. (2010). Tensile fracture properties of an Ultra High Performance Fiber Reinforced Concrete (UHPFRC) with steel fiber. *Composite Structures*. **92**(1): p. 61-71.

[24]. Kwon, S.H. (2013). Tensile stress-crack opening relationship of ultra high performance cementitious composites (UHPCC) used for bridge decks. *Journal of the Korea institute for structural maintenance and inspection*. **17**(1): p. 46-54.

[25]. Ryu, G.S. (2012), Mechanical behavior of UHPC (ultra high performance concrete) according to hybrid use of steel fibers. in *Advanced Materials Research*. Trans Tech Publ.

[26]. Park, S.H. (2012). Tensile behavior of ultra high performance hybrid fiber reinforced concrete. *Cement and Concrete Composites*. **34**(2): p. 172-184.

[27]. Wille, K., Kim, D.J., and Naaman, A.E. (2011). Strain-hardening UHP-FRC with low fiber contents. *Materials and structures*. **44**(3): p. 583-598.

[28]. Kang, S.-T. and Kim, J.-K. (2012). Investigation on the flexural behavior of UHPCC considering the effect of fiber orientation distribution. *Construction and Building Materials*. **28**(1): p. 57-65.

[29]. Kim, D.J. (2011). Comparative flexural behavior of hybrid ultra high performance fiber reinforced concrete with different macro fibers. *Construction and Building Materials*. **25**(11): p. 4144-4155.

[30]. Yoo, D.-Y., Lee, J.-H., and Yoon, Y.-S. (2013). Effect of fiber content on mechanical and fracture properties of ultra high performance fiber reinforced cementitious composites. *Composite Structures*. **106**: p. 742-753.

[31]. Lee, N.P. and Chisholm, D.H. (2006), Reactive Powder Concrete, in Study Report SR 146.

[32]. Hoang, K. (2008), Influence of types of steel fiber on properties of ultra high performance concrete. in *The 3rd AFC International Conference ACG/VCA*.

[33]. Ghorpade, V.G. (2010), An Experimental Investigation on Glass Fibre reinforced High Performance Concrete with Silicafume as Admixture. in *35th Conference on Our World in Concrete & Structures, Singapore*.

[34]. Yoo, D.-Y. and Yoon, Y.-S. (2015). Structural performance of ultra-high-performance concrete beams with different steel fibers. *Engineering Structures*. **102**: p. 409-423.

[35]. Aydın, S. and Baradan, B. (2013). The effect of fiber properties on high performance alkali-activated slag/silica fume mortars. *Composites Part B: Engineering*. **45**(1): p. 63-69.

[36]. Yoo, D.-Y., Kang, S.-T., and Yoon, Y.-S. (2014). Effect of fiber length and placement method on flexural behavior, tension-softening curve, and fiber distribution characteristics of UHPFRC. *Construction and Building Materials*. **64**: p. 67-81.

[37]. Ketema, E. (2005), design aid for composite columns. *aau*.

[38]. Bedage, S. and Shinde, D. (2015). Concrete filled steel tubes subjected to axial compression. *International Journal of Research in Engineering and Technology* **Volume: 04 Available @ http://www.ijret.org** (Issue: 06): p. eISSN: 2319-1163 |pISSN: 2321-7308.

[39]. Lu, Z.-H. and Zhao, Y.-G. (2010). Suggested empirical models for the axial capacity of circular CFT stub columns. *Journal of Constructional Steel Research*. **66**(6): p. 850-862.

[40]. Kirankumar, T.P.R. (2016). Comparative Study of Concrete Filled Steel Tube Columns under Axial Compression *International Journal of Constructive Research in Civil Engineering (IJCRCE)*. **2**(Issue 2,): p. PP 11-17

[41]. Furlong, R.W. (1967). Strength of steel-encased concrete beam columns. *Journal of the Structural Division*. **93**(5): p. 113-124.

[42]. Han, L.-H., Li, W., and Bjorhovde, R. (2014). Developments and advanced applications of concrete-filled steel tubular (CFST) structures: members. *Journal of Constructional Steel Research*. **100**: p. 211-228.

[43]. Shanmugam, N. and Lakshmi, B. (2001). State of the art report on steel–concrete composite columns. *Journal of constructional steel research*. **57**(10): p. 1041-1080.

[44]. Abed, F., AlHamaydeh, M., and Abdalla, S. (2013). Experimental and numerical investigations of the compressive behavior of concrete filled steel tubes (CFSTs). *Journal of Constructional Steel Research*. **80**: p. 429-439.

[45]. Webb, J. (1993). High-strength concrete: economics, design and ductility. *Concrete international*. **15**(1): p. 27-32.

[46]. Liu, D. and Gho, W.-M. (2005). Axial load behaviour of high-strength rectangular concrete-filled steel tubular stub columns. *Thin-Walled Structures*. **43**(8): p. 1131-1142.

[47]. Banthia, N. (2012). FRC: Milestone in international research and development. *proceedings of FIBCON2012, ICI, Nagpur, India, February*: p. 13-14.

[48]. James, I., Gopalaratnam, V., and Galinat, M. (2002). State-of-the-art report on fiber reinforced concrete. *Manual Concr Practice*. **21**: p. 2-66.

[49]. Labib, W. and Eden, N. (2006). An investigation into the use of fibres in concrete industrial ground-floor slabs. *Liverpool John Moores University, Liverpool*.

[50]. Roumaldi, J. and Batson, G.B. (2008), Mechanics of crack arrest in concrete.

[51]. Beckett, D. (2003). Concrete industrial ground floors: aspects of crack control. *Concrete*. **37**(8): p. 14-16.

[52]. Biryukovich, K., and Yu, DL. (1965). Glass Fiber Reinforced Cement," translated by GL Cairns, CERA Translation. *Civil Eng. Res. Assoc., No. 12*.

[53]. Majumdar, A.J. (1976). Properties of Fiber Cement Composites. *Proceedings, RILEM Symp., London, 1975, Construction Press, Lancaster*: p. pp. 279-314.

[54]. Monfore, G. (1968). A review of fiber reinforcement of Portland cement paste, mortar, and concrete. *Journal Pca Res & Dev Laboratories*.

[55]. Goldfein, S. (1963), plastic fibrous reinforcement for Portland Cement. *DTIC Document*.

[56]. Krenchel, H. (1985). Applications of polypropylene fibers in Scandinavia. *Concrete International*. **7**(3): p. 32-34.

[57]. Naaman, A.E., Shah, S.P., and Throne, J.L. (1984). Some developments in polypropylene fibers for concrete. *Special Publication*. **81**: p. 375-396.

[58]. Naaman, A.E. (1985). "Fiber Reinforcement for Concrete," *Concrete International: Design and Construction*. **Vol. 7, No. 3,**: p. pp. 21-25.

[59]. Nataraja, M., Dhang, N., and Gupta, A. (1998). Steel fibre reinforced concrete under compression. *Indian concrete journal*. **72**(7): p. 353-356.

[60]. Zollo, R.F. (1997). Fiber-reinforced concrete: an overview after 30 years of development. *Cement and Concrete Composites*. **19**(2): p. 107-122.

[61]. Shah, S.P. (1981). Fibre reinforced concretes, a review of capabilities. . *University of Illinois at Chicago Circle.*: p. 48.

[62]. Rai, A. and Joshi, D.Y. (2014). Applications and properties of fibre reinforced concrete. *Int. Journal of Engineering Research and Applications*. **4**(5): p. 123-131.

[63]. ASTMA820. Standard Specification for Steel Fibers for Fiber-Reinforced Concrete Active Standard A | Developed by Subcommittee: . *ASTM A820 / A820M*. **A01.05**.

[64]. Grosse, W.a. (1996). Pullout behaviour of fibers in steel fiber reinforced concrete.

[65]. Nataraja, M. (2011). Fiber reinforced concrete-behaviour properties and application. *Sri Jayachamarajendra College of engineering*.

[66]. Bentur, A. and Mindess, S. (1990). Fibers reinforced cementous composites. *Elsevier*. **3**(2): p. 440-9.

[67]. Majumdar, A.J. and Ryder, J. (1968). Glass fibre reinforcement of cement products.

[68]. Cem-FIL (1998). GRC Technical Data, Cem-FIL International Ltd, Vetrotex, UK.

[69]. Liang, W. (2002). Improved properties of GRC composites using commercial E-glass fibers with new coatings. *Materials research bulletin*. **37**(4): p. 641-646.

[70]. Rai, A. and Joshi, D.Y. (2014). Applications and properties of fibre reinforced concrete. *International Journal of Engineering Research and Applications*. **4**(5): p. 123-131.

[71]. Zollo, R.F. and Hays, C.D. (1991). Fibers Versus WWF as Non-Structural Slab Reinforcement. *Concrete International*. **13**(11): p. 50-55.

[72]. Tang, M.-C. (2012), High performance concrete—past, present and future. in *Proceedings of the International Symposium on Ultra High Performance Concrete. Kassel, Germany*.

[73]. Spasojevic, A. (2012), Possibilites for Structural Improvements in the Design of Concrete Bridges. in *Proceedings of the 6th Int. PhD Symposium in Civil Engineering, Zurich 2006*. Proceedings of the 6th Int. PhD Symposium in Civil Engineering, Zurich 2006.

[74]. Schmidt, M. (2012), Von der Nanotechnologie zum Ultra-Hochfesten Beton. in *The 16th International Conference on Building materials (ibausil), Weimar, Germany*.

[75]. Aïtcin, P.-C. (2011), High performance concrete. 2011: *CRC Press*.

[76]. Aïtcin, P.-C. (2000). Cements of yesterday and today: concrete of tomorrow. *Cement and Concrete research*. **30**(9): p. 1349-1359.

[77]. Vande, Voort T., Suleiman M., and Sritharan S. (2008). Design and performance verification of UHPC piles for deep foundations. *IHRB Project TR-558, Center for Transportation Research and Education, Iowa State University, Ames, IA*.

[78]. Rossi, P. (2005). Development of new cement composite materials for construction. *Proceedings of the Institution of Mechanical Engineers, Part L: Journal of Materials Design and Applications*. **219**(1): p. 67-74.

[79]. Jungwirth, J. and Muttoni, A. (2013), Structural behavior of tension members in Ultra High Performance Concrete. in *International symposium on ultra high performance concrete*. International Symposium on Ultra High Performance Concrete.

[80]. Gao, R. (2012), Static properties of plain reactive powder concrete beams. in *Key Engineering Materials*. Trans Tech Publ.

[81]. Dauriac, C. and Dowd, B. (1996). Reactive powder concrete. *The Construction Specifier*. **12**: p. 47-51.

[82]. Walraven, J. (2002), From Design of Structures to Design of Materials. Innovations and Developments in Concrete Materials and Construction. in

Proceedings of the International Conference Held at the University of Dundee, Scotland, UK on.

[83]. Ma, J. and Schneider, H. (2002). Properties of ultra-highperformance concrete. *Leipzig Annual Civil Engineering Report (LACER)*. **7**: p. 25-32.

[84]. Schmidt, M. and Fehling, E. (2005). Ultra-high-performance concrete: research, development and application in Europe. *ACI Special publication*. **228**: p. 51-78.

[85]. Spasojevic, A. (2008). Structural implications of ultra-high performance fibre-reinforced concrete in bridge design.

[86]. Wille, K., Naaman, A.E., and Parra-Montesinos, G.J. (2011). Ultra-High Performance Concrete with Compressive Strength Exceeding 150 MPa (22 ksi): A Simpler Way. *ACI Materials Journal*. **108**(1).

[87]. Rossi, P. (2005). Bending and compressive behaviours of a new cement composite. *Cement and Concrete Research*. **35**(1): p. 27-33.

[88]. Sobolev, K. (2004). The development of a new method for the proportioning of high-performance concrete mixtures. *Cement and Concrete Composites*. **26**(7): p. 901-907.

[89]. Vernet, C.P. (2004). Ultra-durable concretes: structure at the micro-and nanoscale. *MRS bulletin*. **29**(05): p. 324-327.

[90]. Stovall, T., De Larrard, F., and Buil, M. (1986). Linear packing density model of grain mixtures. *Powder Technology*. **48**(1): p. 1-12.

[91]. Kosmatka, S.H., Panarese, W.C., and Kerkhoff, B. (2002). Design and control of concrete mixtures.

[92]. Ma, J., Dietz, J., and Dehn, F. (2002). Ultra high performance self compacting concrete. *Lacer*. **7**: p. 33-42.

[93]. Teichmann, T. and Schmidt, M. (2004), Influence of the packing density of fine particles on structure, strength and durability of UHPC. in *First international symposium on ultra high performance concrete, Kassel*.

[94]. Lubbers, A.R. (2003), Bond performance between ultra-high performance concrete and prestressing strands. *Ohio University*.

[95]. Buitelaar, P. and ApS, C. (2004). Ultra High Performance Concrete: Developments and Applications during 25 years.

[96]. Sadrekarimi, A. (2004). Development of a light weight reactive powder concrete. *Journal of Advanced Concrete Technology*. **2**(3): p. 409-417.

[97]. Perry, V. (2012), A revolutionary new material for new solutions. in *Technical Forum Presentation*.

[98]. Klemens, T. (2004). Flexible Concrete Offers New Solutions. *Concrete Construction*. **49**(12): p. 72.

[99]. Droll, K. (2012), Influence of additions on ultra high performance concretes–grain size optimisation. in *Proceedings of the International Symposium on Ultra-High Performance Concrete, Kassel, Germany, Sept. 13*.

[100]. Brown, J.L. (2006). Highway Span Features Ultra-High-Performance Concrete. *Civil Engineering*. **76**(7).

[101]. Blais, P.Y. and Couture, M. (1999). Precast, prestressed pedestrian bridge: World's first Reactive Powder Concrete structure. *PCI journal*. **44**(5): p. 60-71.

[102]. America, L.N. (2007). Product Information. http://www.lafargenorthamerica.com. *Lafarge North America*.

[103]. Lafarge (2007). Ductal® -Applications and References. http://www.ductal-lafarge.com /wps/portal/Ductal/ApplicationsAndReference.

[104]. Hajar, Z. (2012), Design and construction of the world first ultra-high performance concrete road bridges. in *Proceedings of the Int. Symp. on UHPC, Kassel, Germany*.

[105]. Resplendino, J. (2012), First recommendations for Ultra-High-Performance Concretes and examples of application. in *International Symposium on Ultra High Performance Concrete*.

[106]. Behloul, M., Causse, G., And Etienne, D. (2012), Grands projets et structures innovantes-Passerelle en DUCTAL de Seoul. in *La Technique Francaise Du Beton-The First Fib Congress 2002, October 13-19 2002, Osaka, Japan*.

[107]. Behloul, M. and Lee, K. (2003). Ductal® Seonyu footbridge. *Structural Concrete*. **4**(4): p. 195-201.

[108]. Rebentrost, M. and Cavill, B. (2006). Reactive Powder Concrete Bridges. 6th Austroads Bridge Conferences, 12–15 September. *Perth, Australia*.

[109]. Semioli, W.J. (2001). The new concrete technology. *Concrete International*. **23**(11): p. 75-79.

[110]. Billon, P., Ed. (2006). A railway bridge that is twice as light. *Ductal® Solutions, The Lafarge Ductal® Newsletter* . **No. 3, March: 3**.

[111]. America, L.N. (2006). Structural Columns to Support a Suspended Floor in a 185-ft Silo. *magineductal.com. http://www.imagineductal.com/imagineductal/public/eng/pdf/Detroit-Columns.pdf.*

[112]. Forum, C.I. (2003). Ultra-High Performance Concrete with Ductility *The World's First Long-Span Roof Constructed in Ductal®. Construction Innovation Forum, 2003 Nova Award Nomination. http://www.cif.org/Nom2003/ Nom22_03.pdf.*

[113]. Reda, M., Shrive, N., and Gillott, J. (1999). Microstructural investigation of innovative UHPC. *Cement and Concrete Research*. **29**(3): p. 323-329.

[114]. Hassan, A. and Kawakami, M. (2005). Steel-free composite slabs made of reactive powder materials and fiber-reinforced concrete. *ACI structural journal*. **102**(5): p. 709.

[115]. Cadoni, E. (2012), FRC in Switzerland: research, applications and perspectives. in *International Workshop on Advanced Fiber Reinforced Concrete*. International Workshop on Advanced Fiber Reinforced Concrete.

[116]. Bindiganavile, V., Banthia, N., and Aarup, B. (2002). Impact response of ultra-high-strength fiber-reinforced cement composite. *ACI Materials journal*. **99**(6): p. 543-548.

[117]. Deem, S. (2002). Concrete Attraction–Something new on the French menu-concrete. *Popular Mechanics*.

[118]. Cheyrezy, M. (1999). Structural applications of RPC. *Concrete*. **33**(1): p. 20-23.

[119]. Yan, Z.G. and Yan, G.P. (2012), Experimental study and finite element analysis on RPC footwalk braces. in *Key Engineering Materials*. Trans Tech Publ.

[120]. Toutlemonde, F. and Sercombe, J. (2012), FRC containers design to ensure impact performance. in *Structures Congress–Proceedings*.

[121. Reineck, K.-H., Lichtenfels, A., and Greiner, S. (2004). Concrete hot water tanks for solar energy storage. *Structural engineering international*. **14**(3): p. 232-234.

[122]. Xing, F. (2013), Static Loading Investigation on Well Cover of Reactive Powder Concrete. in *Key Engineering Materials*. Trans Tech Publ.

[123]. Dallaire, E., Aitcin, P.-C., and Lachemi, M. (1998). High-performance powder. *Civil Engineering*. **68**(1): p. 48.

[124]. Schmidt, M. (2003). Concrete Technology-Ultra-high performance concrete: Perspective for the precast concrete industry. *Betonwerk und Fertigteiltechnik*. **69**(3): p. 16-29.

[125]. Berge, M. (1998). Composite columnsMaster's Thesis, New Jersey Institute of Technology, USA.

[126]. Nethercot, D. (2003), Composite construction. 2003: *CRC Press*.

[127]. Hull, B.K. (1998). Experimental behavior of high strength concrete filled tube columns.

[128]. Ajel, H.A. and Abbas, A.M. (2015). Experimental and Analytical Investigations of Composite Stub Columns. *International Journal of Innovative Research in Science, Engineering and Technology*. **Vol. 4**(Issue 2).

[129]. Hu, Y. (2010), Behaviour and modelling of FRP-confined hollow and concrete-filled steel tubular columns. *The Hong Kong Polytechnic University*.

[130]. Morino, S. and Tsuda, K. (2003). Design and construction of concrete-filled steel tube column system in Japan. *Earthquake Engineering and Engineering Seismology*. **4**(1): p. 51-73.

[131. Roeder, C.W., Macrae, G., and Waters, C. (2000). Seismic behavior of steel braced frame connections to composite columns.

[132]. Tarenaka, C. (2001). "Features of CFT structure system", Concrete-Filled steel tube structural system CFT, www.Tarenaka e/quake e/cft/cft-htm.

[133]. Hubert, G. (2001). Semi-continuous beam-to-column joints at the Millennium Tower in Vienna, Austria. *Steel & Composite Structures*. **1**(2): p. 159-170.

[134]. Viest, I.M. (1997). Composite construction design for buildings.

[135]. Wong, R. (2012), The construction of Super High-rise Composite Structures in Hong Kong. in *Structural & Construction Conf*. CRC Press.

[136]. Chandresh, C. (2016). Composite Construction of Buildings. Available at http://civildigital.com/composite-construction-buildings-composite-beams/. Accessed 01.05.2016.ital.com.

[137]. Samhâl, E. (2005). Composite Construction. European Steel Computer Aided Learning (Lecture 1.1).

[138]. Sakino, K. (2004). Behavior of centrally loaded concrete-filled steel-tube short columns. *Journal of Structural Engineering*. **130**(2): p. 180-188.

[139]. Giakoumelis, G. and Lam, D. (2004). Axial capacity of circular concrete-filled tube columns. *Journal of Constructional Steel Research*. **60**(7): p. 1049-1068.

[140]. Schneider, S.P., Kramer, D.R., and Sarkkinen, D.L. (Year), The design and construction of concrete-filled steel tube column frames. in *13th World Conference on Earthquake Engineering, Vancouver, BC, Canada*.

[141]. Gupta, P., Sarda, S., and Kumar, M. (2007). Experimental and computational study of concrete filled steel tubular columns under axial loads. *Journal of Constructional Steel Research*. **63**(2): p. 182-193.

[142]. Evirgen, B., Tuncan, A., and Taskin, K. (2014). Structural behavior of concrete filled steel tubular sections (CFT/CFSt) under axial compression. *Thin-Walled Structures*. **80**: p. 46-56.

[143]. Güneyisi, E.M., Gültekin, A., and Mermerdaş, K. (2016). Ultimate capacity prediction of axially loaded CFST short columns. *International Journal of Steel Structures*. **16**(1): p. 99-114.

[144]. Hafiz, F. (2016). Analytical and Numerical Study on Behavior of Concrete Filled Steel Tabular Columns Subjected To Axial Compression Loads. *International Journal of Scientific & Engineering Research*. **7**(Issue 9,).

[145]. Ellobody, E., Young, B., and Lam, D. (2006). Behaviour of normal and high strength concrete-filled compact steel tube circular stub columns. *Journal of Constructional Steel Research*. **62**(7): p. 706-715.

[146]. Liu, D. (2006). Behaviour of eccentrically loaded high-strength rectangular concrete-filled steel tubular columns. *Journal of Constructional Steel Research*. **62**(8): p. 839-846.

[147]. Yu, Q., Tao, Z., and Wu, Y.-X. (2008). Experimental behaviour of high performance concrete-filled steel tubular columns. *Thin-Walled Structures*. **46**(4): p. 362-370.

[148]. Liew, J.R. and Xiong, D. (2012). Ultra-high strength concrete filled composite columns for multi-storey building construction. *Advances in Structural Engineering*. **15**(9): p. 1487-1503.

[149]. Liew, J. and Xiong, D. (2010). Experimental investigation on tubular columns infilled with ultra-high strength concrete.

[150]. Guler, S., Copur, A., and Aydogan, M. (2013). Axial capacity and ductility of circular UHPC-filled steel tube. *Magazine of Concrete Research*. **65**(15): p. 898-905.

[151]. Lu, Y.-y. (2015). Experimental investigation of axially loaded steel fiber reinforced high strength concrete-filled steel tube columns. *Journal of Central South University*. **22**: p. 2287-2296.

[152]. Zhang, F. (2016). Experimental study of CFDST columns infilled with UHPC under close-range blast loading. *International Journal of Impact Engineering*. **93**: p. 184-195.

[153]. Zhang, F. (2015). Residual axial capacity of CFDST columns infilled with UHPFRC after close-range blast loading. *Thin-Walled Structures*. **96**: p. 314-327.

[154]. Xiong, M.-X., Xiong, D.-X., and Liew, J.R. (2017). Flexural performance of concrete filled tubes with high tensile steel and ultra-high strength concrete. *Journal of Constructional Steel Research*. **132**: p. 191-202.

[155]. Xiong, M.-X., Xiong, D.-X., and Liew, J.R. (2017). Axial performance of short concrete filled steel tubes with high-and ultra-high-strength materials. *Engineering Structures*. **136**: p. 494-510.

[156]. Kharoob, O., Ghazy, M., and Yossef, N. (2017). Behavior of beam-high performance fiber reinforced CFST column joints. *Thin-Walled Structures*. **113**: p. 217-227.

[157]. Al Zand, A.W. (2017). Rehabilitation and strengthening of high-strength rectangular CFST beams using a partial wrapping scheme of CFRP sheets: Experimental and numerical study. *Thin-Walled Structures*. **114**: p. 80-91.

[158]. EN T. (2002). 197-1. *Çimento-Bölüm*. **1**: p. 33-42.

[159]. C494M-16 A.C. (2013). Standard Specification for Chemical Admixtures for Concrete. *ASTM International, West Conshohocken, PA*.

[160]. EFNARC S. guidelines for self compacting concrete. Feb.(2002). *Free pdf copy downloadable from http://www. efnarc. org*: p. 29-35.

[161]. C39M-16b A.C. (2016). Standard test method for compressive strength of cylindrical concrete specimens. *ASTM International, West Conshohocken, PA*.

[162]. C1144-89 A. (2011). Standard Test Method for Splitting Tensile Strength for Brittle Nuclear Waste Forms. *ASTM International, West Conshohocken, PA*.

[163]. C469M-14 A.C. (2014). Standard Test Method for Static Modulus of Elasticity and Poisson's Ratio of Concrete in Compression. *ASTM International, West Conshohocken, PA*.

[164]. Hillerborg, A., Modéer, M., and Petersson, P.-E. (1976). Analysis of crack formation and crack growth in concrete by means of fracture mechanics and finite elements. *Cement and concrete research*. **6**(6): p. 773-781.

[165]. Recommendation, R.D. (1985). Determination of the Fracture Energy of Mortar and Concrete by Means of Three-Point Bend Tests on Notched Beames. *Materials and Structures*. **18**(106): p. 285-290.

[166]. Ravindra, K. and Henderson, N. (1999), Specialist Techniques and Materials for Concrete Production. *Thomas Telford Publishing, Thomas Telford Ltd*.

[167]. Akcay, B. (2012). Interpretation of aggregate volume fraction effects on fracture behavior of concrete. *Construction and Building Materials*. **28**(1): p. 437-443.

[168]. Hillerborg, A. (1985). The theoretical basis of a method to determine the fracture energyG F of concrete. *Materials and structures*. **18**(4): p. 291-296.

[169]. C157M-04 A.C. (West Conshohocken, PA, 2004). Standard Test Method for Length Change of Hardened Hydraulic-Cement, Mortar, and Concrete. *ASTM International*.

[170]. Akçay, B. (2007), Effects of lightweight aggregates on autogenous deformation and fracture of high performance concrete.

[171]. Grzybowski, M. and Shah, S.P. (1990). Shrinkage cracking of fiber reinforced concrete. *Materials Journal*. **87**(2): p. 138-148.

[172]. Shh, S., Krguller, M., and Sarigaphuti, M. (1992). Effects of shrinkage-reducing admixtures on restrained shrinkage cracking of concrete. *Materials Journal*. **89**(3): p. 289-295.

[173]. Sargaphuti, M., Shah, S., and Vinson, K. (1993). Shrinkage cracking and durability characteristics of cellulose fiber reinforced concrete. *Materials Journal*. **90**(4): p. 309-318.

[174]. Wiegrink, K., Marikunte, S., and Shah, S.P. (1996). Shrinkage cracking of high-strength concrete. *Materials Journal*. **93**(5): p. 409-415.

[175]. Skazlić, M., Serdar, M., and Bjegović, D. (2013), Influence of test specimen geometry on compressive strength of ultra high performance concrete. in *Second International Symposium on Ultra High Performance Concrete*.

[176]. Graybeal, B. and Davis, M. (2008). Cylinder or cube: strength testing of 80 to 200 MPa (11.6 to 29 ksi) ultra-high-performance fiber-reinforced concrete. *ACI Materials Journal*. **105**(6): p. 603-609.

[177]. Kazemi, S. and Lubell, A.S. (2012). Influence of specimen size and fiber content on mechanical properties of ultra-high-performance fiber-reinforced concrete. *ACI Materials Journal-American Concrete Institute*. **109**(6): p. 675.

[178]. Eurocode (2004). Design of composite steel and concrete structures. Part 1.1, General rules and rules for buildings. EN 1994-1-1. *European Committee for Standardization: British Standards Institution*.

[179]. ACI (2005). Building code requirements for structural concrete (ACI 318-05) and commentary (ACI 318R-05). *American Concrete Institute*.

[180]. AISC (2005). Load and resistance factor design (LRFD) specification for structural steel buildings. Chicago (IL, USA). *American Institute of Steel Construction*.

[181]. AIJ (1997). Recommendations for design and construction of concrete filled steel tubular structures. Tokyo (Japan) [in Japanese]. *Architectural Institute of Japan*.

[182]. AIJ (2001). Standards for structural calculation of steel reinforced concrete structures 5th ed. Tokyo (Japan) [in Japanese]. *Architectural Institute of Japan*.

[183]. DL/T (1999). Chinese design code for steel-concrete composite structures, in Chinese. *Chinese Electricity Press*.

[184]. Yu, R., Spiesz, P., and Brouwers, H. (2014). Static properties and impact resistance of a green Ultra-High Performance Hybrid Fibre Reinforced Concrete (UHPHFRC): experiments and modeling. *Construction and Building Materials*. **68**: p. 158-171.

[185]. Gibbs, J. and Zhu, W. (1999), Strength of hardened self-compacting concrete. in *Proceedings of First international RILEM Symposium on Self-Compacting Concrete (PRO 7), Stockholm, Suede*.

[186]. Dehestani, M., Nikbin, I., and Asadollahi, S. (2014). Effects of specimen shape and size on the compressive strength of self-consolidating concrete (SCC). *Construction and building materials*. **66**: p. 685-691.

[187]. Hamad, A.J. (2015). Size and shape effect of specimen on the compressive strength of HPLWFC reinforced with glass fibres. *Journal of King Saud University-Engineering Sciences*.

[188]. Griffith, A.A. (1921). The phenomena of rupture and flow in solids. *Philosophical transactions of the royal society of london. Series A, containing papers of a mathematical or physical character*. **221**: p. 163-198.

[189]. Iqbal, S., et al. (2015). Mechanical properties of steel fiber reinforced high strength lightweight self-compacting concrete (SHLSCC). *Construction and Building Materials*. **98**: p. 325-333.

[190]. Mahdi, B. (2009), Properties of self compacted reactive powder concrete exposed to saline solution. *Ph. D. Thesis, Building and Construction Engineering Department, University of Technology, Baghdad*.

[191]. Sanal, I. and Ozyurt, N. (2012), Effects of formwork dimensions on the performance of fiber-reinforced cement based materials. in *Proceedings of the 9th international congress on advances in civil engineering*.

[192]. Tassew, S. and Lubell, A. (2014). Mechanical properties of glass fiber reinforced ceramic concrete. *Construction and Building Materials*. **51**: p. 215-224.

[193]. Yoo, D.-Y., Yoon, Y.-S., and Banthia, N. (2015). Flexural response of steel-fiber-reinforced concrete beams: Effects of strength, fiber content, and strain-rate. *Cement and Concrete Composites*. **64**: p. 84-92.

[194]. Gao, J., Sun, W., and Morino, K. (1997). Mechanical properties of steel fiber-reinforced, high-strength, lightweight concrete. *Cement and Concrete Composites*. **19**(4): p. 307-313.

[195]. Hassanpour, M., Shafigh, P., and Mahmud, H.B. (2012). Lightweight aggregate concrete fiber reinforcement–a review. *Construction and Building Materials*. **37**: p. 452-461.

[196]. Hussein, L. and Amleh, L. (2015). Structural behavior of ultra-high performance fiber reinforced concrete-normal strength concrete or high strength concrete composite members. *Construction and Building Materials*. **93**: p. 1105-1116.

[197]. Grunewald, S. (2004), Performance-based design of self-compacting fibre reinforced concrete. 2004: *Delft University Press*.

[198]. 544 A.C. (1988, Reapp '94). Fiber-Reinforced Concrete. *ACI Committee 544*.

[199]. Lawler, J. (2003). Fracture processes of hybrid fiber-reinforced mortar. *Materials and Structures*. **36**(3): p. 197-208.

[200]. Gesoglu, M. (2016). Strain hardening ultra-high performance fiber reinforced cementitious composites: Effect of fiber type and concentration. *Composites Part B: Engineering*. **103**: p. 74-83.

[201]. Gopalaratnam, V., Shah, S., and John, R. (1984). A modified instrumented Charpy test for cement-based composites. *Experimental mechanics*. **24**(2): p. 102-111.

[202]. Vandewalle, L. (2000). RILEM TC 162-TDF: Test and design methods for steel fibre reinforced concrete. *Materials and structures*. **33**(225): p. 3-6.

[203]. Garas, V., Kahn, L., and Kurtis, K. (2009), Preliminary investigation of the effect of steel fibers on the tensile creep and shrinkage of ultra-high performance concrete. in *Proceedings of the 8th International Conference on Creep, Shrinkage and Durability Mechanics of Concrete and Concrete Structures*.

[204]. Swamy, R. and Stavrides, H. (2012), Influence of fiber reinforcement on restrained shrinkage and cracking. in *Journal Proceedings*.

[205]. Jensen, O.M. and Hansen, P.F. (2001). Water-entrained cement-based materials: I. Principles and theoretical background. *Cement and concrete research*. **31**(4): p. 647-654.

[206]. Tazawa, E.-i. (1999), Autogenous shrinkage of concrete. 1999: *CRC Press*.

[207]. Farhat, F. (2007). High performance fibre-reinforced cementitious composite (CARDIFRC)–Performance and application to retrofitting. *Engineering fracture mechanics*. **74**(1): p. 151-167.

[208]. Kalingarani, K., Shanmugavalli, B., and Sundarraja, M. (2014). Axial Compressive Behavior of Slender CFST members–Analytical Investigation. *International Journal of Innovative research in science, Engineering and Technology*. **3**: p. 22-25.

PERSONAL INFORMATION

Name and Surname: Guler Fakhraddin MUHYADDIN

Nationality: Iraqi

Birth place and date: Iraq-Erbil/01-January-1984

Marital status: married

Phone number: +90 539 645 8484

+964 750 448 0587

Email: gulerasaad2009@yahoo.com

guler.asaad@hotmail.com

gulerasaad2009@gmail.com

EDUCATION

PhD degree /College of engineering/ Civil engineering/ College of Engineering

Master degree /College of engineering/ Civil engineering/ College of Engineering

Bachelor's degree/College of Engineering /Civil Eng. Department/ College of Engineering

Work experience

	Place	Enrollment
2006-Present	Ministry of Higher Education	Civil Engineer

PUBLICATIONS

<u>Published SCI& SCI-Expanded Articles:</u>

1. Gesoglu, M., Güneyisi, E., Asaad, D.S. and **Muhyaddin, G.F.**, 2016. Properties of low binder ultra-high performance cementitious composites: Comparison of nanosilica and microsilica. *Construction and Building Materials*, *102*, pp.706-713.

2. Gesoglu, M., Güneyisi, E., **Muhyaddin, G.F**. and Asaad, D.S., 2016. Strain hardening ultra-high performance fiber reinforced cementitious composites: Effect of fiber type and concentration. Composites Part B: Engineering, 103, pp.74-83.

3. Güneyisi, E.M. and **Muhyaddin, G.F**., 2014. Comparative Response Assessment of Different Frames with Diagonal Bracings under Lateral Loading. Arabian Journal for Science and Engineering, 39(5), pp.3545-3558.

FOREIGN LANGUAGE

Turkish
English
Kurdish
Arabic
Turkmen